Synthesis and Evaluation of Novel Inhibitors of 1-Deoxy-D-xylulose-5-phosphate Reductoisomerase as Potential Antimalarials

A thesis submitted in fulfilment of the requirements for the degree of

Master of Science

of

Rhodes University

by

Anne Claire Conibear

B.Sc.Hons (Rhodes University)

August 2010

Abstract

Malaria continues to be an enormous health-threat in the developing world and the emergence of drug resistance has further compounded the problem. The parasite-specific enzyme, 1-deoxy-D-xylulose-5-phosphate reductoisomerase (DXR), has recently been validated as a promising antimalarial drug target. The present study comprises a combination of synthetic, physical organic, computer modelling and bioassay techniques directed towards the development of novel DXR inhibitors. A range of 2-heteroarylamino-2-oxoethyl- and 2-heteroarylamino-2-oxopropyl phosphonate esters and their corresponding phosphonic acid salts have been synthesised as analogues of the highly active DXR inhibitor, fosmidomycin. Treatment of the heteroarylamino precursors with chloroacetyl chloride or chloropropionyl chloride afforded chloroamide intermediates, Arbuzov reactions of which led to the corresponding diethyl phosphonate esters. Hydrolysis of the esters has been effected using bromotrimethylsilane. Twenty-four new compounds have been prepared and fully characterised using elemental (HRMS or combustion) and spectroscopic (1- and 2-D NMR and IR) analysis. A ^{31}P NMR kinetic study has been carried out on the two-step silylation reaction involved in the hydrolysis of the phosphonate esters and has provided activation parameters for the reaction. The kinetic analysis was refined using a computational method to give an improved fit with the experimental data.

Saturation transfer difference (STD) NMR analysis, computer-simulated docking and enzyme inhibition assays have been used to evaluate the enzyme-binding and -inhibition potential of the synthesised ligands. Minimal to moderate inhibitory activity has been observed and several structure-activity relationships have been identified. *In silico* exploration of the DXR active site has revealed an additional binding pocket and information on the topology of the active site has led to the *de novo* design of a new series of potential ligands.

Acknowledgements

I would like to express my sincere thanks to my supervisors Prof. P. Kaye and Dr K. Lobb for all they have taught me as well as their continued support and guidance throughout the project. I have particularly appreciated Prof. Kaye's wisdom and gentle encouragement to keep going. Dr Lobb's patience in teaching me the computational and NMR skills and his encouragement to try new techniques is also much appreciated.

The *Ec*DXR inhibition assays were carried out by Taryn Bodill at the Rhodes University Centre for Chemico- and Biomedicinal Research and I would like to thank her for her organisation, care and perseverance in getting the assays up and running. I also extend my gratitude to Matthew Adendorff for help with using AutoDock and to Jessica Goble for technical assistance in the expression and purification of *Ec*DXR and for the use of the *Pf*DXR homology model.

The Chemistry Department at Rhodes University has been a very enjoyable and fulfilling place in which to work and I would like to thank all the academic, technical and support staff and students for creating such a supportive work environment. I would especially like to thank Prof. M. Davies-Coleman and Dr R. Klein for their mentorship and unwavering support.

I owe much thanks to my family and friends for their moral support, prayers, interest and encouragement which have so often kept me going.

I am also extremely grateful to the Beit Trust and Rhodes University for a joint Beit-Rhodes Postgraduate Scholarship which has enabled me to undertake this study. I appreciate not only their financial support but their organisation and continued interest.

"For from Him and through Him and to Him are all things. To Him be the glory forever."
Romans 11:36 (NIV)

Table of Contents

[handwritten note: Make your own notes, NEVER underline or write in ...]

1. INTRODUCTION

2. RESULTS AND DISCUSSION

3. EXPERIMENTAL

4. REFERENCES

5. SUPPLEMENTARY DATA (Provided on CD)

1. INTRODUCTION

1.1. Malaria

1.1.1. The world-wide burden of malaria

Man has battled with malaria for thousands of years and its associated, recurring fevers are alluded to in some of the earliest historical records.[1] Spreading from a few isolated regions as populations grew and new territories were colonised, malaria became a world-wide disease by the early 1800's.[1] Little was known about the vector or causative agent of malaria until the 1880's when Charles Laveran identified the plasmodium parasite in the blood of infected patients.[1] In 1897, Ronald Ross demonstrated that malaria is transmitted by mosquitoes, a discovery for which he won a Nobel Prize in 1902.[1] However, the full life cycle of the parasite, including its various tissue stages, was not discovered until 1948 when it was first described by Garnham and Shortt.[1]

Malaria can be caused by any of the four plasmodium species *Plasmodium falciparum* (*P. falciparum*), *Plasmodium ovale* (*P. ovale*), *Plasmodium vivax* (*P. vivax*), or *Plasmodium malariae* (*P. malariae*).[2] *P. falciparum* is the most common of the plasmodium species and, in 2004, was one of the highest causes of death world-wide from a single infectious agent.[3] Recent statistics indicate that there are 3.3 billion people in the world at risk from malaria, 247 million reported cases of the disease annually and the disease is estimated to cause almost a million deaths each year. Of these deaths, 91% occur in Africa – 85% in children under the age of five.[3,4] As illustrated in Figure 1, there are 109 countries in which malaria is endemic, 45 of which are in Africa.[3] In the 1970's, Africa accounted for only half of the world's malaria burden, whereas currently, about 90% of the world's cases occur in sub-Saharan Africa.[3] In sharp contrast to these statistics, according to Casman and Dowlatabadi, only 10% of international funding assigned to fighting malaria is spent in this region.[5]

There is a significant correlation between malaria endemic regions and lack of development, the disease being generally most severe amongst people living in poor socio-economic circumstances. This results in a vicious cycle in which the prevalence of malaria interferes with the survival and education of children and the productivity of the working population as well as straining the resources of governments.[4]
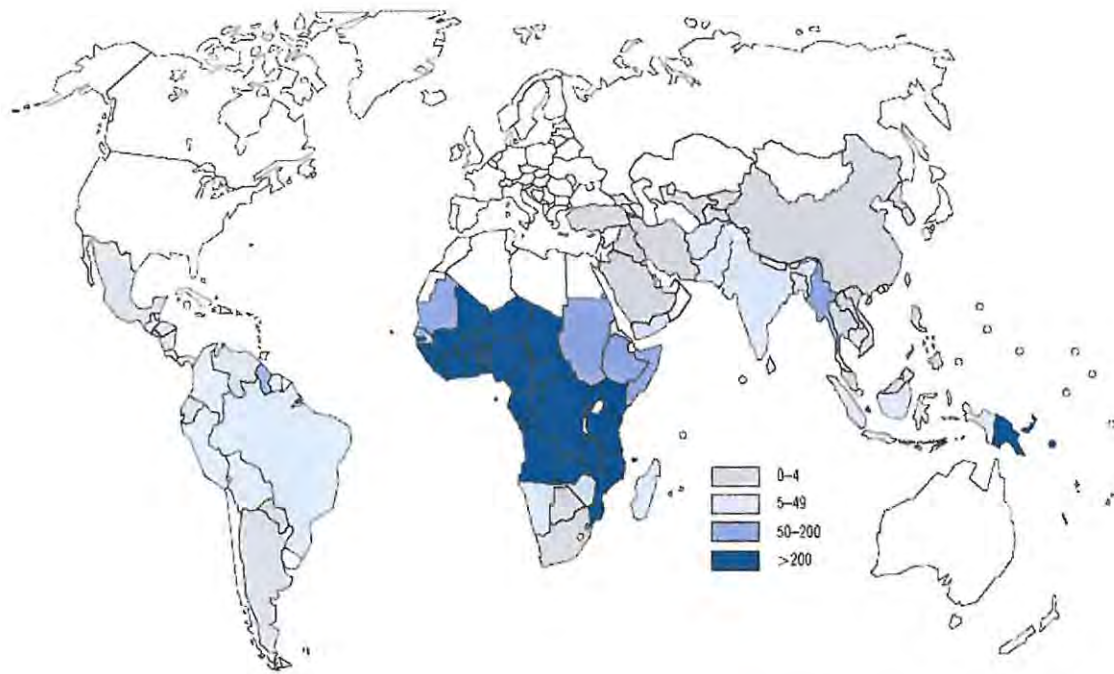
1

Figure 1. Estimated world-wide incidence of malaria per 1000 population, 2006.[3](Reproduced with permission from the World Health Organisation.)

In addition to many localised efforts, the World Health Organisation (WHO) has made efforts to control and eradicate malaria world-wide with a combination of preventative measures including:- long-lasting insecticidal nets; indoor spraying of insecticides; artemisinin-based combination therapy; and intermittent preventive treatment in pregnancy.[3] Apart from a small number of countries which have significantly decreased their malaria burden, the majority operate far below the targets set for the different prevention and control measures. These targets are based on the Millennium Development Goals which include the aim that "by 2015,... malaria is no longer a major cause of mortality and no longer a barrier to social and economic development and growth anywhere in the world."[6] Since its inception in 1998, the "Roll Back Malaria" campaign has taken on this task, aiming to reduce malaria mortality by 50% by 2010 and 75% by 2015.[4] Litsios, however, concludes that the approaches used thus far to control malaria need to be re-assessed, as the public health systems currently in place are incapable of effecting the required response; he calls for an "educated response", "community collaboration" and "the attention of the entire scientific community."[5]

Many factors such as poverty, population growth and movement, social unrest, government instability and climate change, need to be taken into account when considering malaria and its potential spread or elimination.[5] Some of the most successful malaria control programmes have been based on dichlorodiphenyltrichloroethane (DDT) spraying and there is much debate

2

as to whether the insecticide's ill-famed environmental effects outweigh its effectiveness in controlling malaria.[5] Many regions of the world, particularly Central and South America, Asia and countries of the former Soviet Union achieved significant reductions in malaria in the 1980's but have since slackened their malaria control programmes and experienced a re-emergence of the disease, in some cases with the additional problem of drug-resistant strains.[5] Parasite resistance to the current antimalarial drugs is particularly severe in the Indochinese peninsula.[4] Although there is little information on the interactions between malaria and the Human Immunodeficiency Virus (HIV), some data suggests that HIV-infected people are more likely to suffer from severe malaria.[2]

Attempts to combat malaria have been hampered to some extent by a lack of economic incentive for pharmaceutical companies to research and develop new antimalarial drugs. As Milhous and Kyle express so succinctly, "From a commercial perspective, it makes little sense to turn out costly pharmaceuticals for people who cannot afford shoes."[7] In response to this, the World Bank and the International Federation of Pharmaceutical Manufacturers Associations have established the Medicines for Malaria Venture which aims to discover, develop and register affordable new drugs.[8] As resistance to current drugs increases, scientists and health authorities are increasingly realising that a continued effort applied to the discovery of new classes of antimalarial drugs is vital in order to have new drugs at hand when resistance to the current drugs develops.[8] Although some success, and even eradication, in some areas has been achieved with the current tools, it is important that these successes do not lead to complacency. New tools for control and new drugs for the treatment of malaria are necessary if such achievements are to be sustained and extended.[4]

1.1.2. The life cycle of the malaria parasite

Despite its small size, the complex biology and life cycle of the malaria parasite, as shown in Figure 2, make it a particularly difficult organism to target in drug development. In addition, the parasite lives within the host cells, out of reach of the immune system, and changes the expression of its genes continually to exploit the different environments it experiences in different host cells.[9] The mechanisms of invasion of host cells, gene expression and signalling pathways are poorly understood but potentially provide many targets for the development of drugs and vaccines.[10]
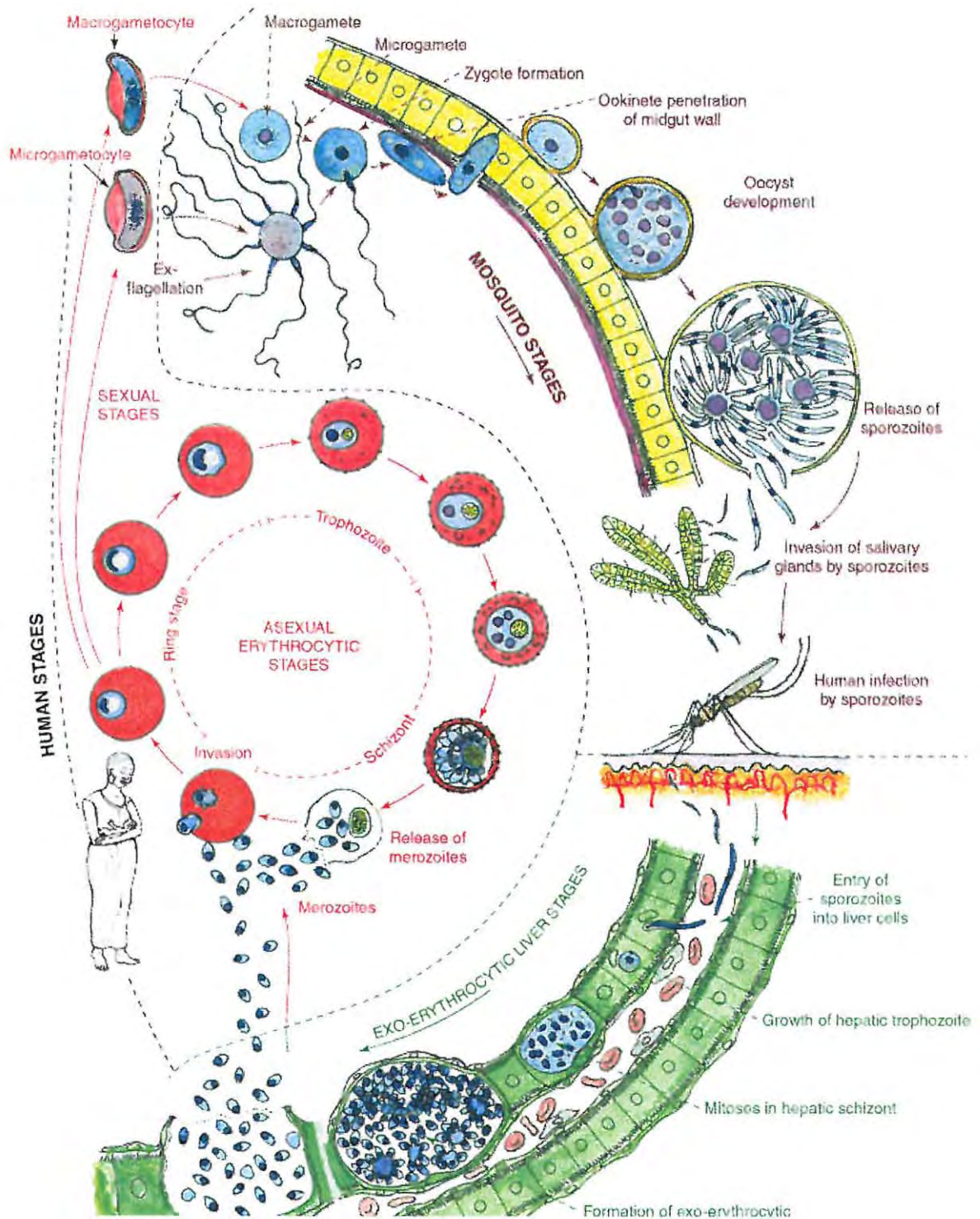
Figure 2. Life cycle of the malaria parasite showing stages in the human and the mosquito.[9](Reproduced with permission.)

When an infected female anopheles mosquito bites a human, it releases sporozoites from its salivary glands into the blood of the human host. The sporozoites invade liver cells (hepatocytes) where they grow and divide for 6 – 15 days (the pre-erythrocytic stage). At the end of this stage, thousands of merozoites are released into the bloodstream where they

attach to and invade red blood cells.[11] This is the part of the life cycle on which most attention has been focused for the development of potential vaccines against malaria.[12]

In the red blood cells, the plasmodium undergoes the asexual erythrocytic stages of its life cycle, the stage targeted by most antimalarial drugs.[9] The parasite forms a thin biconcave disc in a sac known as the parasitophorous vacuole. Here it feeds on haemoglobin and sequesters nutrients from the plasma. The product of haemoglobin digestion crystallises out as a dark pigment called haemozoin. The merozoites excrete proteins which modify the red blood cell membrane so that it sticks to the lining of the blood vessels, thus minimising the transport and destruction of infected red blood cells by the liver and spleen. The merozoites grow into trophozoites which are the most active in feeding and red blood cell modification.[9] The trophozoites mature into schizonts and the nucleus of each schizont divides, resulting in about 16 nuclei which form into merozoite buds. The red blood cell then bursts, releasing the small, egg-shaped, merozoites. The free merozoites then adhere to and invade new red blood cells, forming a new parasitophorous vacuole.[9] This 48 − 72 hour cycle is responsible for the recurring fevers and chills which are the most well known clinical symptoms of malaria.[10,11]

Some merozoites eventually differentiate into sexual forms (gametocytes), an important step in the life cycle which provides an intriguing target for arresting parasite development.[13] If the gametocytes are taken up by another female mosquito in a blood meal, they mature into male and female gametes and fertilisation occurs, forming a zygote which matures into an ookinete. This ookinete is motile and burrows into the mid-gut wall of the mosquito to form an oocyst.[11,13] The ookinetes divide mitotically, filling the oocycsts with sporozoites. When the oocyst bursts, the sporozoites migrate to the salivary glands from which they may be injected into a new human host.[11] The cycle in the mosquito takes approximately 7 − 18 days and involves six different forms of the plasmodium, a factor which complicates the potential control of the parasite in the mosquito vector.[13]

1.1.3. Current antimalarial drugs: targets and resistance

Attempts to make a malaria vaccine date back as far as 1912 but have thus far been unsuccessful, due mostly to the complex nature and life cycle of the parasite.[8] Each stage of the life cycle produces a different immune response, generally weak and poorly understood. There have, however, been some promising new developments, involving deoxyribonucleic acid (DNA) vaccines and synthetic and recombinant antigen production, which are in clinical trials.[14,15,8] Milhous and Kyle, however, have advised that "we should not dilute the search for new drugs with overly optimistic expectations for a vaccine."[7]

The current antimalarial drugs mostly target the asexual erythrocytic stages of the parasite life cycle and are classified into four main families, *viz.*, the antifolates, the hydroxynapthoquinones, the quinolines and artemisinin derivatives.[7] The structures of a selection of the current antimalarials are shown in Figure 3.
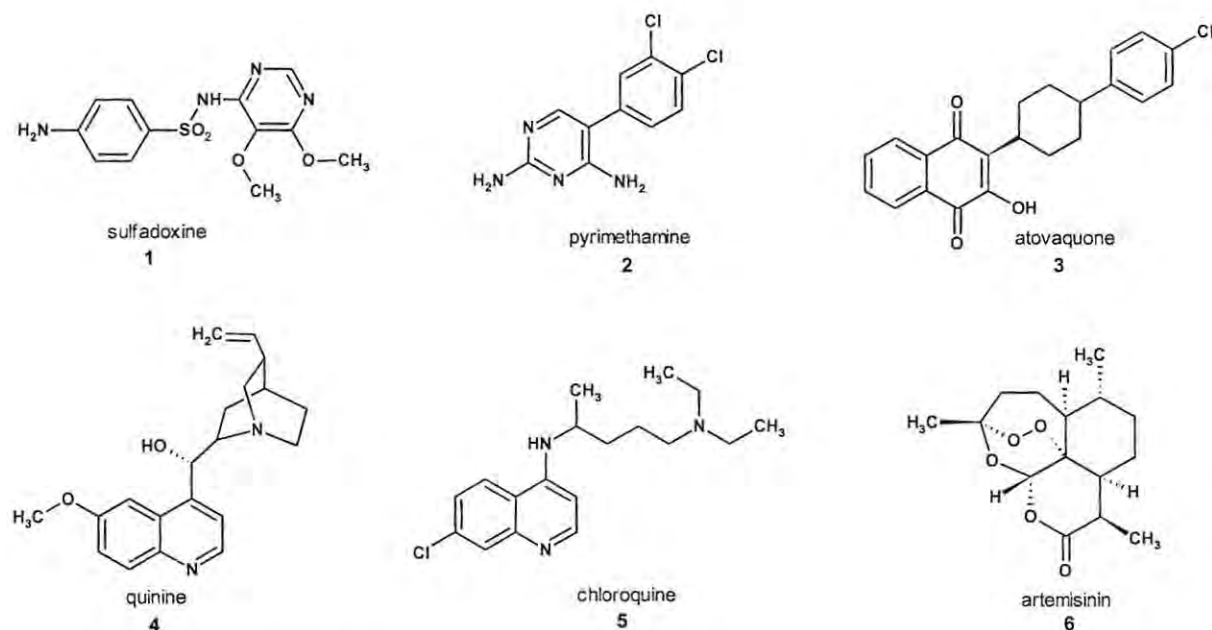
Figure 3. Structures of some current antimalarial drugs showing examples from each of the four main classes.[1]

The **antifolates** (sulfadoxine **1**, pyrimethamine **2**, cycloguanil, trimethoprim, chlorproguanil and the sulfonamides) target the plasmodial enzymes dihydrofolate reductase (DHFR) and dihydropteroate synthase (DHPS) which form part of the folate biosynthetic pathway.[7,16] The sulfa drugs, such as sulfadoxine **1**, inhibit DHPS and are *p*-aminobenzoic acid analogues which act as antagonists.[16] They are also widely used as antibacterial agents.[16] Pyrimethamine **2** and sulfadoxine **1** (Fansidar) act synergistically and are particularly effective in combination as they target both DHFR and DHPS in the folate biosynthetic pathway, decreasing purine and pyrimidine synthesis and thereby inhibiting the synthesis of DNA. Generally, resistance to DHFR and DHPS inhibitors in malaria parasites is due to point mutations in the target enzymes. Some parasites, however, achieve partial resistance simply by expressing more of the relevant enzyme and thus increasing the ratio of enzyme to inhibitor.[16] When designing new drugs in this class of antimalarials, consideration needs to be given to their potential effectiveness against current drug-resistant strains and the possible inclusion of features to counter the parasite's ability to adapt.[16]

6

Atovaquone **3** belongs to the class of **hydroxynapthoquinones** which inhibit mitochondrial respiration by disrupting electron transport in the parasite.[7] Atovaquone is often combined with proguanil in the drug Malarone.[8] Resistance to atovaquone, used alone, arises quite rapidly and has been attributed to mutations in the cytochrome *b* gene.[17]

The most well-known member of the **quinoline** class of antimalarials is quinine **4**, the oldest antimalarial drug in Western medicine, and still widely used as a last recourse for severe malaria.[18] Quinine, a 4-aminoquinoline derivative, is a natural-product drug, extracted from the bark of cinchona trees native to South America. The active ingredient, quinine, was isolated in 1820 and is thought to act by interfering with the formation of haemozoin, the malarial pigment, from haeme. Resistance to quinine has arisen in several scattered regions around the world but the mechanism of the resistance is not fully known, although mutations in the *pfcrt* gene are thought to be involved.[18,19] Resistance to quinine is not wide-spread in sub-Saharan Africa and this compound still finds use as a fast-acting and effective antimalarial drug.[2] Chloroquine **5**, a 4-aminoquinoline derivative, has been a widely-used and very valuable antimalarial because it is:- active against all four plasmodial species which infect humans; safe for pregnant women and children; and inexpensive.[20] Chloroquine is thought to act by interfering with the function of the parasite food vacuole, possibly preventing the detoxification of haeme (in a similar manner to quinine), inhibiting haemoglobin protease activity or raising the pH of the vacuole.[20] The wide-spread use of chloroquine as an antimalarial drug has been very successful in reducing the malaria burden in some areas but the emergence of resistance has curtailed its effectiveness world-wide.[20] Resistance to chloroquine was first noticed in the 1960's and has been partly attributed to population migration, poor health services and improper use of antimalarial drugs.[4] The mechanism of resistance to chloroquine has not been fully determined but it has been found that the accumulation of chloroquine in the food vacuoles of resistant parasites is far less than in susceptible parasites.[7] Chloroquine resistance-reversers, which would be co-administered with chloroquine to restore its effectiveness, are being investigated.[7] Studies on the design of new aminoquinolines have given rise to compounds which show some promising action against chloroquine-resistant parasites.[20]

Artemisinin **6** is the active principle in the extract of the sweet wormwood tree, *Artemisia annua*, and has been used as a herbal medicine in China for over 2000 years.[18] The mechanism of action has been suggested to involve iron-dependent free-radical generation.[7] The endo-peroxide bridge in the structure of artemisinin has been found to be crucial for its activity and

is thought to interact with the iron in haeme resulting in the formation of the free radicals.[18] Artemisinin is usually used in combination with other drugs as recrudescence is common due to the drug's short half-life when it is used alone, especially for short periods.[2,7] Since there is a potential problem with neurotoxicity caused by artemisinin, derivatives, such as synthetic trioxanes and tetraoxanes, are being explored.[7] Although resistance to artemisinin is not wide-spread, there have been reports of reduced efficacy of the drug in some areas.[21] An additional drawback of this drug is that the cost per treatment is prohibitively high for most people in sub-Saharan Africa.[8,18]

In addition to the above four classes, some antibiotics such as tetracyclines and macrolide antibiotics are effective antimalarials and these compounds are thought to act by inhibiting protein synthesis in the mitochondrion or the plastid.[17] Knowledge of the mechanisms of resistance to the current drugs can aid in the design of new drugs in addition to seeking to target parasite-specific pathways in rational drug design,[7] particularly as the emergence of resistance has been recorded for all the current antimalarial drugs.[22] Several routes to new drug discovery are being pursued in attempts to counter the emergence of resistance. These include:- natural product screening; investigating traditional medicine leads; structure-based drug design and molecular modelling; and molecular biology techniques to identify potential targets.[7]

1.2. New targets for antimalarial drugs based on the non-mevalonate pathway

1.2.1. The non-mevalonate pathway for isoprenoid biosynthesis

Isoprenoids are found in all living organisms and carry out a wide variety of functions.[23] Some isoprenoids are essential metabolites, such as sterols involved in membrane stabilisation, quinones in the electron transport chain and carotenoids involved in photosynthesis; others are used in the synthesis of secondary metabolites.[24] The mevalonate pathway for the synthesis of isoprenoids is well known and has been extensively studied for over 50 years.[25] This pathway involves condensation of three molecules of acetyl coenzyme A to form 3-hydroxy-3-methylglutaryl coenzyme A, which is then converted, *via* mevalonate, to isopentenyl pyrophosphate (IPP).[26] IPP and its isomer, dimethylallyl pyrophosphate (DMAPP), form the universal building blocks for isoprenoids.[27] In 1993 it was discovered that an alternative pathway for the synthesis of isoprenoids exists and this was termed the non-mevalonate or DOXP/MEP pathway, shown in Figure 4.[25] Rohmer and co-workers established that pyruvate **7** and glyceraldehyde-3-phosphate **8** are the precursors which combine to form

1-deoxy-D-xylulose-5-phosphate (DOXP) **9**, a reaction catalysed by DOXP synthase.[25,28] An intramolecular rearrangement and reduction is then effected by DOXP reductoisomerase (DXR) to convert DOXP to 2-C-methyl-D-erythritol-4-phosphate (MEP) **10**[28] – a transformation found to require nicotinamide adenine dinucleotide phosphate (NADPH) and a cofactor:- Mn^{2+}; Mg^{2+}; or Co^{2+}. The intermediate aldose phosphate is produced between the isomerisation and reduction steps.[24] In the third step, MEP is linked to cytidine triphosphate (CTP) to form compound **11**, and phosphorylation of the 2-hydroxy group of MEP in an adenosine triphosphate (ATP)-dependent reaction yields compound **12**.[28] This is followed by cyclisation to 2-C-methyl-D-erythritol-2,4-cyclodiphosphate **13** and intramolecular elimination of the diphosphate. The final conversion to IPP **14** is achieved by two reduction and two dehydration steps.[28]

The DOXP/MEP pathway contains promising potential target enzymes for drug development because it is used in several pathogenic species of bacteria and protozoa but not in humans.[29] In addition to being present in species of both Gram-positive and Gram-negative bacteria, the DOXP/MEP pathway is also found in many eukaryotes such as algae and higher plants.[24,29] In higher plants, the mevalonate pathway is utilised in the cytoplasm for the synthesis of sterols whilst the non-mevalonate pathway is utilised in the chloroplasts for the synthesis of photosynthesis-related isoprenoids.[23] Attention has been focused on the development of inhibitors for DOXP/MEP pathway enzymes in pathogenic species such as *Helicobacter pylori* *(H. pylori)*, *Mycobacterium tuberculosis* *(M. tuberculosis)*, *Escherichia coli* *(E. coli)* and, most importantly in the present context, *P. falciparum*.[29]
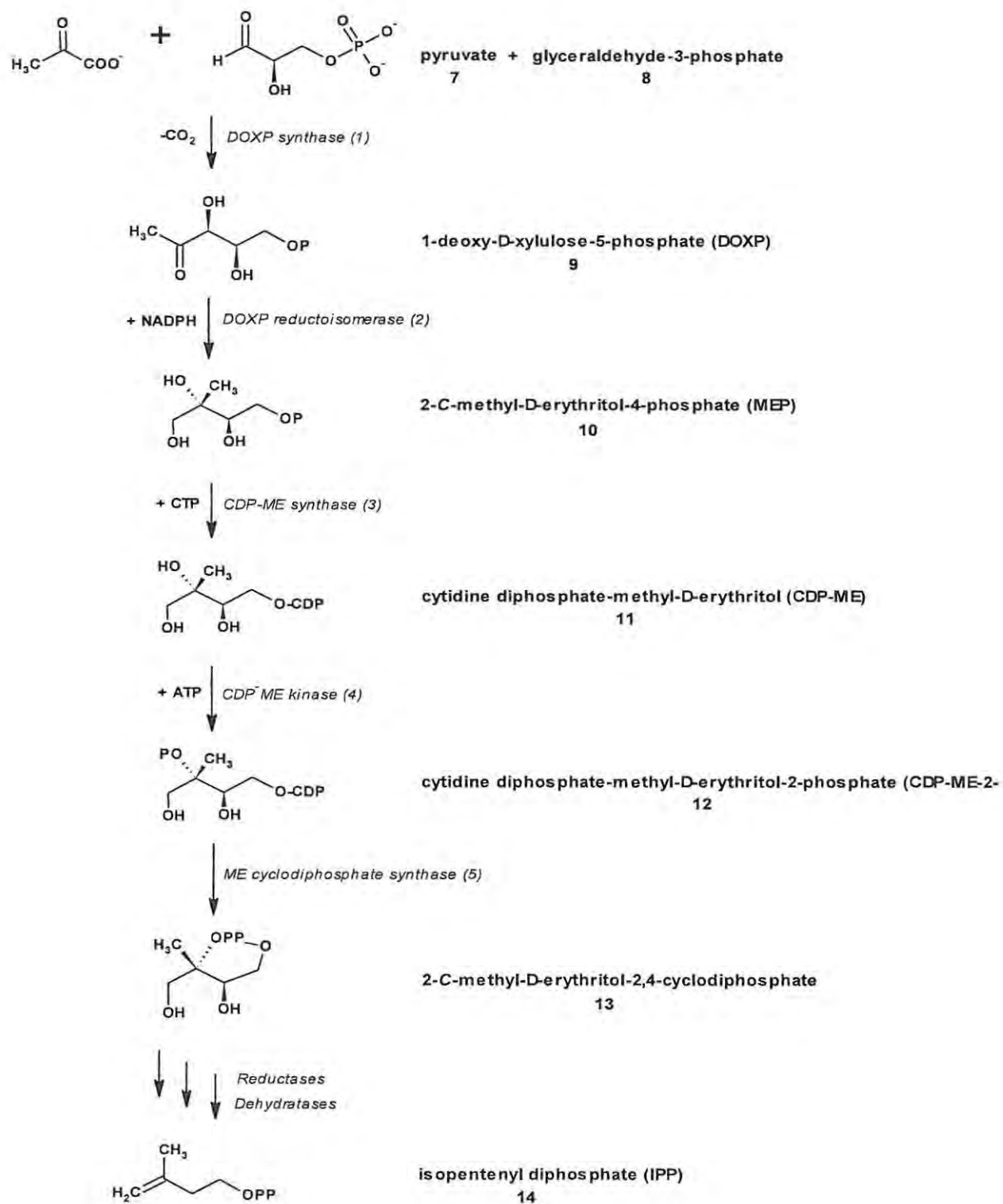
Figure 4. DOXP/MEP pathway showing the enzymes involved.[28]

Structures and labels within the figure:

pyruvate + glyceraldehyde-3-phosphate
7   8

$-CO_2$ DOXP synthase (1)

1-deoxy-D-xylulose-5-phosphate (DOXP)
9

+ NADPH   DOXP reductoisomerase (2)

2-C-methyl-D-erythritol-4-phosphate (MEP)
10

+ CTP   CDP-ME synthase (3)

cytidine diphosphate-methyl-D-erythritol (CDP-ME)
11

+ ATP   CDP-ME kinase (4)

cytidine diphosphate-methyl-D-erythritol-2-phosphate (CDP-ME-2-
12

ME cyclodiphosphate synthase (5)

2-C-methyl-D-erythritol-2,4-cyclodiphosphate
13

Reductases
Dehydratases

isopentenyl diphosphate (IPP)
14

10

1.2.2. Mechanism of the 1-deoxy-D-xylulose-5-phosphate reductoisomerase (DXR) catalysed conversion of 1-deoxy-D-xylulose-5-phosphate (DOXP) to 2-C-methyl-D-erythritol-4-phosphate (MEP)

The DXR-catalysed conversion of DOXP to MEP has been shown to proceed *via* the intermediate 2-C-methylerythrose-4-phosphate **15** but there has been no conclusive evidence for the detailed mechanism by which the reaction occurs.[30] In the first proposed mechanism, a retro-aldol/aldol rearrangement, the 4-hydroxyl group of DOXP **9** is oxidised and the C(3)–C(4) bond cleaved in a retro-aldol process to give the enol/enolate of hydroxyacetone and glycoaldehyde phosphate, as shown in Figure 5a;[30,31] an aldol reaction between these two intermediates then gives 2-C-methylerythrose-4-phosphate **15**.[30,31] The second proposed mechanism parallels the ketol acid reductoisomerase pathway and involves an α-ketol rearrangement, as shown in Figure 5b.[32] In this mechanism, the 3-hydroxyl group of DOXP is deprotonated and oxidised to a carbonyl group, followed by migration of C-4 to C-2 to give the common aldehyde intermediate **15**.[30,31] Argyrou and Blanchard mention a third possibility involving a 1,2-hydride shift followed by a 1,2-methyl shift, as shown in Figure 5c, but this mechanism was not supported by the results of NMR experiments using ^{13}C-labelled material.[30]

The 2-C-methylerythrose-4-phosphate intermediate **15** formed by one (or more) of the above mechanisms is then reduced by NADPH, converting the aldehyde moiety to a primary alcohol.[30] The stereochemistry of the product **10** is determined by preferential migration of the C-4 moiety to the *re*-face at C-2; this is then followed by *re*-face attack of NADPH on the intermediate, as shown in Figure 6. The pro-S-hydrogen at C-1 of MEP is derived from the C-3 hydrogen of DOXP, whilst the pro-R-hydrogen at C-1 originates from the 4-S-hydrogen of NADPH in the subsequent reduction step.[33-36]

11

a) retro-aldol/aldol rearrangement

b) α-ketol rearrangement

2-C-methylerythrose-4-phosphate
15

MEP
10
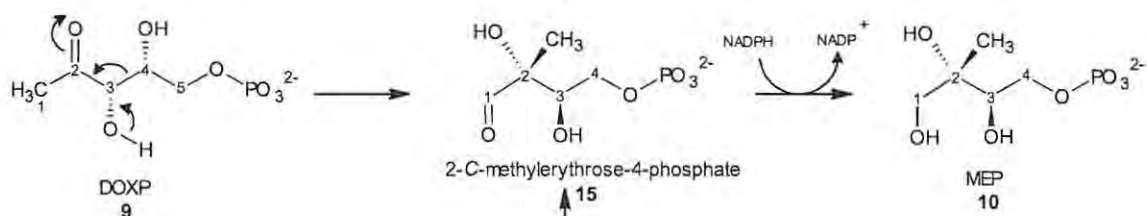
c) 1,2-hydride shift

Figure 5. Three possible mechanisms for the conversion of DOXP **9** to 2-C-methylerythrose-4-phosphate **10**:- a) retro-aldol/aldol rearrangement; b) α-ketol rearrangement; c) 1,2-hydride shift.[30,31]
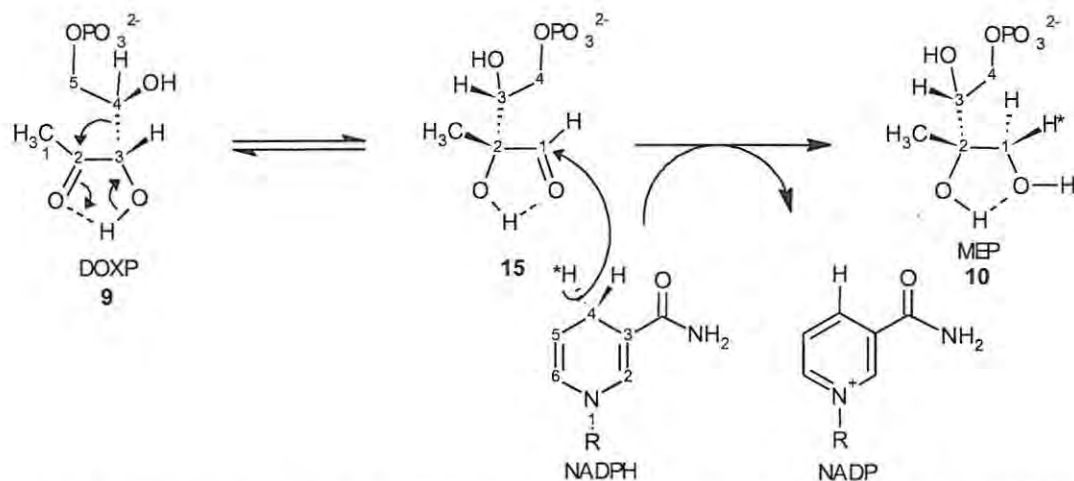
Figure 6. Stereochemical aspects of the DXR reaction *via* the α-ketol pathway (Fig. 5b). Attack of C-4 on C-2 from the back (*re*-face attack on the DOXP C-2 carbonyl) followed by attack of NADPH pro-*S* hydrogen (marked with *) from the front (*re*-face attack on the C-1 carbonyl of the intermediate **15**).[34,35]

12

Hoeffler *et al.* (2002) attempted to verify the existence of the α-ketol rearrangement mechanism of the isomerisation step by synthesising DOXP analogues lacking the 3- or 4-hydroxyl group (**16** and **17**, respectively; Figure 7). The first step of this mechanism involves deprotonation of the 3-hydroxyl group, and would result in the formation of the MEP analogue **18** if the 3-hydroxy compound **16** were used as the substrate. If the 4-hydroxy isomer **17** were used as the substrate, the α-ketol rearrangement mechanism would not be possible. When these analogues were tested as substrates for DXR, however, it was found that both compounds **16** and **17** failed to act as substrates for DXR, as NADPH was not oxidised, but did reversibly inhibit the enzyme.[37] Although these experiments were unable to prove the α-ketol rearrangement, they did establish the importance of both the 3- and 4-hydroxy groups in the enzyme substrate. A further experiment was undertaken using C-1 ^{13}C-labelled DOXP, but formation of ^{13}C-labelled hydroxyacetone, which would be produced by the retro-aldol/aldol mechanism, could not be confirmed.[37] Moreover, the two putative intermediates, hydroxyacetone and glycoaldehyde phosphate, were not recognised by DXR and the experiments proved inconclusive. [37]
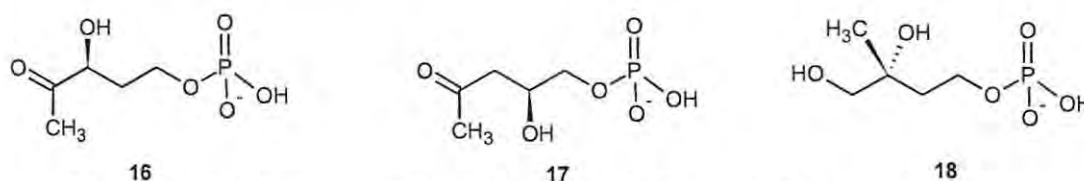

Figure 7. Structures of DOXP analogues **16** and **17** and the MEP analogue **18**.[37]

1.2.3. Discovery of fosmidomycin and its potential as a DXR inhibitor

The natural product fosmidomycin **19**, shown in Figure 8, was isolated from *Streptomyces lavendulae* in the 1970's and found to have antibiotic and herbicidal properties.[28,29,38,39] Once the DOXP/MEP pathway was known, Kuzuyama *et al.* investigated the effect of fosmidomycin on bacteria with and without this pathway and established that fosmidomycin is an inhibitor of the DOXP/MEP pathway.[40] Shortly afterwards, it was found that fosmidomycin inhibits DXR in a dose-dependent manner, as does its acetyl derivative FR900098 **20**.[38,41] The antimalarial properties of these two compounds were reported by Jomaa *et al.* who found that these compounds showed low toxicity and were able to clear mice of the rodent malaria parasite *Plasmodium vinckei*.[41] In humans, fosmidomycin was shown to be effective as a treatment for uncomplicated *P. falciparum* malaria but a high rate of recrudescence was observed with short treatment courses.[29,38] Additional disadvantages encountered in the use of fosmidomycin are its very short half-life in the blood and its low lipophilicity which leads to poor absorption in

the gut and difficulty in crossing phospholipid membranes.[38] As a result, combination therapies with other antimalarials have been investigated and the combination of fosmidomycin with clindamycin has shown a synergistic effect.[29] The high levels of DXR inhibition by fosmidomycin and FR900098, however, make these compounds particularly promising lead compounds which may be modified to produce effective antimalarial drugs.[38]
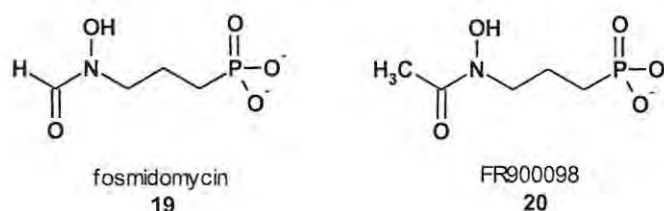

Figure 8. Structures of the lead compounds fosmidomycin 19 and FR900098 20.

1.3. Properties and structural features of 1-deoxy-D-xylulose-5-phosphate reductoisomerase (DXR)

1.3.1. Kinetic properties of DXR

The enzyme DXR is found in the apicoplast of malaria plasmodia.[41] The apicoplast is a non-photosynthetic, plastid-like organelle, found at the anterior end of the cell. It is thought to be involved in penetrating host tissues although its metabolic function has still not been fully determined.[8,41,42,43] Secondary endosymbiosis of an alga is thought to have been the origin of this organelle's presence in the phylum Apicomplexa.[41,43] The apicoplast is an organelle not present in human cells and therefore the DXR enzyme presents a promising drug target, especially as it is essential for the survival of the parasite.

The characterisation of DXR has been well summarised by Proteau in terms of its cofactor requirements, mechanism and kinetic parameters.[34] Some of the first investigations into the nature of EcDXR were carried out by Takahashi et al. in 1998.[44] These studies revealed that NADPH is used as the coenzyme rather than nicotinamide adenine dinucleotide (NADH) and the optimum pH was proposed to lie between 7.5 and 8.0.[44] Kuzuyama et al., however, found the optimum pH to be between pH 7.0 and 8.5 (greater than 75% of maximum activity) and maximum activity was obtained between 40 and 60 °C, although the enzyme was not heat stable above 50 °C.[45] Studies on the metal cation revealed that one of the cations Mn^{2+}, Co^{2+} or Mg^{2+} is required; no activity was detected in the presence of Ca^{2+}, Ni^{2+}, Zn^{2+}, Cu^{2+}, Fe^{2+} or ethylenediaminetetraacetic acid (EDTA).[44] The enzyme has a half-life of approximately 3 days at 4 °C but retains almost all of its activity for a year when stored at -20 °C in 50% glycerol.[30]

14

When stored at 4 °C in 100 mM Tris-HCl buffer (pH 7.5), the enzyme was found to have retained 90% of its activity after one month.[45]

The Michaelis Constant, K_M, of an enzyme is defined as the substrate concentration at which the velocity of the reaction is half of its maximum value.[46] A small K_M value means that the enzyme achieves maximum catalytic efficiency at low substrate concentrations and hence K_M can also be used as a measure of the affinity of an enzyme for its substrate.[46] The catalytic constant or turnover number of an enzyme, k_{cat}, is the ratio of the maximal velocity to the total enzyme concentration and indicates the number of reaction processes each active site catalyses per unit time.[46] The catalytic efficiency of an enzyme is measured by the quantity k_{cat}/K_M, the apparent second-order rate constant of the enzymatic reaction.[46] Argyrou and Blanchard point out that, due to the presence of inactive enzyme which contributes to the protein concentration, experimental k_{cat} and k_{cat}/K_M values must be regarded as lower limits.[30]

The kinetic parameters for DXR from several organisms have been investigated by a number of authors. Argyrou and Blanchard carried out experiments to determine the k_{cat}, K_M and k_{cat}/K_M values of *M.tuberculosis* DXR (*Mt*DXR) for each of the metal cofactors (Mn^{2+}, Mg^{2+} and Co^{2+}) for both the forward and reverse reactions. The reciprocal plots showed lines intersecting left of the *y*-axis and above the *x*-axis, suggesting a sequential mechanism.[30] Studies of the pH dependence of the kinetic parameters indicated the presence of two deprotonated groups (with pK_a values of *ca.* 7.4) which are predicted to bind to the metal cation.[30] Mac Sweeney *et al.*[47] determined the K_M values of *Ec*DXR for the three metal cofactors (Mn^{2+}, Mg^{2+} and Co^{2+}) at pH values of 7.8 and 6.0 and found them to be similar to those of *Mt*DXR for Mn^{2+} and Co^{2+}; the K_M for Mg^{2+} was higher than that for the other two metals but lower than that determined for *Mt*DXR or *Synechocysitis* DXR. For both *Mt*DXR and *Ec*DXR, the K_M increased as the pH decreased and this was attributed to protonation at low pH of the carboxylate-containing residues binding to the metal ion, resulting in a decreased metal affinity.[47] Kuzuyama *et al.* also determined the kinetic parameters of *Ec*DXR for each of the metal cofactors and concluded that the enzyme activity depends significantly on the *in vivo* concentration of each cation.[45]

1.3.2. Crystal structures of DXR

There are several crystal structures of DXR available in the Protein Data Bank (PDB; E.C. 1.1.1.267), from *E.coil*, *Z.mobilis* and *M.tuberculosis* but none as yet for DXR from *P. falciparum*.[48] The crystal structure of *E. coli* DXR (*Ec*DXR) obtained by Mac Sweeney *et al.*[47] verified previous proposals[36,49] that DXR exists as a 'V'-shaped, 86 kDa homodimer, comprising

three domains.[36,47] The large *N*-terminal domain (residues 1-150) contains the NADPH cofactor binding site and is comprised of a seven-stranded parallel β-sheet and seven α-helices, as shown in Figure 9.[47,50] The structure of this domain, however, needs to be accepted with caution as Hoeffler *et al.* point out that studies undertaken on histamine-tagged proteins must take into account the potential interference of the His-tag with cofactor binding.[37] A connective region made up of residues 150-285 includes most of the active site as well as a flexible 'lid' (residues 206-216), which closes over the substrate or inhibitor and excludes solvent from the active site.[36,47] The *C*-terminal domain (residues 312-398) is thought to play a structural role in supporting the active site and is made up of a four-helix bundle.[36,47] In the model of *P. falciparum* DXR (*Pf*DXR) published by Goble *et al.*, the corresponding domains were found to be residues 1-160 for the *N*-terminal domain, residues 161-340 for the connective domain and residues 341-417 for the *C*-terminal domain.[51] The overall structure, as well as the orientations of the catalytic residues in *Pf*DXR, was found to be similar to that of *Ec*DXR.[51]
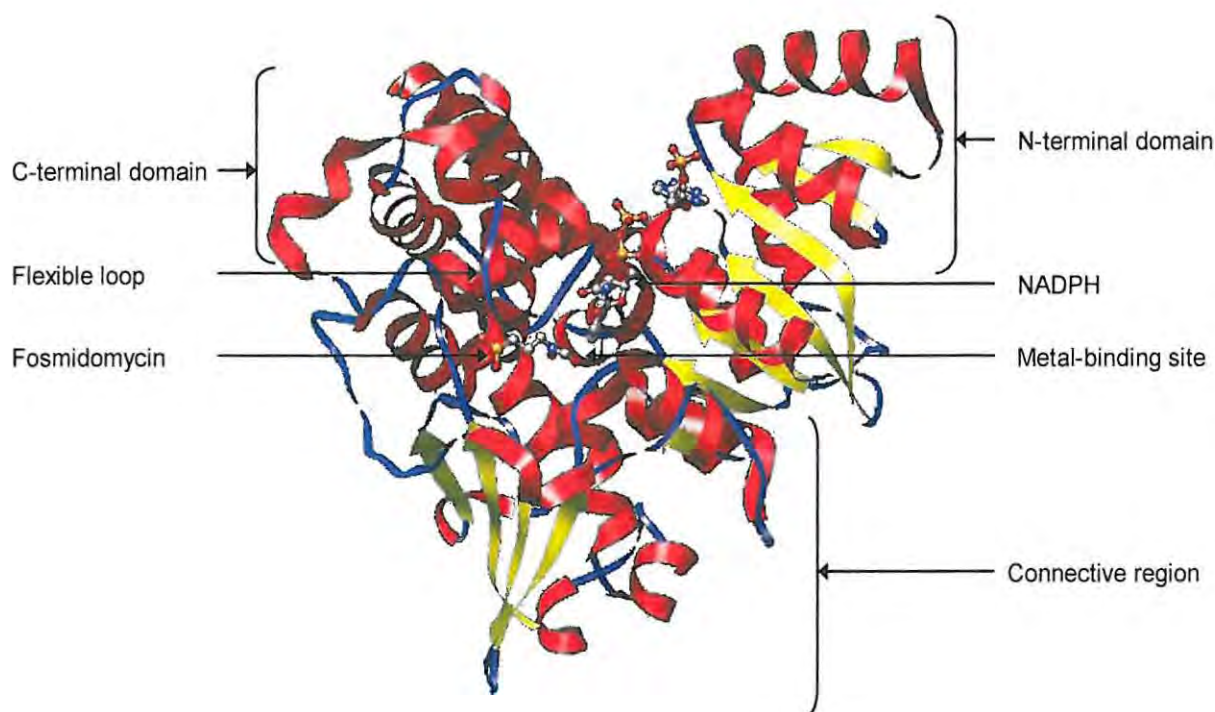
Figure 9. Diagram of *Ec*DXR showing secondary structure. α-Helices are shown in red, β-sheets in yellow and turns in blue. Bound fosmidomycin **19** and NADPH are shown in ball-and-stick format, coloured by atom type. The diagram was created from PDB structure 1Q0L.[47]

The structure of the apo-enzyme (1ONN) revealed several different loop conformations, showing the flexibility of this region when no ligand or cofactor is bound.[36,52] In 2002, Yajima *et al.* produced the first crystal structure with NADPH bound and this structure (1JVS) showed a

more ordered loop region.[49] This structure contains a sulphate ion positioned in the region in which the phosphonate group of the substrate or inhibitor would bind.[49] The binding of the inhibitor was investigated by Steinbacher et al. who published an EcDXR crystal structure containing fosmidomycin and Mn^{2+} in the active site and identified the metal-coordinating residues and ligand-binding interactions.[36] Although the electron density observed for the loop region was more ordered in this structure than that of the apo-enzyme, it was still partly disordered and the NADPH-binding site was blocked by the C-terminal region of a neighbouring molecule.[36] Two structures obtained for the enzyme from Z. Mobilis (ZmDXR); (1ROK and 1ROL) were very similar in overall structure and active-site architecture to that of EcDXR except for some differences in the interactions with the adenine ring of NADPH.[50,52] Yajima et al. published EcDXR structures (1T1S and 1T1R) with bisphosphonate inhibitors which bound differently to fosmidomycin, with the bisphosphonate moiety displacing the metal ion.[49] The tight-binding structure of EcDXR with fosmidomycin and NADPH (1Q0L) and the DOXP-NADPH-DXR ternary structure (1Q0Q) released by Mac Sweeney et al. revealed the interactions of the active-site residues with the inhibitor and the substrate and also showed a fully ordered loop region interacting with the ligand in a closed conformation.[47,50] Unfortunately, the crystals were obtained at pH 5.0 at which value the metal binding is very weak and DXR is not catalytically active.[47] Silber et al. have suggested that the interactions identified from this structure are likely to be different to those taking place in vivo because of different protonation states of the active-site residues.[34,52] Several structures of MtDXR with different combinations of cofactors and inhibitors published by Henriksson et al. show the active-site residues and reveal certain differences between MtDXR and EcDXR, especially relating to the metal coordination.[33] Instead of regarding crystallography as a static picture, these authors aimed to use the binding of different substrates and cofactors to reveal some of the dynamic properties of the enzyme.[33]

The quaternary complex of EcDXR with fosmidomycin, NADPH and Mg^{2+} (2EGH) obtained by Yajima et al. in 2007 revealed that the electron density data for the loop region could be resolved and that interactions of the loop with the inhibitor could be observed.[53] Comparison of the quaternary complex with that of a structure lacking NADPH revealed small differences, which suggested that DXR is structurally flexible and that both cofactors are needed for correct positioning of the substrate in the active site.[53] However, the only metal ion to be successfully incorporated into the crystal structure was Mg^{2+}, despite the authors' attempts to obtain crystals with Mn^{2+} and Co^{2+} as cofactors.[53]

In the absence of a reported crystal structure of *Pf*DXR, a 3-D model of *Pf*DXR was built by Singh *et al.*, using comparative protein modelling techniques, based on the crystal structures of *Ec*DXR (1Q0L) and *Zm*DXR (1R0L).[50] Comparison of this *Pf*DXR model with *Ec*DXR indicated that the overall structures and interactions with fosmidomycin are largely similar.[50] Verification of the model using docking studies, including the metal cofactor, showed good correlation between the docking scores and the IC_{50} values and indicated substrate-like binding of inhibitors and common binding modes.[50] Unfortunately, since this model was not publically available, another homology model of *Pf*DXR has been developed by Goble *et al.*, which incorporates the results of further docking studies and more recent inhibition studies on *Pf*DXR.[51,54] Comparison of this *Pf*DXR model with the *Ec*DXR crystal structure 1Q0L revealed largely similar structures, corresponding regions in the Ramachandron plots and similar catalytic residues.[51] Although the NADPH-binding residues appear to be largely the same in both *Ec*DXR and *Pf*DXR, some differences in the loop region were noted and it was predicted that the loop is likely to change conformation significantly on binding of the inhibitor.[51]

1.3.3. Role and binding of the divalent metal cation

It is well established that DXR requires the presence of a divalent metal cation for its catalytic activity, and the position of the metal in the active site is reasonably well defined.[24] In the *Mt*DXR crystal structure,[33] a Mn^{2+} ion is present with an octahedral geometry involving coordination to three water molecules and the active-site residues Asp151, Glu153 and Glu222;[33] the corresponding residues in *Ec*DXR are Asp150 (D_{150}), Glu152 (E_{152}) , Glu231 (E_{231}).[36,47]
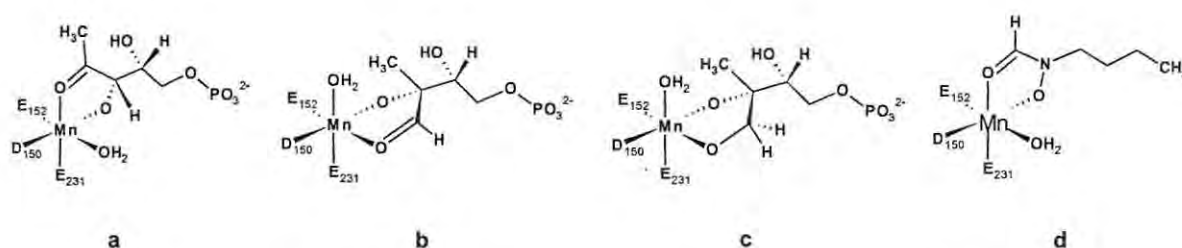
Figure 10. Binding of Mn^{2+} to active-site residues (in *E.coli*) and ligands:- a) DOXP **9**; b) 2-*C*-methylerythrose-4-phosphate **15**; c) MEP **10**; and d) fosmidomycin **19**.[36,47,53]

As shown in Figure 10, coordination of fosmidomycin **19** (d) to the metal cation (*via* axial and equatorial interactions) is considered to be the same as that exhibited by the substrate, DOXP **9** (a).[36,47] Steinbacher *et al.*, however, suggest that coordination of the intermediate **15** (b) and the product **10** (c) is diequatorial, stating that coordination of these compounds *trans* to Asp150 and Glu231 would lead to incorrect stereochemistry in the product.[36,47] Henriksson, on

18

the other hand, has proposed that the divalent metal cation (M^{2+}) serves as an anchor for the O-2 and O-3 atoms of the substrate, DOXP **9**, and that these remain coordinated during the rearrangement and become the O-1 and O-2 hydroxyl groups of MEP **10**.[33] Mac Sweeney, however, reported that the role of the M^{2+} in the isomerisation step is not known but that it is necessary for the subsequent reduction.[33,47] Comparison of *Mt*DXR structures in the presence and absence of the cofactors has indicated that the Mn^{2+} coordination is not greatly affected by the binding of NADPH.[33] The (*N*-formyl-*N*-hydroxy)amino group of fosmidomycin **19** and the metal-binding residues are thought to undergo slight conformational changes in order to coordinate to the metal,[33] but this has yet to be confirmed for *Ec*DXR as the only available structure containing both fosmidomycin and NADPH (1Q0L) fails to show binding of fosmidomycin to the metal.[47] The reason given for the absence of the metal is that the crystal was obtained at pH 5.0, at which value the metal-binding affinity of DXR is thought to be reduced.[47] At this pH, the conformations of the acidic residues expected to coordinate Mg^{2+} also do not adopt the required octahedral geometry as they are not protonated and are therefore expected to interact differently.[47,52] Magnesium (as Mg^{2+}) is thought to be the cofactor present *in vivo* as its intracellular concentration is similar to the k_{cat} value of the enzyme.[30,55] However, DXR can use Mn^{2+}, Co^{2+} or Mg^{2+} and the specificity of *Mt*DXR for the metal was found to follow the order:- $Co^{2+} > Mn^{2+} > Mg^{2+}$.[30] Hoeffler *et al.* found that a lower concentration of Mn^{2+} than Mg^{2+} gave maximum activity, and suggested that DXR has a higher affinity for Mn^{2+} than for Mg^{2+} although the intermediate, methylerythrose phosphate **15** was found to bind more efficiently to Mg^{2+} than Mn^{2+}.[37] According to Bock *et al.*, the ionic radius of Mn^{2+} (0.75 Å) is larger than that of Mg^{2+} (0.65 Å) and therefore Mn^{2+}, as the softer acid, prefers to bind to a site containing both nitrogen and oxygen donors, whereas Mg^{2+}, a harder acid, prefers oxygen donors alone – as in compound **15**.[56] For their docking studies using AutoDock, Silber *et al.* and other researchers have replaced Mn^{2+} in the binding site by Mg^{2+}. The justification given is that either metal can be utilised by active DXR, as the coordination chemistry of the two metals is very similar, but that Mg^{2+} is better parameterised for use with the docking programme.[52,57] The mechanism, however, is thought to be the same whichever metal is involved.[45]

Analysis of the crystal structure of *Ec*DXR (1Q0L) reveals a distorted octahedral coordination sphere around Mg^{2+} involving Glu152, Glu231, Asp150, Lys125 and the 2-carbonyl and 3-hydroxyl oxygens of DOXP.[47] Perruchon *et al.* have argued that, in order to inhibit the enzyme, the divalent cation must be complexed and that the hydroxamate group suits the metal-coordination sphere best.[52,57] This proposal has been supported by Giessmann *et al.* who

found that replacing the hydroxamate group in the inhibitor, fosmidomycin **19**, with other metal-coordinating groups led to a decrease in the inhibitory properties.[54] The pK_a of the fosmidomycin hydroxamate group is thought to be influenced by the coordinated metal ion resulting in deprotonation of the *N*-hydroxyl group and a planar arrangement of the hydroxamate group.[52,54] The hydroxamate moiety is also well oriented for coordination to the metal as the distances from the metal centre to each of the oxygen atoms are fairly similar (M···O(H)N: 2.1 Å; C=O···M: 2.4 Å).[52]

Argyrou and Blanchard have proposed that the divalent metal ion is involved in facilitating ionisation of the substrate hydroxyl group and stabilising the intermediate by electrostatic interactions with the coordinating hydroxyl groups;[30] when the loop region closes over the active site, the change in the dielectric conditions is thought to increase the strength of these interactions.[52] The pK_a values of the three carboxylate moieties of the coordinating active-site residues are higher than might otherwise be expected due, it is thought, to their proximity to each other. As a result, unless a suitable metal cation is present, these moieties are predominantly protonated at neutral pH.[30]

1.3.4. Ligand-binding residues of DXR

The active-site residues of DXR have been identified from the available crystal structures containing fosmidomycin **19** or DOXP **9** as bound ligands. The enzyme is relatively flexible, and it is thought to rearrange considerably during substrate and NADPH binding to form a catalytic pocket over which a loop closes to isolate the active site.[47,54] The resulting active site has been described as having three regions, namely, a phosphonate-binding pocket, a narrow region accommodating the carbon backbone of the ligand and a metal-coordination site which also binds the hydroxamate moiety of fosmidomycin **19**.[47]

In all of the published DXR crystal structures, fosmidomycin **19** binds in the active site with the hydroxamate group oriented towards the metal cation and the phosphonate group occupying a positively charged phosphonate-binding pocket.[33,47,52] There is little evidence of 'reverse' binding in which the phosphonate group coordinates to the metal.[58] Cheng and Oldfield have suggested that phosphonate-metal chelation would involve a strained four-membered ring whereas hydroxamate-metal chelation would afford a more relaxed five-membered ring, assuming two coordination sites are occupied in each case, as illustrated in Figure 11.[58]
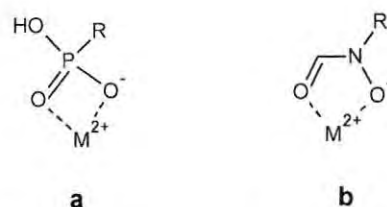
a   b

Figure 11. Suggested coordination of the divalent metal M^{2+} with a) the phosphonate group to afford a 4-membered chelate; and b) the hydroxamate group to afford a 5-membered chelate.[58]

The phosphonate-binding region involves the residues Ser186, Ser222, Asn227 and Lys228 (residue numbering from 1Q0L as shown in Figure 12), which act as hydrogen-bond donors to the negatively charged phosphonate oxygen atoms.[54,57] This phosphonate-receptor charge interaction was shown to be important following experiments in which ligands which were uncharged, but had suitable hydrogen-bonding groups, displayed no inhibitory activity against DXR.[57] The hydrophobic backbone of fosmidomycin is shielded from the solvent by the active-site 'lid' (residues 206-216) and is positioned approximately parallel to the β-indole ring of Trp212 which lies *ca.* 4 Å away (Figure 12).[47] Two of the six coordination sites of the metal are occupied by the fosmidomycin hydroxamate group which is thought to adopt a planar arrangement and to be deprotonated.[52] The residues Glu231, Glu152 and the backbone nitrogen of Ser151 are also thought to interact with the hydroxamate moiety.[47]
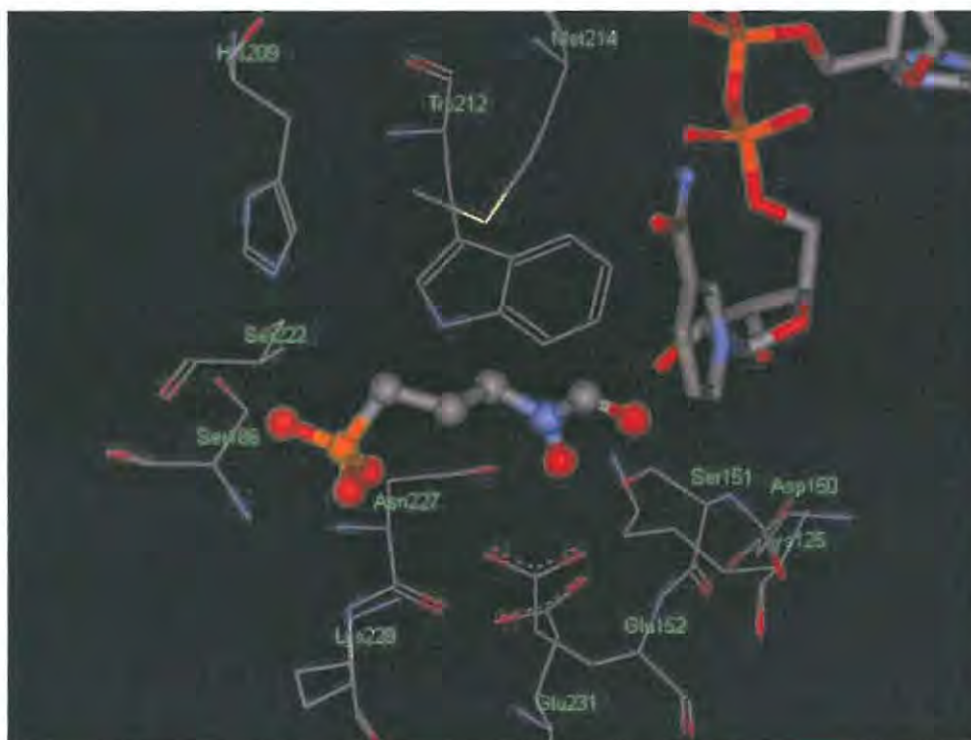

Figure 12. Illustration of the active site of *Ec*DXR (PDB code 1Q0L) showing significant binding residues. Bound fosmidomycin **19** is shown in ball-and-stick format, NADPH as sticks and protein residues in wireframe with the amino acids labelled. All structures are coloured according to element. (Generated using the Discovery Studio Visualizer 2.0.)

21

The substrate DOXP **9** interacts with DXR in a similar fashion to fosmidomycin **19** with the phosphate group forming hydrogen bonds to Ser186, Asn227 and Lys228, as shown in Figure 13.[47] There is a difference, however, in that His209 hydrogen bonds to the alkyl oxygen of the DOXP phosphate moiety whilst the phosphonate moiety of fosmidomycin shows no such interaction with this residue.[47] The histidine residues His153, His209 and His257 have all been found to be essential for DXR activity and are thought to play a role either in catalysis or in the positioning of the substrate.[45,47] As is the case with fosmidomycin **19**, the DOXP backbone lies roughly parallel to the β-indole ring of Trp212[47] and the 2-carbonyl oxygen is hydrogen-bonded to Glu152 and the amide nitrogen of Ser151. The 3-hydroxyl group of DOXP **9** is involved in hydrogen-bonding interactions with Lys125 and Glu231, while the 4-hydroxyl group is hydrogen-bonded to Glu152, Asn227 and Lys228.[47] Glu222 (in *Mt*DXR) is thought to deprotonate the 3-hydroxyl group of DOXP **9**[33] and, from comparisons of the wild-type enzyme with mutant varieties, Glu231 is considered to play a crucial role in the DOXP-MEP reaction.[45]
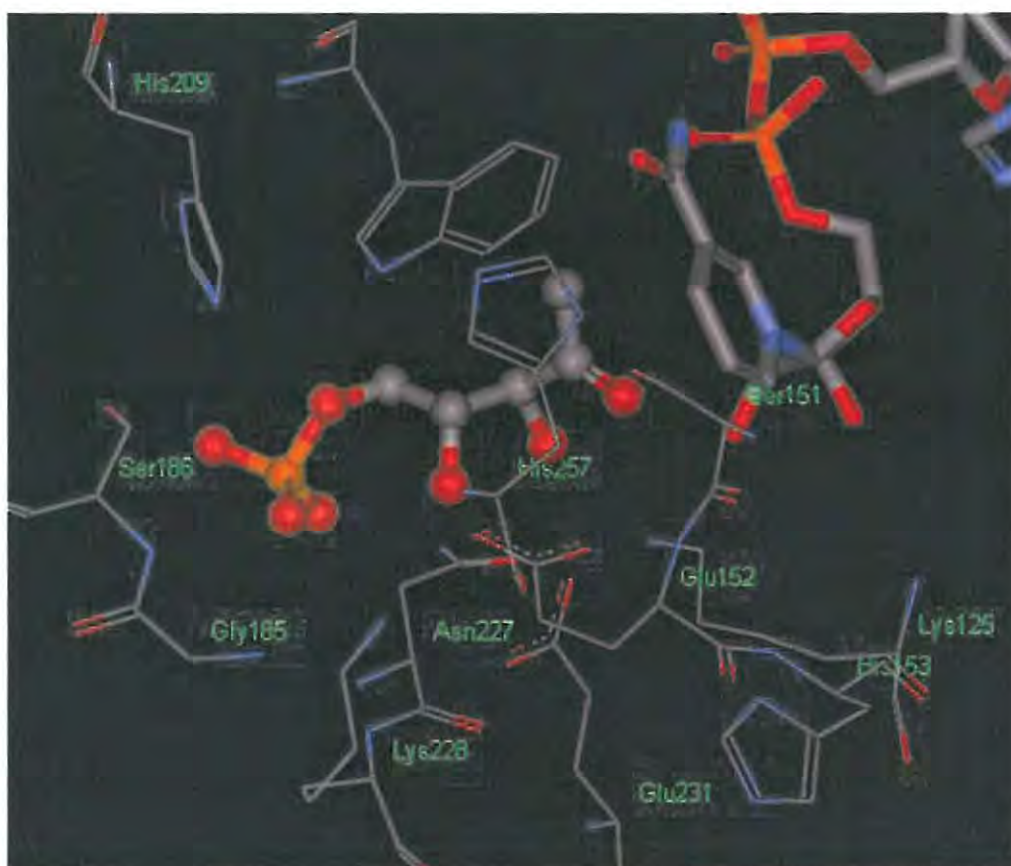

Figure 13. Illustration of the active site of *Ec*DXR (PDB code 1Q0Q) showing significant binding residues. Bound DOXP **9** is shown in ball-and-stick format, NADPH as sticks and protein residues in wireframe with the amino acids labelled. All structures are coloured according to element. (Generated using the Discovery Studio Visualizer2.0.)

The NADPH-binding region consists of a conserved group of residues at the N-terminus of the protein.[44] Experiments in which Gly14 was substituted with aspartic acid suggest that Gly14 may play an important role in maintaining the secondary and tertiary structure of the protein as well as being part of the NADPH-binding region.[45] Henriksson identified the residues in MtDXR which interact with NADPH and found that NADPH is positioned close to both the inhibitor fosmidomycin 19 and Mn^{2+}.[33] This observation was considered to restrict the length of potential fosmidomycin analogues although Henriksson has argued that longer compounds could project into a nearby hydrated cavity lined by Thr175, Ser245 and His248 (in MtDXR).[33] He proposed that binding of the substrate or inhibitor increases the binding of NADPH. The binding of NADPH, however, was found to have minimal effect on Mn^{2+} coordination.[33] NADPH is considered to bind prior to the inhibitor or substrate and to stabilise the hydrogen bonds formed when the 'lid' closes.[47] The close proximity of NADPH to the substrate is necessary for the second part of the reaction in which the pro-S-hydrogen of C-4 on the nicotinamide ring of NADPH is transferred to C-2 of 2-C-methylerythrose-4-phosphate.[47] Henriksson has suggested that the NADPH-binding site, in addition to the active site, could be investigated as a potential binding region in the design of new inhibitors.[33]

Closure of the flexible loop (Ser186-Arg216 in EcDXR) is effected by a hydrogen bond between Ser186 and His209 and is thought to lead to the tight-binding conformation of the ligand,[52] which is then shielded from the solvent by the 'lid'. The two residues Ser186 and His209 are brought together as the lid closes, with Gly185 acting as a 'hinge'.[47] Met214 is also part of the hinge and Ortmann et al. have proposed that the backbone N-H of this residue could hydrogen-bond with a suitably placed ligand or inhibitor.[59] Silber et al. have shown the loop region to have significantly different conformations in the apo-enzyme, the fosmidomycin-Mn^{2+} complex and the NADPH complex, and suggest that only relatively small ligands will allow the loop to close properly.[52]

1.4. Structure-activity relationships of fosmidomycin and DOXP analogues

Many analogues of DOXP 9, fosmidomycin 19 and FR900098 20 have been synthesised and have been investigated in terms of their inhibitory properties. Although very few of these have proven more effective than fosmidomycin in inhibiting EcDXR, the structure-activity data they provide can be used to direct the design of further analogues. For closely related compounds, there appears to be a good correlation between the IC_{50} values of the ligands in both EcDXR and PfDXR, showing that EcDXR is a useful model for the less stable PfDXR.[60]

The phosphate group of DOXP **9** is involved in interactions with the active-site residues in a similar manner to that of the phosphonate group of fosmidomycin and several studies have been carried out to establish the importance of this group.[47] In one such study, it was found that neither deoxyxylulose nor erythrose-4-phosphate act as substrates for DXR.[34] Due to the susceptibility of the phosphate O-P bond to cleavage by phosphatases, the phosphonate group which contains the more stable C-P bond is commonly used in the design of potential inhibitors; this substitution appears to have little detrimental effect on the inhibition properties.[61] The phosphonate derivative of DOXP, compound **21** (Figure 14), serves as an alternative substrate for DXR but has lower activity than DOXP.[34] Giessmann *et al.*, however, have pointed out that the additional oxygen atom of a phosphate group would have the ability to form additional hydrogen bonds with nearby residues.[54, 61]
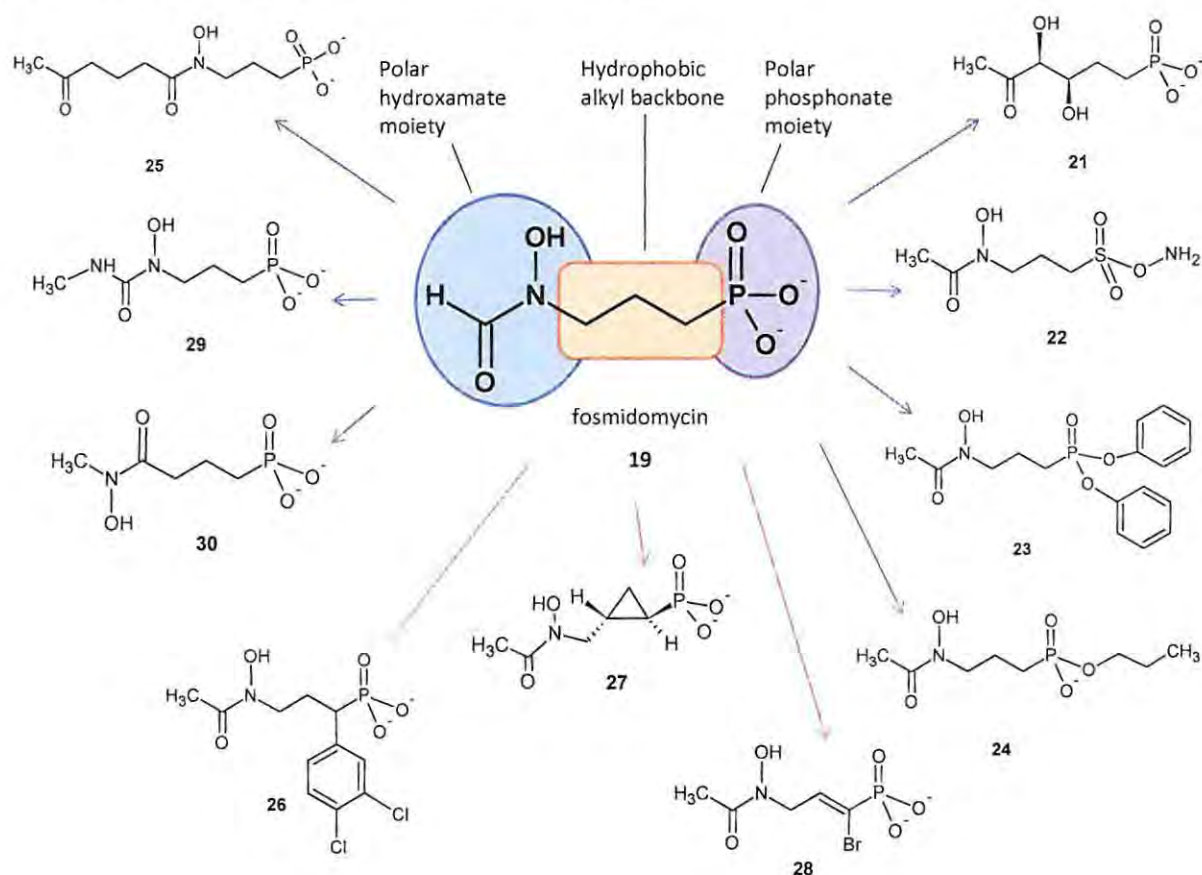
Figure 14. Structures of selected DOXP and fosmidomycin analogues **21-30** showing variation of the phosphonate moiety, backbone region and hydroxamate moiety.

The necessity of having a negative charge on the phosphonate group was studied by investigating the binding potential of structural analogues which are intrinsically neutral but are still able to form hydrogen bonds with the active-site residues.[57] Both sulfone and sulphonamide moieties, such as compound **22**, were tested on DXR but proved to have no activity as inhibitors, illustrating the importance of both the negative charge on the

24

phosphonate moiety and of hydrogen-bonding potential.[57] Compounds with only a single negative charge showed greatly reduced activity relative to fosmidomycin, further supporting this finding.[57]

One explanation for the limited efficacy of fosmidomycin is that its overall hydrophilicity results in poor absorption, and, consequently, Reichenburg et al. investigated diaryl ester pro-drugs of fosmidomycin based on the rationale that the ester linkages would be cleaved in vivo by non-specific plasma esterases. Diphenyl phosphonate analogues, such as compound 23, proved, in fact, to be more active than FR900098 20 when administered orally. However, substitution on the phenyl rings tended to decrease activity, possibly due to a reduction in the rate of ester cleavage caused by steric hindrance.[62] An interesting observation was made by Courtois et al. who found that, in some cases, hydrolysis of the diethyl phosphonates to the acids led to a reduction in inhibitory activity in plant cells.[63]

Considering the dimensions of the binding site, it appears that there is little scope for the design of inhibitors much larger than fosmidomycin 19 which would be able to occupy the same binding site. The active-site cleft is, in fact, relatively small and Mac Sweeney et al. have suggested that any inhibitors longer than fosmidomycin are likely to displace NADPH or bind to the open conformation of DXR.[47] Several studies, however, have suggested the presence of adjacent pockets which may have the potential to bind bulky and hydrophobic groups. In one such study by Giessmann et al., the relatively high inhibitory activity of an O-phenyl-substituted fosmidomycin analogue was considered to support the existence of a hydrophobic binding region some distance from the active site.[54] In fact, the study of fosmidomycin analogues with large hydrophobic groups attached to the phosphonate moiety has indicated the existence of an additional lipophilic binding region beyond the phosphonate-binding site. Interactions of these hydrophobic groups with the protein have been found to partially compensate for the resultant loss of one negative charge on the phosphonate moiety.[57] Contrary to expectations, the activities of the mono-methyl, -ethyl and -propyl phosphonate esters of FR900098, such as compound 24, have been observed to increase with increasing length of the alkyl chain, supporting the presence of a hydrophobic pocket adjacent to the binding site.[57] The acyl residue which distinguishes FR9000098 20 from fosmidomycin 19 is thought to be the limit to which the hydroxamate moiety can be extended.[54] Elongation of the acyl chain beyond the hydroxamate moiety has, in fact, led to a decrease in activity, although the addition of a carbonyl group, as in compound 25, appeared to mitigate this, possibly by acting as a hydrogen-bond acceptor from the backbone NH of Met214 (E.coli).[59] Substitution

at the α-position of the backbone region suggested the presence of a hydrophobic pocket close to the phosphonate-binding region.[60] This was supported by the promising activity of α-substituted fosmidomycin analogues, of which the 3,4-dichlorophenyl substituent, compound **26**, was the most effective.[60] A hydrated cavity bound by the residues Thr175, Ser245 and His248 (in *Mt*DXR) has also been identified as a possible binding pocket for fosmidomycin analogues containing a phenyl group attached to C-4.[33] These studies show that the design of novel DXR inhibitors need not be limited to compounds which only occupy the fosmidomycin binding site. Incorporation of a hydrophobic alkyl or aryl group capable of occupying an adjacent pocket could enhance a ligand's membrane permeability, receptor-binding and inhibiting potential.[57,59,60]

Few variations in the three-carbon spacer of fosmidomycin have been explored, possibly because the binding of the phosphonate and hydroxamate groups anchor the molecule in the DXR binding cavity, leaving little scope for variation at these points. Experiments involving a shorter carbon spacer have shown that the three-carbon distance between the phosphonate and hydroxamate moieties is crucial.[54] Rotationally restricted fosmidomycin analogues incorporating a three-membered ring, such as compound **27** (Figure 14), have been synthesised and shown to inhibit DXR.[65] The stereochemistry at the two chiral centres proved to be significant as the enantiomerically pure *trans*-inhibitor was much more effective than the corresponding racemic mixture.[65] Based on this work and the success of α-aryl substituted analogues, Devreux *et al.* synthesised analogues containing both an α-aryl substituent and an α,β-unsaturated moiety, such as compound **28**, but these all showed minimal activity, suggesting that the combination of these two groups limited the rotational freedom excessively.[66]

Although the coordination of the hydroxamate moiety of fosmidomycin to the metal ion has been shown to be important, several other metal-coordinating groups have been explored.[54] Hydroxyurea and carboxylic acid analogues of fosmidomycin, such as compound **29**, have been synthesised by Kurz *et al.*; unfortunately, no binding or inhibition assay data appear to have been published on these compounds.[67,68] A reversal of the order of the hydroxamate moiety of fosmidomycin to form hydroxamic acids, such as compound **30**, resulted in inhibitors showing almost the same activity as fosmidomycin.[69] These compounds were also found to inhibit the growth of *E. coli* strains, including a strain resistant to fosmidomycin.[69]

The study of analogues of DOXP **9**, the intermediate 2-*C*-methyl-D-erythrose-4-phosphate **15** and MEP **10** has highlighted crucial structural features in these molecules. The 3-hydroxyl

group does not appear to be essential for binding but is important for catalysis, as is the 4-hydroxyl group.[54,70] Hoeffler *et al.* have shown that the methyl group of the intermediate **15** is vital for binding to the enzyme although elongation of this group to ethyl, as in compound **31** (Figure 15), decreases activity, implying that the metal-coordination site is sterically constrained.[37,70] Replacement of the methyl ketone moiety of DOXP with an amide moiety, as in compound **32**, and variations in the stereochemistry of the hydroxyl groups has resulted in compounds which failed to act as substrates for DXR but proved to be weak inhibitors.[70] Successive replacement of the 1-methyl hydrogens of DOXP with fluorine atoms was carried out by Fox and Poulter;[71] the di- and tri-fluorinated analogues acted as moderate DXR inhibitors, whilst the mono-fluorinated analogue **33** proved to be a good substrate for the enzyme.[71]
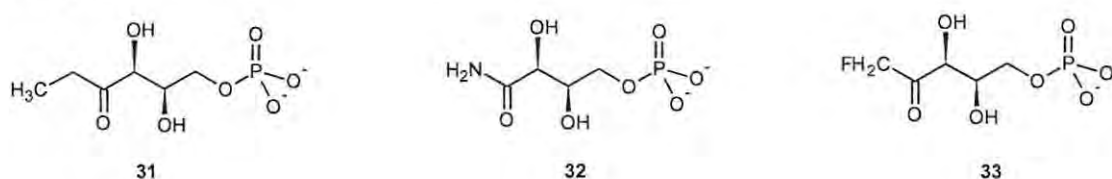

Figure 15. Structures of selected DOXP analogues.

## 1.5. Aims of the present investigation

Understanding the global importance of malaria and the potential of DXR as a promising drug target, the overall aim of this project has been to synthesise and evaluate a series of potential DXR inhibitors. More specifically, this has involved the following objectives.

i) Synthesis of a series of diethyl 2-heteroarylamino-2-oxoethyl- and 2-heteroarylamino-2-oxopropyl-phosphonate esters and their corresponding phosphonic acid salts.

ii) Investigation of the use of the saturation transfer difference (STD) experiment as a nuclear magnetic resonance (NMR) screening tool to study the ability of the synthesised compounds to bind to DXR.

iii) Testing of the synthesised compounds in a DXR-inhibition assay to determine their inhibitory activity and to explore structure-activity relationships.

iv) Simulated docking studies of the inhibitors to investigate their ability to fit in the DXR active site and their potential interactions with the active-site residues.

v) Exploration of the active sites of EcDXR and PfDXR to highlight any differences between them and to identify any nearby potential binding pockets or residues.

vi) Design of a series of novel DXR inhibitors incorporating known structure-activity relationships and any information brought to light in the above investigations.

2. RESULTS AND DISCUSSION

2.1. Synthesis of potential DXR inhibitors

During the investigation of glutamine synthetase inhibitors as potential antituberculosis agents, compound **34** was found to exhibit binding to *Ec*DXR in STD NMR experiments and a low level of *Ec*DXR inhibition in enzyme inhibition assays.[72] Several series of analogues of compound **34**, with various substituents on the phenyl ring, were consequently prepared in a cognate study in our group, and some of these compounds showed binding in STD experiments.[73] The phosphonated acetanilide **34** was therefore identified as a possible lead compound for the design of novel inhibitors of DXR and, in the present study, attention has been given to the synthesis of analogues in which the benzene ring is replaced by a heterocyclic system.

34
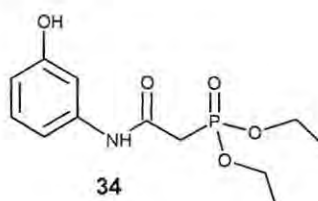
Structure-activity studies of fosmidomycin and its analogues have highlighted the importance of a metal-coordinating moiety (especially nitrogen- or oxygen-containing functionalities) for binding to the hard divalent metal cation in the DXR active site.[74] The heterocyclic and amide moieties in compounds **35a-e** (Figure 16) were expected to serve this function in addition to providing a degree of rigidity and hydrophobicity. In studies by Kuntz *et al.*, reversal of the hydroxamate moiety of fosmidomycin **19** did not appear to decrease the inhibitory activity and it was hoped that the amide moiety would have similar interactions with the active-site residues.[69] Ester pro-drugs of fosmidomycin analogues have been shown to exhibit increased lipophilicity and absorption,[62,75,76] and the phosphonate esters **35a-e** were expected to provide similar advantages.
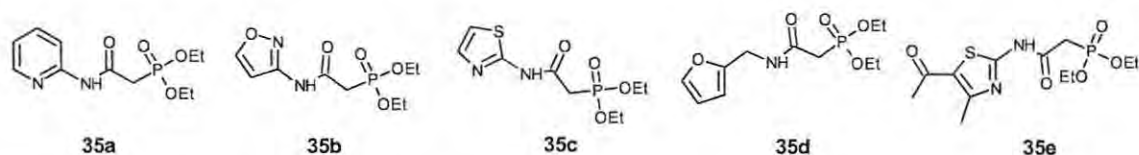
Figure 16. Initial set of phosphonate ester targets **35a-e**.

Since the phosphonate esters **35a-e** could well be hydrolysed *in vivo*, it was decided that the disodium salts **36a-e** of the corresponding acids (Scheme 1) should also be prepared and subjected to enzyme-binding and -inhibition studies. Access to the phosphonate esters **35a-e** and the disodium salts **36a-e** is outlined in Scheme 1.
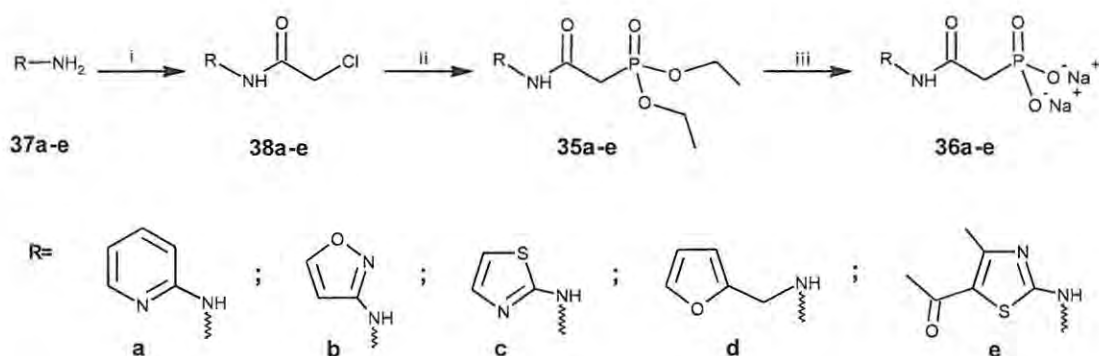
Scheme 1. Synthesis of phosphonate esters **35a-e** and the disodium salts **36a-e** of the corresponding phosphonic acids.
Reagents and conditions:- (i) NaH, chloroacetyl chloride, THF, 6 h, r.t.; (ii) triethyl phosphite, 9 h, reflux (110 °C); (iii) TMSBr, DCM, overnight, r.t. and then 0.4M-NaOH.

The formation of the amide bond in the α-chloroamides **38a-e** is achieved by reaction of chloroacetyl chloride with the respective primary amines **37a-e** in THF, sodium hydride serving to deprotonate, and thus enhance the nucleophilicity of, the amines. Nucleophilic acyl substitution with loss of chloride occurs preferentially at the less hindered and more electrophilic carbonyl carbon in chloroacetaldehyde, as shown in Figure 17.

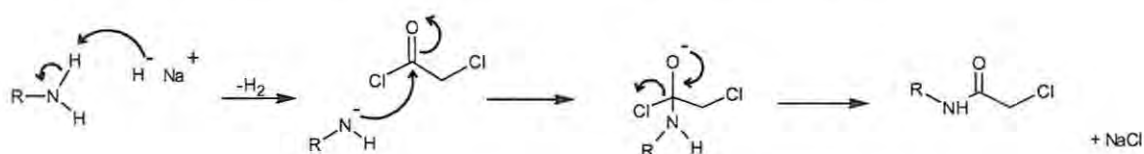**Figure 17.** Mechanism of the formation of the amide bond between a primary amine and chloroacetyl chloride.

Thus, acylation of the respective primary amines **37a-e** with chloroacetyl chloride afforded the known chloroacetamides **38b-e** in yields in excess of 70% and in sufficient purity (after washing with hexane), as indicated by ^{1}H and ^{13}C NMR analysis, to be used without further

29

purification. The pattern of signals between 0.5 and 2.0 ppm in Figure 18 was observed in the NMR spectra of all the crude products, and was attributed to high-boiling alkanes present in the mineral oil used to store the NaH. Repeated washing of the products with hexane successfully removed the oil. Each of the products was characterised by the presence of the chloromethylene singlet at *ca.* 4.2 ppm in the ^{1}H NMR spectrum as shown in Figure 18. The 2-aminopyridine derivative **38a**, however, required chromatographic purification prior to use to remove residual starting material and other impurities. Intramolecular cyclisation or polymerisation are possible competition reactions and could account for the lower yields obtained in repeated preparations of compound **38a** (Table 1, p. 34).
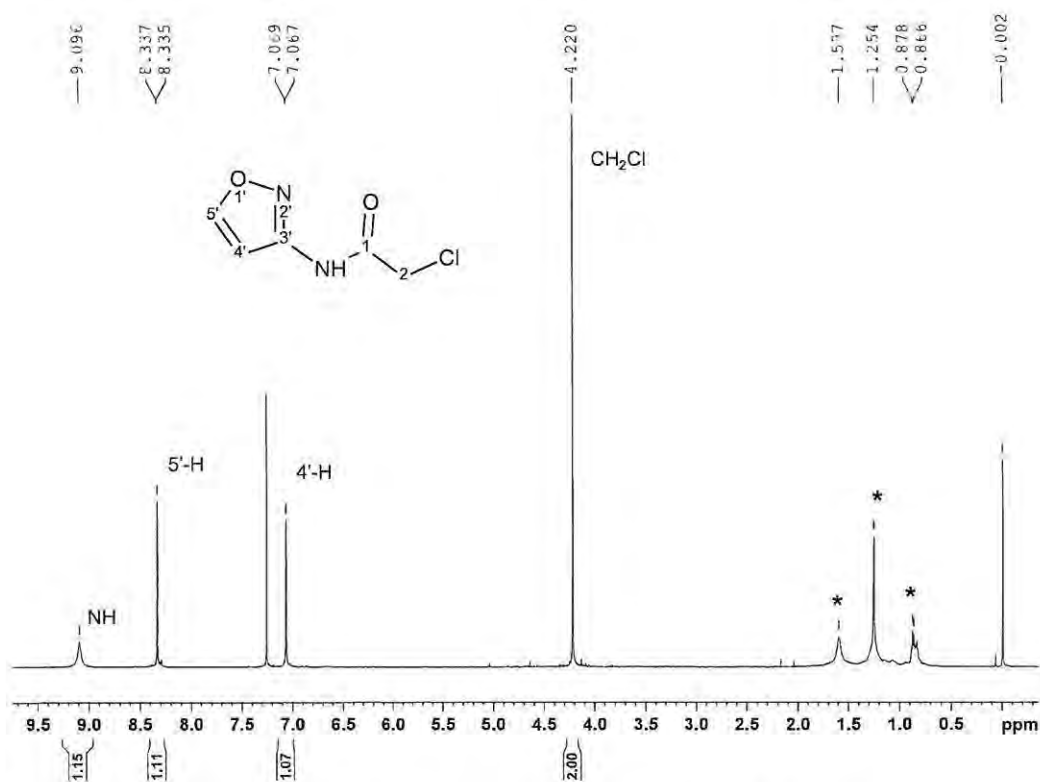
Figure 18. ^{1}H NMR spectrum of compound **38b** (CDCl$_3$, 600 MHz); *mineral oil impurities.

An alternative procedure was explored for the synthesis of compounds **38a** and **38d**. This method[77] involves direct addition of chloroacetyl chloride to the amine in dichloroethane followed by neutralisation with aqueous sodium hydroxide, and appeared to work well for the furfurylamine derivative **38d**, giving a clean product after work-up with a yield of 91%. However, this approach failed to give the 2-aminopyridine derivative **38a**; analysis of the crude reaction mixture showed the presence of 2-aminopyridine **37a** but none of the expected product **38a**. A microwave-assisted variation of this method also failed to yield the desired product **38a**.

30

The next step involved introduction of the phosphonate ester moiety *via* the Arbuzov reaction. Each of the chloroacetamides **38a-e** was heated under reflux with neat triethyl phosphite for 9 hours to yield the diethyl phosphonates **35a-e**. In this reaction, the trivalent phosphorus attacks the chloromethylene carbon, displacing chloride to form an intermediate phosphonium salt, which cleaves to afford ethyl chloride and the pentavalent phosphonate ester as shown in Figure 19.[78]

Figure 19. Mechanism of the Arbuzov reaction.[78]

The diethyl phosphonates **35b-e** were readily isolated in reasonable yields (48% to 100%; Table 1, p. 34), the excess 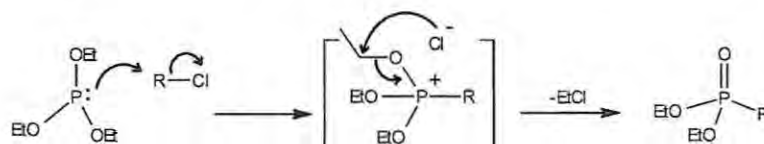triethyl phosphite being effectively removed by repeated washing with hexane and evaporation under high vacuum for several hours. ^{1}H NMR analysis of the products clearly showed the disappearance, in each case, of the chloromethylene singlet at *ca.* 4.2 ppm and the appearance of a methylene proton doublet at *ca.* 3 ppm as shown in Figure 20. Coupling to the adjacent ^{31}P nucleus results in splitting of the methylene signal, with a characteristic coupling constant of *ca.* 21 Hz. As with the chloroacetylation step, the 2-aminopyridine derivative **35a** was obtained, repeatedly, in lower yields (12%) and purity than the other phosphonate esters. Since attempts to purify compound **35a** on silica gel proved unsuccessful, the subsequent hydrolysis step was carried out on the crude material and the product, **36a**, was purified by reverse-phase chromatography on a C18 column followed by reverse-phase HPLC. As the aim was to obtain the compounds for bioassay, further optimisation of the synthetic method was not explored.

All of the phosphonate esters **35a-e** are new and were fully characterised by elemental (HRMS) and spectroscopic (IR and 1- and 2-D NMR) analysis. The characteristic coupling to the adjacent ^{31}P nucleus seen in the ^{1}H NMR spectrum (Figure 20) was also observed in the proton decoupled ^{13}C spectrum of compound **35b** (Figure 21). Coupling to the adjacent ^{31}P nucleus results in splitting of the methylene carbon signal at *ca.* 36 ppm with a large coupling constant of 131 Hz and the splitting (*J*=4.5 Hz) can even be observed in the carbonyl carbon signal at 162.5 ppm. The C-5' nucleus is highly deshielded by the adjacent oxygen atom and the signal was assigned by analysis of the multiplicity-edited HSQC NMR spectrum. The HMBC NMR spectrum for compound **35b** (Figure 22) reveals the correlation between the CH$_2$P protons and the carbonyl carbon as well as between the 4'- and 5'-methine protons and the C-3' carbon.
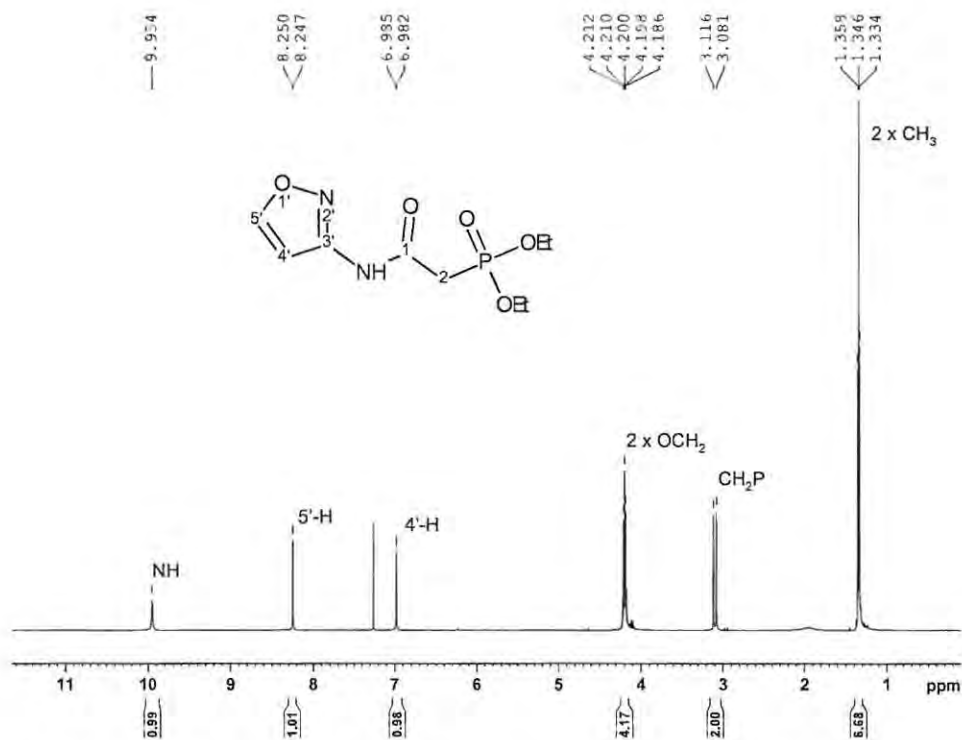
31

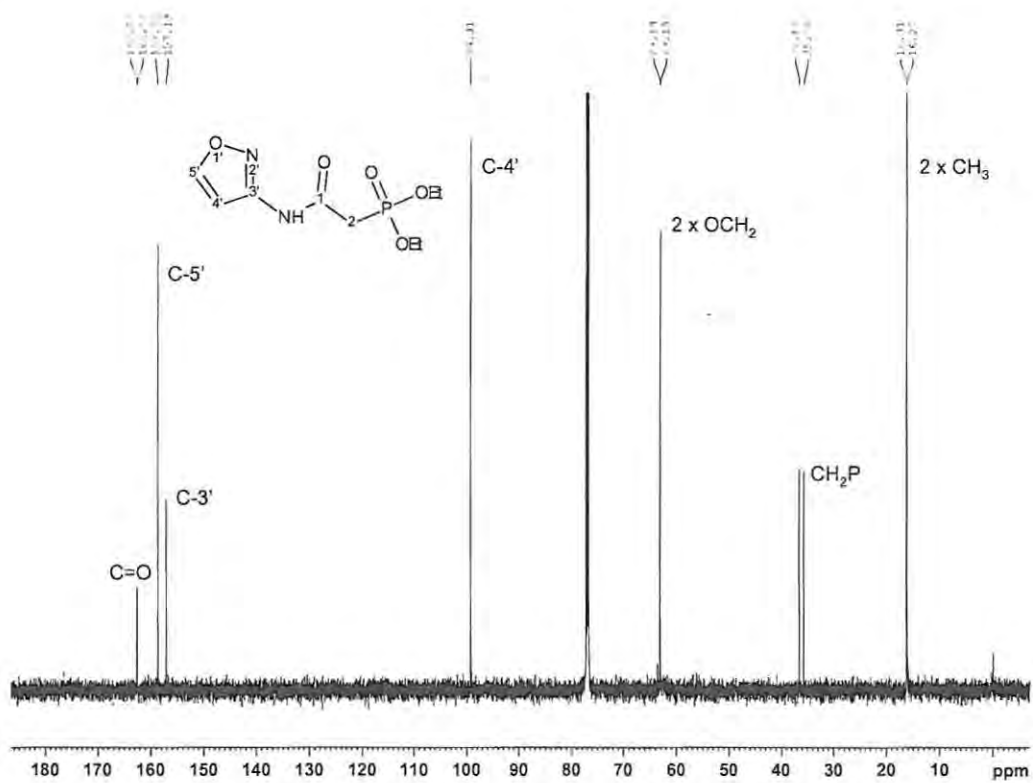**Figure 20.** ^{1}H NMR spectrum of compound **35b** showing coupling of CH$_2$ to ^{31}P (CDCl$_3$, 600 MHz).

Figure 21. Proton decoupled ^{13}C NMR spectrum of compound **35b** (CDCl$_3$, 150 MHz).
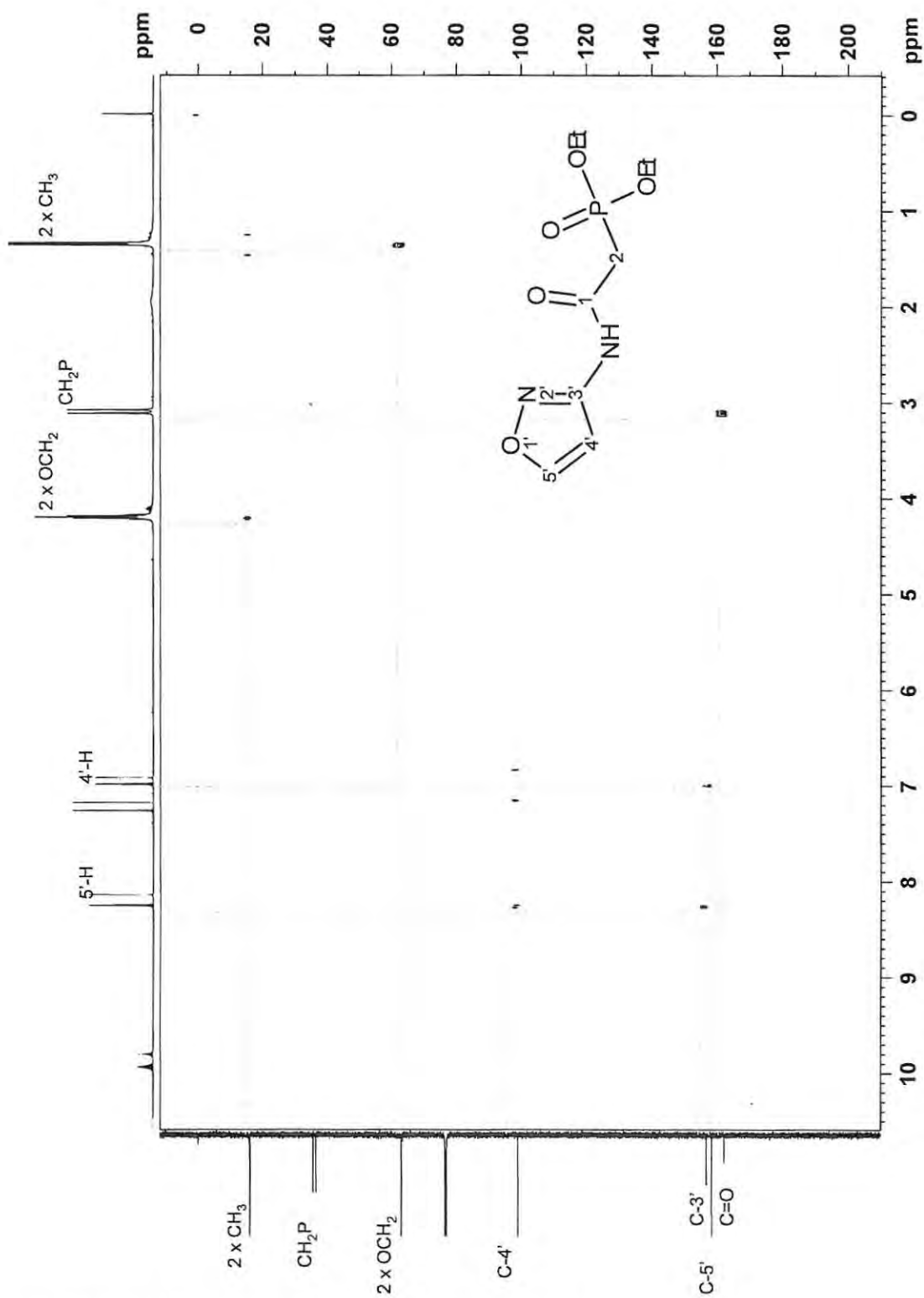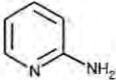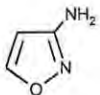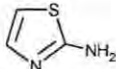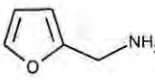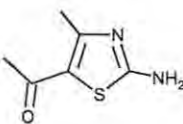
Figure 22. HMBC NMR spectrum of compound **35b** (CDCl₃, 600 MHz).

Table 1. Percentage isolated yields of chloroacetamides **38a-e**, phosphonate esters **35a-e** and disodium phosphonate salts **36a-e**.

	R-NH$_2$ 37a-e	RNHCO.CH$_2$Cl 38a-e	RNHCO.CH$_2$P(O)OEt$_2$ 35a-e	RNHCO.CH$_2$P(O)O$_2$Na$_2$ 36a-e
a		21	12	2.3
b		100	48	100
c		70	59	100
d		84 (91)[a]	62	100
e		74	67	100

[a] Synthesis by direct addition of chloroacetyl chloride to furfurylamine.[77]

Since hydrolysis of the phosphonate esters **35a-e** is expected to occur *in vivo*,[65,62,79,80] the disodium salts **36a-e** of the corresponding phosphonic acids were also required for *in vitro* enzyme inhibition assays. Microwave-assisted hydrolysis of the esters **35b-d** in acetonitrile,[81] a method used successfully in our group on similar compounds,[73] was attempted using bromotrimethylsilane (TMSBr) in acetonitrile but there was little or no evidence of the hydrolysis products despite several attempts.[†] Several methods for the conversion of phosphonate esters to the corresponding phosphonic acids have been reported. Phosphonation using dibenzyl phosphite followed by hydrogenolysis with hydrogen gas and palladium-on-carbon catalysis has proved successful in many instances,[59] and the transformation has also been achieved by treatment of phosphonate esters with TMSBr at room temperature in dichloromethane followed by hydrolysis (Scheme 4, p. 53).[54,82] The latter method[54] was attempted for the hydrolysis of the phosphonate ester **35e**, followed by

---

[†] Subsequently, however, it was discovered that the temperature control on the microwave rotor had been malfunctioning and this may have been the cause of the failure of the reaction.

treatment with aqueous sodium hydroxide and extraction into ethyl acetate, but NMR analysis of the organic phase showed that only starting material was present. The reported procedure[54] requires reaction of the phosphonate ester with TMSBr for 2 hours. It was therefore decided to monitor the reaction over an extended period of time using ^{31}P NMR spectroscopy and it was found that stirring the reaction mixture overnight followed by titration with aqueous sodium hydroxide generally afforded the disodium salts of the respective phosphonic acids in quantitative yield (Table 1). The 2-aminopyridine system, however, again presented difficulties with the disodium salt **36a** being obtained, after purification by reverse-phase HPLC, in only 2.3% yield. Having established the suitability of ^{31}P NMR spectroscopy to follow the reaction with TMSBr, it was decided to undertake a full kinetic study of the reaction, the details of which are discussed in Section 2.2.

Comparison of the ^{1}H NMR spectra of the phosphonate ester **35b** and the disodium salt **36b** (Figure 23) clearly shows the disappearance of the signals corresponding to the ethyl groups at *ca.* 1.3 and 4.1 ppm. All hydrolysis products were purified by reverse-phase column chromatography and compounds **36a** and **36c** were further purified by reverse-phase HPLC. The disodium salts **36b-e** are all new compounds and were fully characterised by elemental (HRMS) and spectroscopic (IR and 1- and 2-D NMR) analysis.
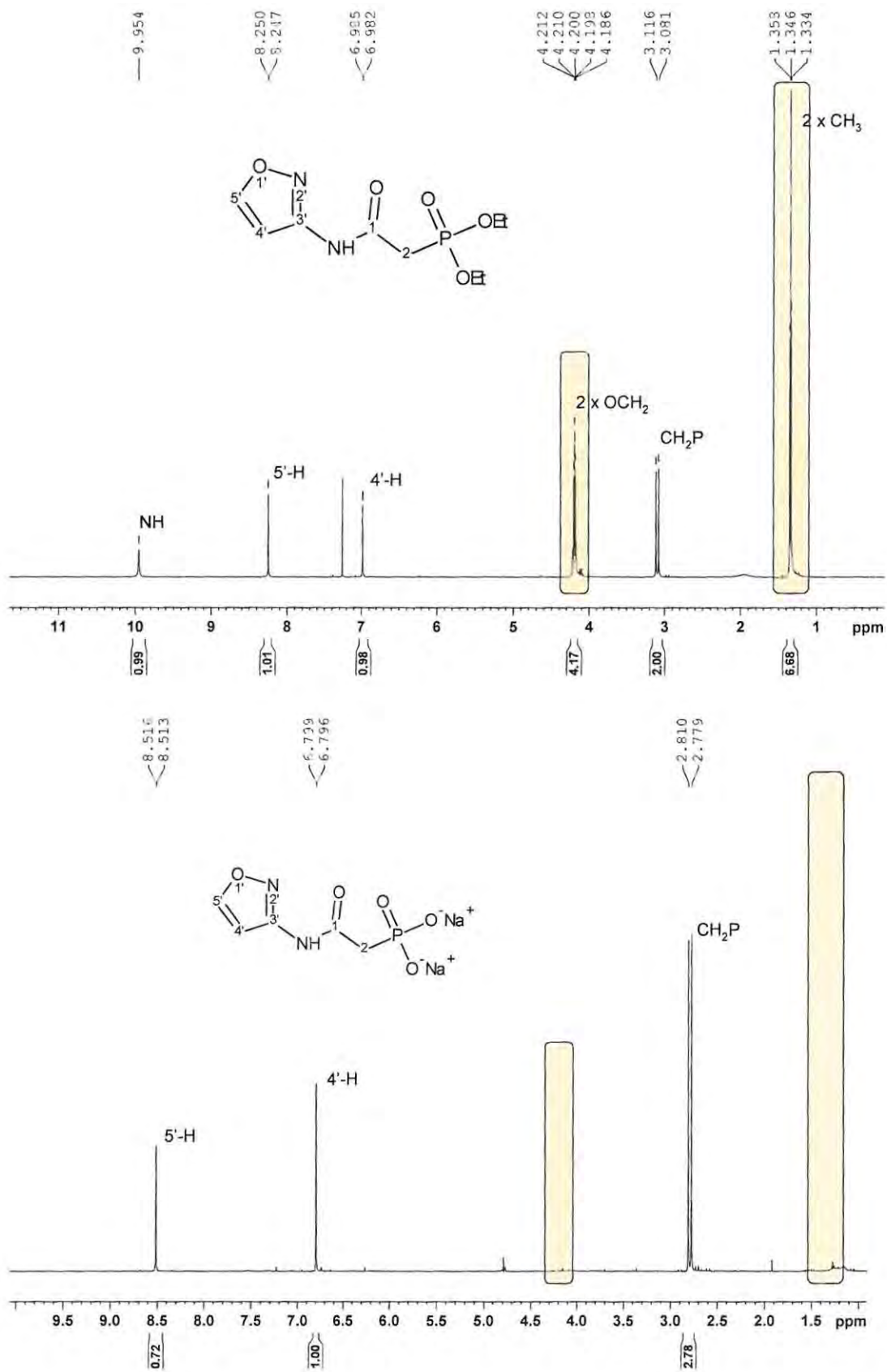
Figure 23. ^{1}H NMR spectra of phosphonate ester **35b** (top; CDCl₃, 600 MHz) and disodium salt **36b** (bottom; D₂O, 600 MHz) showing disappearance of ethyl ester signals (highlighted in orange) on hydrolysis.

A dynamic NMR study was carried out to investigate the rotameric possibilities of the phosphonic acid salts. Delocalisation of the amide nitrogen lone-pair electrons, as shown in Figure 24 for compound **36c**, confers a degree of rigidity on the amide bond and may result in the existence of two conformers interconversion of which occurs on the NMR timescale. A variable temperature NMR study may therefore be used to determine the presence of the two rotamers and, if such rotamers exist, the energy barrier to rotation.
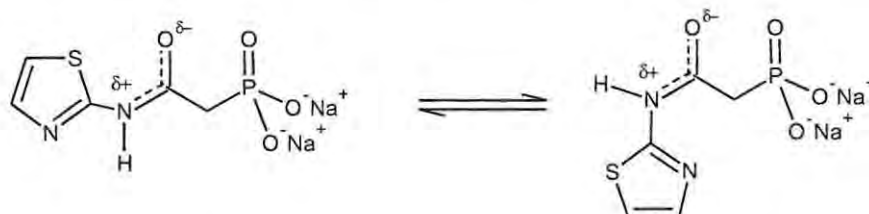
Figure 24. Two possible rotamers of compound **36c** due to restricted rotation about the amide N-CO bond.

Compound **36c** was selected for the dynamic NMR study as apparent doubling of the signals was observed in the ^{1}H NMR spectrum at 297 K (Figure 25). ^{1}H NMR spectra of compound **36c** were recorded as the temperature was increased in 5 K increments from 283 K to 333 K. If the doubling of the signals at 297 K were due to the presence of rotamers, it was expected that, as the temperature increased, the signals would move closer together and eventually coalesce as distinct populations of the two conformers become indistinguishable on the NMR timescale. Selected ^{1}H NMR spectra of compound **36c** at temperatures between 283 K and 333 K are shown in Figure 26 and it is clear that there is no variation in the chemical shift difference between the signals over this temperature range. The dynamic NMR study therefore excluded the possibility of rotamers at 297 K and it was concluded that steric factors result in the existence of only one rotamer within the temperature range studied. HPLC purification of compound **36c** subsequently confirmed these results, showing that the low intensity signals observed in Figure 25 were due to residual starting material, compound **35c**!
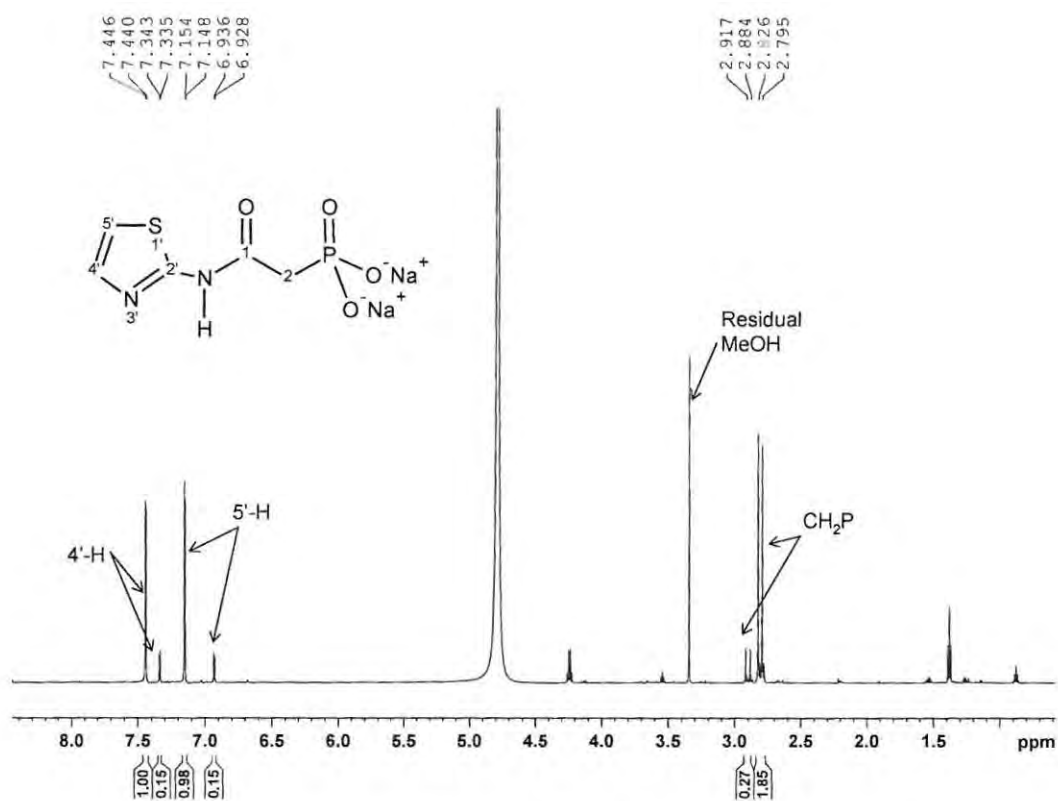
Figure 25. ^{1}H NMR spectrum of compound **36c** showing doubling of the CH$_2$P, 4'-H and 5'-H signals (D$_2$O, 600 MHz).
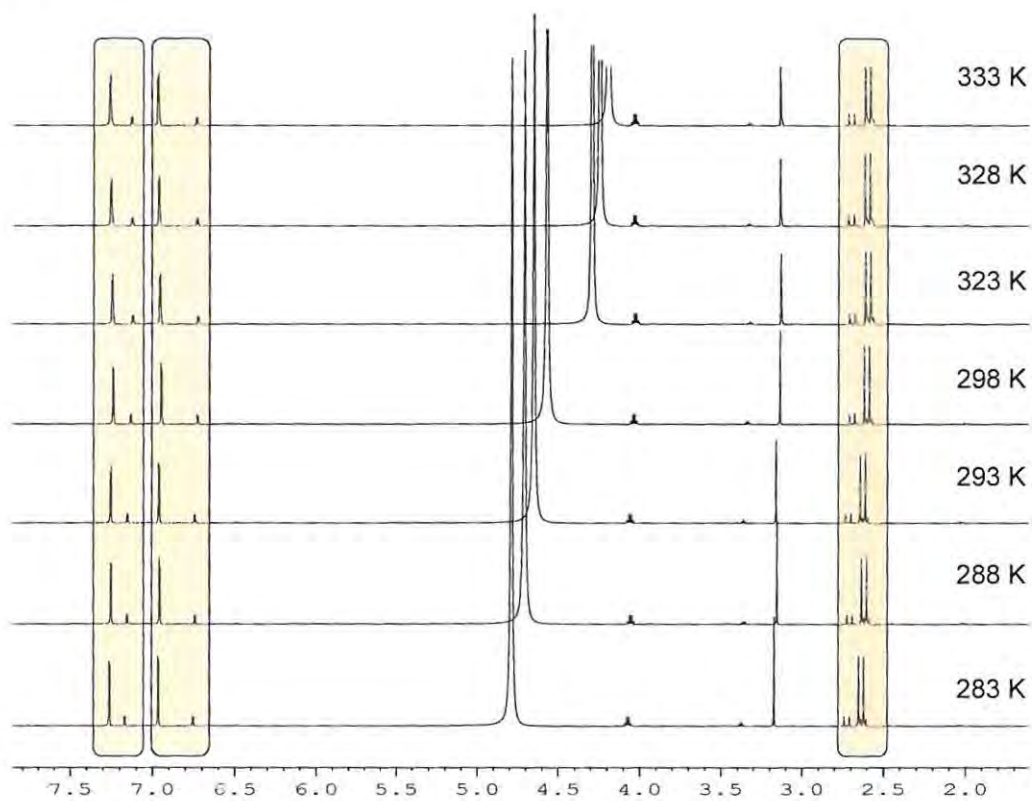
Figure 26. ^{1}H NMR spectra (D$_2$O, 600 MHz) of compound **36c** at selected temperatures. The pairs of signals (CH$_2$P, 4'-H and 5'-H) analysed are highlighted.

38

Comparison of the structure of fosmidomycin **19** and several of the fosmidomycin analogues (such as compounds **23**[62] and **30**[69]) reported in the literature suggested that an increase in inhibitory activity may be achieved by increasing the distance between the amide and phosphonate moieties in compounds **35a-e** and **36a-e**. The active-site cleft of DXR is relatively small and it is considered that analogues either much shorter or much longer than fosmidomycin are unlikely to be effective inhibitors.[47,64] Analogues of compound **34** incorporating an ethylene rather than a methylene spacer between the amide and phosphonate moieties, have been prepared in our group and have shown increased inhibition in *Ec*DXR enzyme-inhibition assays,[72,73,83] and the heterocyclic analogues, **39a-e** (Figure 27) and their corresponding disodium phosphonic acid salts **40a-e**, were therefore prepared.
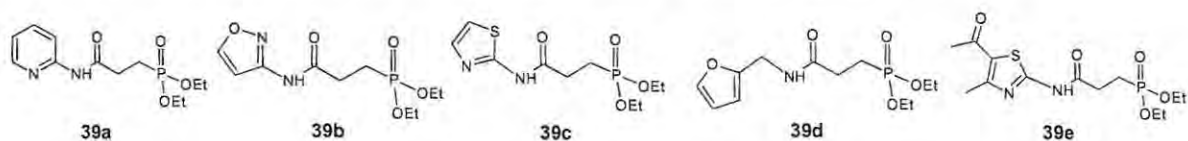
Figure 27. Structures of the second set of phosphonate esters **39a-e**.

Access to the phosphonate esters **39a-e** and the disodium salts **40a-e** of the corresponding phosphonic acids is outlined in Scheme 2.
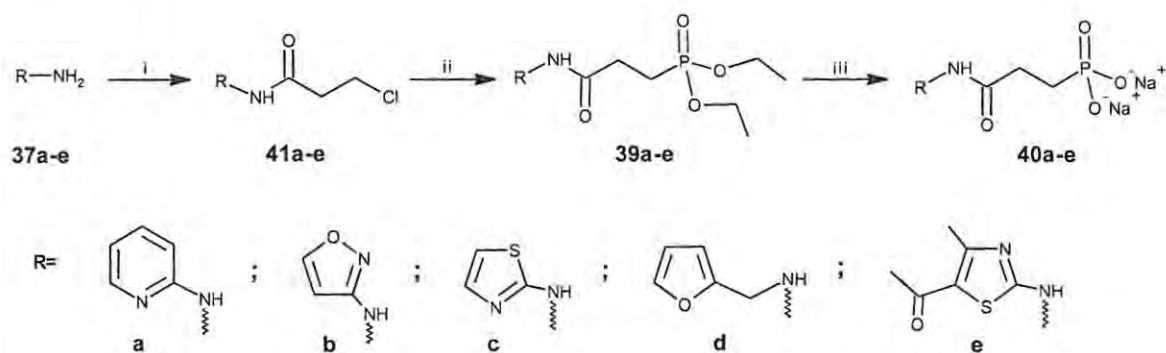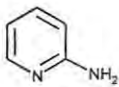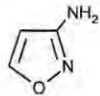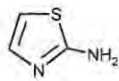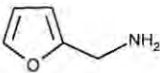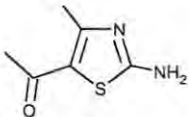
Scheme 2. Synthesis of phosphonate esters **39a-e** and the corresponding phosphonic acid salts **40a-e**. *Reagents and conditions*:- (i) NaH, chloropropionyl chloride, THF, overnight, r.t.; (ii) triethyl phosphite, 9 h, reflux (110 °C); (iii) TMSBr, DCM, overnight, r.t. and then 0.4M-NaOH.

The 3-chloropropionyl derivatives **41a-e** were synthesised by the reaction of chloropropionyl chloride with the respective primary amines **37a-e**, following the methodology used for the methylene analogues **38a-e**, and were were isolated in reasonable yields ranging from 36% to 100% (Table 2). After washing with hexane to remove residual high-boiling alkanes, compounds **41b**, **41c** and **41d** were used without further purification whilst compounds **41a** and **41e** required purification by column chromatography before they could be used in the phosphonation step. The presence of a pair of methylene triplets at *ca.* 3.0 and 3.9 ppm in the

^{1}H NMR spectra of each of the 3-chloropropionyl derivatives **41a-e** confirmed the presence of the ethylene linking group. Low intensity signals at *ca.* 5.9, 6.4 and 6.6 ppm were commonly observed in the ^{1}H NMR spectra of the crude products, suggesting that loss of HCl may have occurred resulting in formation of the α,β-unsaturated amides as minor products.

Table 2. Percentage isolated yields of β-chloroamides **41a-e**, phosphonate esters **39a-e** and disodium phosphonic acid salts **40a-e**.

	R-NH$_2$ 37a-e	RNHCO.CH$_2$CH$_2$Cl 41a-e	RNHCO.CH$_2$CH$_2$P(O)OEt$_2$ 39a-e	RNHCO.CH$_2$CH$_2$P(O)O$_2$Na$_2$ 40a-e
a	(2-aminopyridine structure)	39	33	100 (crude)
b	(3-aminoisoxazole structure)	100	74	27
c	(2-aminothiazole structure)	62	69	13.9
d	(furfurylamine structure)	63	80	81
e	(2-amino-4-methyl-5-acetylthiazole structure)	84	40	61

Reverse-phase HPLC was used to separate the mixture of products formed during the synthesis of compound **41a** and characterisation of the compounds in the fractions obtained (Figure 28) gave some insight into the reason for the low yields obtained in this case. The first fraction was the desired product **41a** which showed that the reaction had been successful to some degree, although the yield following HPLC was only 39%. The second fraction contained a mixture of compound **41a** and the imide **42**, resulting from reaction of two chloropropionyl chloride molecules with the amine **37a**, followed by loss of HCl from one of the 3-chloropropionyl moieties to give the α,β-unsaturated amide. The third fraction contained compound **43**, also an imide but containing a second pyridine ring; its formation is attributed to conjugate addition of a second molecule of 2-aminopyridine **37a** to the α,β-unsaturated imide **42**. Loss of HCl from the product **41a** resulted in the formation of the α,β-unsaturated

40

amide **44** which was isolated in only 2% yield from the fourth fraction. Formation of small amounts of the α,β-unsaturated amides during the synthesis of the other compounds in this series **41b-d** is no doubt due to the added stability afforded by the extended conjugation. Interestingly, there was no evidence of the formation of the side-products corresponding to compounds **42** and **43** in the synthesis of the analogues **41b-e**.
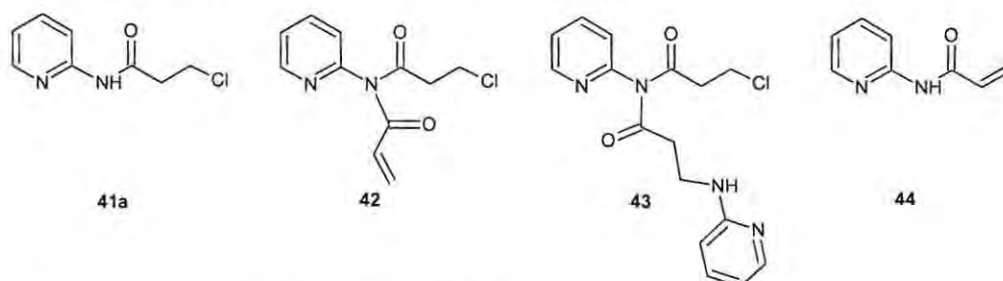
Figure 28. Products formed during the synthesis of compound **41a**.

The 1- and 2-D NMR spectra used to characterise compound **43** are shown in Figures 29-34. Integration of the ^{1}H NMR spectrum (Figure 29) indicated the presence of two pyridine and two ethylene moieties and the absence of signals between 5.5 and 6.5 ppm showed that no α,β-unsaturated system was present. Comparison of the ^{1}H-^{1}H coupling constants and analysis of the COSY spectrum (Figure 30) confirmed the presence of two ethylene moieties by showing the coupling of 2-CH$_2$ with 3-CH$_2$ and 2''-CH$_2$ with 3''-CH$_2$. The aromatic proton signals from the two pyridine rings were assigned following identification of the 6'''-H signal at 8.32 ppm, deshielded by the adjacent nitrogen atom, and the coupling between the 6'''- and 5'''-, the 6'- and 5'-, the 4'''- and 3'''- and the 4'- and 3'- protons. The ^{13}C DEPT 135 spectrum (Figure 31) clearly showed the CH$_2$ signals of the two ethylene moieties and allowed identification of the quaternary carbon signals in the proton decoupled ^{13}C spectrum (Figure 32). Assignment of the CH and CH$_2$ carbon signals was assisted by analysis of the multiplicity-edited HSQC spectrum (Figure 33) in which the CH$_2$ signals (negative phasing) are shown in blue and the CH (and CH$_3$) signals (positive phasing) are shown in red. Analysis of the HMBC spectrum, shown in Figure 34, confirmed the assignment of the aromatic proton and carbon signals and allowed assignment of the C(O)-1 and C(O)-1'' signals due to their correlation with the 2- and 3-CH$_2$ and 2''- and 3''-CH$_2$ protons, respectively. Correlation between the C-2' carbon signal and the 3'- and 6'-H proton signals and, likewise, the C-2''' carbon signal and the 3'''- and 6'''-H proton signals was used to assign these two quaternary carbon signals, as shown in Figure 34.

41

Figure 29, ^{1}H NMR spectrum of compound 43 (D$_2$O, 600 MHz).
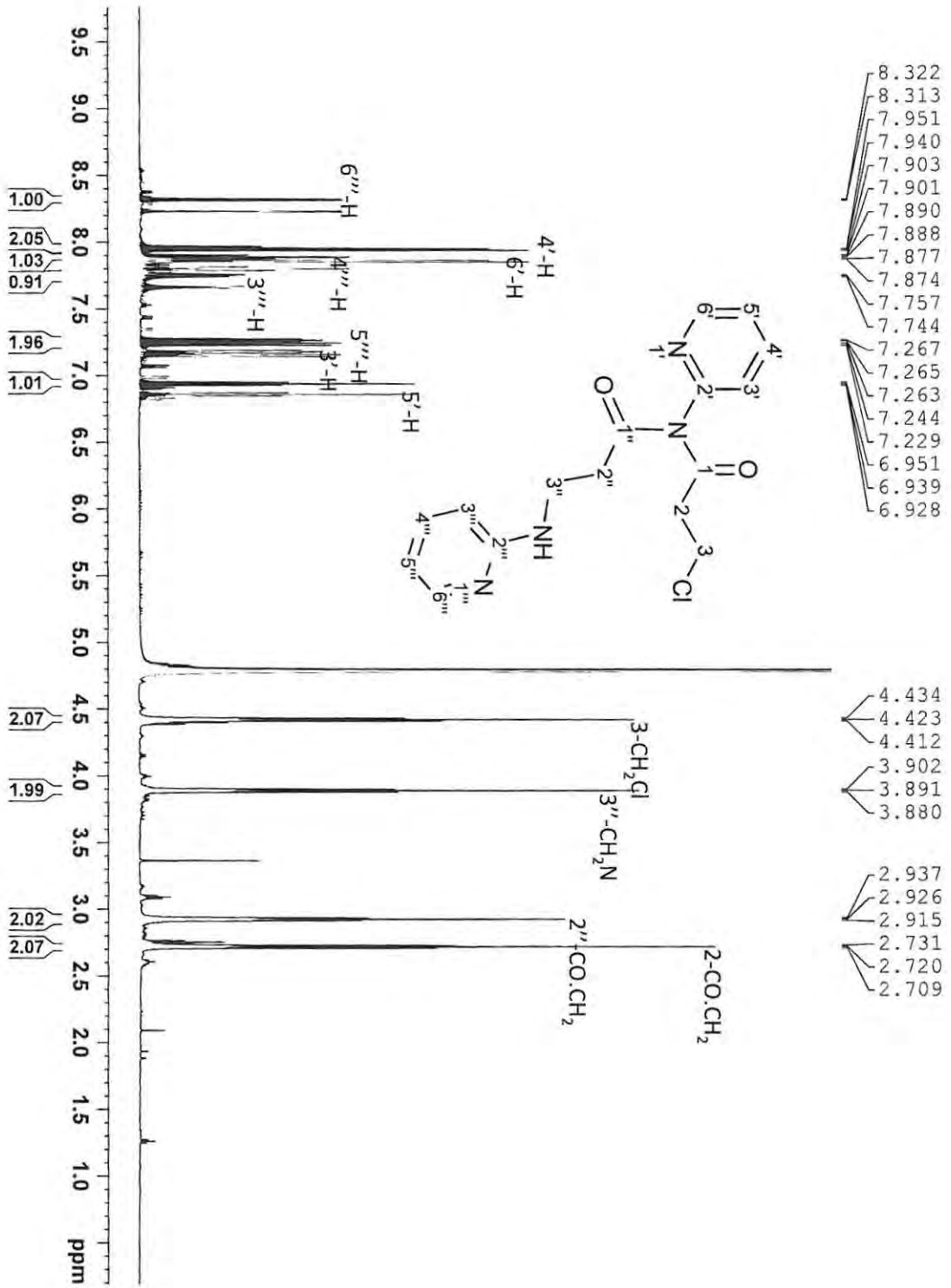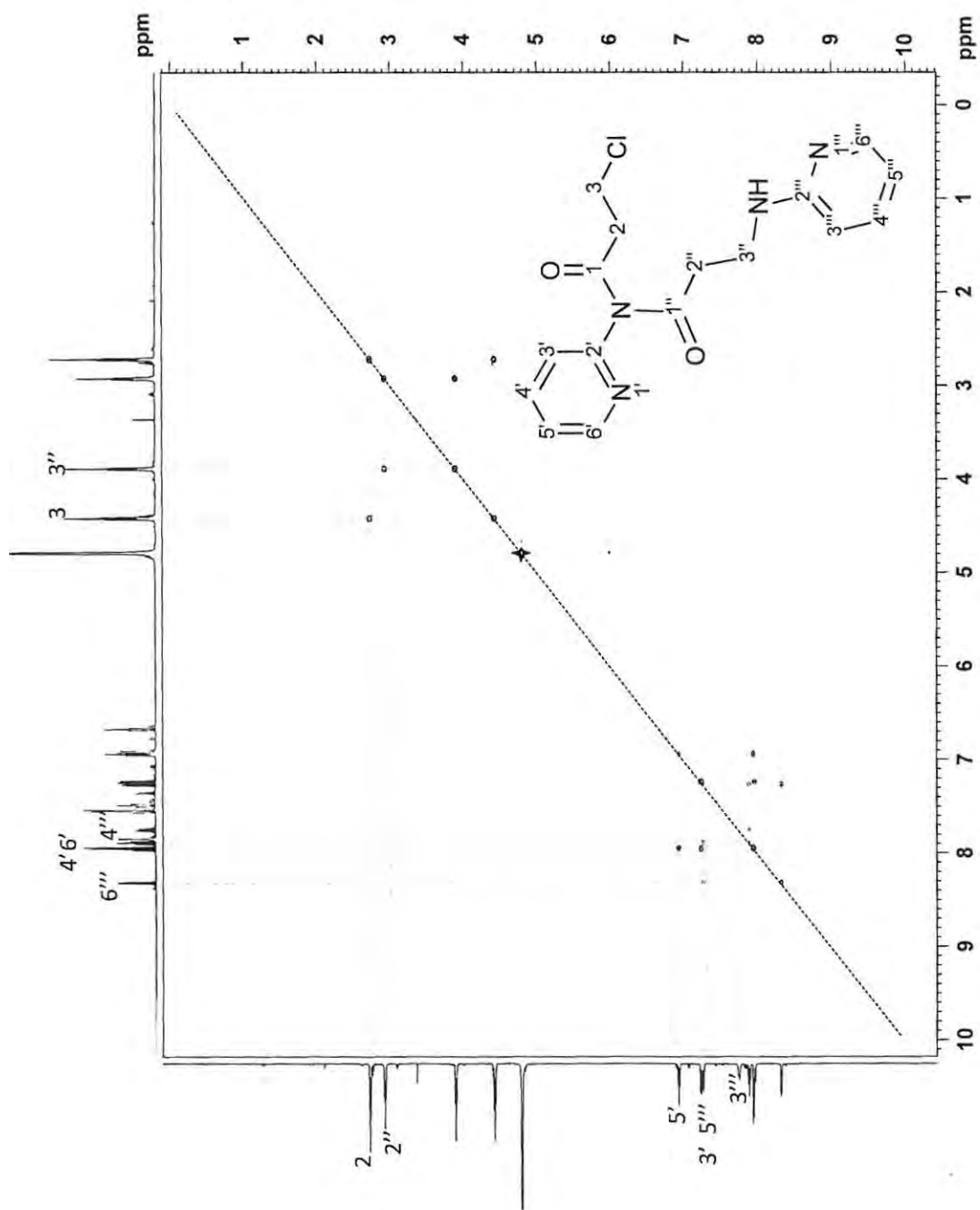
Figure 30. COSY NMR spectrum of compound **43** (D$_2$O, 600 MHz).
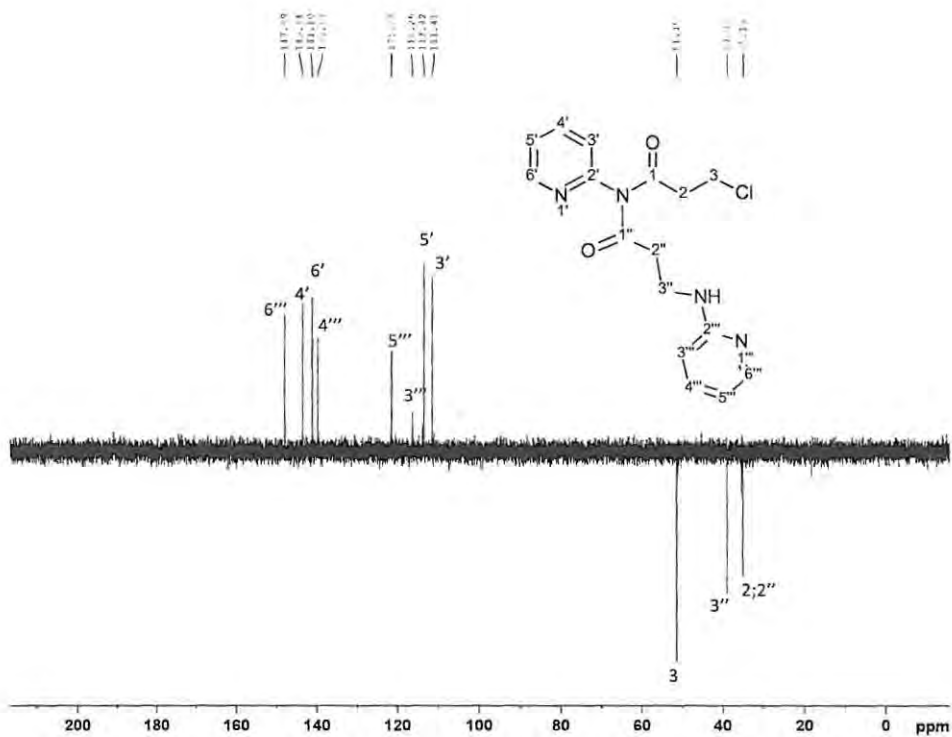
Figure 31. ^{13}C DEPT 135 NMR spectrum of compound **43** (D$_2$O, 150 MHz).
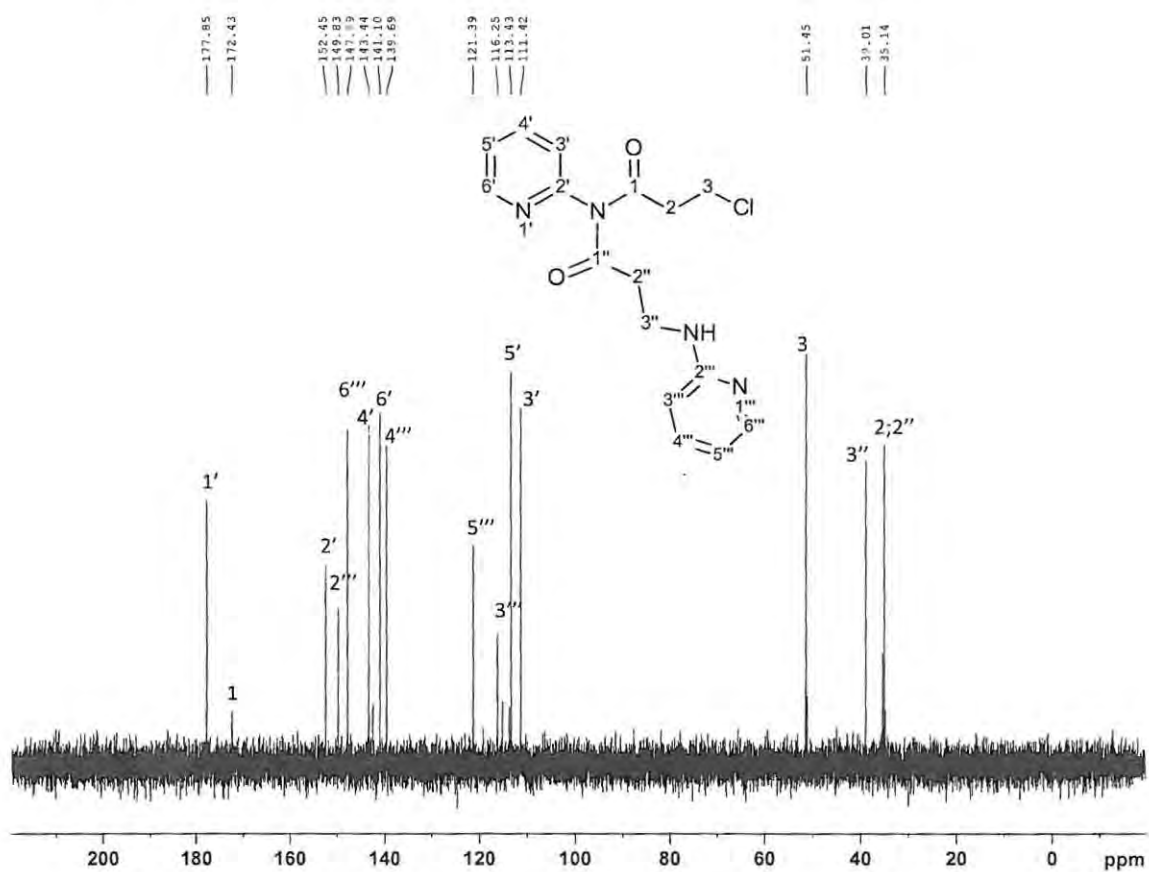
Figure 32. Proton decoupled ^{13}C NMR spectrum of compound **43** (D$_2$O, 150 MHz).

44
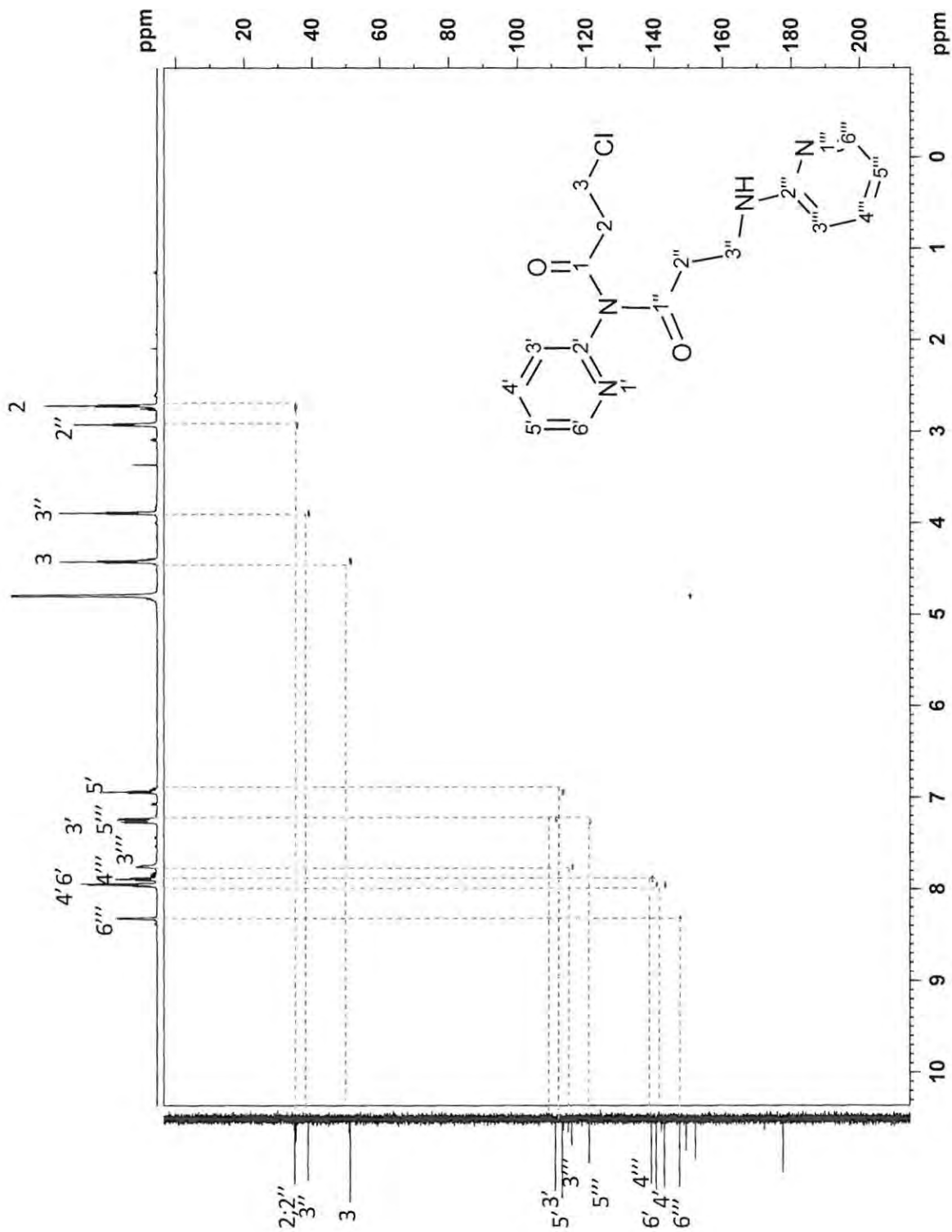
Figure 33. Multiplicity-edited HSQC NMR spectrum of compound **43** (D$_2$O, 600 MHz).

45
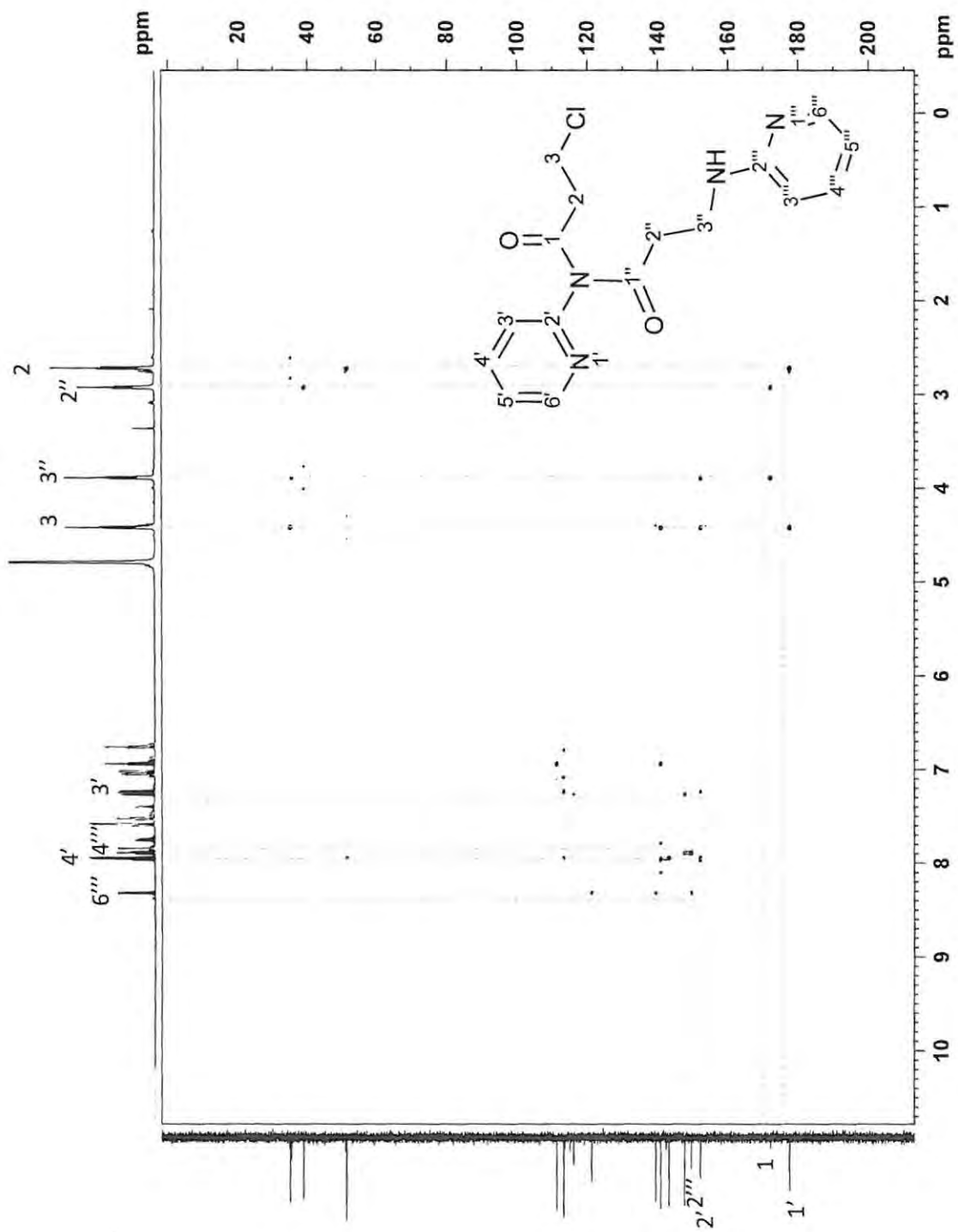
Figure 34. HMBC NMR spectrum of compound **43** (D$_2$O, 600 MHz).

Arbuzov phosphonation of the β-chloroamides **41a-e** proceeded smoothly, affording the phosphonate esters **39a-e** in moderate to good yields (Table 2). Several washings with hexane were required to remove the excess triethyl phosphite but, in general, the phosphonation reaction proved to be a very clean reaction. Compounds **39a**, **39b**, **39d,** and **39e** were all oils but the thiazole derivative **39c** crystallised out on the addition of hexane yielding crystals of high purity. Splitting of the signals due to coupling to ^{31}P can be observed in both the ^{1}H and ^{13}C spectra, even as far down the chain as the amide carbonyl signal.

Employing the variation of Giessman's method[54] described earlier, the phosphonate esters **39a-e** were hydrolysed to afford the disodium salts **40a-e** of the corresponding phosphonic acids. Purification of the salts was attempted using HP20 resin chromatography but this approach proved unsuccessful due to the high aqueous solubility of the sodium salts which precluded adequate retention by the stationary phase. Reverse-phase HPLC, eluting with water, was therefore used to purify the final products for full characterisation and bioassay. The absence of the ethyl ester signals in the ^{1}H NMR spectra of the disodium salts provided clear evidence of the success of the hydrolysis reaction.

The 1- and 2-D NMR spectra obtained for compound **40c** are shown in Figures 35-40 and were used to characterise this compound. The ^{1}H NMR spectrum (Figure 35) clearly shows the two aromatic and two methylene proton signals, with the complex splitting patterns of the methylene signals arising from their proximity to the ^{31}P nucleus. The downfield signal at 7.39 ppm was assigned to the 4'- proton on the basis of the expected deshielding by the adjacent nitrogen atom, and hence, the signal at 7.11 ppm was assigned to the 5'- proton. Coupling between these two protons and the 2- and 3-methylene protons is evident in the COSY spectrum (Figure 36). The amide proton signal could not be observed due to exchange of this proton with the D$_2$O solvent. The ^{13}C DEPT 135 spectrum (Figure 37) clearly shows the two methylene carbon nuclei while the absence of signals at 158.9 and 174.5 ppm in the DEPT spectrum permitted their assignment in the proton decoupled ^{13}C spectrum to the quaternary carbon nuclei. The splitting (J=130.5 Hz) of the signal at 24.3 ppm in the proton decoupled ^{13}C spectrum (Figure 38) permitted assignment of this signal to the 3-methylene carbon adjacent to the ^{31}P. Once this signal had been assigned, analysis of the HSQC spectrum (Figure 39) led to the assignment of the corresponding methylene proton signal at 1.73 ppm and, hence, the remaining signal at 2.65 ppm to the 2-methylene protons. Assignment of the ^{13}C signal at 136.8 ppm to the C-4' nucleus also reflects the deshielding by the adjacent nitrogen atom. The HMBC spectrum (Figure 40) shows correlation of C-2' to the 4'- and 5'-methine protons and

the carbonyl carbon to the 2- and 3-methylene protons, thus allowing assignment of the two remaining ^{13}C signals at 158.9 and 174.5 ppm to C-2' and the carbonyl carbon respectively. Doublets observed in the HMBC spectrum were attributed to one-bond couplings between carbon and proton nuclei and were identified by comparison with the HSQC spectrum. The ^{31}P spectrum of compound **40c** shows a single signal at 20.9 ppm, illustrating that complete hydrolysis of the phosphonate ester **39c** had taken place.
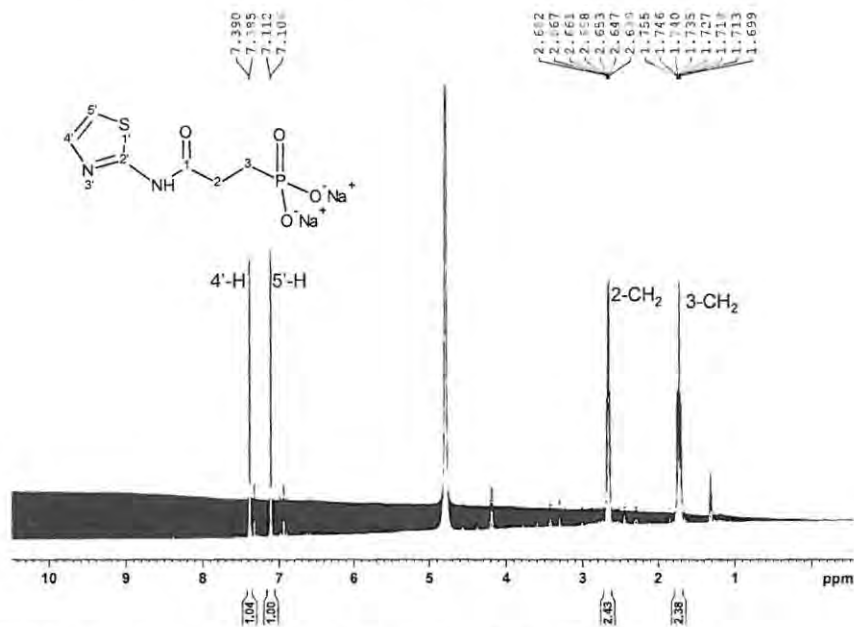
Figure 35. ^{1}H NMR spectrum of compound **40c** after HPLC (D$_2$O, 600 MHz).
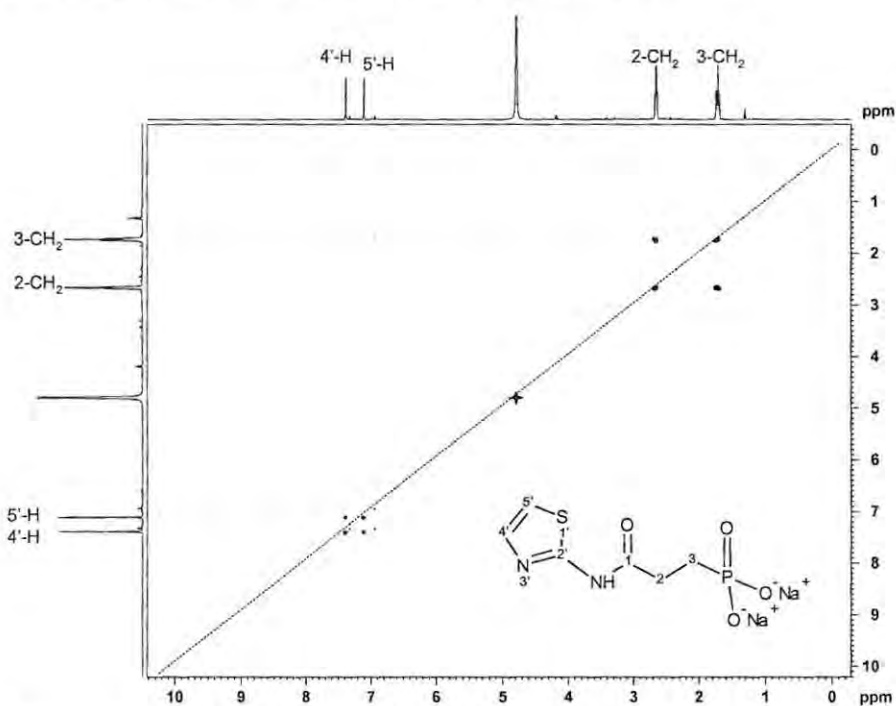
Figure 36. COSY NMR spectrum of compound **40c** after HPLC (D$_2$O, 600 MHz).
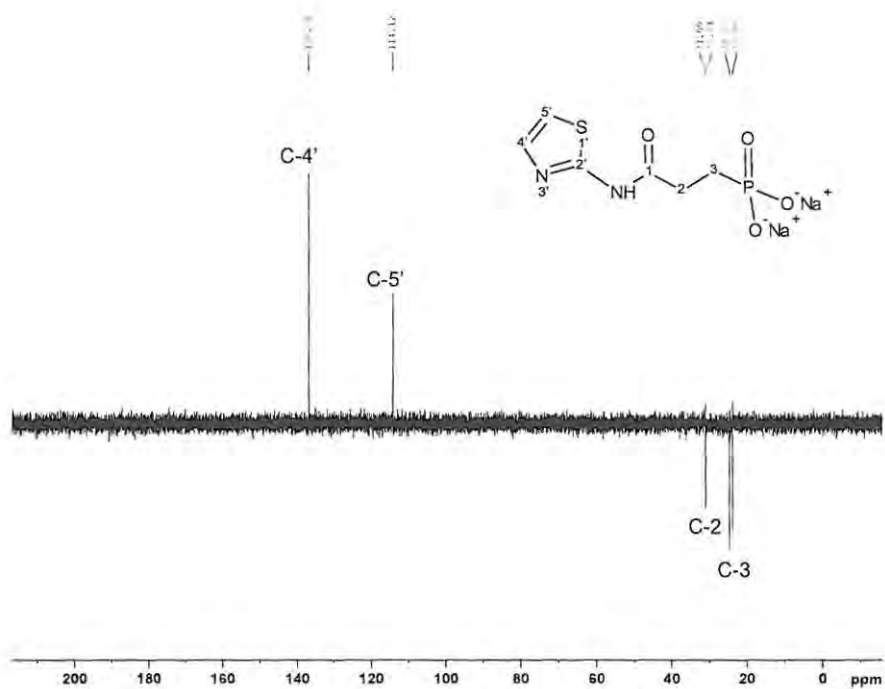
Figure 37. ^{13}C DEPT 135 NMR spectrum of compound **40c** after HPLC (D$_2$O, 150 MHz).
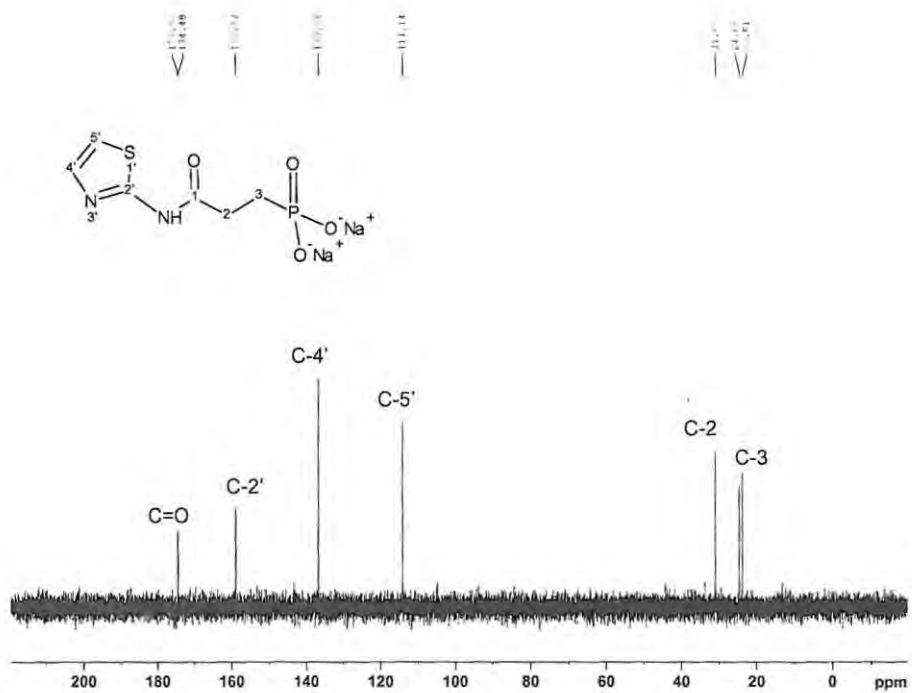
Figure 38. Proton decoupled ^{13}C NMR spectrum of compound **40c** after HPLC (D$_2$O, 150 MHz).

49
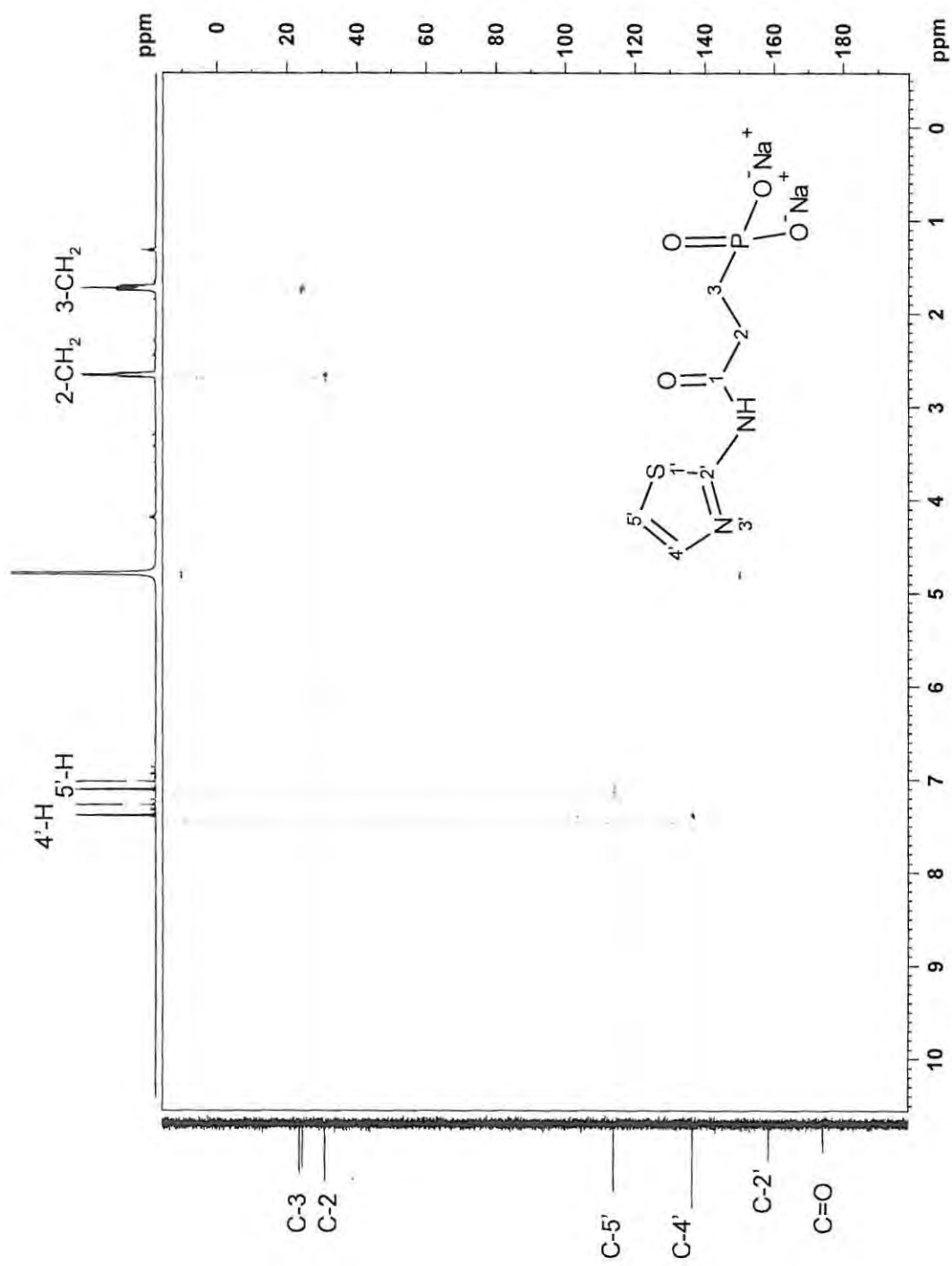
Figure 39. HSQC NMR spectrum of compound **40c** after HPLC (D₂O, 600 MHz).
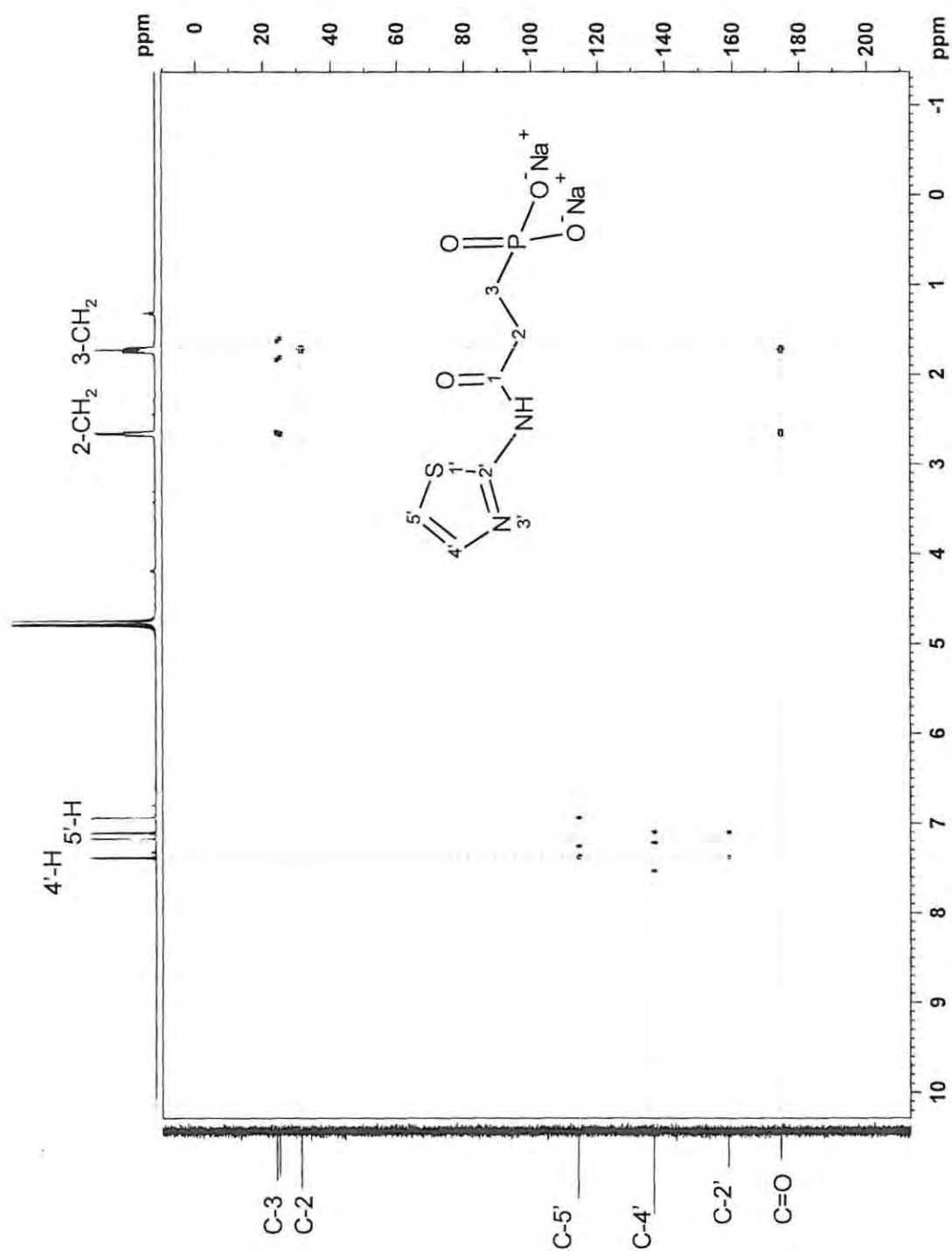
Figure 40. HMBC NMR spectrum of compound **40c** after HPLC (D₂O, 600 MHz).

51

For comparative purposes, the phosphonate ester **45** and the disodium phosphonate salt **46** were prepared from 3-chloropropiophenone **47** as illustrated in Scheme 3. Separation of the phosphonate ester **45** from the excess triethyl phosphite proved particularly difficult as the product was miscible with the hexane used for washing. The ^{31}P NMR spectrum indicated the presence of a mixture of phosphorus-containing products and column chromatography was used to purify the phosphonate ester **45**, subsequent hydrolysis of which afforded the disodium salt **46** which was included in the *Ec*DXR enzyme assays (Section 2.3.2.).
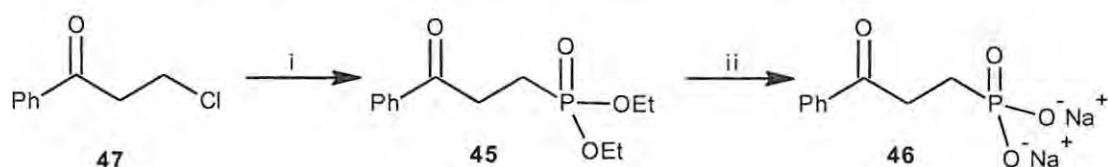
Scheme 3. Synthesis of the β-keto phosphonate **45** and corresponding disodium salt **46**.
Reagents and conditions:- (i) triethyl phosphite, 9 h, reflux (110 °C); (ii) TMSBr, DCM, overnight, r.t. and then 0.4M-NaOH.

2.2. Kinetic study of the reaction of phosphonate esters with bromotrimethylsilane

As indicated earlier, attempts to hydrolyse the phosphonate esters **35b**, **35c** and **35d** using the method of Kumar[81] were unsuccessful and the synthesis of the disodium salt **36e**, using the method of Geissmann,[54] appeared to require a longer reaction time than indicated in the literature. In order to elucidate the process, the kinetics of the consecutive trans-esterification reactions leading to the formation of the bis(silyl) ester **48** from the phosphonate ester **35e** (Scheme 4) were investigated. The bis(silyl) ester **48** hydrolyses readily to the phosphonic acid salt **36e** on treatment with aqueous NaOH. The use of bromotrimethylsilane (TMSBr) to form bis(silyl) esters was introduced by McKenna in 1977 and, while the reaction progress has been monitored previously by ^{1}H and ^{31}P NMR spectroscopy, no kinetic studies have been carried out.[82] Although some studies have employed ^{31}P NMR to investigate the kinetics of binding to a sorbent[84] and to measure the *in vivo* levels of phosphate metabolites,[85] the technique has not been widely used to study the kinetics of reactions in organic synthesis.
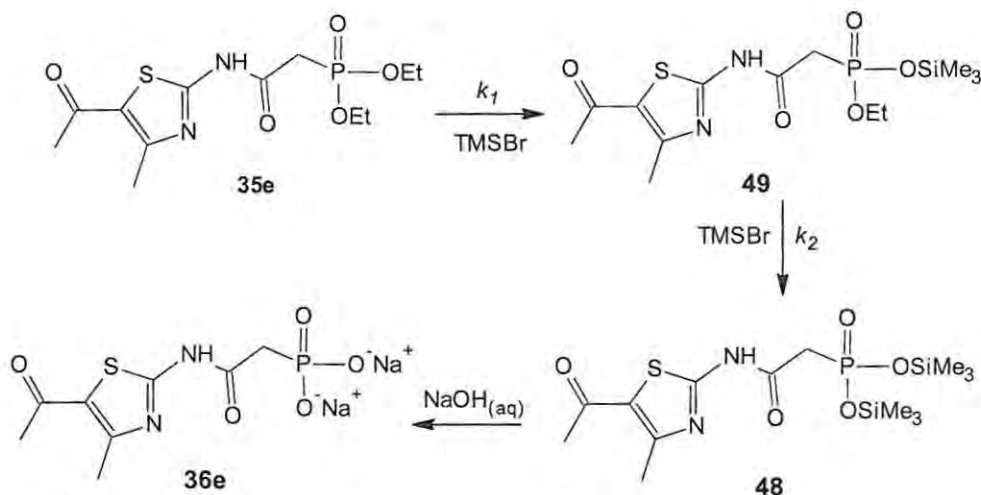
Scheme 4. Two-step reaction between the phosphonate ester **35e** and TMSBr.

Characterisation of the bis(trimethylsilyl)phosphonates **48** and **50** (Figure 41) was carried out in the reaction mixture due to the highly labile nature of these compounds. The NMR signals of these compounds were well resolved from those of the by-product ethyl bromide (EtBr), excess TMSBr and the 1,3,5-trimethoxybenzene (TMB) used as an internal standard. The NMR spectra used to characterise compound **48** are shown in Figures 42 and 43.
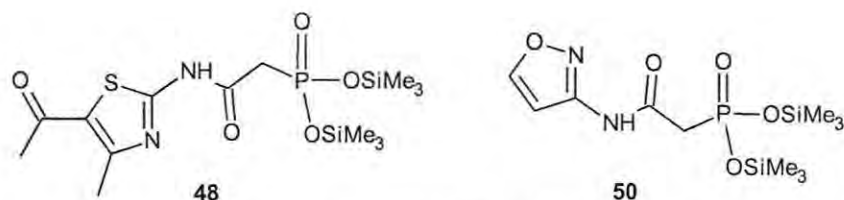
Figure 41. Structures of the bis(trimethylsilyl)phosphonates **48** and **50**.

The ^{1}H NMR spectrum of the bis(trimethylsilyl)phosphonate **48** (Figure 42) indicated the presence of the two trimethylsilyloxy groups, with the highly shielded protons resonating as a singlet at -0.03 ppm with a relative integral of 18. The signal due to excess TMSBr was identified as the broad singlet at 0.43 ppm. The characteristic doublet at 3.45 ppm was assigned to the methylene protons adjacent to the ^{31}P nucleus and the two singlets due to the TMB standard were identified by their 1:3 integral ratio and the deshielding of the methoxy protons. Assignment of the signals at 1.57 and 3.32 ppm to the EtBr byproduct was made by analysis of the COSY spectrum. The signals in the proton decoupled ^{13}C spectrum (Figure 43) were assigned following analysis of the multiplicity-edited HSQC spectrum and HMBC spectrum. The ^{31}P NMR spectrum showed a single signal at -0.69 ppm.
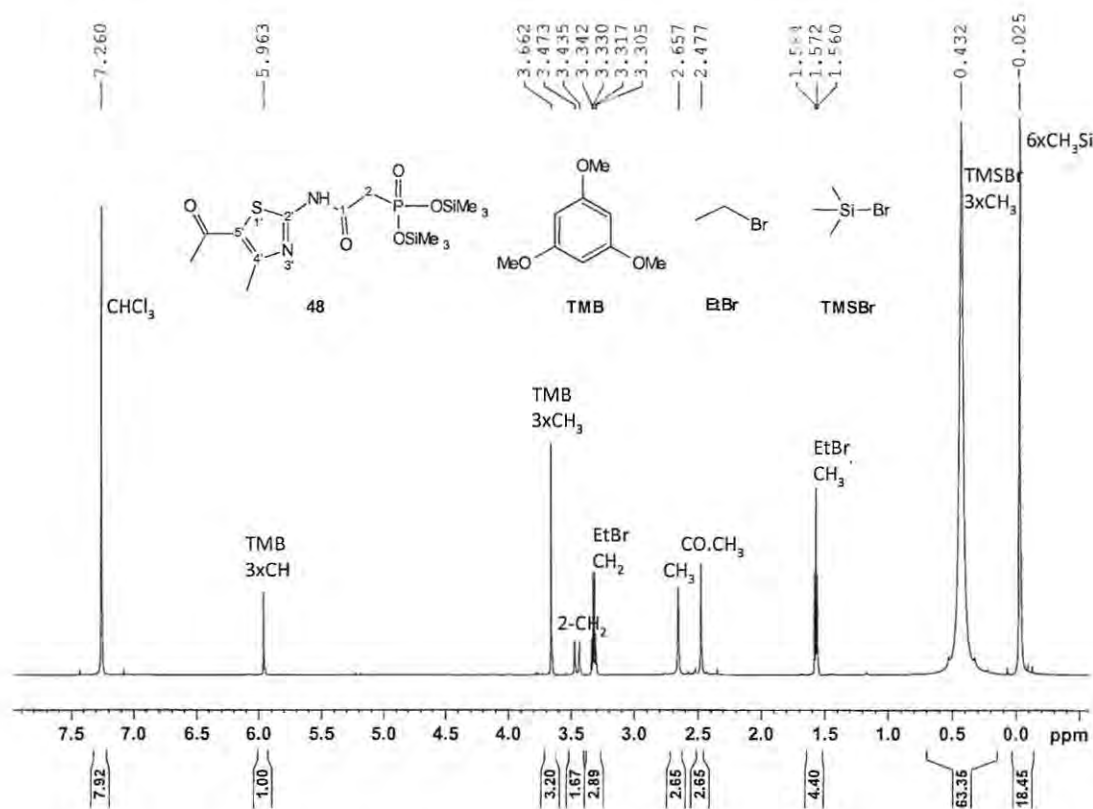
Figure 42. ^{1}H NMR spectrum of compound **48** together with EtBr, TMSBr and TMB (CDCl$_3$, 600 MHz).

54
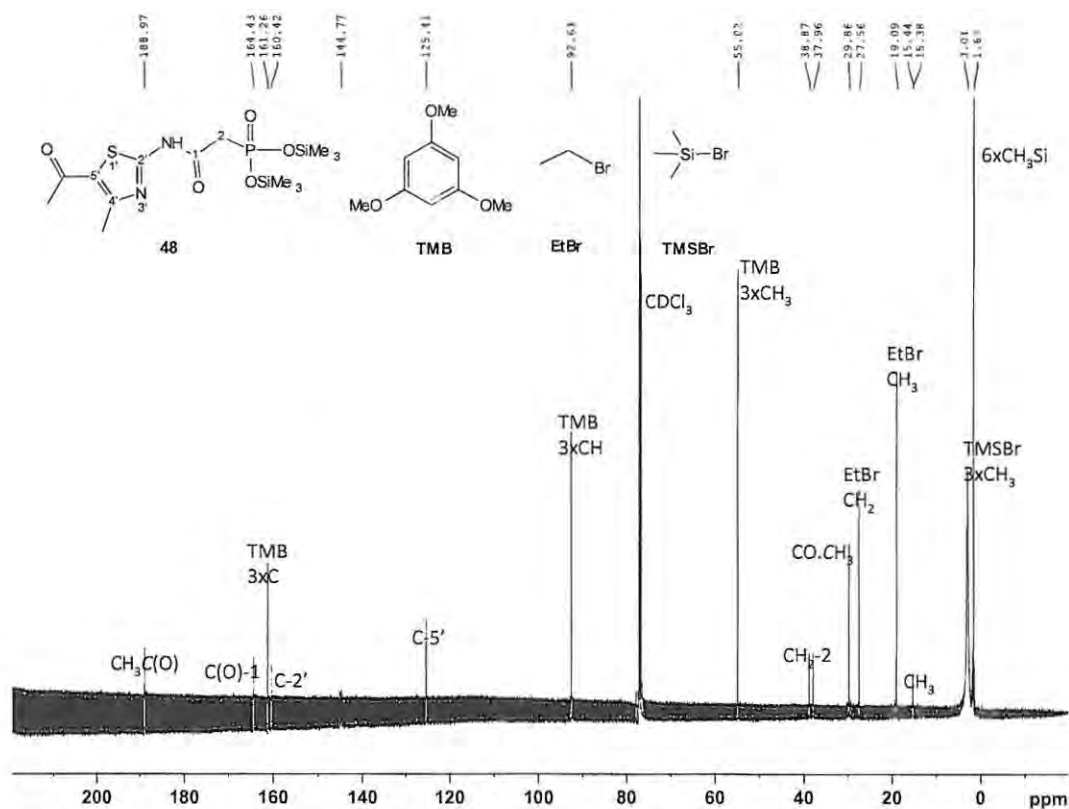
Figure 43. Proton decoupled ^{13}C NMR spectrum of compound **48** together with EtBr, TMSBr and TMB (CDCl$_3$, 150 MHz).

Conversion of the diethyl phosphonate **35e** to the bis(trimethylsilyl)phosphonate **48** involves the replacement of two ethyl groups by two trimethylsilyl groups, and is presumed[82] to follow a mechanism (Scheme 5) similar to that of the Arbuzov reaction.
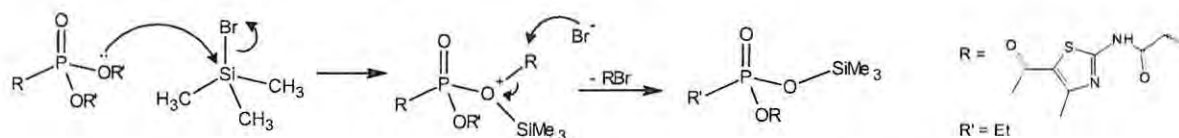
Scheme 5. Proposed mechanism for the reaction of a phosphonate diester with TMSBr.[82]

^{1}H and ^{31}P NMR spectra were obtained for solutions of the substrate **35e** in dry CDCl$_3$ at 90 s intervals during the course of the reaction, and the concentrations of the three phosphorus-containing species (**35e**, **49** and **48**) were determined from the relative integral data. The ^{31}P T$_1$ relaxation times for each of these species were measured to ensure that the recycle (acquisition + delay) time used (2.9 s) permitted complete relaxation of the phosphorus nuclei and, hence, that the integral data are proportional to their relative concentrations. Inverse-gated proton decoupling was also used. Concentrations of TMSBr were determined from the corresponding ^{1}H NMR spectra, using 1,3,5-trimethoxybenzene (TMB) as an internal standard.

55

The ^{31}P T_1 relaxation times and ^{31}P chemical shift values (relative to that of the phosphoric acid standard) are shown in Table 3. It is apparent, from the ^{31}P spectra illustrated in the stack-plot (Figure 44), that the signals of the three phosphorus nuclei are well resolved and that the phosphorus nuclei are progressively shielded as the ethyl groups are replaced by trimethylsilyl groups.

Table 3. ^{31}P Chemical shift values and T_1 relaxation times of phosphorus-containing species.

Compound	δ (ppm)	T_1 (ms)
35e	19.19	536
49	9.37	542
48	-0.69	553
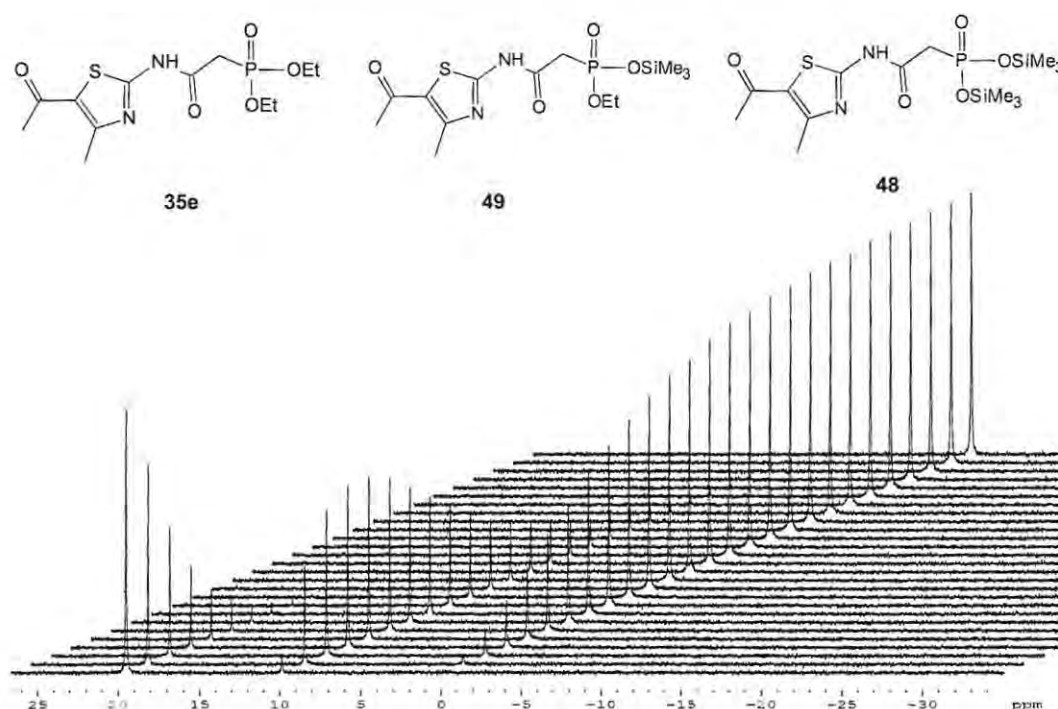
Figure 44. Stack-plot illustrating ^{31}P NMR signals for starting material **35e**, intermediate **49**, and product **48** at 30 min intervals, at 285 K.

A plot of the concentrations of the starting material **35e** and the mono- and disilylated derivatives (**49** and **48**, respectively) against time (Figure 45) reveals curves, which are typical of a two-step reaction in which $k_1 \approx k_2$.[86] As expected, the curve for the formation of the product **48** is sigmoidal in shape and has a point of inflexion at the time corresponding to $[49]_{max}$.[86] The

56

delay in the appearance of the product **48** (which is responsible for the sigmoidal curve) implies involvement of an intermediate in the reaction.[86]
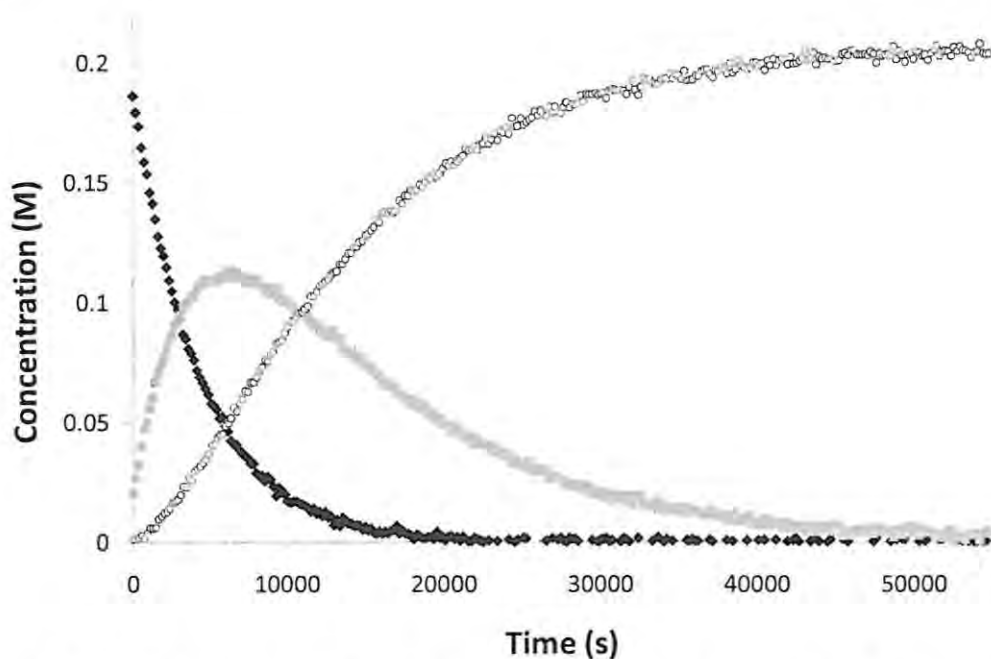
Figure 45. Graph of concentration against time for the reaction of phosphonate ester **35e** with TMSBr, at 283 K, showing the three phosphorus-containing species:- starting material **35e** as black diamonds; intermediate **49** as grey squares and product **48** as open circles.

Analysis of the first step, involving consumption of the starting material **35e**, indicated that it follows second-order rather than the simple first-order kinetics used in the treatment provided by Schmid and Sapunov.[86] Consequently, the reaction was attempted under pseudo first-order conditions by using 32 equivalents of TMSBr. Under these conditions, however, the ^{31}P signals broadened significantly and changes in the chemical shift values were noted. In order to avoid unnecessary complications (involving, perhaps, the formation of polysilylated products, such as compound **51**),[87] the well-resolved, second-order data were used.
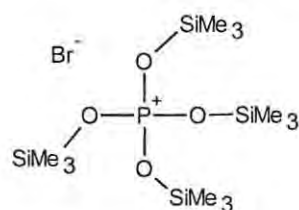
51

Frost and Schwemer,[88] have integrated the differential rate equations for competitive consecutive second-order reactions based on very similar reactions, viz., the saponification of ethyl adipate and ethyl succinate, and their treatment was extended into a computer

57

programme by Burkhard.[89] Unfortunately, these approaches only apply to the use of stoichiometrically equivalent amounts of the two reactants. However, the system we examined involves the reaction between the phosphonate ester **35e** and four equivalents of TMSBr and our analysis has been based on a consideration of two, separate, second-order reactions of the general form:-

$$A + B \rightarrow P$$
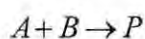
The rate of such a reaction is given by equation 1 in which k is the second-order rate constant:-

$$\frac{-d[A]}{dt} = k[A][B] \qquad \text{Eqn. 1}$$

When the starting concentrations $[A]_o$ and $[B]_o$ of the two reactants are different, the variable x is used such that $[A]_o - x = [A]$ and $[B]_o - x = [B]$, and equation 1 becomes:-

$$\frac{dx}{([A]_o - x)([B]_o - x)} = kdt \qquad \text{Eqn. 2}$$

After partial fraction expansion and integration, equation 2 becomes:-

$$\frac{1}{[B]_o - [A]_o} \ln \frac{[A]_o - x}{[B]_o - x} = kt + C \qquad \text{Eqn. 3}$$

where $C = \dfrac{1}{[B]_o - [A]_o} \ln \dfrac{[A]_o}{[B]_o}$ when $x = 0$ and $t = 0$

$$\ln \frac{[B]_o[A]}{[A]_o[B]} = kt([B]_o - [A]_o) \qquad \text{Eqn. 4}$$

As the reactant concentrations [A] and [B] can be measured using the NMR integral data, equation 4 (developed by Keusch),[90] was used to calculate the rate constants, k_1 and k_2 for the first and second steps respectively. For the first step, A_o = initial concentration of the substrate **35e**, while B_o = initial concentration of TMSBr. $\ln(B_o A / A_o B)$ was plotted against time and the gradient for the initial linear portion of the graph was divided by $(B_o - A_o)$ to afford the rate constant k_1 for the first step (**35e** → **49**). The second-order component of the second step (**49** → **48**) occurs upon complete consumption of the substrate **35e**, at which stage the only reaction occurring involves conversion of the monosilylated intermediate **49** to the product **48**. At this point, A_o = [49] and B_o = [TMSBr] and equation 4 was again used to determine the

second-order rate constant for the second step, k_2. The linearity of the second-order kinetic plots confirms that both steps are second-order – observations which are consistent with the mechanism proposed by McKenna (Scheme 5).[82]

Reactions were conducted at various temperatures between 283 and 303 K and Arrhenius plots for the first (**35e** → **49**) and second steps (**49** → **48**) permitted evaluation of the respective activation energies E_a using equation 5 (Table 4). The Eyring equation (equation 6) provides an alternate treatment of the activation parameters,[91] and Eyring plots (Figure 46) permitted direct evaluation of the activation parameters $\Delta H^{\ddagger}$ and $\Delta S^{\ddagger}$ (Table 4) and, thence, using equation 7, $\Delta G^{\ddagger}$ at 298.15 K. Uncertainties were calculated from the respective standard error values of the slope and intercept for each graph.

$$k = Ae^{-Ea/RT}$$

Eqn. 5

$$\ln\frac{k}{T} = \frac{\Delta H^{\ne}}{RT} + \ln\frac{k_B}{h} + \frac{\Delta S^{\ne}}{R}$$

Eqn. 6

$$\Delta G^{\ne} = \Delta H^{\ne} - T\Delta S^{\ne}$$

Eqn. 7
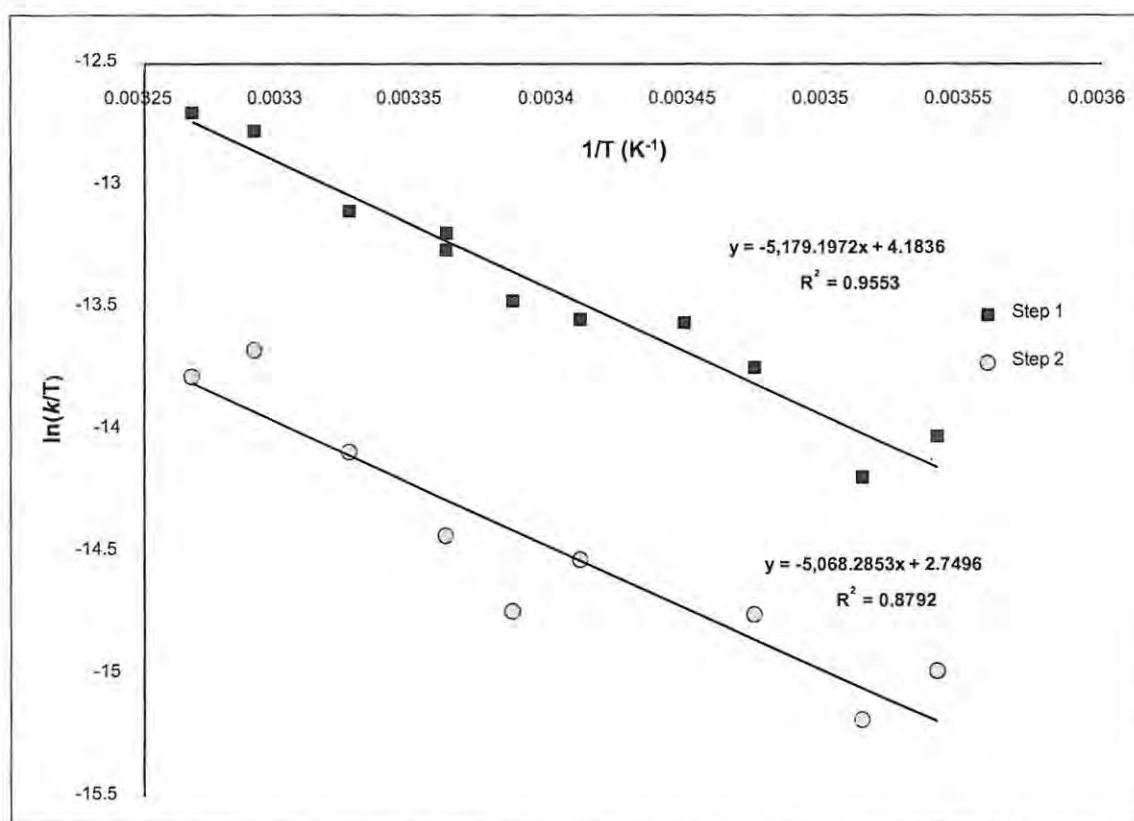
Figure 46. Eyring plot of $\ln(k/T)$ against $1/T$ (K^{-1}) for step 1 (shown in black squares) and step 2 (shown in grey circles) for the reaction between **35e** and TMSBr.

59

Table 4. Kinetic parameters of the reaction between phosphonate ester **35e** and TMSBr.

Parameter	Calculated value (kcal.mol⁻¹)	
	Step 1	Step 2
E_a	11.63 ± 0.80	10.7 ± 1.4
$\Delta H^{\ddagger}$	10.29 ± 0.74	10.1 ± 1.4
$\Delta S^{\ddagger}$	-38.9 ± 2.5[a]	-41.8 ± 4.8[a]
$\Delta G^{\ddagger}$	21.9 ± 1.5	22.5 ± 1.6

[a] cal.K^{-1}.mol⁻¹

A computational method was then employed to refine the estimates of the activation parameters obtained using equation 4 and improve the fit with the experimental data. Using the values of k_1 and k_2 calculated by the above method as initial estimates, the concentrations of each of the species **35e**, **49** and **48** were predicted at one second intervals from the second-order rate equation (equation 1). Building on a method used in earlier work,[92] k_1 and k_2 were varied independently within a range of ± 50% of their initial values. For each pair of k_1 and k_2, the resultant curve of the calculated concentrations was compared with the experimental values and an R^2 value was calculated. The values of k_1 and k_2 giving the minimum R^2 value were easily identified and were considered to correspond to the best fit with the experimental data. These calculations were carried out using a specially written computer programme (Supplementary Data).[93] For each experiment, graphs were plotted (Supplementary Data) comparing the experimental data with those calculated using:- a) the original k_1 and k_2 obtained from equation 4; and b) the optimised k_1 and k_2 calculated using the above method (Table 5). An example of the distinct improvement in the fit with the experimental data using the optimised k_1 and k_2 values is shown in Figure 47 for the experiment at 297 K. The linearity of the Arrhenius and Eyring (Figure 48) plots is also improved, thus giving activation parameters (Table 6) with smaller uncertainty values, particularly for the second step of the reaction. As expected for a bimolecular reaction, $\Delta S^{\ddagger}$ is negative due to the decrease in entropy when **35e** and TMSBr combine.

Table 5. Values of k_1 and k_2 obtained at different temperatures using the two methods.

T (K)	Equation 4		Model	
	k_1 (L.mol^{-1}.s^{-1})	k_2 (L.mol^{-1}.s^{-1})	k_1 (L.mol^{-1}.s^{-1})	k_2 (L.mol^{-1}.s^{-1})
282.46	-2.290E-04	-8.747E-05	-1.535E-04	-6.735E-05
282.46	-1.520E-04	—^{a}	-1.231E-04	—^{a}
284.61	-1.953E-04	-7.221E-05	-1.875E-04	-8.232E-05
287.83	-3.091E-04	-1.123E-04	-2.906E-04	-1.269E-04
289.98	-3.742E-04	-2.896E-04	-3.330E-04	-1.506E-04
293.20	-3.835E-04	-1.433E-04	-3.682E-04	-1.562E-04
295.35	-4.164E-04	-1.169E-04	-4.080E-04	-1.590E-04
297.49	-5.545E-04	-1.604E-04	-5.213E-04	-2.181E-04
297.49	-5.178E-04	-8.373E-05	-4.556E-04	-1.256E-04
300.71	-6.129E-04	-2.285E-04	-5.884E-04	-2.582E-04
303.93	-8.601E-04	-3.500E-04	-8.515E-04	-3.955E-04
306.08	-9.348E-04	-3.165E-04	-8.881E-04	-3.703E-04

^{a} The experiment at 282.46 K was interrupted by a power failure so only k_1 could be calculated.
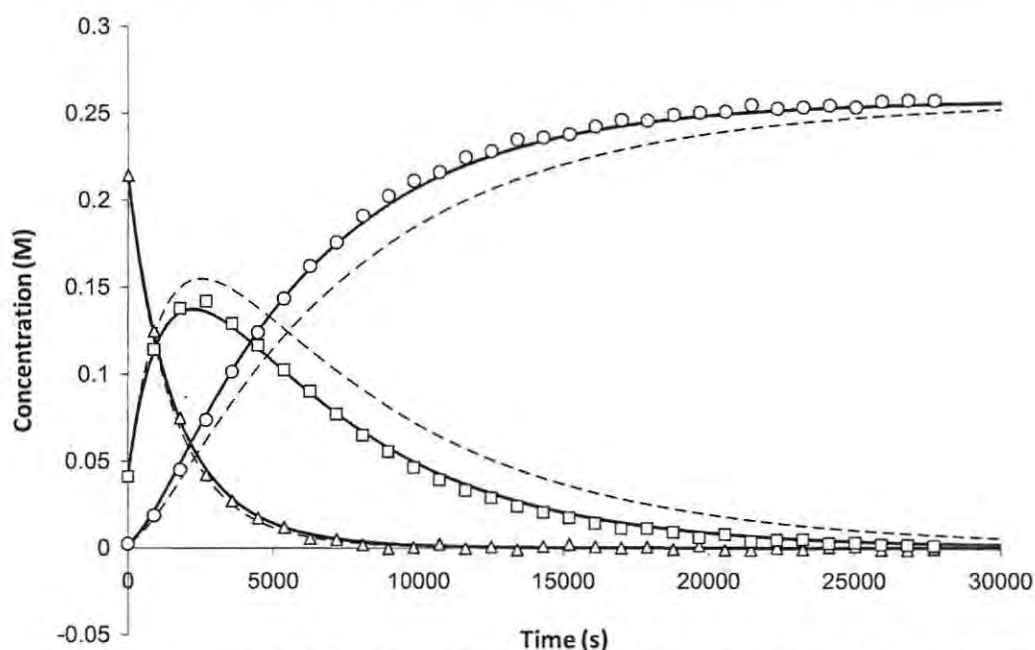
Figure 47. Plots of concentration against time for the reaction of phosphonate ester **35e** with TMSBr at 297 K, showing the three phosphorus-containing species:- starting material **35e** as open triangles; intermediate **49** as open squares and product **48** as open circles. The fit of the experimental data with the values of k_1 and k_2 obtained from equation 4 is shown by dashed lines. The significantly improved fit of the experimental data with the computationally optimised k_1 and k_2 values is shown by solid lines. For clarity, only a limited number of points are plotted for each curve.

61

Table 6. Kinetic parameters of the reaction between phosphonate ester **35e** and TMSBr using optimised k_1 and k_2 values.

Parameter	Calculated value (kcal.mol^{-1})	
	Step 1	Step 2
E_a	13.07 ± 0.76	12.44 ± 0.81
$\Delta H^{\ddagger}$	11.67 ± 0.64	11.86 ± 0.81
$\Delta S^{\ddagger}$	-34.4 ± 2.2^{a}	-35.4 ± 2.7^{a}
$\Delta G^{\ddagger}$	21.9 ± 1.3	22.4 ± 1.6

^{a} cal.K^{-1}.mol^{-1}
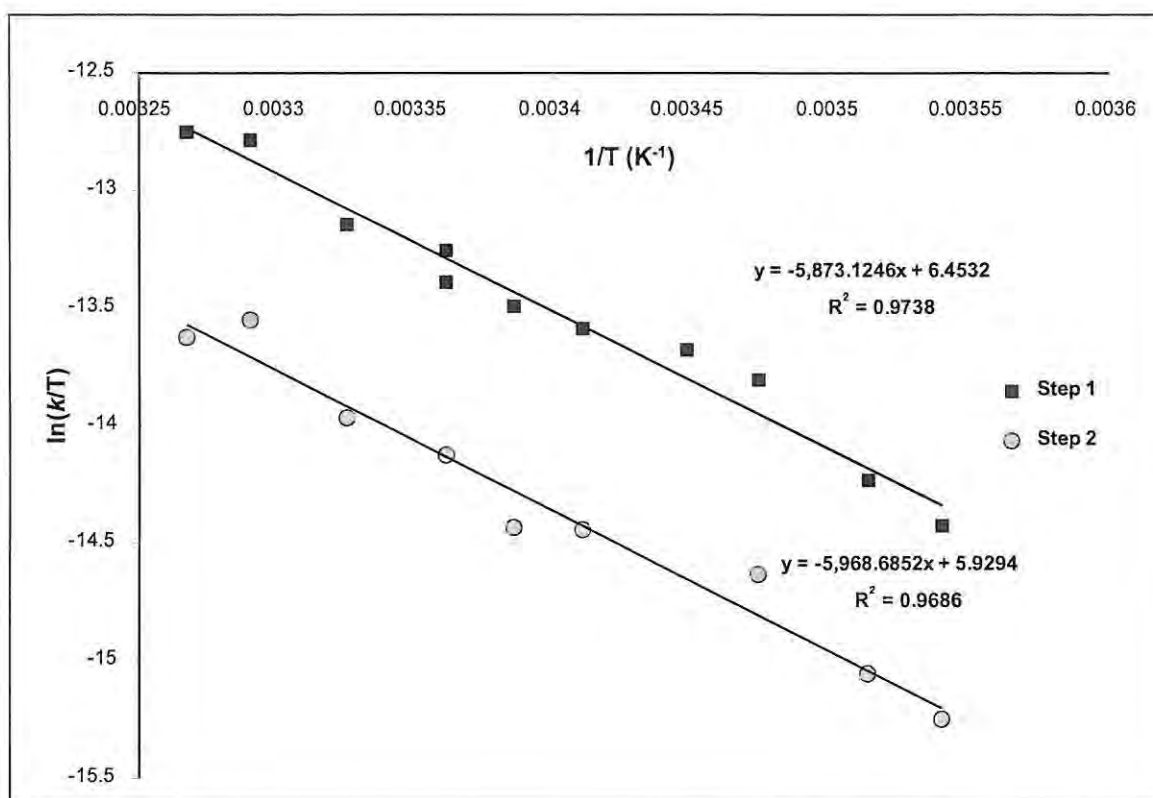
Figure 48. Eyring plot of ln(k/T) against 1/T (K^{-1}) for step 1 (shown in black squares) and step 2 (shown in grey circles) for the reaction between **35e** and TMSBr using optimised k_1 and k_2 values.

These results show that the second-order rate equation gives an accurate description of each step of the reaction, supporting the mechanism proposed by McKenna[82] (Scheme 5). The initial estimates of k_1 and k_2, calculated using equation 4, fit well with the experimental data but only for the initial parts of the two reactions **35e** → **49** and **49** → **48** as only the initial linear portions of the graphs were used to calculate k_1 and k_2. The optimised values of k_1 and

k_2 provided by the model, however, fit the experimental data much better for the entire course of the transformation:- **35e → 49 → 48**. This kinetic study has thus illustrated the use of both an approximate and a more accurate method for the analysis of second-order kinetic data which does not require equimolar amounts of the starting materials or pseudo first-order conditions. These analyses have provided rate constants and activation parameters for each of the consecutive reactions. In addition, the study has highlighted the value of ^{31}P NMR spectroscopy for kinetic studies with the advantages of uncluttered spectra and short relaxation times enabling accurate determination of the concentrations of the species involved. The results of this kinetic study have been accepted for publication.[94]

2.3. Enzyme-binding and inhibition studies

2.3.1. Saturation transfer difference (STD) NMR experiments

The saturation transfer difference (STD) experiment[95] is based on the nuclear Overhauser effect (NOE) and uses the difference between two spectra to determine whether a small molecule (ligand) binds to a protein.[96] Provided that their ^{1}H NMR spectra are sufficiently different, a set of 5 to 7 ligands can be studied in one experiment and so the STD experiment can be used as a screening assay for potential drug molecules.[95] To obtain the STD spectrum, the protein is irradiated at a frequency at which the ligands do not absorb – usually the upfield region of the protein spectrum. In large molecules such as proteins, fast spin diffusion leads to rapid saturation of the whole protein due to an intramolecular NOE effect.[96] If a ligand in the set binds to the protein, intermolecular spin diffusion results in the ligand resonances becoming saturated as well. The second, reference, spectrum is obtained by irradiating the protein-ligand mixture at a frequency at which none of the ligand or protein nuclei resonate (off-resonance irradiation) and therefore the signal intensities remain unchanged as all species are equally saturated.[96] Subtraction of the two spectra yields a spectrum in which only the signals whose intensities have changed are present, thus enabling identification of the ligands which bind to the protein.[96] Differences between the two spectra due to temperature differences or magnetic field homogeneity are greatly reduced by phase cycling between the on- and off-resonances.[96] According to Mayer and Meyer, the STD NMR method can be applied to ligands which bind to a protein with dissociation constants K_D between 10^{-3} and 10^{-8}.[95] The STD technique can also be extended to enable identification of the ligand moieties which interact with the protein as the degree of saturation of the ligand resonances is proportional to their distance from the protons in the protein.[96,97]

In order to confirm that the STD pulse programme and parameters were set up correctly and to determine whether the assay could be carried out in H_2O rather than D_2O, an STD experiment was carried out using bovine serum albumin (BSA) as the protein and glucose and L-tryptophan as the ligands. This standard STD assay is expected to show that L-tryptophan binds to the protein[98] whilst glucose does not.[99] As shown in Figure 49, the results of this STD experiment carried out in H_2O suggest that both glucose and L-tryptophan bind to BSA as signals for both ligands could be observed in the STD difference spectrum.
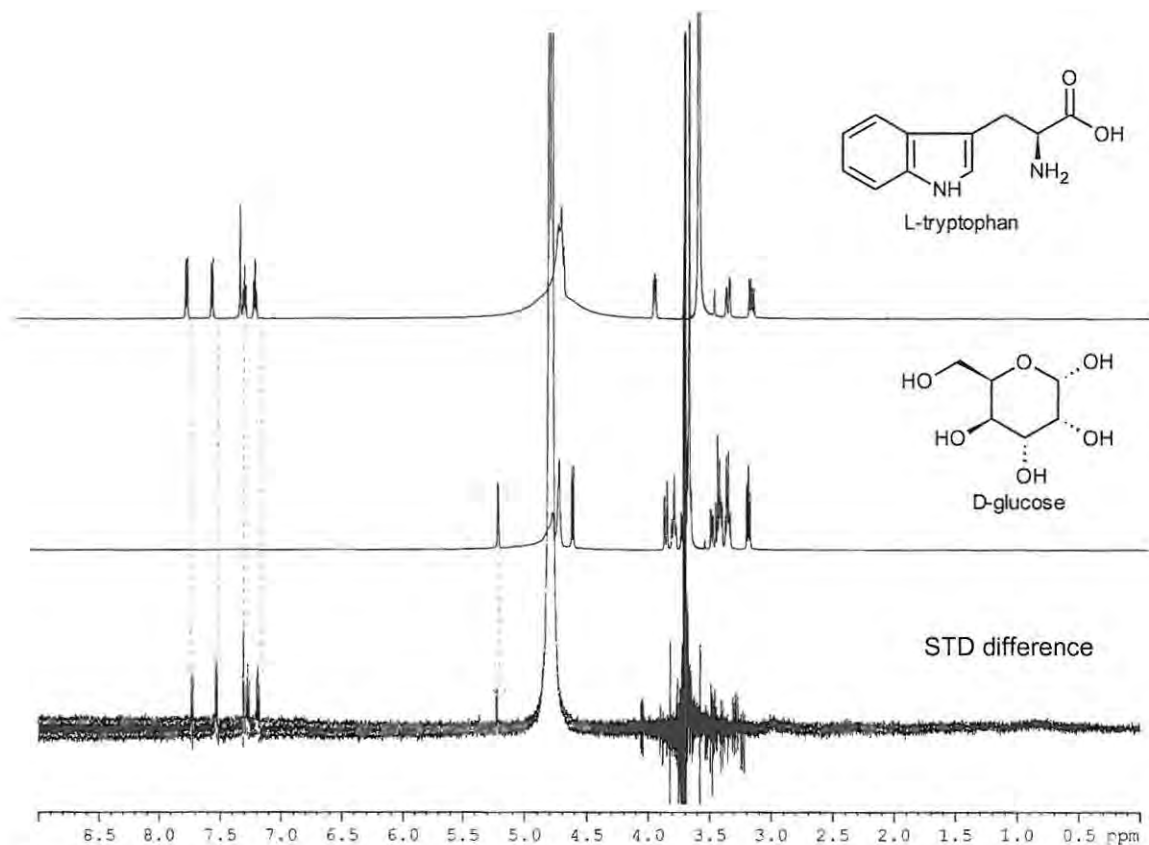
Figure 49. BSA STD difference spectrum (bottom) resulting from an STD experiment carried out in H_2O with ^1H NMR spectra of ligands glucose (middle) and *L*-tryptophan (top), showing the presence of both glucose and *L*-tryptophan signals in the difference spectrum (dashed arrows).

These results indicate that H_2O is not a suitable solvent in which to carry out the STD experiments. This could be due to saturation transfer between the protein and unbound ligand mediated by intervening solvent protons. This problem would be avoided if D_2O was used as the solvent. The use of D_2O, however, means that it is necessary to freeze-dry the protein solution and re-suspend it in D_2O, a process which may result in some denaturation of the protein. The experiment was therefore repeated using D_2O as the solvent and the resultant difference spectrum is shown in Figure 50.

The glucose signals in this second experiment are much lower than those observed in H_2O. The fact that weak signals corresponding to the glucose resonances can still be seen may be due to the presence of a low concentration of HOD or H_2O in the D_2O, thus permitting the transfer of magnetisation to the ligand. Alternatively, there may be a weak interaction between glucose and BSA.
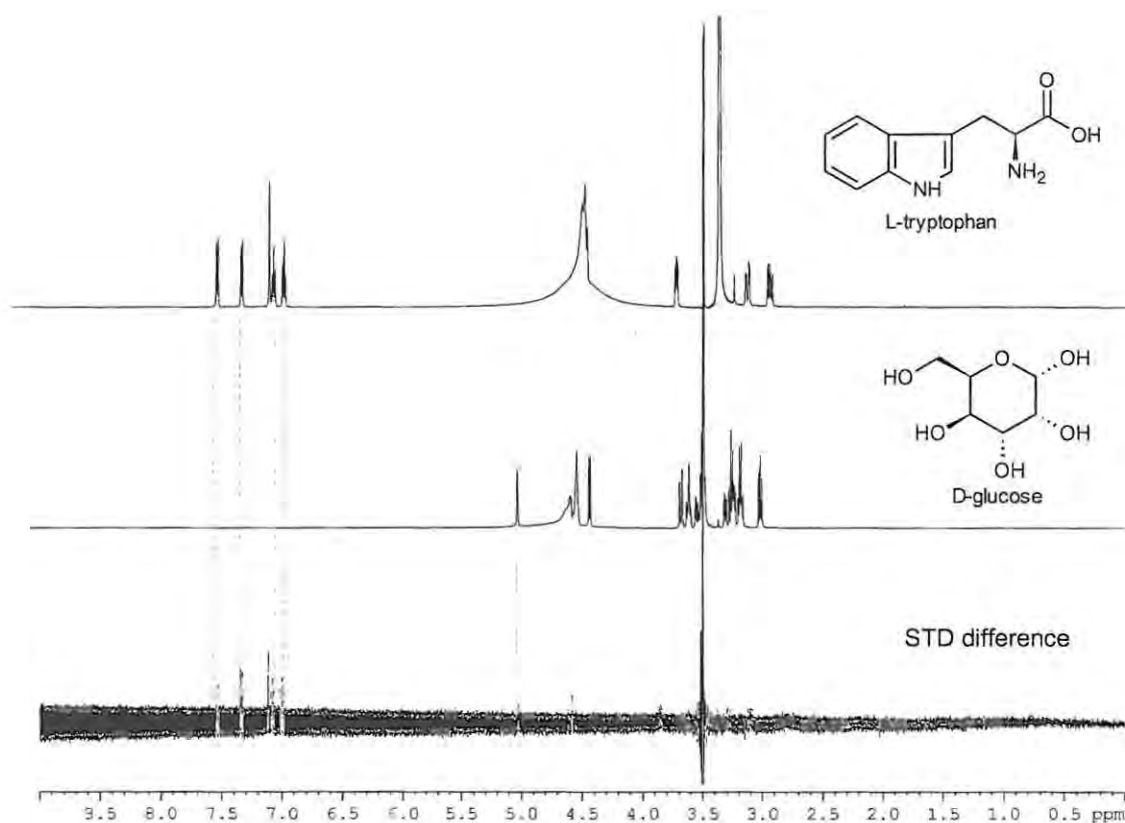
Figure 50. BSA STD difference spectrum (bottom) resulting from an STD experiment carried out in D_2O with ^1H NMR spectra of ligands glucose (middle) and *L*-tryptophan (top), showing the presence of *L*-tryptophan signals in the difference spectrum (dashed arrows) and a very weak glucose signal (dotted arrow).

The use of STD NMR has not been very widely reported, but the examples in the literature appear to be inconclusive as to which solvent should be used. Ji and co-workers carried out successful STD NMR studies in an aqueous sodium phosphate buffer, with 10% D_2O added for the frequency lock, and used a WATERGATE (water suppression by gradient-tailored excitation) pulse sequence to suppress the water signal.[98] Mayer and Meyer carried out their experiments in D_2O but claim that the STD experiment works just as well in H_2O.[95] A comparison between spectra obtained in H_2O and D_2O was carried out by Mayer and James for paromycin binding to RNA targets.[100] It was found that the STD signal was smaller for spectra recorded in H_2O, as compared to D_2O, and rapidly reached its maximum intensity of about 40% as the saturation transfer time was increased. In contrast, the signal intensity of spectra recorded in D_2O increased steadily as the saturation transfer time was increased. These observations have been attributed to the faster longitudinal relaxation rate of the receptor protein in H_2O, due, in turn, to the abundant unsaturated water protons which readily accept the magnetisation. Mayer and James have therefore concluded that, although the STD

66

experiment can be carried out in H_2O, the use of D_2O is preferable, especially if the signal intensities are low.[100]

The ligands to be tested for binding to *Ec*DXR were divided into four sets (**35a-e**, **36b-e**, **39a-e** and **40b-e** + **36a**) and an STD experiment was carried out for each set. In each experiment, *Ec*DXR in sodium phosphate buffer was freeze-dried and re-suspended in D_2O and the set of ligands was dissolved in the protein solution to give a 1:40 protein to ligand molar ratio (except for the set **35a-e** which was prepared with a 1:80 protein to ligand molar ratio). For the first group of ligands, the STD difference spectrum showed very weak signals and increasing the number of scans resulted in little improvement. Although the *Ec*DXR concentration was relatively low for the first experiment (4.6 μM), the STD experiment is one of the most sensitive ligand-detected screening methods and protein concentrations as low as 100 nM[96] and even 1 nM[95] have been reported. A possible reason for the lack of sensitivity, despite the large number of scans, could be the length of the protein pre-saturation time. In this experiment, only 4 Gaussian-shaped pulses were applied whilst the use of 40,[95] and even 58, has been reported.[98] If the protein was not fully saturated by the on-resonance pulse, spin diffusion would lead to further reduction of the saturation, resulting in very little being transferred to the binding ligands. An alternative explanation for the weak signals could be competitive binding between the ligands in the set due to their similar chemical properties, thus resulting in decreased saturation transfer to all of the ligands.

The parameters used in the STD experiment were therefore optimised in terms of the number of Gaussian pre-saturation pulses, the power used for saturation and the number of scans, and it was found that the sensitivity of the experiment improved significantly when 40 Gaussian-shaped pre-saturation pulses were applied at an attenuation of power of only 40 dB. Once the experiment had been optimised, STD experiments were carried out on the four sets of ligands using *Ec*DXR at a concentration of *ca.* 15 μM. The resulting STD spectra and spectra of the individual ligands are shown as stacked plots in Figures 51-54. The underlying protein spectrum is visible in Figure 51 as, during the STD experiment on the first set, a spin-lock filter was not used. All other STD experiments included a spin-lock filter.
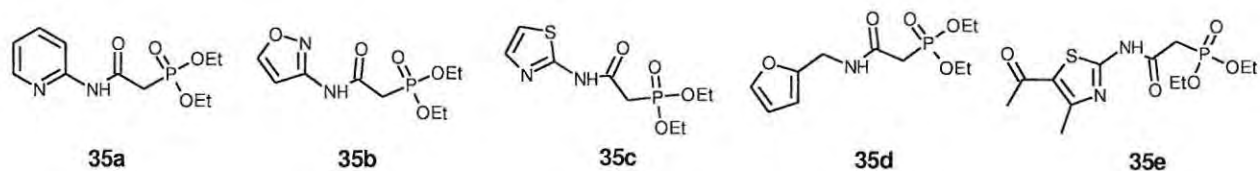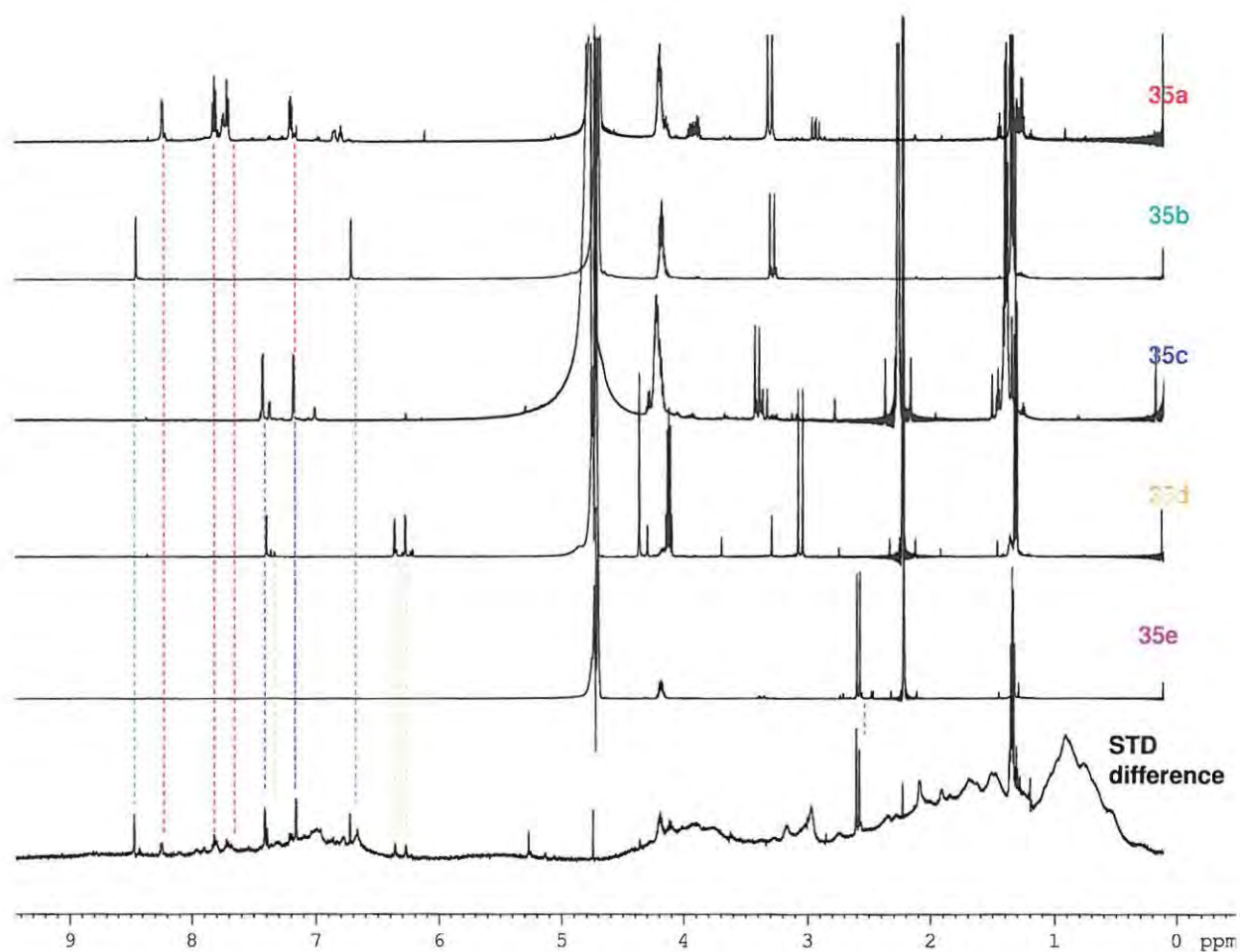
Figure 51. *Ec*DXR STD difference spectrum for the first set of ligands (**35a-e**) showing correlations between characteristic ligand signals and signals in the STD difference spectrum (coloured dashed lines). Individual ligand spectra in D$_2$O are shown from top to bottom:- **35a**, **35b**, **35c**, **35d** and **35e**.
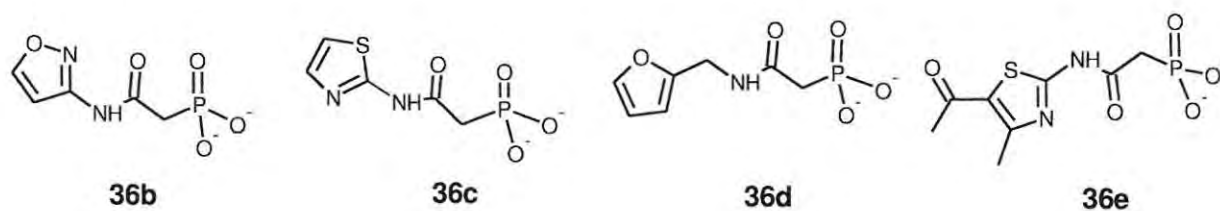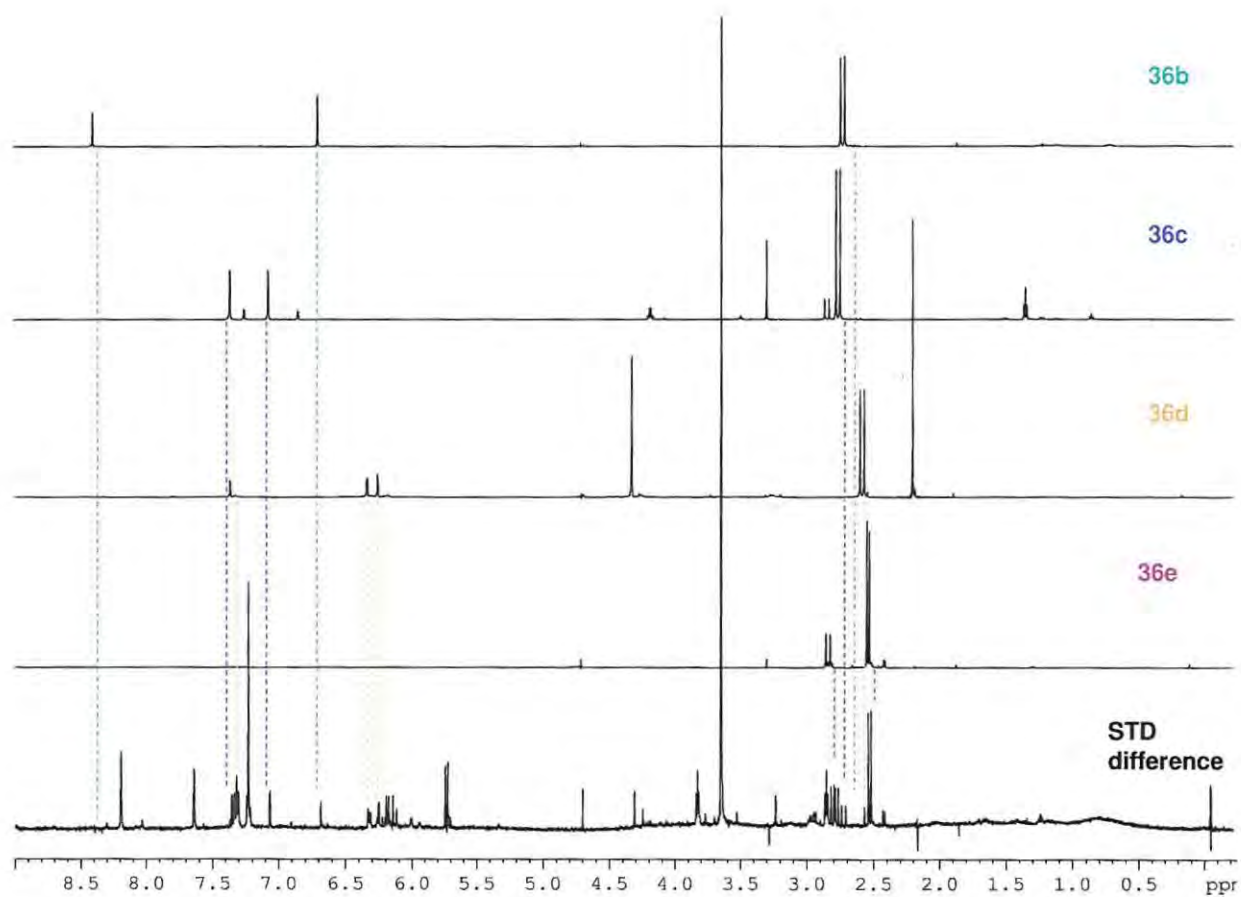
Figure 52. *Ec*DXR STD difference spectrum for the second set of ligands (**36b-e**) showing correlations between characteristic ligand signals and signals in the STD difference spectrum (coloured dashed lines). Individual ligand spectra in D₂O are shown from top to bottom:- **36b**, **36c**, **36d** and **36e**.
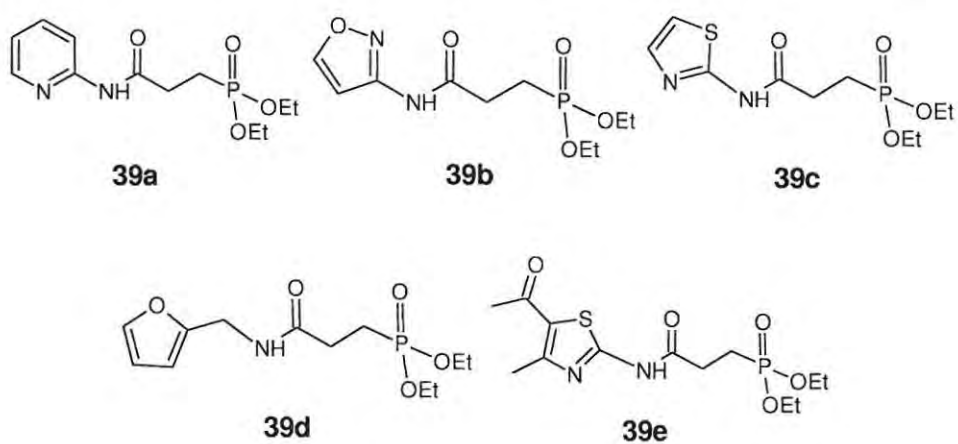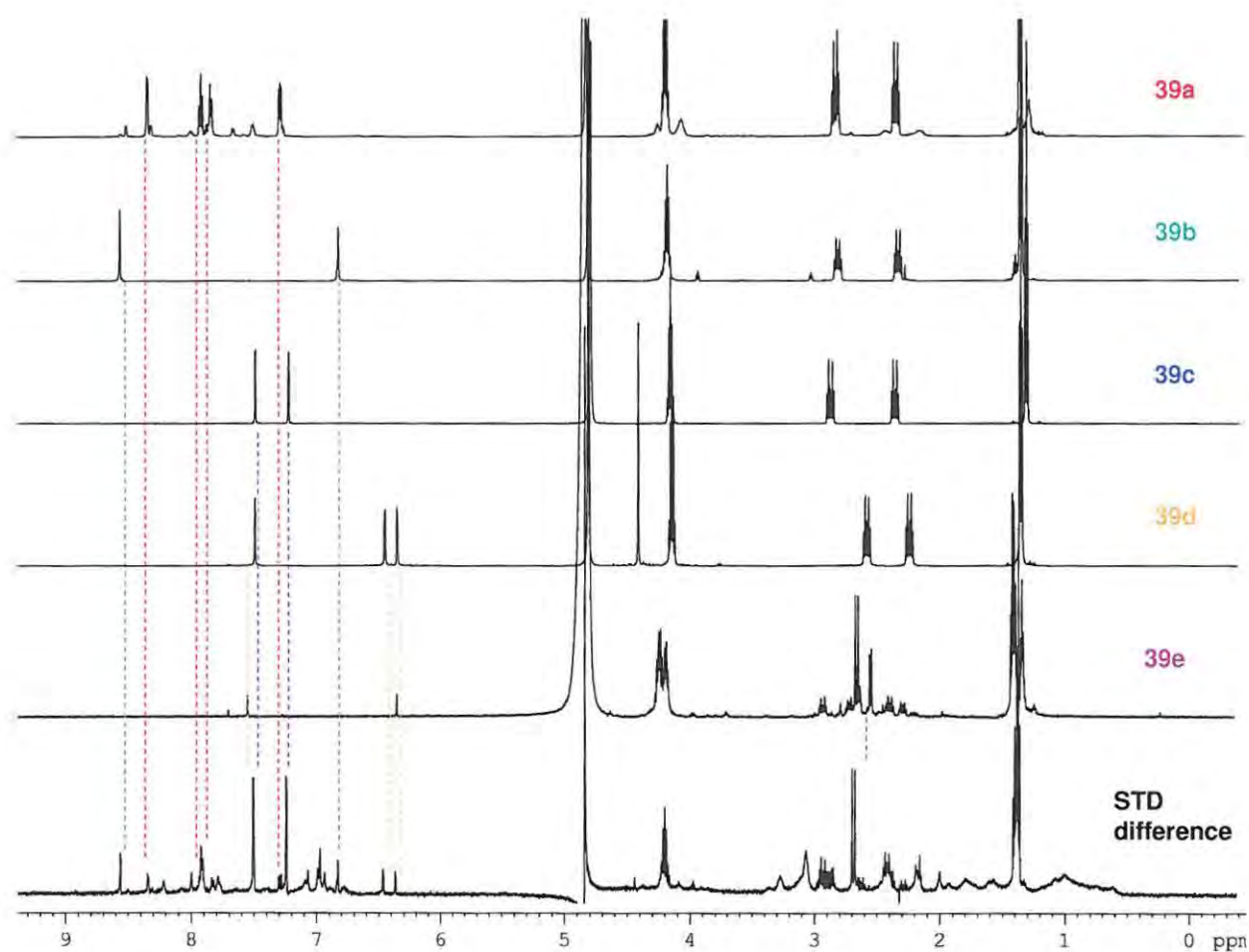
Figure 53. *Ec*DXR STD difference spectrum for the third set of ligands (**39a-e**) showing correlations between characteristic ligand signals and signals in the STD difference spectrum (coloured dashed lines). Individual ligand spectra in D₂O are shown from top to bottom:- **39a**, **39b**, **39c**, **39d** and **39e**.
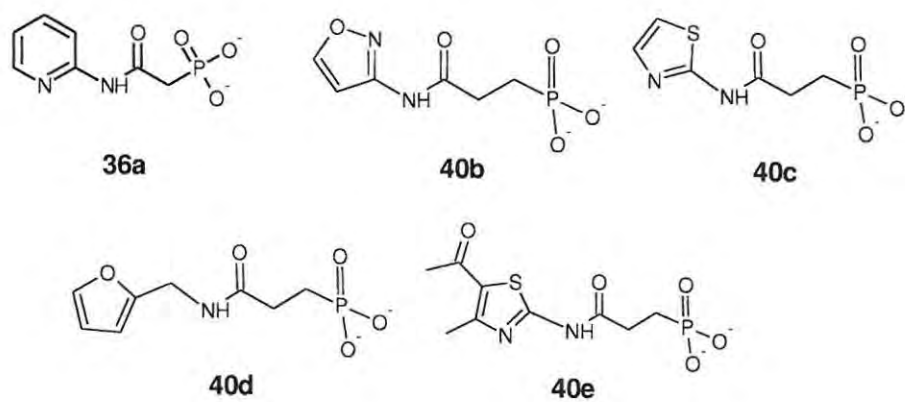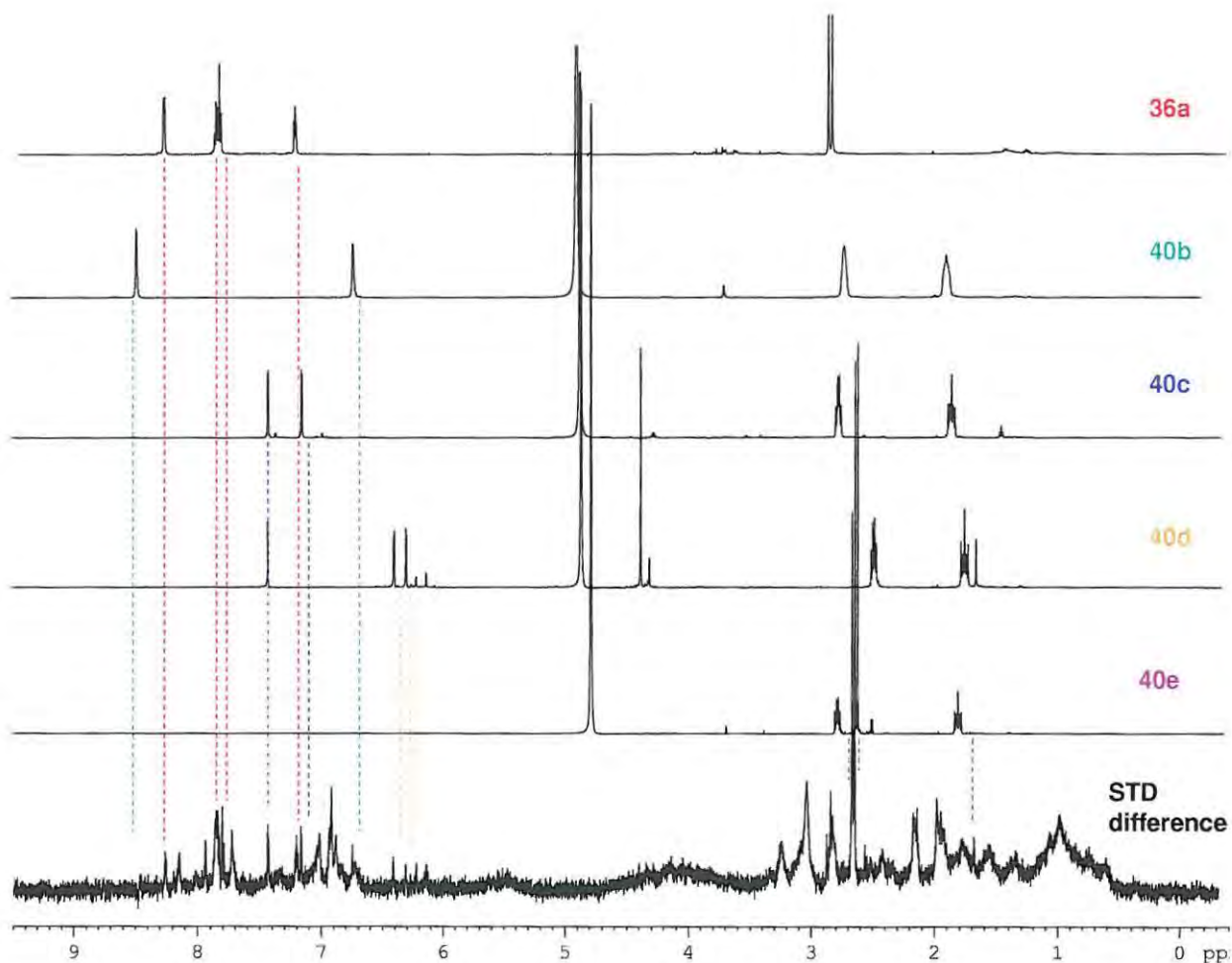
Figure 54. *Ec*DXR STD difference spectrum for the fourth set of ligands (**36a** and **40b-e**) showing correlations between characteristic ligand signals and signals in the STD difference spectrum (coloured dashed lines). Individual ligand spectra in D$_2$O are shown from top to bottom:- **36a**, **40b**, **40c**, **40d** and **40e**.

Comparison of the individual ligand spectra with the STD difference spectra shows that all of the ligands appear to bind to EcDXR. This is surprising as the phosphonate esters **35e** and **39e** are bulky and were not expected to fit into the restricted active-site cavity.[50] The phosphonate esters appear to bind as well as the phosphonate salts indicating that, perhaps, the more hydrophobic phosphonate esters favour the more hydrophobic enzyme environment over the polar solvent, despite their larger size. In Figure 52, the signal at 8.51, corresponding to the 5' aromatic proton in ligand **36b**, does not appear in the STD difference spectrum whilst the signal corresponding to the 4' aromatic proton does. This may be due to a difference in the T_1 relaxation times of the two protons or it could mean that the 5' proton is not sufficiently close to the protein to experience saturation transfer. Interestingly, the corresponding signal for ligand **40b** is also absent in Figure 54, but is observed for the esters **35b** and **39b**.

Since the STD experiments were run for *ca.* 12 hours, the stability of EcDXR was tested to ensure that the protein remains active during the course of the STD experiment. A sample of EcDXR in sodium phosphate buffer was left at room temperature for 24 hours and was found to have retained 88% of its activity after this period. The protein was therefore considered to be sufficiently active during the 12 hour STD experiments to provide accurate binding data. In addition to determining binding ligands from a mixture, the STD experiment, once it has been optimised for a particular ligand, can be used to explore competition effects and calculate binding affinities.[98,100] Such experiments, however, require successive titrations of ligand with the protein followed by a lengthy STD experiment after each titration, and were only considered to be warranted for ligands which exhibited really promising enzyme inhibition activity (see Section 2.3.2.).

Although the STD results indicate binding for all the ligands examined, the enzyme inhibition assays show that the ligands have, at best, relatively low inhibitory activity. This highlights the fact that, although the STD data provide an indication of protein-ligand binding, the possibility of non-specific binding in regions other than the active site cannot be excluded.[98] In fact, the presence of ligands in very high concentrations relative to the protein may promote non-specific binding to regions other than the active site.[98] In order to determine if the observed binding was specific or allosteric, the highly active inhibitor fosmidomycin was added to the assay mixtures of the last two groups of compounds after the STD experiment and the experiment was re-run under exactly the same conditions. The STD difference and reference spectra for the fourth set of ligands (**36a** and **40b-e**) with and without fosmidomycin are shown in Figure 55.
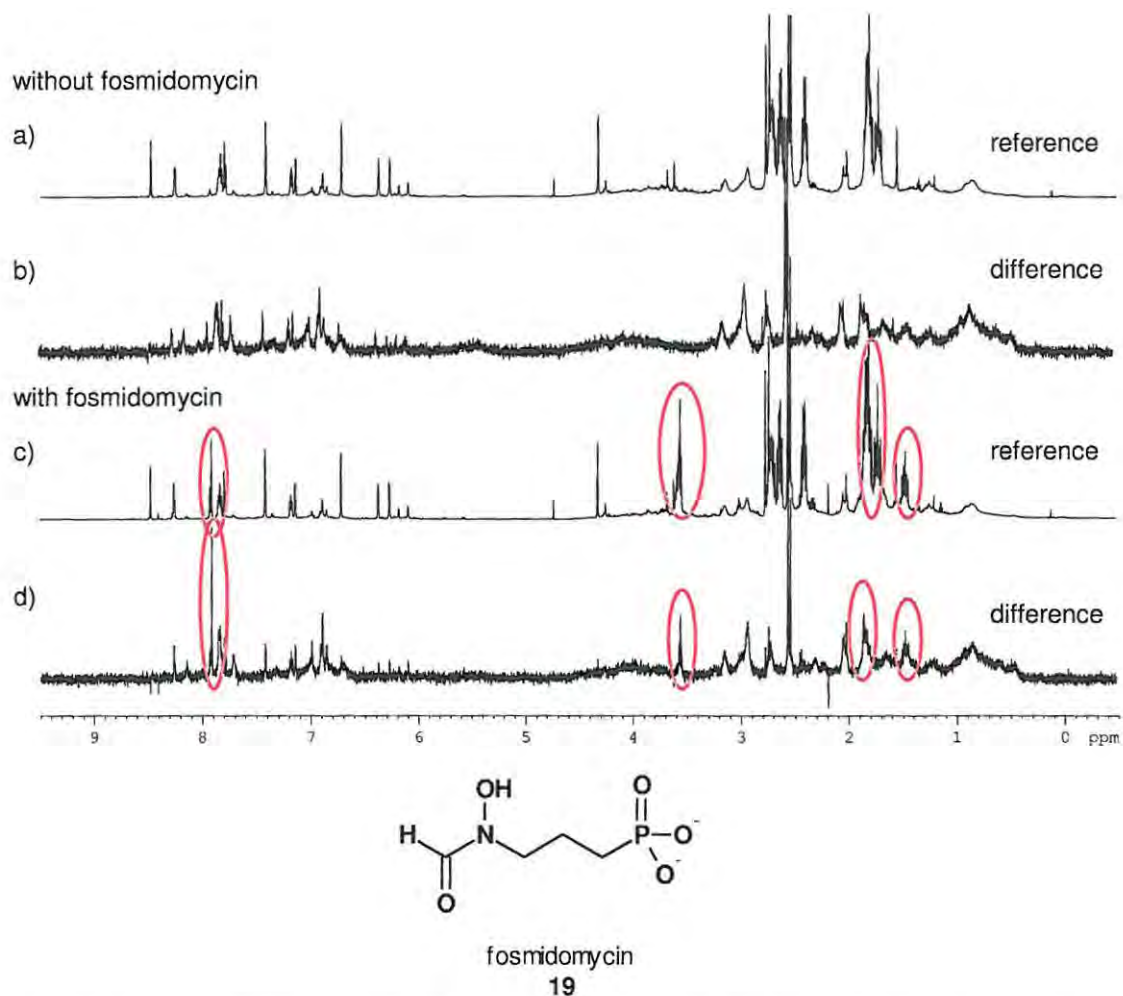
Figure 55. *Ec*DXR STD difference and reference spectra for the fourth set of ligands (**36a** and **40b-e**) without (a, b) and with (c, d) fosmidomycin **19** present. Fosmidomycin signals are indicated by red circles.

As a highly active inhibitor, fosmidomycin **19** is assumed to bind tightly in the active site and to displace any weakly bound ligands. The STD technique relies on saturation transfer followed by exchange of the ligands, and is therefore unable to identify ligands which bind so tightly to the protein that they undergo slow chemical exchange on the NMR timescale.[98] Hence, the presence of fosmidomycin signals in the difference spectrum (Figure 55) implies that, although fosmidomycin is a highly active inhibitor, its exchange in and out of the active site must be sufficient to permit its resonances to be observed. The appearance of the ligand signals in the difference spectrum when fosmidomycin is present indicates that the ligands are not completely displaced by fosmidomycin and therefore still bind to the protein to some degree. This binding could therefore be either weak binding in the active site or binding to some site other than the active site. These conclusions are consistent with the enzyme assay results discussed in Section 2.3.2. and suggest that the weak inhibition observed by most of the ligands is due either to weak active-site binding or to allosteric inhibition.

73

As the STD experiment is based on the detection of ligand signals, it is a valuable technique for proteins which cannot be labelled, have high molecular weights, are membrane-bound or can only be obtained in small quantities.[99] The disadvantage is that the binding site in the protein cannot be determined easily by this method.[96] Although the sensitivity and applications of the STD technique have been illustrated by the above experiments, the possibility of apparently positive results caused by non-specific binding has been highlighted. In addition, the importance of optimising the experiment in terms of the solvent used and the pre-saturation frequency and number of pulses has been emphasised. The STD experiment provides a useful initial screen for ligand binding of several compounds simultaneously but a thorough understanding of the technique, as well as its limitations, is necessary before any firm conclusions about inhibition potential can be drawn from the results.

2.3.2. Enzyme inhibition assays

Binding assays may provide a useful initial screen for binding of a ligand to the enzyme of interest, but the binding must result in inhibition if the ligand is to be of any potential medicinal benefit. Biological assays are therefore crucial for determining the potential of synthesised molecules as well as guiding the design of new ones. The standard assay for determining EcDXR inhibition has been described by Kuzuyama.[101] This assay has been widely used as an indication of PfDXR inhibition potential and was the assay which first established fosmidomycin as an inhibitor of DXR.[41,54,60] Although it only affords a measure of DXR inhibition ability and not necessarily anti-parasitic activity, the DXR inhibition assay gives a quick and inexpensive indication of the activity of the ligands tested. Once promising compounds have been identified, a parasite growth inhibition assay, such as the 8-[^{3}H]hypoxanthine incorporation assay, can be carried out.[102] EcDXR is used in the DXR inhibition assay as it can be easily expressed and purified in large quantities and is more stable than PfDXR[65] and, for closely related compounds, there appears to be a good correlation between the IC_{50} values of the ligands in both EcDXR and PfDXR.[60]

The assay is based on the spectrophotometric measurement of the conversion of NADPH to NADP which occurs when DOXP is converted to MEP by DXR.[40] The ligands were tested on behalf of the author[103] at concentrations between 10 µM and 500 µM for compounds **35a-e** and **36a-e** and 10µM and 1000 µM for **39a-e** and **40a-e**. In each assay, the slope of the initial linear portion of the absorbance-time graph was determined and taken to indicate the reaction rate. Rates of decrease in absorbance were compared with the respective control experiments and a percentage relative inhibition was determined in triplicate for each ligand by considering the enzyme activity in the absence of inhibitor to be 100% (*i.e.* 0% inhibition). Under these conditions, fosmidomycin **19** at 0.3 µM exhibited 99.3% inhibition. Plots of the absorbance-time graphs for the control, the mild inhibitor **35c** and the highly active inhibitor fosmidomycin **19** are shown in Figure 56.
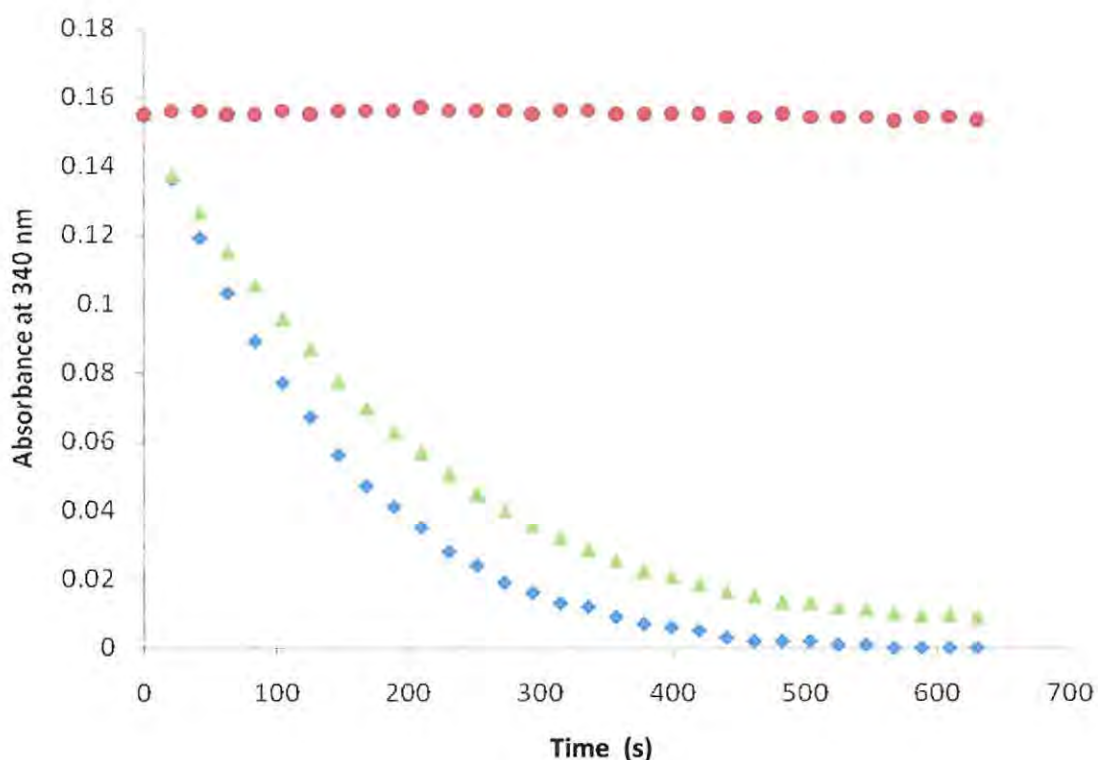
Figure 56. Absorbance-time graphs showing progress of the reaction catalysed by *Ec*DXR in the presence of inhibitor **35c** (250 µM), shown as triangles, and fosmidomycin **19** (0.3 µM), shown as circles. The control experiment is shown as diamonds. Absorbance values, which reflect the decreasing concentration of NADPH, have been scaled to account for differences in the initial absorbance readings.

Fosmidomycin is a slow, tight-binding inhibitor of DXR[55] and, consequently, the compounds to be tested were pre-incubated with the enzyme for 5 minutes before the reaction was started by addition of the enzyme-inhibitor mixture to the substrate, cofactor and buffer mixture. Other authors have accommodated a pre-incubation time by adding the substrate last to initiate the reaction.[57,59] NADPH has been found to bind before either DOXP or fosmidomycin in the ordered reaction mechanism[55] and this should be taken into account when deciding on the order in which to add compounds to the assay mixture. As shown in Figure 56, the absorbance decreased immediately, suggesting that, either DOXP very quickly replaces any bound ligand, or that the ligand binds allosterically and therefore does not interfere with DOXP binding. In some reports, bovine serum albumin (BSA) was added to the assay mixture to stabilise the enzyme at low concentrations.[55] However, this was not deemed to be necessary in our assays as the enzyme concentration was higher than that used by other authors and no problems with stability were encountered.

For each of the ligands, the percentage inhibition was plotted against the ligand concentration and, by extrapolation of the trend-line, IC_{50} values were calculated. The percentage inhibition at 500 µM and the IC_{50} values determined for the synthetic ligands are summarised in Table 7.

Table 7. Results of *Ec*DXR inhibition assays at 500 μM and IC_{50} values calculated for each of the ligands.

Compound	Inhibition[a] at 500 μM (%)	IC_{50} (μM)
35a	58.5	472
35b	11.7	1171
35c	28.9	730
35d	67.7	408
35e	21.6	1286
36a	—[b]	—[b]
36b	12.2	>1500
36c	7.4	>1500
36d	30.0	1027
36e	16.6	>1500
39a	-0.1	>1500
39b	0.0	>1500
39c	0.1	>1500
39d	0.2	>1500
39e	0.3	>1500
40a	0.0	>1500
40b	0.2	>1500
40c	0.2	>1500
40d	0.3	>1500
40e	0.0	>1500
46	10.1	1006

[a] Activity in the absence of inhibitor set at 100%
[b] Anomalous result suggesting enzyme activation (negative % inhibition)

While most of the percentage inhibition values are relatively low and the IC_{50} values relatively high, several of the ligands exhibit IC_{50} values in the micromolar range, the most active of these being the furan and pyridine derivatives **35d** and **35a**, respectively. Compared to the most active inhibitors reported in the literature,[38,104] with IC_{50} values in the nanomolar range (30 to 459 nM), the inhibition observed for the tested compounds is relatively low. Nevertheless, the fact that some measure of inhibition is shown by the ligands, which differ quite significantly from the fosmidomycin structure, provides a starting-point for the design of more effective DXR inhibitors.

Interestingly, the phosphonate esters **35a-e** appear to exhibit significantly lower IC_{50} values than the corresponding phosphonic acid salts **36a-e** – due, perhaps, to their more hydrophobic character and, hence, their relative preference for the enzyme environment rather than the aqueous environment. Perruchon et al.[57] explored the effect of extending the phosphonate ester groups and suggested that the negative effect of decreasing the charge on the phosphonate moiety may be partly counteracted by the occupation of a nearby hydrophobic pocket by the alkyl ester groups.[57] Occupation of such a pocket by the phosphonate ester groups in our ligands may well account for the higher inhibition levels exhibited by the phosphonate esters compared to the phosphonic acid salts. (See Section 2.4.2. for discussion on the topology of the receptor cavity.)

The ligands with two methylene groups (**39a-e** and **40a-e**) show significantly lower percentage inhibition and higher IC_{50} values than their analogues containing one methylene group (**35a-e** and **36a-e**). Thus, whilst compounds **35a-e** and **36a-e** show minimal to moderate inhibition, compounds **39a-e** and **40a-e** show almost no inhibition at all, illustrating the importance of the length of the carbon backbone in the ligands examined here. The restricted length of the DXR active site, with the phosphonate-binding region at one end and the metal cation and NADPH at the other, has been considered to limit the length of potential fosmidomycin analogues.[33] The acyl residue, which distinguishes FR900098 **20** from fosmidomycin **19**, is thought to be the limit to which the length of the molecule can be extended if it is to occupy the same binding site.[54] Interestingly, however, data from a cognate study using anilide derivatives has revealed that ligands containing two methylene groups between the polar termini are better DXR inhibitors than their analogues containing one.[83]

The STD experiments (Section 2.3.1.) have indicated that the compounds all show binding to EcDXR, but this binding may be weak or non-specific as the ligands did not appear to be completely displaced by fosmidomycin in the STD experiment. The results displayed in Table 7 seem to confirm this conclusion in that, despite positive STD binding results, little inhibition was observed for most of the ligands.

Compounds **35a-e** and **36a-e** were also subjected to a set of qualitative assays to determine whether they had any biological activity against some common pathogens. The GIBEX (Global Institute for Bioexploration)[105] assays have been designed as field-based assays to screen crude plant extracts for antibacterial, antifungal, antiprotozoan and antimycobacterial activity. The assays were designed to be quick and involve minimal equipment but provide only qualitative results indicating either a positive or negative inhibition of growth. Extracts

78

exhibiting some inhibitory activity against one or more of the representative pathogens can then be studied further. The GIBEX antibacterial assay was modified for use[103] on the pure compounds **35a-e** and **36a-e** but no inhibition of bacterial growth was observed at a concentration of 1 mM. The DOXP/MEP pathway is found in many Gram-positive and Gram-negative bacteria[24] and, not surprisingly, fosmidomycin **19** has been found to completely inhibit the growth of *E. coli* at a concentration of 3.13 µg/mL.[40]

Although the ligands prepared in this study have not exhibited significant DXR inhibitory activity, the bioassays have provided some interesting structure-activity data for use in the design of future inhibitors as discussed in Section 2.4.2.

2.4. *In silico* studies

2.4.1. *Molecular modelling and simulated docking of synthetic ligands*

Simulated docking studies were carried out to:- i) predict the DXR binding affinity of the ligands **35a-e** and **36a-e**; ii) explore the topology of the DXR binding site; and iii) identify additional binding regions which could be exploited in the modification and design of potential inhibitors. An *in vacuo* global minimum was located for each of the ligands by means of a systematic conformational search using Cerius^2.[106] Solvent-corrected, energy-minimised structures (including frequency calculations) were then obtained at the density functional theory (DFT) level using Gaussian 03.[107] AutoDock version 4.0[108] was used for the docking studies, Discovery Studio Visualizer 2.0[109] to visualise the docked conformations and UCSF Chimera[110] to explore the active site.

AutoDock uses a genetic algorithm to perform a search of the possible orientations, positions and conformations of a ligand in the active site of a protein.[108] A genetic algorithm is an efficient search method which utilises the biological concepts of genetics and evolution, encoding the position, orientation and conformation of a ligand on a 'chromosome'. The information on the ligand's chromosome (its genotype) determines its atomic coordinates (its phenotype).[108] An initial population is randomly generated and 'crossover' of the genes occurs during 'mating' of random pairs of individuals in which the 'progeny' inherit genes from both 'parents'.[108] The 'fitness' of the progeny is determined by the total interaction energy between the ligand and the protein and therefore, on 'selection', only the individuals best suited to their environment survive to 'reproduce'.[108,111] A user-defined level of random mutation is also included to ensure adequate sampling of the docking possibilities. The Lamarkian genetic algorithm includes a further step (in which it deviates from Mendelian genetics), allowing the results of a local search (the individual's phenotype) to be mapped back onto the genotype for further optimisation.[108,111]

Preliminary *in silico* docking of the phosphonate esters **35a-e**, the corresponding phosphonic acids and their dianions **36a-e**, was explored using the active site (from which fosmidomycin **19** and the solvating water molecules had been removed) in the crystal structure 1Q0L[47] of *Ec*DXR (which includes bound fosmidomycin **19** and NADPH). In order to simulate coordination to the divalent metal cation, Mn^{2+} was included in the model and positioned according to its location relative to fosmidomycin **19** and the coordinating ligands Asp150, Glu231 and Glu152 in the *Ec*DXR crystal structure 1ONP.[36] A charge of +2 was manually assigned to the manganese ion. The active-site residues Ser186, Asn227, Lys228 and Glu231 (residue

numbering from 1Q0L) were defined as flexible residues and simulated dockings were carried out with each of the ligands **35a-e** and **36a-e** (as both the free acids and deprotonated analogues) as well as with DOXP **9**, MEP **10**, fosmidomycin **19**, FR900098 **20** and the intermediate 2-C-methylerythrose-4-phosphate **15**. Examination of the docked conformations of each of the ligands relative to the crystal structure conformation of fosmidomycin **19** (from 1Q0L) and the proximal amino acid residues in the active site of the EcDXR crystal structure 1Q0L permitted potential hydrogen-bonding and Mn^{2+}-coordination distances to be determined. The relative docked conformations of the phosphonate ester, phosphonic acid and corresponding dianionic form of each phosphonic acid were also compared.

While the conformations of the majority of the docked ligands appeared to differ little from their minimum energy conformers, the solvent-corrected energies calculated for the docked ligands were all higher (by 32-84 $kcal.mol^{-1}$) than the corresponding energies for their undocked conformers. The energy differences between the solvent-corrected, energy-minimised and docked conformers are shown in Table 8 and give an indication of the conformational cost of binding which must be compensated for by the protein-ligand interaction energy.

Table 8. Conformational binding cost on docking of phosphonate esters **35a-e** and their corresponding acids in DXR.

Compound	Conformational binding cost ($kcal.mol^{-1}$)
35a	31.92
35b	54.45
35c	67.10
35d	81.01
35e	66.08
36a[a]	84.47
36b[a]	45.02
36c[a]	44.79
36d[a]	47.06
36e[a]	41.60

[a] As the protonated phosphonic acid

81

In most cases, the ligands exhibited, unexpectedly, docking orientations opposite to that of fosmidomycin **19** (as illustrated in Figure 57). In all of the crystal structures which include bound fosmidomycin, the hydroxamate moiety coordinates to the metal ion, close to NADPH, while the phosphonate group occupies a well-defined phosphonate-binding pocket. In the case of the natural substrate DOXP **9**, this orientation is crucial as coordination of the α-hydroxy ketone to the metal anchors the substrate in a suitable position for catalysis, locating the aldehyde moiety of the intermediate **15** close to NADPH for the reduction step.[30] However, this does not preclude competitive 'reverse' binding of DOXP **9**, nor would it necessarily prevent a 'reverse'-bound ligand from acting as an inhibitor. The most likely explanation for the observed 'reverse' binding is the electrostatic attraction between the negatively charged phosphonic acid moiety of the ligands and the divalent metal cation. Although the 'reverse'-binding mode is chemically feasible, Cheng and Oldfield have pointed out that the resultant 4-membered ring would be more strained than the 5-membered ring formed by 'normal' coordination of the hydroxamate moiety in fosmidomycin **19** to the metal cation (Figure 11, p. 21).[58] There may, of course, be several plausible orientations of fosmidomycin **19** in the active site and the orientation found in the crystal structure may merely be a static representation of a dynamic system.
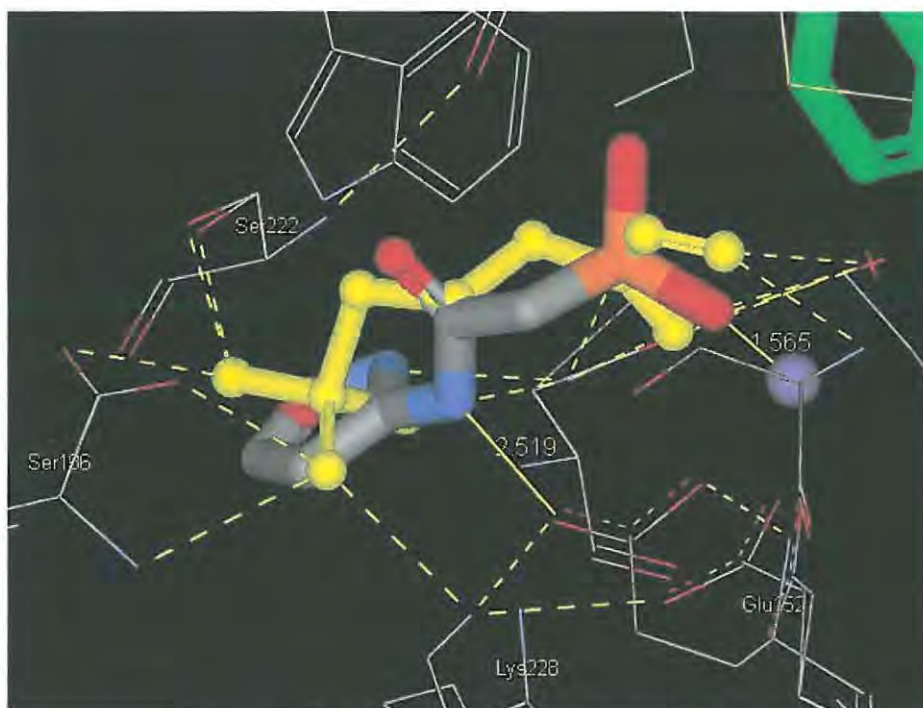
Figure 57. Docked conformation of phosphonic acid dianion **36b** in the EcDXR active site (1Q0L) with Mn^{2+} added, showing 'reverse' binding of the ligand relative to fosmidomycin **19**. Protein active-site residues are shown in wireframe and coloured by atom type, NADPH as green sticks, Mn^{2+} as a purple sphere, and the ligand as sticks coloured by atom type. The crystal structure conformation of fosmidomycin **19** is shown in yellow ball-and-stick format. Hydrogen atoms have been omitted for clarity and hydrogen-bonding distances (in Å) are shown as yellow dashed lines.

The most active inhibitors against *Pf*DXR reported so far are analogues of fosmidomycin containing an aromatic ring α to the phosphonate moiety.[76,104] No docking studies have yet been reported for these compounds but the results observed for ligands **35a-e** and **36a-e** (Figure 58) strongly suggest the existence of an additional binding pocket adjacent to the phosphonate-binding pocket and lined by the residues, His257, Thr184, Glu152, Trp212 and the backbone atoms of Ser254 and Gly185.
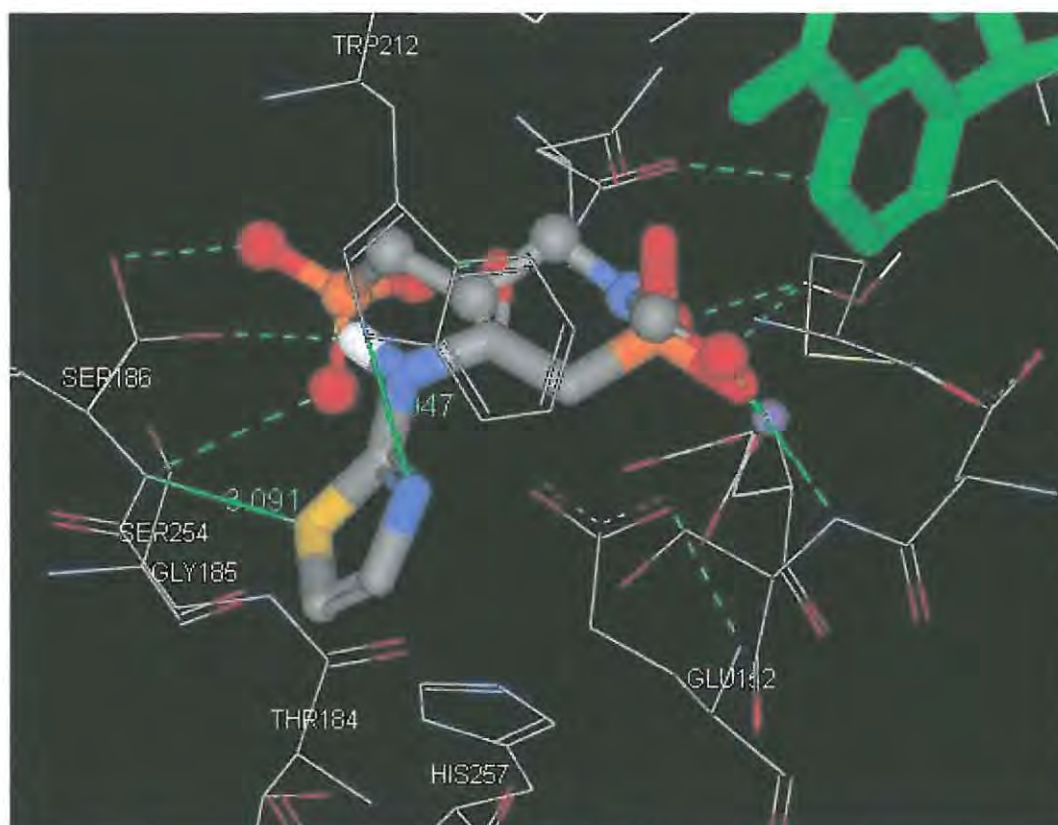
Figure 58. Docked conformation of phosphonic acid dianion **36c** in the *Ec*DXR active site (1Q0L) with Mn^{2+} added, showing the thiazole ring occupying a pocket adjacent to the phosphonate-binding site. Protein active-site residues are shown in wireframe and coloured by atom type, NADPH as green sticks, Mn^{2+} as a purple sphere, and the ligand as sticks coloured by atom type. The crystal structure conformation of fosmidomycin **19** is shown in ball-and-stick format and coloured by atom type. Hydrogen atoms have been omitted for clarity and hydrogen-bonding distances (in Å) are shown as green dashed lines.

The phosphonate esters **35a-e** are intended to act as pro-drugs as it is anticipated that the ester moieties would be hydrolysed *in vivo* by cellular esterases.[62,76] Not surprisingly, the docking results suggest that the phosphonate esters are too large to fit the 'normal' binding site, and many of the phosphonate esters adopt the orientation shown in Figure 59 – an arrangement in which crucial interactions with the metal cation and phosphonate-binding residues would not be possible.[54,76] Subsequent docking studies were therefore carried out only on the deprotonated phosphonic acid forms of the ligands.
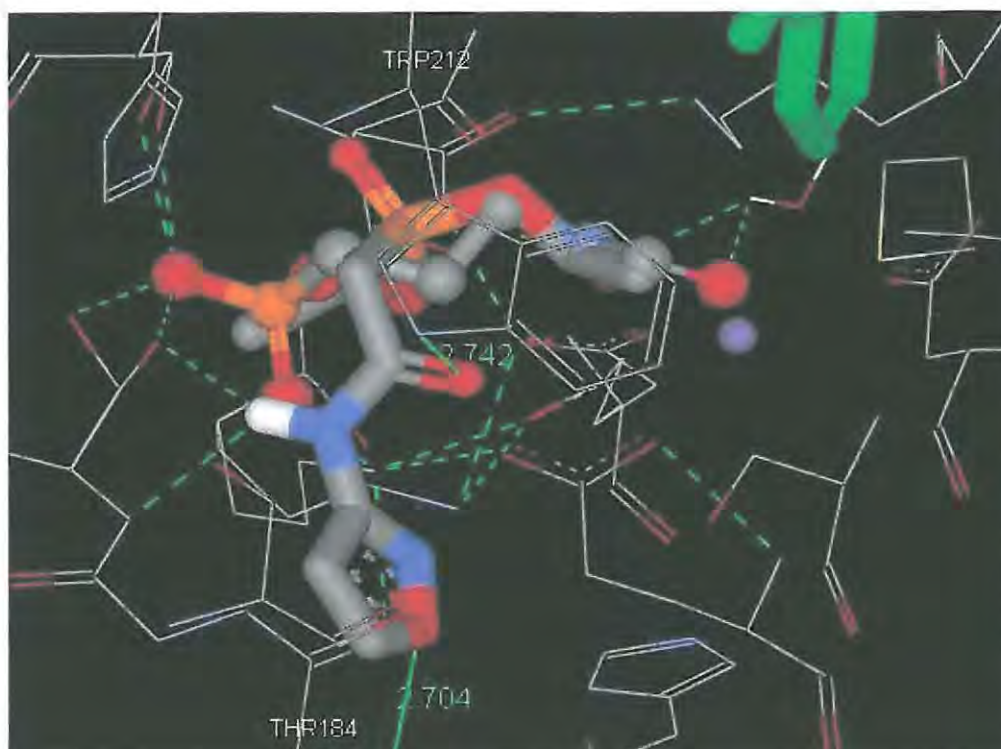
Figure 59. Docked conformation of the phosphonate ester **35b** in the *Ec*DXR active site (1Q0L) with Mn^{2+} added, showing alignment of the ethyl ester groups along the fosmidomycin backbone and projection of the isoxazole ring into a pocket adjacent to the phosphonate-binding site. Protein active-site residues are shown in wireframe and coloured by atom type, NADPH as green sticks, Mn^{2+} as a purple sphere, and the ligand as sticks coloured by atom type. The crystal structure conformation of fosmidomycin **19** is shown in ball-and-stick format and coloured by atom type. Hydrogen atoms have been omitted for clarity and hydrogen-bonding distances (in Å) are shown as green dashed lines.

The close alignment with fosmidomycin observed for the phosphonic acid dianions **36b**, **36d** and **36e** (Figure 60), despite the 'reverse' docking, would suggest that these ligands could show favourable chemical interactions with DXR and thus prove to be good inhibitors. The enzyme inhibition assay results, however, revealed that compounds **36a-e** exhibit minimal inhibition, indicating that, although they may fit into the active site, there are insufficient chemical interactions with the protein for effective binding and inhibition to occur. In the docked conformations, the majority of the ligands appear to be anchored at either end by the metal-binding and phosphonate-binding receptor-site residues, with some degree of conformational flexibility in between. This agrees with the proposed mechanisms of the DOXP-MEP reaction in which the central region of the active site would need to accommodate the re-arrangement of the carbon backbone.[30] Perruchon *et al.*[57] found that a methyl extension to the phosphonate group increased activity and the ability of such elongated ligands to fit into the active site is supported by the observation that even some of the larger ligands such as **36d** and **36e** appear to fit into the active site, even though they project beyond fosmidomycin **19**.

Figure 60. Docked conformation of phosphonic acid dianion **36d** in the EcDXR active site (1Q0L) with Mn^{2+} added, illustrating the potential for variability in the conformation of the linking region between the phosphonate-binding and metal-coordinating ends. Protein active-site residues are shown in wireframe and coloured by atom type, NADPH as green sticks, Mn^{2+} as a purple sphere, and the ligand as sticks coloured by atom type. The crystal structure conformation of fosmidomycin **19** is shown in ball-and-stick format and coloured by atom type. Hydrogen atoms have been omitted for clarity and potential hydrogen bonds are shown as green dashed lines.

Little attention appears to have been given to placing the M^{2+} cation in the protein model and to assigning a realistic charge to the metal centre. Typically, in docking studies which actually include the metal cation, Mg^{2+} has been used and has either been assigned a full +2 charge or the docking programme has been allowed to calculate a charge.[50,58] Although Silber et al.[52] and Perruchon et al.[57] state that Mg^{2+} is better parameterised than Mn^{2+} in AutoDock, a Gasteiger[112] charge of 0.00 is automatically assigned to either metal in AutoDock 4.0. Neither a charge of +2 nor 0 is likely to model the metal co-factor realistically in the presence of the surrounding, negatively charged, coordinating ligands. The importance of substrate or inhibitor binding to the metal cation[30,74] surely requires that attention be given to including a well-parameterised and accurately charged metal cation when carrying out docking studies on DXR. Consequently, in order to investigate the effect of the ligands on the +2 charge, the Mg^{2+} cation, its coordinating residues (Asp149, Glu151 and Glu230), a water molecule and fosmidomycin **19** were all removed, as a group, from the crystal structure 2EGH,[53] and the group was energy-minimised, using a Hartree-Fock calculation (Figure 61).[107] This calculation afforded a charge of +1.058 on the Mg cation – a value consistent with significant dissipation of the formal +2 charge by the coordinating ligands. The calculated Mulliken charges on all of

the atoms in the energy-minimised group were transferred to the input files used by AutoDock and, when fosmidomycin **19** (with its Hartree-Fock calculated charges) was docked into the modified protein model, an increase in the number of correctly oriented dockings was observed. Replacement of the empirical charges with quantum-mechanical-calculated values in the force-field parameters of docking algorithms has also been shown by other researchers to increase the accuracy of the calculation of the electrostatic interactions.[113] As the electrostatics term in the free-energy equation is independent of the other terms, replacement of the empirical charges with quantum-mechanical-calculated values does not affect the other terms[114] and the quantum-mechanics-refined parameters were then used in subsequent docking experiments.

Figure 61. Magnesium cofactor (shown in green) with surrounding ligands, Asp149, Glu151, Glu230, H_2O and fosmidomycin **19** following Hartree-Fock energy minimisation, showing Mulliken charges assigned to each atom. All atoms are coloured by atom type.

AutoDock 3.0[108] appears to give very reproducible docking results and has been widely used for DXR docking studies.[57-59] The use of the more recent version, AutoDock 4.0, however, has not yet been reported for DXR docking studies and, therefore, a series of docking runs was performed to determine the effectiveness of AutoDock 4.0 for the reliable prediction of inhibition. The *Ec*DXR crystal structure 2EGH[53] was prepared as the receptor and Mulliken

86

charges, obtained from the energy minimisation process described above, were substituted for Gasteiger charges on the atoms of the active-site residues Glu230, Asp149, Glu151, the coordinating water molecule, the Mg cation and fosmidomycin **19**. The Ser221, Lys227, Ser185, His256, Met213, Asp149, Glu230 and Glu151 residues were defined as flexible, having been identified by others as being involved in the binding of either fosmidomycin **19** or DOXP **9** to the active site.[47,50,51]

To validate the docking protocol and determine reproducibility, fosmidomycin **19** was removed from the model and then subjected to three docking experiments, each experiment using the same parameters and generating ten docking results. Analysis of the results was based on the clustering of the results and the closeness of the docked conformations to that of the crystal structure. The clustering of the docking results gives an indication of the similarity of the docked structures to each other, based on the root-mean-square-deviation (rmsd) between the atomic coordinates.[115] The docking results are ranked according to energy and the lowest energy (best) docked structure is placed in the first cluster. Calculation of the rmsd between the lowest and second-lowest energy structures then determines whether the second structure is placed in the first cluster or becomes the reference for a second cluster, depending on the cut-off rmsd value (default 2.0 Å). This process is repeated until each of the docking results is placed in a cluster.[115] The number and distribution of the clusters gives an indication of the reliability of the docking method and it is assumed that increasing the number of energy evaluations within each docking run will increase the likelihood that similar low-energy docks will be achieved in each of the docking runs and therefore the number and distribution of the clusters will decrease.[115] In each of the three replicates of the fosmidomycin docking, eight or more clusters were generated, indicating that, within each experiment, the docked conformations were significantly different to each other.

On visual inspection of the three docking experiments, the lowest energy docks appear to align most closely with the crystal structure conformation of fosmidomycin **19** whilst the higher energy docks appear to bind in the channel region. Although this confirms the correct positioning of the grid box for the docking, the variability in the docking results indicates that, either fosmidomycin **19** can adopt several binding orientations and conformations, or that the programme does not consistently converge to the minimum energy docked conformation. Figure 62 shows the ten docking results obtained in one of the docking experiments with fosmidomycin.

Figure 62. Docked conformations of fosmidomycin **19** in the *Ec*DXR active site (2EGH) with Mulliken charges added, illustrating the variability in the docked conformations when several flexible residues are chosen. Protein active-site residues are shown in wireframe coloured by atom type, docked fosmidomycin conformations as sticks coloured by atom type and the crystal structure fosmidomycin in ball-and-stick format, coloured yellow.

Increasing the number of docking runs or increasing the number of energy evaluations within each run did not appear to substantially improve the results or decrease the number and distribution of clusters. Energy minimisation and subsequent docking of DOXP **9** yielded similar results; with only one or two docks looking feasible. Replacment of the Gasteiger charges on DOXP **9** with Mulliken charges also appeared to make little difference.

Unlike AutoDock 3.0, AutoDock 4.0 allows the selection of flexible residues in the receptor in order to better approximate the 'hand and glove' concept of a ligand binding to a protein. There is no limit to the number of flexible residues which can be selected but the maximum number of torsions in the ligand and flexible residues combined may not exceed 32.[115] In order to ascertain the effect that the choice and number of flexible residues has on the docking results, the input file was altered to include only Ser221 as a flexible residue. Ser221 was chosen as it is found at the edge of the active site and only has two torsion angles in the side

88

chain. This was the minimum which could be selected as a completely rigid dock is not possible in AutoDock 4.0. Docking of fosmidomycin **19** into this model produced surprisingly different results. For the default, medium length, run, only three clusters were generated with eight of the ten conformations in the lowest energy cluster. In addition, all of the eight lowest energy conformations aligned very closely with the crystal structure fosmidomycin as shown in Figure 63.

Figure 63. Docked conformations of fosmidomycin **19** in the *Ec*DXR active site (2EGH) with Mulliken charges added, illustrating the reproducibility of the docked conformations when only one flexible residue (Ser221) is chosen. Protein active-site residues are shown in wireframe coloured by atom type, docked fosmidomycin conformations as sticks coloured by atom type and the crystal structure fosmidomycin in ball-and-stick format, coloured yellow.

Increasing the length of the run increased the reproducibility of the results with nine out of ten docks showing close alignment and low energy. These experiments show that the choice and number of flexible residues significantly influences the docking results. Although the choice of fewer flexible residues leads to greater reproducibility, the simulation system then deviates considerably from the biological system in which the enzyme is flexible.

The experiments described above were used to validate the docking results obtained with AutoDock in terms of the parameterisation of the metal cation, the reliability of the docking and the influence of the number of flexible residues. The results obtained show the importance of gaining a good understanding of the parameters used and of how the docking programme works before attempting to interpret the docking results. It is also important to balance the reproducibility of 'good' *in silico* results with their correspondence to the real enzyme-ligand system. In subsequent docking experiments, the Mulliken charge was substituted for the automatically-assigned Gasteiger charge on the metal cofactor, the clustering of the docking results was analysed and the number of flexible residues was limited.

2.4.2. Exploration of the DXR active site and design of novel inhibitors

Many analogues of fosmidomycin **19** and FR900098 **20** have been synthesised and evaluated as DXR inhibitors but few have proved to be more active than these two lead compounds. Most analogues have been based on chemical modifications of the lead compounds and attempts to probe the DXR active site. Although this is a valid and rational approach to drug discovery, little use appears to have been made of computational techniques to study the topology and properties of the active site for *de novo* inhibitor design; this, however, is an approach which we have begun to explore.

Significant binding residues in DXR have been identified previously from the available crystal structures and Giessman *et al.* have summarised the essential features of fosmidomycin **19** and DOXP **9** and their interactions with the protein in order to highlight opportunities for the variation of ligand structure.[47,53,54] The importance of a metal-coordinating moiety has been stressed by Deng *et al.*[74] and hard ligands, such as hydroxamate or catechol groups, have been suggested as suitable Lewis bases for coordination to the hard Mg^{2+} ion.[74] However, due to their possible degradation *in vivo* by several pathways, hydroxamate groups appear to confer poor pharamacokinetic properties on potential medicinal compounds. Consequently, there is a need to consider other metal-coordinating moieties.[74] Variations on the length and properties of the 3-carbon spacer have been largely unsuccessful in increasing inhibition, supporting the assumption that closure of the loop region of the enzyme results in a relatively narrow active site,[36,54] while the significance of a double negative charge on the phosphonate group has been highlighted by Perruchon *et al.*[57] With these known structure-activity relationships in mind, we have explored both the EcDXR and PfDXR active sites to identify residues with binding potential or adjacent pockets which may be exploited in the design of novel inhibitors.

Analysis of the ligand docking results revealed that some of the docked ligands occupied a pocket adjacent to the phosphonate-binding site. This prompted further investigation into the dimensions, shape and properties of this cavity in DXR. Visualisation was achieved with Chimera[110] using the EcDXR crystal structure (2EGH)[53] as this model contains bound fosmidomycin **19**, NADPH and Mg^{2+}. Measurements of the pocket occupied by fosmidomycin **19** revealed a narrow elongated pocket with the metal ion at one end, near to the channel through which the ligand enters, a narrow central region and a phosphonate-binding site as shown in Figure 64. The largely polar nature of the active site of DXR is also highlighted in Figure 64 with a highly polar region (shown in blue) at the back of the pocket and in the vicinity of the metal cation, and a more hydrophobic area (shown in orange) towards the top of the pocket and close to the channel due, mostly, to the presence of Ile217.
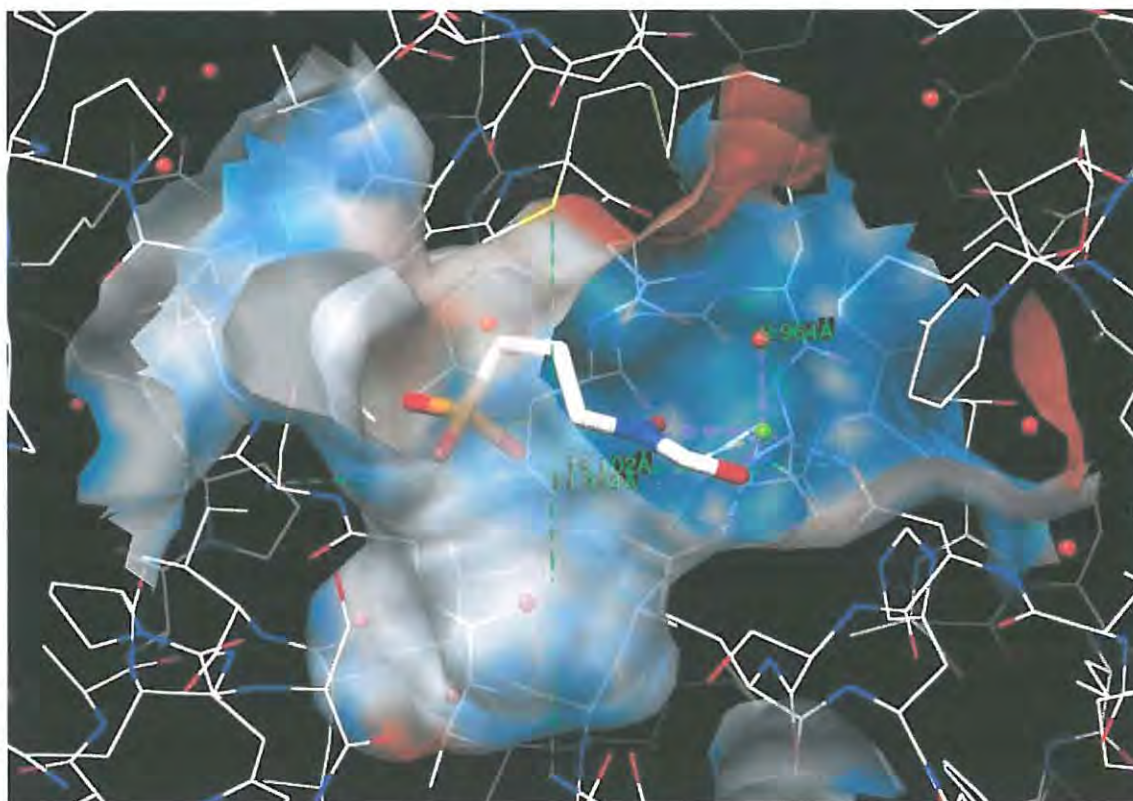
Figure 64. Active site of *Ec*DXR (2EGH), showing some dimensions and the polarity of the cavity around fosmidomycin **19**. The surface zone at 7.7 Å from fosmidomycin is shown with 40% transparency and coloured by hydrophobicity [polar (blue), non-polar (white), hydrophobic (orange)]. Protein residues are shown in wireframe, coloured by atom type, fosmidomycin as sticks, coloured by atom type, Mg^{2+} as a green sphere and the crystal structure water molecules as red spheres.

Analysis of the docking results revealed the existence of a pocket (I) adjacent to the phosphonate-binding region. Figure 65 shows the phosphonic acid dianion **36c** docked in *Ec*DXR (1Q0L) with the thiazole ring occupying the pocket (I) 'in front' of the phosphonate-binding region. This pocket was regularly occupied by the heterocyclic moieties of the docked ligands and, of the ligands docked, the thiazole ring appears to fit best into pocket I although many of the other ligands, including fosmidomycin **19**, were observed to bend 'forward' into this pocket. In Figure 64, three crystal structure water molecules can be seen occupying this pocket, highlighting its relatively hydrophilic nature. Fosmidomycin analogues containing an aryl group α to the phosphonate moiety have shown increased inhibition but, as yet, the cavity in which this moiety binds has not been identified.[76,104] The size and shape of pocket (I) 'in front' of the phosphonate-binding site suggest that this may, in fact, be the region in which these α-aryl compounds bind and also, possibly, the same region in which Perruchon *et al.*[57] reported binding of a propyl extension to the phosphonate group. Deng *et al.* also suggest the presence of a hydrophobic pocket near the DOXP binding site which may be occupied by phenyl or benzyl groups.[74]
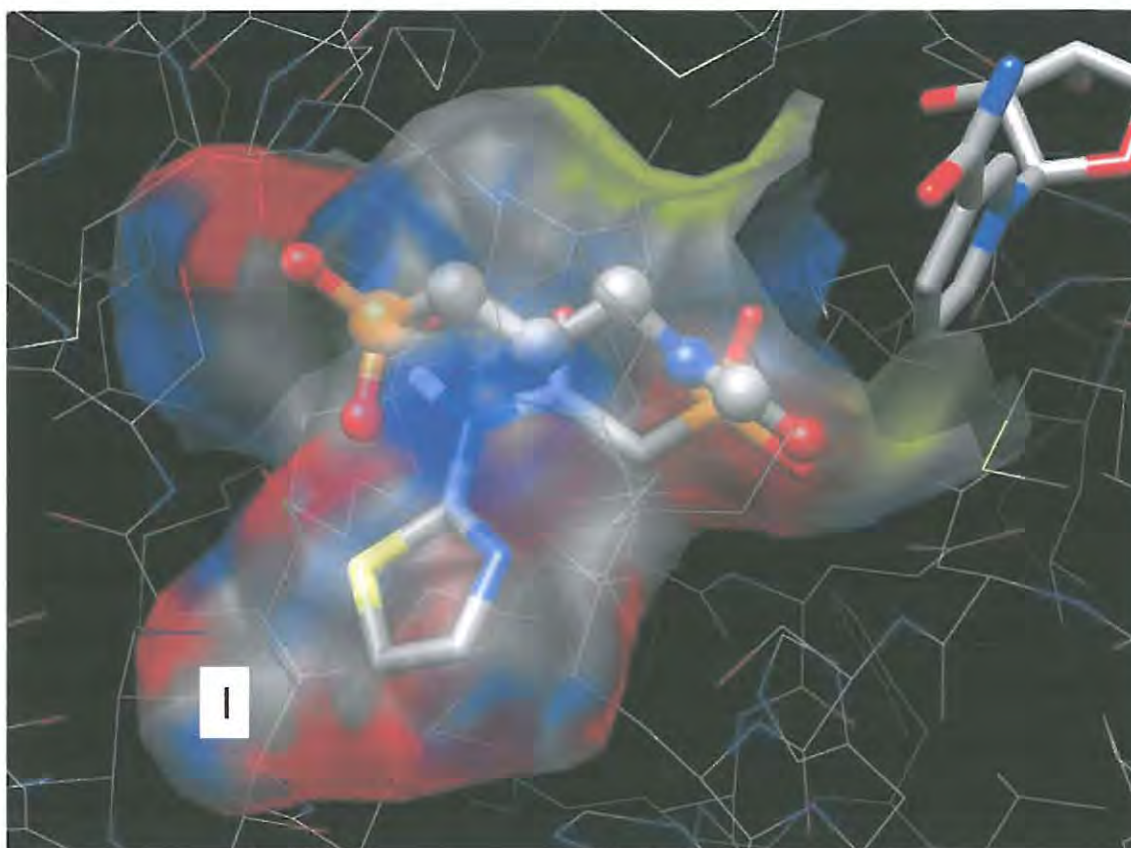
Figure 65. Docking of the phosphonic acid dianion **36c** in EcDXR (1Q0L) showing the pocket (I) 'in front' of phosphonate-binding site occupied by thiazole ring. The surface zone at 4.1 Å from fosmidomycin **19** is shown with 50% transparency and coloured by atom type. Protein residues are shown in wireframe, coloured by atom type, the crystal structure fosmidomycin in ball-and-stick format coloured by atom type and ligand **36c** and NADPH as sticks coloured by atom type.

Further exploration of the cavities around the phosphonate-binding region revealed two additional pockets (II and III; Figure 66) which could be exploited in the design of new inhibitors. The first, a small, generally hydrophobic pocket (II) 'behind' the phosphonate group may well accommodate the methyl ester moiety in a ligand described by Perruchon *et al.*,[57] and the small size of this pocket could explain why the methyl ester was found to be more active than the ethyl ester. A second, relatively large cavity (III) extends 'above' the phosphonate-binding region, as shown in Figure 66. A number of docking results suggest occupation of this pocket and Deng *et al.* also mention a hydrophobic pocket which may be occupied by a phenyl ring.[74] Figure 66 shows a 'front' view of the active site illustrating the positions of the three pockets (I, II and III) close to the phosphonate-binding region. In contrast, the space around the central region is relatively restricted and the metal-binding site is constrained by the metal cation, the bound NADPH and the channel.

Figure 66. Active site of *Ec*DXR (2EGH), showing the three available pockets (I, II and III) close to the phosphonate-binding site. The surface zone at 7.7 Å from fosmidomycin **19** is coloured by hydrophobicity [polar (blue), non-polar (white), hydrophobic (orange)] and clipped in front. Protein residues are shown in wireframe, coloured by atom type, fosmidomycin in ball-and-stick format coloured by atom type, NADPH as sticks coloured by atom type, Mg^{2+} as a green sphere and the crystal structure water molecules as red spheres.

Although several crystal structures of *Ec*DXR are available, none has yet been elucidated for *Pf*DXR and, therefore, the homology model developed by Goble *et al.* was used to compare the properties of the active sites of *Ec*DXR and *Pf*DXR.[51] It is widely accepted that, in enzyme assays, the inhibition of *Ec*DXR is a reasonable indicator of *Pf*DXR inhibition potential; however, small differences between the two enzymes may provide useful guides for the design of better *Pf*DXR inhibitors.[60] As the model developed by Goble *et al.* does not include fosmidomycin **19** or Mg^{2+}, these structures were extracted from the 2EGH[53] crystal structure and superimposed on the *Pf*DXR model by overlaying corresponding residues. The active-site residues of the two models superimposed very closely, enabling the inhibitor and metal cofactor to be positioned with confidence. Table 9 shows the dimensions of the active sites of the *Ec*DXR crystal structure (2EGH)[53] and the *Pf*DXR model[51] with distances measured between corresponding residues in the two structures. The active site of *Pf*DXR appears to be slightly shorter and deeper than the *Ec*DXR counterpart but, as the active-site residues are highly conserved, the receptor cavities in *Pf*DXR and *Ec*DXR are very similar in shape.[50,51] Significantly, however, in *Pf*DXR, a cysteine residue (Cys267) replaces the smaller Ser253 in *Ec*DXR (2EGH)[53]

resulting in the presence of two cysteine residues (Cys197 and Cys267) in pocket I 'in front' of the phosphonate-binding site as shown in Figure 67. The larger size of the cysteine residue in PfDXR slightly decreases the size of pocket I, and this difference, as well as the differences in polarity and chemical properties between serine and cysteine could be exploited in the design of new PfDXR-specific inhibitors.

Table 9. Comparison of the dimensions of the EcDXR (2EGH) and PfDXR (homology model) active sites.

Dimension	Distance (Å)		Corresponding amino acid residues	
	EcDXR	PfDXR	EcDXR	PfDXR
Length	12.2	10.3	Ser185 OG - Asp149 OD	Ser199 OG - Asp160 OD
Width	8.9	9.9	Trp211 CD - Glu230 OE	Trp225 CD - Glu244 OE
Height	9.6	10.2	Ile217 C(O) - Glu151 OE	Ile231 C(O) - Glu162 OE
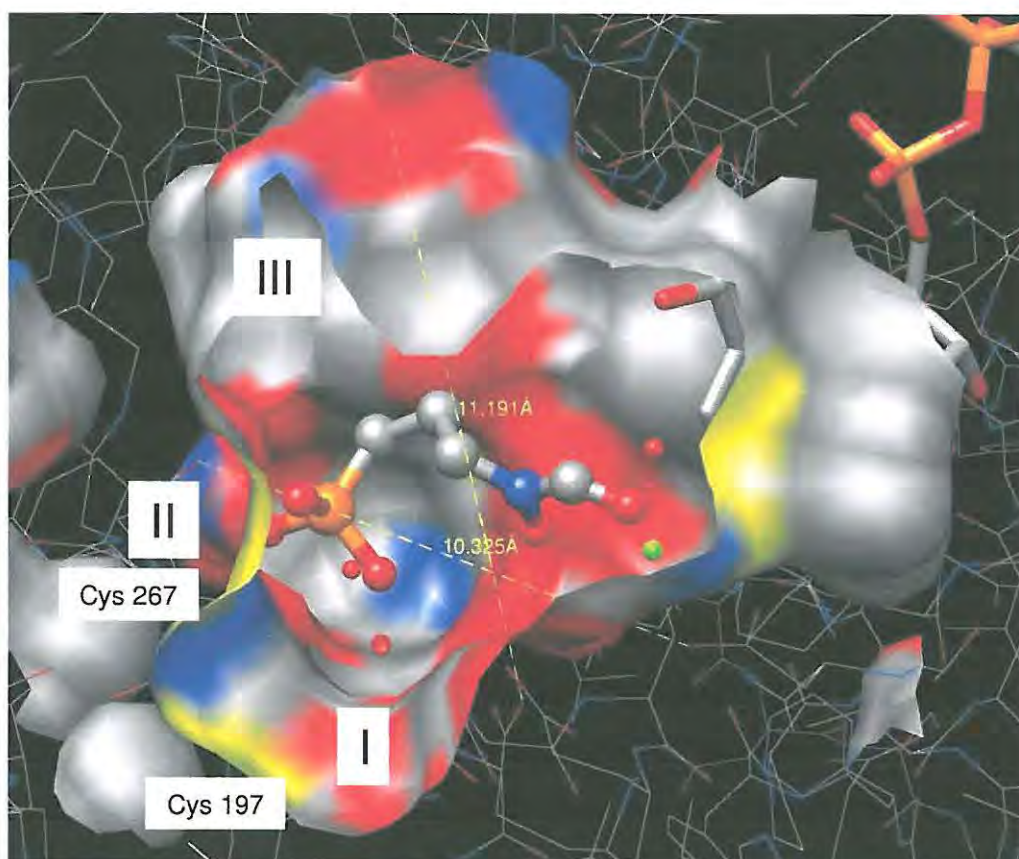
Figure 67. Active site of PfDXR with Mg^{2+}, NADPH and fosmidomycin **19** from 2EGH, showing some dimensions of the cavity, the pockets (I, II and III) and highlighting differences between EcDXR and PfDXR. The surface zone at 7.3 Å from fosmidomycin is coloured by atom type and clipped in front. Protein residues are shown in wireframe, coloured by atom type, NADPH as sticks coloured by atom type, fosmidomycin in ball-and-stick format, coloured by atom type, Mg^{2+} as a green sphere and water molecules as red spheres.

In *Pf*DXR, as in *Ec*DXR, there are three pockets close to the phosphonate-binding site (Figure 67). Compared with the corresponding pockets in *Ec*DXR, pocket I in *Pf*DXR is smaller and less flattened, pocket II is slightly larger and pocket III is wider. The distances measured from the phosphate atom in fosmidomycin **19** to the end of each of the three pockets (I, II and III) are shown in Figure 68, as is the height of pocket I. Binding of the active ligand **26**[104] (Figure 14, p. 24) may well involve occupation of either pocket I or pocket III by the 3,4-dichlorophenyl ring. Distances such as those shown in Figure 68 can, however, only be taken as approximations since the dynamic nature of the enzyme structure allows a degree of conformational flexibility.
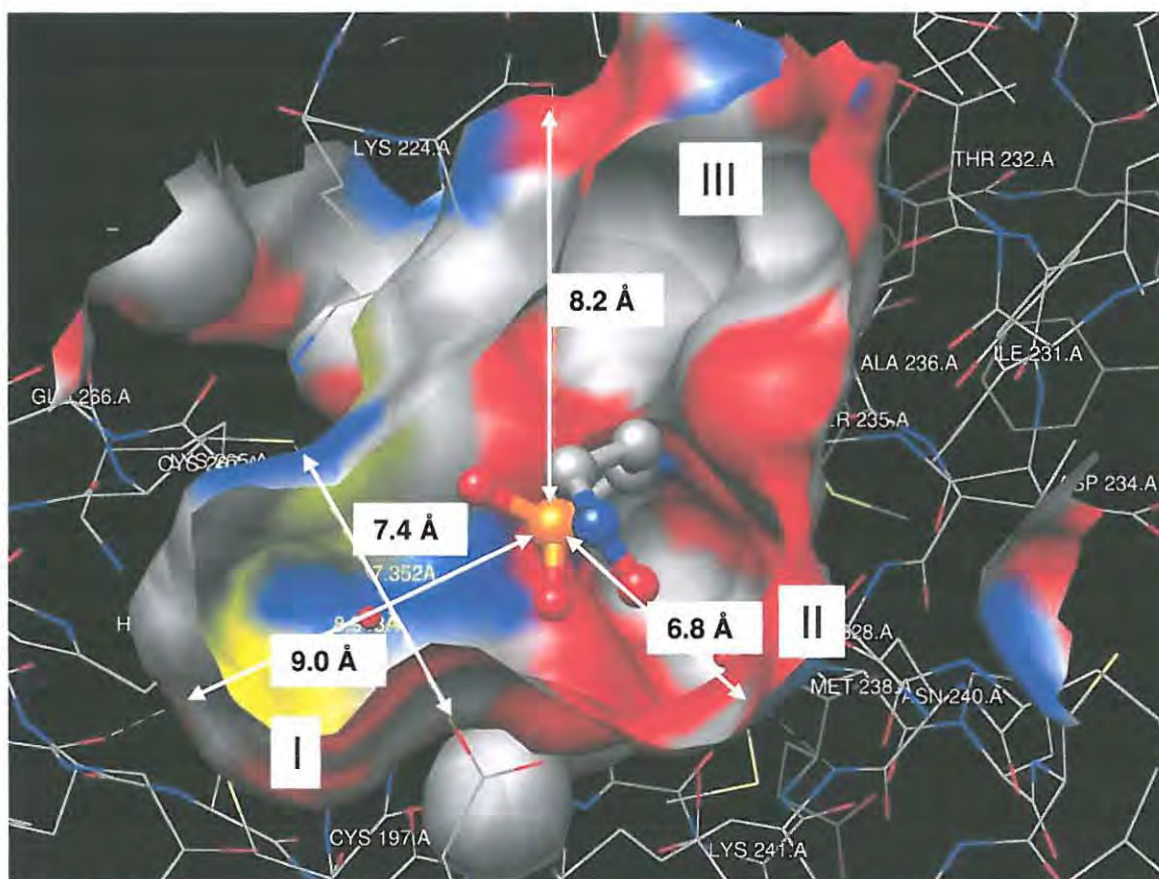
Figure 68. Active site of *Pf*DXR with Mg^{2+}, NADPH and fosmidomycin **19** from 2EGH, viewing along the axis of fosmidomycin **19** towards the phosphonate group and showing the dimensions of the nearby pockets (I, II and III). The surface zone at 8.0 Å from fosmidomycin is coloured by atom type and clipped in front. Protein residues are shown in wireframe, coloured by atom type, and residues less than 8.0 Å away from fosmidomycin are labelled. Fosmidomycin is shown in ball-and-stick format, coloured by atom type and water molecules are shown as red spheres.

Figure 69 highlights the polarity of the cavity in *Pf*DXR and shows some of the surrounding residues, while the narrowness of the central portion of the binding site is illustrated in Figure 70. The latter figure shows a view down the length of the cavity from the phosphonate end, with the central region clearly bordered by the planar β-indole ring of Trp225 in the front and by Ser235 at the back.

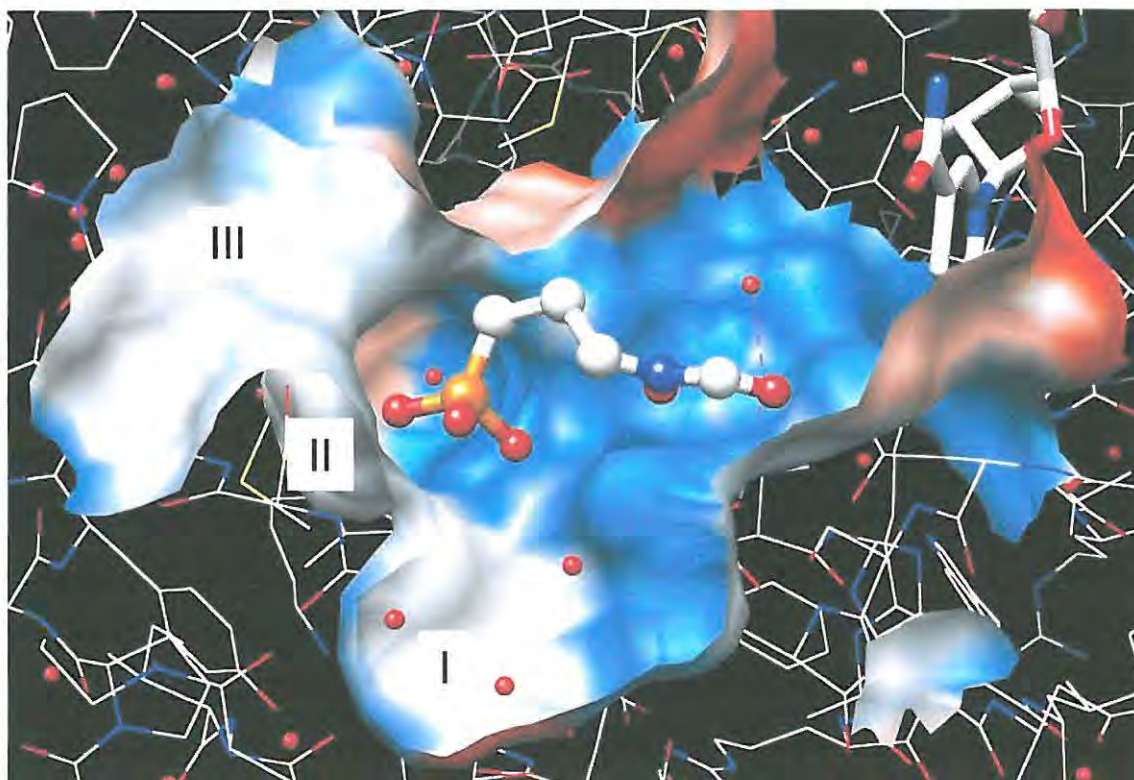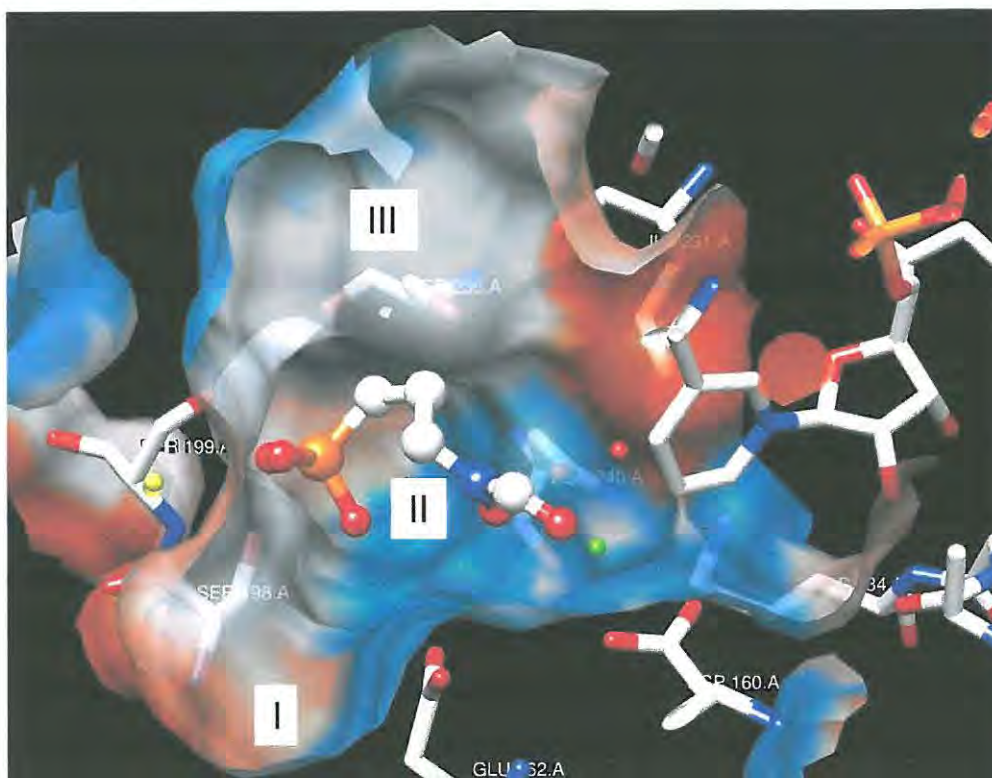**Figure 69.** Active site of *Pf*DXR, showing the three available pockets (I, II and III) close to the phosphonate-binding site. The surface zone at 8.0 Å from fosmidomycin **19** is shown with 30% transparency, coloured by hydrophobicity [polar (blue), non-polar (white), hydrophobic (orange)] and clipped in front. Protein residues are shown as sticks, coloured by atom type and residues less than 8.0 Å away from fosmidomycin are labelled. Fosmidomycin is shown in ball-and-stick format, coloured by atom type, NADPH as sticks coloured by atom type, Mg^{2+} as a green sphere and the coordinating water molecule as a red sphere.

The information obtained from this study of the topology of the *Ec*DXR and *Pf*DXR active sites, structure-activity relationship data reported in the literature and the pharmaco-kinetic observations detailed below were used to design a set of potential inhibitors. It is widely accepted that the cause of the limited plasma half-life of fosmidomycin **19** is its high hydrophilicity which leads to low membrane permeability.[38] A possible solution to this problem is the synthesis of phosphonate ester pro-drugs which can be hydrolysed *in vivo* to yield the active phosphonic acids. The rate of hydrolysis of the phosphonate ester linkages can be decreased by increasing the bulkiness of the ester group,[79] and diaryl, acyloxyalkyl and pivaloyloxymethyl ester analogues of fosmidomycin have been synthesised and have shown increased plasma levels after oral administration.[62,75,76] The phosphonate moiety has been widely used because it is more stable than the phosphate moiety found in DOXP **9**. Additional disadvantages of phosphates as potential drug molecules are their lower membrane solubility and greater susceptibility to hydrolysis compared to phosphonates.[79,116] The importance of a metal-coordinating group, on one hand, and a dianionic phosphonate group, on the other, has

97

been highlighted, and the studies of the active site described above suggest that the distance between these two functionalities needs to correspond to a 3 carbon atom chain for the groups to reach their respective binding sites.[57,74] The decrease in activity in the enzyme inhibition assays observed on increasing the number of methylene groups (Section 2.3.2.) supports this assumption. Attempts to place substituents at positions β and γ to the phosphonate on the carbon chain have led to a decrease in inhibition – an observation attributed to the narrowness and highly polar nature of the central region of the cavity.[70,76] Only α-substituted fosmidomycin analogues such as **26**[104] have shown higher inhibition properties than fosmidomycin **19** and this is probably due to occupation of one of the pockets (I or III) described above, by the α-substituent.
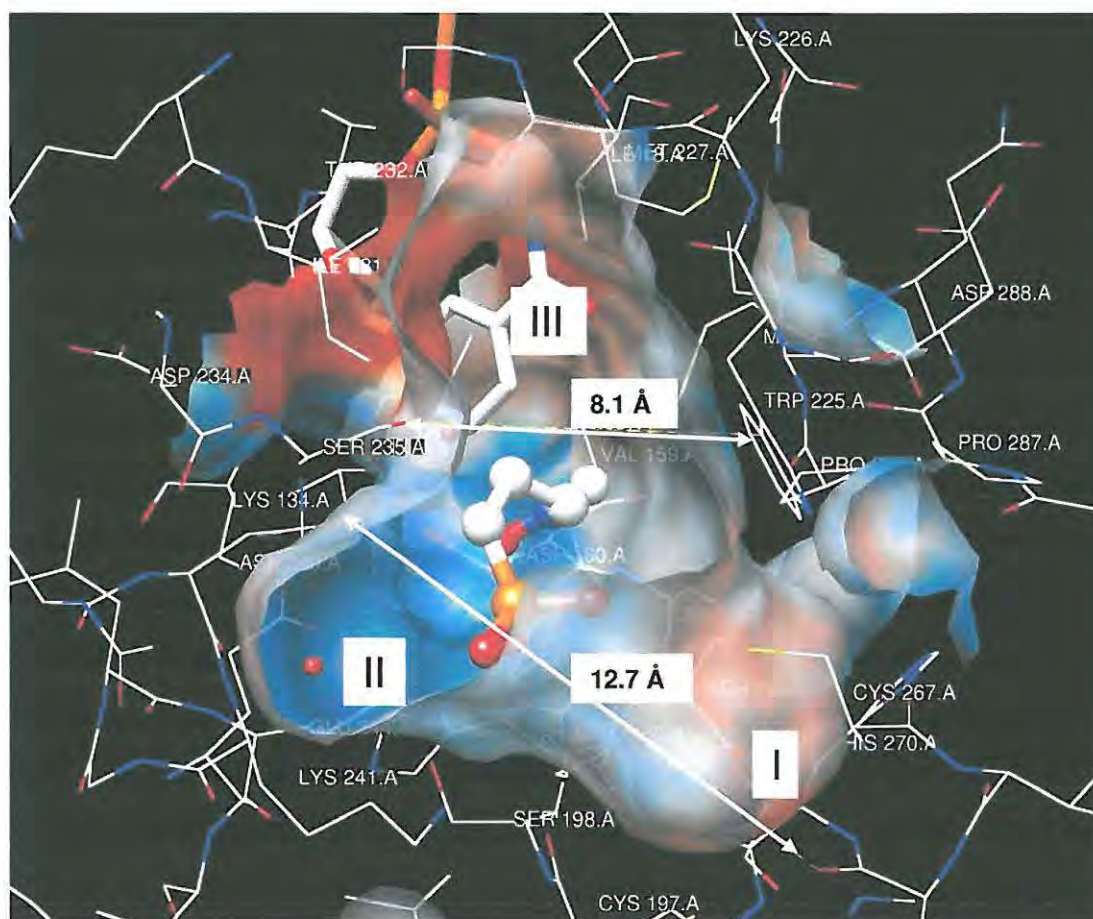
Figure 70. Active site of *Pf*DXR with Mg^{2+}, NADPH and fosmidomycin **19** from 2EGH, viewing along the axis of fosmidomycin towards NADPH and showing the dimensions of the pocket at the widest (12.7 Å) and narrowest (8.1 Å) points. The surface zone at 8.0 Å from fosmidomycin is shown with 30% transparency, coloured by hydrophobicity [polar (blue), non-polar (white), hydrophobic (orange)] and clipped in front. Protein residues less than 10 Å away from fosmidomycin are shown in wireframe, coloured by atom type, and residues less than 8.0 Å away from fosmidomycin are labelled. Fosmidomycin is shown in ball-and-stick format, coloured by atom type, NADPH as sticks coloured by atom type and the crystal structure water molecules as red spheres.

Consideration of the above requirements led to the design of compounds **52a-e** (Figure 71), as potential *Pf*DXR inhibitors. Whilst maintaining the phosphonate and hydroxamate moieties of fosmidomycin **19**, the α-carbon has been replaced by a nitrogen atom to:- i) provide a point of attachment for α-substituents; ii) provide a hydrogen-bonding atom in the α-position similar to the DOXP phosphate group; and iii) avoid introducing a chiral centre at the α-position, thus facilitating synthesis. Instead of the aromatic α-substituents employed by Kurz *et al.* and Haemers *et al.*,[60,76] less bulky ethyl substituents were proposed for compounds **52b-d** with terminal atoms designed to permit interaction with serine or cysteine residues close to the phosphonate-binding site. Such interactions could involve the formation of covalent disulphide or thioether links between the inhibitor and the enzyme receptor site.
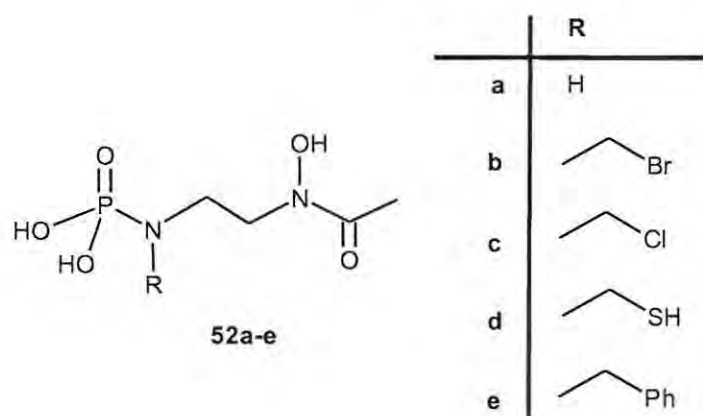
Figure 71. Structures of the proposed novel ligands **52a-e**.

2.5. Preliminary studies towards the synthesis of novel, customised ligands

As indicated in the previous section, analysis of the molecular topology of the DXR active site led to the design of compounds **52a-e** and, although time was limited, it was decided to, at least, commence an approach to their synthesis. The synthetic strategy outlined in Scheme 6 was adapted from established syntheses of fosmidomycin **19** and its analogues,[59,68,75,80,117] a variation being the introduction of a nitrogen atom α to the phosphonate group to facilitate attachment of α-substituents to occupy pocket I and enhance activity.[104] In addition, attachment of such subsituents to the nitrogen avoids the introduction of chirality which would have to be considered if the attachment was to an sp^3 hybridised carbon atom.
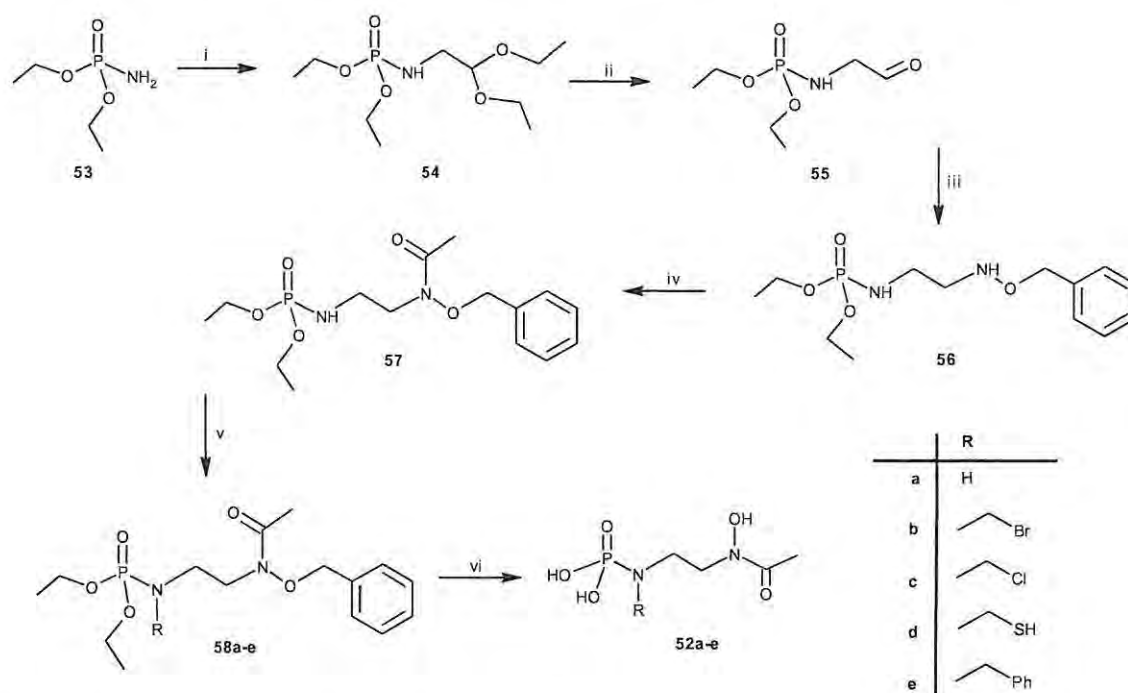
Scheme 6. Proposed synthesis of novel ligands **52a-e**.
Proposed reagents:- (i) NaH, bromoacetaldehyde diethylacetal; (ii) 2M-HCl; (iii) O-benzylhydroxylamine; NaCNBH$_3$; (iv) acetyl chloride, Et$_3$N; (v) NaH, RCl; (vi) H$_2$, Pd/C or acetyl chloride, EtOH.

Zwierzak has reported that monoalkylation of diethyl phosphoramidate **53** gave poor results – due mainly to formation of a mixture of the mono- and dialkylated products – but found that this problem could be avoided by protecting the primary amide.[117] Following Zwierzak's method,[117] diethyl phosphoramidate **53** was reacted with hexamethyldisilazane in refluxing benzene (Scheme 7)[117] to afford the protected amide **59** as an oil which, on cooling, crystallised as off-white, highly hygroscopic crystals. The reaction was high-yielding (95-97%) and the product **59** was very clean as shown in the ^{1}H NMR spectrum (Figure 75).
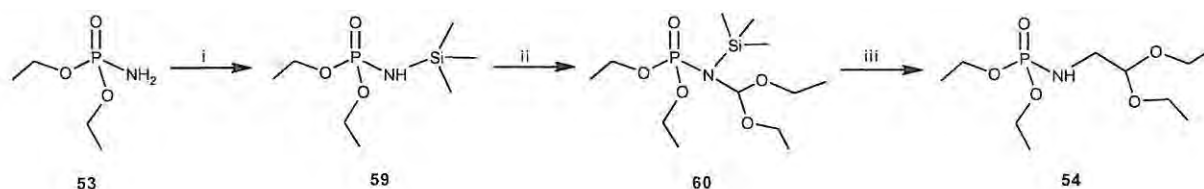
Scheme 7. Monoalkylation of diethyl phosphoramidate **53**.[117]
Reagents and conditions:- (i) Hexamethyldisilazane (20 % mol excess), C_6H_6, 3 h, reflux (80 °C); (ii) NaH (1.2 eq.), C_6H_6, r.t.; bromoacetaldehyde diethylacetal, tetrabutylammonium bromide (10 mol%), C_6H_6, 4 h, reflux (80 °C); (iii) EtOH, 1 h, 80 °C.

Alkylation of the protected phosphorus amide **59** was achieved by deprotonation of the amide using sodium hydride followed by reaction with bromoacetaldehyde diethyl acetal in the presence of 10 mol% tetrabutylammonium bromide to afford compound **60** (Scheme 7).[117] The role of tetrabutylammonium bromide is not clear but it has been suggested that the catalyst may facilitate formation of a reactive ionised species.[117] Deprotection of the amide **60** was carried out *in situ* by the addition of ethanol, and, after work-up, compound **54** was isolated in 90% yield. Comparison of the ^{1}H NMR spectra of the protected substrate **59** and the deprotected product **54** (Figure 72) reveals the presence of the signals due to the trimethylsilyl protons at 0.18 ppm in the protected substrate **59** and their subsequent disappearance in the deprotected product **54**. Integration of the signals in the ^{1}H NMR spectrum of the product **54** indicates that the protection method successfully prevented dialkylation of the diethyl phosphoramidate. The methylene signals of the diethyl acetal moiety appear as a doublet of quartets due to coupling to the methyl protons and to each other, as confirmed by the COSY NMR spectrum. This is due to the chemical non-equivalence of these two protons and therefore their magnetic non-equivalence and consequent geminal coupling.

101

Figure 72. ^{1}H NMR spectra of (i) protected phosphorus amide **59**, and (ii) alkylated phosphoramidate **54** (CDCl$_3$, 600 MHz).
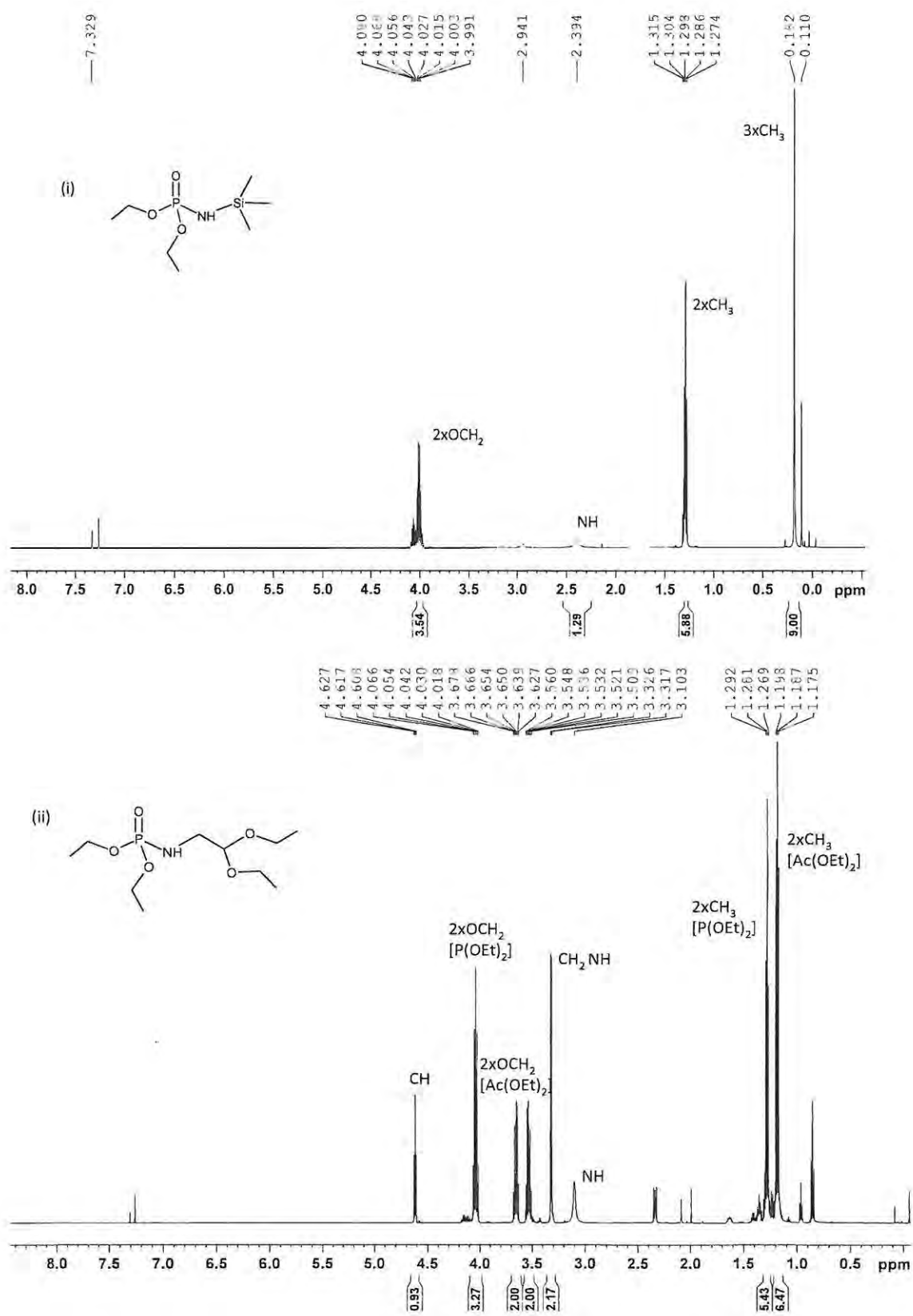
The next step in the synthesis involves cleavage of the diethyl acetal **54** (Scheme 8). This is a well-established procedure but application of the methods used by Ortmann *et al.* and Perruchon *et al.*[57,75] failed to yield the desired product **55**. The reaction was repeated several times and the reaction time was varied as shown in Scheme 8. Analysis of the crude products by ^{1}H NMR spectroscopy suggested that very little of the desired aldehyde **55** was formed and that cleavage may also have occurred elsewhere. As time was limited, this reaction could not be investigated further but exploration of different methods for the cleavage of the diethyl acetal **54** is being continued in our group and the synthesis of compounds **52a-e** will be pursued.
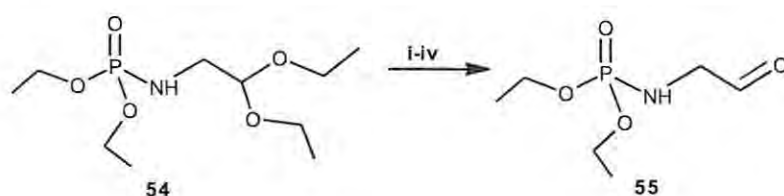
Scheme 8. Attempted cleavage of diethyl acetal **54** to the aldehyde **55**.
Reagents and conditions:- 2M-HCl; (i) r.t., overnight; (ii) r.t., 3.5 days; (iii) r.t., 3 h; (iv) 40 °C, 4h.

2.6 Conclusions

The phosphonate esters **35a-e** and the corresponding phosphonic acid salts **36a-e** have been successfully synthesised as fosmidomycin **19** analogues. Reaction of a series of heterocyclic amines with chloroacetyl chloride, followed by phosphonation with triethyl phosphite led to the esters **35a-e**, hydrolysis of which afforded the disodium salts **36a-e**. A second series of phosphonate esters **39a-e** and their corresponding phosphonic acid salts **40a-e** with a bimethylene spacer have also been synthesised, using 3-chloropropionyl chloride in place of chloroacetyl chloride, to investigate the effect of lengthening the carbon backbone of fosmidomycin **19** analogues. Further investigation into some of the reactions employed led to the purification and characterisation of various side products formed during the synthesis of the 2-aminopyridine derivative **41a**. All of the above compounds, with the exception of the salt **36a**, are new and have been fully characterised using elemental (HRMS or combustion analysis) and spectroscopic (1- and 2-D NMR and IR) techniques. A kinetic study of the transesterification reaction between the phosphonate esters and bromotrimethylsilane employed for hydrolysis of the phosphonate esters was undertaken and illustrated the use of ^{31}P NMR for following the reaction progress. Rate constants for the two, consecutive, second-order reactions involved and activation parameters for the reactions were calculated following variable temperature studies and a computational method was developed for the optimisation of the rate constants.

The phosphonate esters **35a-e** and **39a-e** and the corresponding phosphonic acid salts **36a-e** and **40b-e** were subjected to preliminary screening for their ability to bind to DXR using the STD NMR technique, following optimisation of the solvent and the pulse sequence parameters. Comparison of the STD difference spectra with the ligand spectra indicated that all of the synthesised ligands exhibited binding to EcDXR, although the STD experiment, used alone, does not distinguish between specific and non-specific binding of the ligand to the protein. A second, competitive binding experiment involving the inclusion of the highly active inhibitor fosmidomycin **19** in the ligand mixture was therefore carried out. The results of this experiment suggested that, either the ligands bind non-competitively at a site other than the active site and, perhaps, cause allosteric inhibition, or that their binding in the active site is much more transient than that of fosmidomycin **19**. Enzyme inhibition assays on the synthesised ligands supported these conclusions as most of the inhibitors were found to exhibit relatively low inhibitory activity compared to fosmidomycin **19**. Several structure-activity relationships were, however, suggested by the enzyme inhibition results. Thus, increasing the length of the carbon spacer in the ligands from one to two methylene groups

decreased the IC_{50} values, the more hydrophobic phosphonate esters generally showed greater inhibition than the corresponding phosphonic acid salts, and the furfuryl-derived ester **35d** and acid salt **36d** showed the greatest inhibition of the ligands tested.

Simulated docking studies using AutoDock revealed the ability of the ligands to fit into the active site of DXR and to form hydrogen-bonding interactions with active-site residues. Repeated observation of a 'reverse' binding orientation for many of the ligands led to an investigation of the effect of the charge assigned to the divalent metal cofactor included in DXR. Substitution of the automatically-assigned charges with quantum-mechanical calculated charges resulted in a decrease in the number of 'reverse' docks. Validation of the docking parameters revealed that decreasing the number of flexible residues selected improved the reproducibility of the docking. However, increasing the rigidity of the model may compromise its approximation to the biological system. Exploration of the DXR active-site topology revealed the presence of three pockets of different sizes in close proximity to the phosphonate-binding site. Occupation of these pockets, and possible chemical interaction with their constituent amino acid residues, was proposed to increase the inhibitory activity of a new generation of DXR inhibitors. Consideration of these results, as well as the structure-activity relationships described above, directed the design of a series of novel, customised inhibitors for *Pf*DXR, compounds **52a-e**, the synthesis of which has been commenced and will be continued within our group.

Overall, the project has involved a combination of various complementary approaches to novel drug discovery. Thus, synthetic, physical organic, computer modelling and biochemical evaluation techniques have all been used and have led to the identification of structure-activity relationships for two series of potential inhibitors and the rational design of a third series of novel DXR inhibitors **52a-e**.

The study of the active-site topology of DXR and the design of compounds **52a-e** has provided a platform for future work on DXR inhibitors, especially those customised for *Pf*DXR, and opportunities for future research include:-

   i)   the design of ligands capable of occupying several of the available pockets;

   ii)   further development of the *Pf*DXR model to include the metal cofactor;

   iii)   extension of the STD NMR technique to permit calculation of binding constants or binding epitopes of the ligands; and

   iv)   following the enzyme inhibition assays with cell-based assays to test the bioavailability and toxicity of the inhibitors.

3. EXPERIMENTAL

3.1. Synthesis of potential DXR inhibitors

General

Synthesis and Purification

Starting materials were obtained from Sigma-Aldrich or Fluka and used without further purification. THF and benzene were distilled from sodium/benzophenone under nitrogen. DCM was stored over $CaCl_2$ overnight and then distilled from CaH_2 under nitrogen. Normal-phase thin layer chromatography was performed on Merck TLC silica gel 60 F_{254} plates, and reverse-phase on Fluka TLC silica gel RP-18 F_{254} plates. Plates were viewed under UV light (254 nm) or developed with iodine vapour. Flash chromatography[118] was performed using silica gel 60 (70-230 mesh) for normal-phase and Sep-Pak Vac 35cc C18 cartridges for reverse-phase. Normal-phase semi-preparative HPLC was performed on a Whatman Partisil 10 column and reverse-phase on a Phenomenex C-18 LUNA column, using a Spectra-Physics Spectra Series P100 isocratic pump and a Waters 401 Differential Refractometer with a Perkin-Elmer 561 Recorder.

Analysis and Characterisation

NMR spectra were recorded on a Bruker Biospin 600 MHz Avance spectrometer at 298 K (except where described otherwise for kinetics experiments) and calibrated on the residual protonated solvent signals (for $CDCl_3$: δ_H = 7.26 ppm; δ_C = 77.00 ppm; for D_2O: δ_H = 4.79 ppm). Multiplicities described for ^{13}C spectra were obtained from the DEPT or multiplicity-edited HSQC spectra and refer to ^{13}C-^{1}H coupling except in the case of ^{13}C-^{31}P coupling where the J_{C-P} values are recorded and the multiplicity refers to this coupling. IR spectra were recorded on a Perkin-Elmer Spectrum 100 FT-IR spectrometer with neat compounds on a diamond window. Melting points were determined using a Reichert hot-stage apparatus and are uncorrected. Low-resolution mass spectrometry was performed on a Finnigan MAT GCQ mass spectrometer, using the electron ionisation mode. High-resolution mass spectra were recorded on Micromass 70-70E (Northwest University, Potchesfstroom, South Africa) and Waters API Q-TOF Ultima spectrometers (University of Stellenbosh, Stellenbosh, South Africa). The names of new compounds are italicised and literature references are cited for known compounds; § denotes that no melting point data were given.

Procedure 1. Synthesis of 2-chloro-*N*-arylacetamides 38a-e.[72]

A solution of the relevant primary amine (**37a-e**) in dry THF was stirred under N_2. NaH (60% dispersion in mineral oil; 1 eq.) was added slowly to allow controlled evolution of H_2. Chloroacetyl chloride (1 eq.) was then added through a septum and the mixture was stirred for *ca.* 6 h. The solvent was removed *in vacuo* and the residue dissolved in EtOAc (2 x 50 mL). The resulting solution was washed sequentially with saturated aqueous $NaHCO_3$ (2 x 100 mL), water (2 x 100 mL) and brine (2 x 100 mL). The combined aqueous layers were then re-extracted with EtOAc (100 mL). The organic layers were combined, dried with anhydrous Na_2SO_4 or $MgSO_4$ and evaporated *in vacuo* to afford the 2-chloro-*N*-arylacetamide product.

2-Chloro-*N*-(pyridine-2-yl)acetamide 38a

The general procedure 1 was followed, using 2-aminopyridine **37a** (2.64 g, 28 mmol), THF (30 mL), NaH (1.20 g, 30 mmol) and chloroacetyl chloride [2.2 mL (3.12 g), 28 mmol]. The crude product (2.65 g, 55%) was isolated as a red-brown oil which partly crystallised on standing. Purification by column chromatography [on silica; elution with hexane-EtOAc (1:3)] afforded 2-chloro-*N*-(pyridine-2-yl)acetamide **38a** as pale purple crystals (0.50 g, 21%), mp 82-86 °C (lit.,[77,119] 110-115 and 123-125 °C); v/cm^{-1} 1676 (C=O); δ_H (600 MHz; CDCl$_3$) 4.19 (2H, s, CH$_2$Cl), 7.10 (1H, dd, *J*=7.2 and 4.8 Hz, 5'-H), 7.73 (1H, dd, *J*=8.5 and 7.2 Hz, 4'-H), 8.19 (1H, d, *J*=8.5 Hz, 3'-H), 8.32 (1H, d, *J*=4.8 Hz, 6'-H) and 8.86 (1H, s, NH); δ_C (150 MHz; CDCl$_3$) 42.7 (t, CH$_2$Cl), 113.9 (d, C-3'), 120.6 (d, C-5'), 138.5 (d, C-4'), 148.1 (d, C-6'), 150.3 (s, C-2') and 164.4 (s, C=O); *m/z* 171 (MH$^+$, 100%).

2-Chloro-*N*-(isoxazole-3-yl)acetamide 38b

The general procedure 1 was followed, using 3-aminoisoxazole **37b** [1.4 mL (1.59 g), 19 mmol], THF (30 mL), NaH (1.20 g, 50 mmol) and chloroacetyl chloride [2.2 mL (3.12 g), 28 mmol]. 2-Chloro-*N*-(isoxazole-3-yl)acetamide **38b** was isolated as a dark brown solid (3.89 g, 100%), mp 109-113 °C (lit.,[120] §); v/cm^{-1} 1715 (C=O); δ_H (600 MHz; CDCl$_3$) 4.22 (2H, s, CH$_2$Cl), 7.07 (1H, d, *J*=1.4 Hz, 4'-H), 8.34 (1H, d, *J*=1.4 Hz, 5'-H) and 9.10 (1H, s, NH); δ_C (150 MHz; CDCl$_3$) 42.5 (t, CH$_2$Cl), 99.1 (d, C-4'), 156.7 (s, C-3'), 159.3 (d, C-5') and 164.4 (s, C=O); *m/z* 161 (MH$^+$, 100%).

2-Chloro-*N*-(1,3-thiazole-2-yl)acetamide 38c

The general procedure 1 was followed, using 2-aminothiazole **37c** (1.90 g, 19 mmol), THF (30 mL), NaH (1.20 g, 30 mmol) and chloroacetyl chloride [2.2 mL (3.12 g), 28 mmol]. 2-Chloro-*N*-(1,3-thiazole-2-yl)acetamide **38c** was isolated as a yellow-brown solid (2.34 g, 70%), mp 111-113 °C (lit.,[121] 162-164 °C); v/cm^{-1} 1701 (C=O); δ_H (600 MHz; CDCl$_3$) 4.28 (2H, s, CH$_2$Cl), 7.05 (1H,

d, J=3.5 Hz, 5'-H) and 7.50 (1H, d, J=3.5 Hz, 4'-H); δ_C (150 MHz; CDCl$_3$) 42.1 (t, CH$_2$Cl), 114.6 (d, C-5'), 137.8 (d, C-4'), 157.4 (s, C-2') and 164.0 (s, C=O); m/z 177 (MH$^+$, 100%).

2-Chloro-*N*-(furan-2-ylmethyl)acetamide 38d

The general procedure 1 was followed, using furfurylamine **37d** [2.5 mL (2.66 g), 28 mmol], THF (30 mL), NaH (1.20 g, 30 mmol) and chloroacetyl chloride [2.2 mL (3.12 g), 28 mmol]. 2-Chloro-*N*-(furan-2-ylmethyl)acetamide **38d** was isolated as a brown solid (3.97 g, 84%), mp 58-60 °C (lit.,[122,123] §); v/cm^{-1} 1645 (C=O); δ_H (600 MHz; CDCl$_3$) 4.07 (2H, s, CH$_2$Cl), 4.48 (2H, d, J=5.4 Hz, CH$_2$N), 6.26 (1H, d, J=3.2 Hz, 3'-H), 6.33 (1H, dd, J=3.2 and 1.9 Hz, 4'-H), 6.89 (1H, s, NH) and 7.37 (1H, d, J=1.9 Hz, 5'-H); δ_C (150 MHz; CDCl$_3$) 36.8 (t, CH$_2$NH), 42.5 (t, CH$_2$Cl), 107.9 (d, C-3'), 110.5 (d, C-4'), 142.6 (d, C-5'), 143.0 (s, C-2') and 150.3 (s, C=O); m/z 173 (M$^+$, 22%) and 343 (100).

N-(5-Acetyl-4-methyl-1,3-thiazol-2-yl)-2-chloroacetamide 38e

The general procedure 1 was followed, using 5-acetyl-2-amino-4-methylthiazole **37e** (2.20 g, 14 mmol), THF (15 mL), NaH (0.67 g, 28 mmol) and chloroacetyl chloride [1.1 mL (1.56 g), 14 mmol]. *N*-(5-Acetyl-4-methyl-1,3-thiazol-2-yl)-2-chloroacetamide **38e** was isolated as a dark brown solid (2.42 g, 74%), mp 148-151 °C (lit.,[124] §); v/cm^{-1} 1713 (C=O); δ_H (600 MHz; CDCl$_3$) 2.52 (3H, s, 4'-CH$_3$), 2.66 (3H, s, CO.CH$_3$) and 4.30 (2H, s, CH$_2$Cl); δ_C (150 MHz; CDCl$_3$) 18.0 (q, CO.CH$_3$), 30.4 (q, CH$_3$-4'), 41.9 (t, CH$_2$Cl), 126.5 (d, C-5'), 156.3 (d, C-4'), 157.5 (s, C-2'), 164.2 (s, NHC=O) and 190.5 (s, CH$_3$C=O); m/z 233 (MH$^+$, 100%).

Procedure 2. Synthesis of 2-chloro-*N*-arylacetamides 38a and 38d in 1,2-dichloroethane (non-microwave).[77]

The relevant amine (**37a** or **37d**) was dissolved in 1,2-dichloroethane and stirred for 10 min under N$_2$ in an ice bath. Chloroacetyl chloride (1 eq.) was added dropwise and, after stirring for 1 h at room temperature, the pH of the solution was adjusted to pH 9 with aqueous NaOH. After separation, the aqueous layer was extracted twice with 1,2-dichloroethane (25 mL) and the organic layers were combined and dried over anhydrous Na$_2$SO$_4$ followed by removal of the solvent *in vacuo*.

Attempted synthesis of 2-chloro-*N*-(pyridine-2-yl)acetamide 38a

The general procedure 2 was followed, using 2-aminopyridine **37a** (2.80 g, 30 mmol), 1,2-dichloroethane (25 mL) and chloroacetyl chloride [2.6 mL (3.69 g), 33 mmol]. Evaporation of

the solvent afforded a red-brown solid (2.03 g), NMR analysis of which showed the presence of the starting material alone.

2-Chloro-*N*-(furan-2-ylmethyl)acetamide 38d

The general procedure 2 was followed, using furfurylamine **37d** [2.7 mL (2.84 g), 30 mmol], 1,2-dichloroethane (25 mL) and chloroacetyl chloride [2.6 mL (3.69 g), 33 mmol]. 2-Chloro-*N*-(furan-2-ylmethyl)acetamide **38d** was isolated as a brown solid (4.70 g, 91%), mp 50-55 °C (lit.,[122,123] §); v/cm^{-1} 1648 (C=O); δ_H (600 MHz; CDCl$_3$) 4.07 (2H, s, CH$_2$Cl), 4.49 (2H, d, *J*=5.4 Hz, CH$_2$N), 6.27 (1H, d, *J*=3.3 Hz, 3'-H), 6.33 (1H, dd, *J*=3.3 and 1.8 Hz 4'-H), 6.88 (1H, s, NH) and 7.37 (1H, d, *J*=1.8 Hz, 5'-H); δ_C (150 MHz; CDCl$_3$) 36.7 (t, CH$_2$NH), 42.5 (t, CH$_2$Cl), 107.9 (d, C-3'), 110.5 (d, C-4'), 142.5 (d, C-5'), 150.2 (s, C-2') and 165.6 (s, C=O).

Procedure 3. Attempted synthesis of 2-chloro-*N*-(pyridine-2-yl)acetamide 38a in 1,2-dichloroethane (microwave method).[77]

A solution of 2-aminopyridine **37a** (0.56 g, 6.0 mmol) in 1,2-dichloroethane (5 mL) was made up in a 10 mL glass microwave tube. Chloroacetyl chloride [0.52 mL (0.74 g), 6.5 mmol] was added dropwise and the tube was sealed with a septum and irradiated at 80 °C for 5 min at 300 W in standard mode, with stirring and 5 min cooling time. The pH of the solution was then adjusted to pH 9 with aqueous NaOH. After separation, the aqueous layer was extracted twice with 1,2-dichloroethane (2 x 5 mL). The organic layers were combined and dried over anhydrous Na$_2$SO$_4$ and then the solvent was removed *in vacuo* to give a red-brown solid (0.23 g), NMR analysis of which showed the presence of only the starting material and impurities.

Procedure 4. Synthesis of phosphonate esters 35a-e.[72]

The relevant α-chloroamide (**38a-e**) was placed in a dry, round-bottomed flask under N$_2$ and triethyl phosphite [P(OEt)$_3$; 5 eq.] was added through a septum. The mixture was boiled under reflux (oil bath at 110 °C) for *ca*. 9 h. After cooling, hexane (20 mL) was added and the mixture stirred for *ca*. 20 min. The hexane was then decanted and stirring and decanting was repeated with three further aliquots (20 mL each) of hexane. Evaporation of residual hexane and P(OEt)$_3$ *in vacuo* afforded the desired ester **35a-e**.

Diethyl [2-oxo-2-(pyridin-2-ylamino)ethyl]phosphonate 35a

General procedure 4 was followed, using **38a** (0.43 g, 2.5 mmol) and P(OEt)$_3$ [2.0 mL (1.94 g), 12 mmol] to yield *diethyl [2-oxo-2-(pyridin-2-ylamino)ethyl]phosphonate* **35a** as a dark brown oil (0.078 g, 12%) (Found: M$^+$, 272.091731. C$_{11}$H$_{17}$N$_2$O$_4$P requires *M*, 272.092596); v/cm^{-1} 1691

(C=O) and 1018 (P-OR); δ_H (600 MHz; CDCl$_3$) 1.35 (6H, t, J=6.6 Hz, 2xCH$_3$), 3.04 (2H, d, J=21.0 Hz, CH$_2$P), 4.20 (4H, q, J=6.6 Hz, 2xOCH$_2$), 7.04 (1H, t, J=6.0 Hz, 5'-H), 7.69 (1H, t, J=7.8 Hz, 4'-H), 8.13 (1H, d, J=8.4 Hz, 3'-H), 8.28 (1H, d, J=4.8 Hz, 6'-H) and 8.96 (1H, s, NH); δ_C (150 MHz; CDCl$_3$) 16.4 (q, 2xCH$_3$), 36.9 (d, J_{C-P}=129.0 Hz, CH$_2$P), 63.0 (t, 2xOCH$_2$), 114.0 (d, C-3'), 120.0 (d, C-5'), 138.3 (d, C-4'), 148.0 (d, C-6'), 151.0 (s, C-2) and 162.7 (s, C=O); m/z 272 (M$^+$, 48%) and 94 (100).

Diethyl [2-(isoxazol-3-ylamino)-2-oxoethyl]phosphonate 35b

General procedure 4 was followed, using **38b** (1.02 g, 6 mmol) and P(OEt)$_3$ [5.2 mL (5.04 g), 30 mmol] to yield *diethyl [2-(isoxazol-3-ylamino)-2-oxoethyl]phosphonate* **35b** as a dark brown oil which crystallised on standing (0.800 g, 48%), mp 60-66 °C (Found: M$^+$, 262.071312. C$_9$H$_{15}$N$_2$O$_5$P requires M, 262.071860); v/cm^{-1} 1693 (C=O) and 1010 (P-OR); δ_H (600 MHz; CDCl$_3$) 1.35 (6H, t, J=7.2 Hz, 2xCH$_3$), 3.10 (2H, d, J=21.0 Hz, CH$_2$P), 4.20 (4H, q, J=7.3 Hz, 2xOCH$_2$), 6.98 (1H, d, J=1.8 Hz, 4'-H), 8.25 (1H, d, J=1.8 Hz, 5'-H) and 9.95 (1H, s, NH); δ_C (150 MHz; CDCl$_3$) 16.3 (q, 2xCH$_3$), 36.2 (d, J_{C-P}=130.5 Hz, CH$_2$P), 63.2 (t, 2xOCH$_2$), 99.3 (d, C-4'), 157.1 (s, C-3'), 158.7 (d, C-5') and 162.5 (s, C=O); m/z 262 (M$^+$, 67%) and 179 (100).

Diethyl [2-oxo-2-(1,3-thiazol-2-ylamino)ethyl]phosphonate 35c

General procedure 4 was followed, using **38c** (1.13 g, 6 mmol) and P(OEt)$_3$ [5.2 mL (5.04 g), 30 mmol] to yield *diethyl [2-oxo-2-(1,3-thiazol-2-ylamino)ethyl]phosphonate* **35c** as a brown oil (1.04 g, 59%) (Found: M$^+$, 278.047217. C$_9$H$_{15}$N$_2$O$_4$PS requires M, 278.049017); v/cm^{-1} 1684 (C=O) and 1015 (P-OR); δ_H (600 MHz; CDCl$_3$) 1.32 (6H, t, J=7.1 Hz, 2xCH$_3$), 3.17 (2H, d, J=21.6 Hz, CH$_2$P), 4.18 (4H, q, J=7.1 Hz, 2xOCH$_2$), 6.96 (1H, d, J=3.0 Hz, 5'-H) and 7.47 (1H, d, J=3.0 Hz, 4'-H); δ_C (150 MHz; CDCl$_3$) 16.2 (q, 2xCH$_3$), 35.6 (d, J_{C-P}=131.3 Hz, CH$_2$P), 63.1 (t, 2xOCH$_2$), 113.6 (d, C-5'), 137.2 (d, C-4'), 158.5 (s, C-2') and 162.4 (s, C=O); m/z 278 (M$^+$, 50%) and 179 (100).

Diethyl {2-[(furan-2-ylmethyl)amino]-2-oxoethyl}phosphonate 35d

General procedure 4 was followed, using **38d** (1.11 g, 6 mmol) and P(OEt)$_3$ [5.2 mL (5.04 g), 30 mmol] to yield *diethyl {2-[(furan-2-ylmethyl)amino]-2-oxoethyl}phosphonate* **35d** as a red-brown oil (1.09 g, 62%) (Found: M$^+$, 275.090706. C$_{11}$H$_{18}$NO$_5$P requires M, 275.092261); v/cm^{-1} 1662 (C=O) and 1015 (P-OR); δ_H (600 MHz; CDCl$_3$) 1.29 (6H, t, J=7.3 Hz, 2xCH$_3$) 2.85 (2H, d, J=20.7 Hz, CH$_2$P), 4.90 (4H, q, J=7.3 Hz, 2xOCH$_2$), 4.42 (2H, d, J=5.7 Hz, CH$_2$N), 6.22 (1H, d, J=3.0 Hz, 3'-H), 6.28 (1H, dd, J=3.0 and 1.7 Hz, 4'-H), 7.17 (1H, s, NH) and 7.31 (1H, d, J=1.7 Hz, 5'-H); δ_C (150 MHz; CDCl$_3$) 16.2 (q, 2xCH$_3$), 35.0 (d, J_{C-P}=129.0 Hz, CH$_2$P), 36.7 (t, CH$_2$NH), 62.7 (t,

2xOCH$_2$), 107.3 (d, C-3'), 110.3 (d, C-4'), 142.1 (d, C-5'), 151.0 (s, C-2') and 163.8 (s, C=O); *m/z* 275 (M$^+$, 22%) and 96 (100).

Diethyl {2-[(5-acetyl-4-methyl-1,3-thiazol-2-yl)amino]-2-oxoethyl}phosphonate 35e

The general procedure 4 was followed, using **38e** (1.49 g, 6 mmol) and P(OEt)$_3$ [5.2 mL (5.04 g), 30 mmol] to yield *diethyl {2-[(5-acetyl-4-methyl-1,3-thiazol-2-yl)amino]-2-oxoethyl}-phosphonate* **35e** as a yellow-brown solid (1.44 g, 67%), mp 151-154 °C [Found: (M-1)$^+$, 333.0667. C$_{12}$H$_{19}$N$_2$O$_5$PS requires *M-1*, 333.0674]; v/cm^{-1} 1682 (C=O) and 1011 (P-OR); δ$_H$ (600 MHz; CDCl$_3$) 1.38 (6H, t, *J*=7.2 Hz, 2xCH$_3$), 2.42 (3H, s, 4'-CH$_3$), 2.49 (3H, s, CO.CH$_3$), 3.19 (2H, d, *J*=22.2 Hz, CH$_2$P) and 4.27 (4H, q, *J*=7.2 Hz, 2xOCH$_2$); δ$_C$ (150 MHz; CDCl$_3$) 16.3 (q, 2xCH$_3$), 18.2 (q, CO.CH$_3$), 30.2 (q, CH$_3$-4') 35.7 (d, *J*$_{C-P}$=129.0 Hz, CH$_2$P), 63.6 (2xOCH$_2$), 125.5 (s, C-5'), 155.4 (s, C-4'), 158.4 (s, C-2'), 162.6 (s, NHC=O) and 190.6 (s, CH$_3$C=O); *m/z* 333 [(M-H)$^+$, 100%].

Procedure 5. Hydrolysis of phosphonate esters 35b-d in acetonitrile.[81]

The phosphonate ester starting material (**35b-d**) was placed in a 10 mL microwave tube and dissolved in acetonitrile (3 mL). The tube was sealed with a septum and trimethylsilyl bromide (TMSBr; 2 eq.) was added. The mixture was irradiated in a microwave at 100 W and 60 °C for 10 min in standard mode with stirring and 2 min allowed for cooling. The reaction was then quenched with 10 mL of a 95:5 methanol-water mixture and stirred for 30 min followed by removal of the solvent *in vacuo*.

Attempted synthesis of [2-(isoxazol-3-ylamino)-2-oxoethyl]phosphonic acid 36b

The general procedure 5 was followed, using **35b** (0.524 g, 2 mmol) and TMSBr [0.53 mL (0.61 g), 4 mmol]. Removal of the solvent gave a dark brown solid, 0.481 g, NMR analysis of which showed very broad signals which could not be assigned to either the desired product or to starting material; δ$_P$ (243 MHz; D$_2$O) -0.43.

[2-Oxo-2-(1,3-thiazol-2-ylamino)ethyl]phosphonic acid 36c

The general procedure 5 was followed, using **35c** (0.557 g, 2 mmol) and TMSBr [0.53 mL (0.61 g), 4 mmol]. Removal of the solvent afforded *[2-oxo-2-(1,3-thiazol-2-ylamino)ethyl]phosphonic acid* **36c** as brown solid (0.613 g); δ$_H$ (600 MHz; D$_2$O) 3.16 (2H, d, *J*=21.6 Hz, CH$_2$P), 6.95 (1H, d, *J*=3.6 Hz, 5'-H) and 7.40 (1H, d, *J*=3.6 Hz, 4'-H); δ$_P$ (243 MHz; D$_2$O) -1.38. Compound **36c** was fully characterised following its synthesis using procedure 7.

111

Attempted synthesis of {2-[((furan-2-ylmethyl)amino]-2-oxoethyl}phosphonic acid 36d

The general procedure 5 was followed, using **35d** (0.550 g, 2 mmol) and TMSBr [0.53 mL (0.61 g), 4 mmol]. Removal of the solvent gave a brown solid, 0.547 g, NMR analysis of which showed very broad signals which could not be assigned to either the desired product or to starting material; δ_P (243 MHz; D_2O) -0.39.

Procedure 6. Attempted synthesis of {2-[(5-acetyl-4-methyl-1,3-thiazol-2-yl)amino]-2-oxoethyl}phosphonic acid 36e.[54]

The phosphonate ester **35e** (0.60 g, 2 mmol) was dissolved in dry CH_2Cl_2 (3 mL) under N_2. TMSBr [0.95 mL (1.10 g), 7 mmol] was dissolved in dry CH_2Cl_2 (3 mL) and added dropwise. The mixture was stirred under nitrogen for 2 h at room temperature. After removal of the volatile compounds *in vacuo*, the residue was dissolved in 0.25M-NaOH. The aqueous layer was washed twice with 20 mL EtOAc and then acidified by adding 2M-HCl dropwise. NaCl was added to the acidic aqueous layer and this was extracted three times with EtOAc. The organic layers were dried with anhydrous $MgSO_4$ and evaporated to afford a dark brown oil (0.025 g), NMR analysis of which showed only the presence of starting material.

Procedure 7. Synthesis of the disodium phosphonates 36a-e.

The relevant phosphonate ester (**35a-e**) was dissolved in dry CH_2Cl_2 (3.5 mL) under N_2 and TMSBr (4 eq.) was added dropwise. The mixture was stirred overnight at room temperature. After removal of the volatile compounds *in vacuo*, the residue was dissolved in water (2 mL) and then titrated with 0.4M-NaOH to a pH of *ca.* 8. After titration, the aqueous solution was added to methanol (*ca.* 200 mL) and evaporated to dryness *in vacuo*. Purification of the products was carried out using reverse-phase column chromatography on C_{18} cellulose, eluting with 1% NH_4OH in MeOH.

Disodium [2-oxo-2-(pyridin-2-ylamino)ethyl]phosphate 36a

The general procedure 7 was followed, using **35a** (0.143 g, 0.52 mmol) and TMSBr [0.28 mL (0.32 g), 2.1 mmol]. Disodium [2-oxo-2-(pyridin-2-ylamino)ethyl]phosphate **36a** was isolated as a red-brown solid which was further purified by reverse-phase HPLC (LUNA 10u C_{18} column, 250 x 10.00 mm; elution with H_2O) (3 mg, 2.3% from HPLC), decomposes above 300 °C (lit.,[125] §); [Found: (MH-Na₂)⁺, 215.0221. $C_7H_8N_2O_4P$ requires *M*, 215.0222]; v/cm⁻¹ 3242 (NH), 1668 (C=O) and 1058 (P-O); δ_H (600 MHz; D_2O) 2.79 (2H, d, *J*=18.6 Hz, CH_2P), 7.23 (1H, t, *J*=6.0 Hz, 5'-H), 7.87 (2H, overlapping m, 3'-H and 4'-H) and 8.31 (1H, d, *J*=4.8 Hz, 6'-H); δ_C (150 MHz; D_2O)

40.1 (d, J_{C-P}=109.5 Hz, CH$_2$P), 115.8 (d, C-3'), 120.8 (d, C-5'), 139.6 (d, C-4'), 147.7 (d, C-6'), 150.4 (s, C-2') and 171.9 (s, C=O); m/z 215 [(MH-Na$_2$)$^+$, 25%] and 218 (100).

Disodium [2-(isoxazol-3-ylamino)-2-oxoethyl]phosphonate 36b

The general procedure 7 was followed, using **35b** (0.300 g, 1.1 mmol) and TMSBr [0.60 mL (0.52 g), 4.6 mmol]. *Disodium [2-(isoxazol-3-ylamino)-2-oxoethyl]phosphonate* **36b** was isolated as a dark brown oil (0.438 g, 100%), mp 283-285 °C [Found: (M+1)$^+$, 250.9806. C$_5$H$_5$N$_2$O$_5$PNa$_2$ requires $M+1$, 250.9810]; v/cm^{-1} 3038 (NH), 1682 (C=O) and 1067 (P-O); δ_H (600 MHz; D$_2$O) 2.79 (2H, d, J=18.6 Hz, CH$_2$P), 6.80 (1H, d, J=1.8 Hz, 4'-H) and 8.51 (1H, d, J=1.8 Hz, 5'-H); δ_C (150 MHz; D$_2$O) 39.5 (d, J_{C-P}=111.0 Hz, CH$_2$P), 99.1 (d, C-4'), 157.2 (s, C-3'), 160.0 (d, C-5') and 170.8 (s, C=O); m/z 251 [(M+1)$^+$, 87%] and 217 (100).

Disodium [2-oxo-2-(1,3-thiazol-2-ylamino)ethyl]phosphonate 36c

The general procedure 7 was followed, using **35c** (0.243 g, 0.87 mmol) and TMSBr [0.46 mL (0.53 g), 3.5 mmol]. *Disodium [2-oxo-2-(1,3-thiazol-2-ylamino)ethyl]phosphonate* **36c** was isolated as a light brown solid which was further purified by HPLC (LUNA 10u C$_{18}$ column, 250 x 10.00 mm; elution with H$_2$O) (0.385 g, 100%), decomposes above 290 °C [Found: (M+1)$^+$, 266.9582. C$_5$H$_5$N$_2$O$_4$SPNa$_2$ requires $M+1$, 266.9581]; v/cm^{-1} 3090 (NH), 1687 (C=O) and 1070 (P-O); δ_H (600 MHz; D$_2$O) 2.80 (2H, d, J=18.6 Hz, CH$_2$P), 7.14 (1H, d, J=3.6 Hz, 5'-H) and 7.43 (1H, d, J=3.6 Hz, 4'-H); δ_C (150 MHz; D$_2$O) 39.1 (d, J_{C-P}=108.0 Hz, CH$_2$P), 114.0 (d, C-5'), 136.8 (d, C-4'), 159.0 (s, C-2') and 170.4 (s, C=O); m/z 267 [(M+1)$^+$, 22%] and 223 (100).

Disodium {2-[(furan-2-ylmethyl)amino]-2-oxoethyl}phosphonate 36d

The general procedure 7 was followed, using **35d** (0.300 g, 1.1 mmol) and TMSBr [0.57 mL (0.66 g), 4.4 mmol]. *Disodium {2-[(furan-2-ylmethyl)amino]-2-oxoethyl}phosphonate* **36d** was isolated as a brown solid (0.567 g, 100%), decomposes above 250 °C [Found: (M+1)$^+$, 264.0010. C$_7$H$_8$NO$_5$PNa$_2$ requires $M+1$, 264.0014]; v/cm^{-1} 2971 (NH), 1643 (C=O) and 1075 (P-O); δ_H (600 MHz; D$_2$O) 2.63 (2H, d, J=19.2 Hz, CH$_2$P), 4.40 (2H, d, CH$_2$N), 6.36 (1H, d, J=3.6 Hz, 3'-H), 6.44 (1H, dd, J=3.6 and 1.8 Hz, 4'-H) and 7.48 (1H, d, J=1.8 Hz, 5'-H); δ_C (150 MHz; D$_2$O) 36.4 (t, CH$_2$NH), 38.2 (d, J_{C-P}=114.0 Hz, CH$_2$P), 107.1 (d, C-3'), 110.5 (d, C-4'), 142.5 (d, C-5'), 151.3 (s, C-2') and 172.1 (s, C=O); m/z 264 [(M+1)$^+$, 3%] and 394 (100).

Disodium {2-[(5-acetyl-4-methyl-1,3-thiazol-2-yl)amino]-2-oxoethyl}phosphonate 36e

The general procedure 7 was followed, using **35e** (0.180 g, 0.54 mmol) and TMSBr [0.28 mL (0.32 g), 2 mmol]. *Disodium {2-[(5-acetyl-4-methyl-1,3-thiazol-2-yl)amino]-2-oxoethyl}-*

113

phosphonate **36e** was isolated as a light brown solid (0.197 g, 100%), decomposes above 290 °C [Found: $(M+1)^+$, 322.9856. $C_8H_9N_2O_5Na_2PS$ requires $M+1$, 322.9843]; v/cm^{-1} 3146 (NH), 1652 (C=O) and 1103 (P-O); δ_H (600 MHz; D_2O) 2.59 (3H, s, CH_3), 2.61 (3H, s, $CO.CH_3$) and 2.90 (2H, d, J=18.6 Hz, CH_2P); δ_C (150 MHz; D_2O) 17.4 (q, CH_3) 29.3 (q, $CO.CH_3$), 38.9 (d, J_{C-P}=109.5 Hz, CH_2P), 125.7 (s, C-4'), 156.3 (s, C-5'), 161.1 (s, C-2'), 170.5 (s, NHC=O) and 195.7 (s, CH_3C=O); m/z 323 [$(M+1)^+$, 100%].

Procedure 8. Synthesis of bis(trimethylsilyl) intermediates 48 and 50.

As the bis(trimethylsilyl) phosphonates hydrolyse on contact with air, compounds **48** and **50** were synthesised in an NMR tube and characterised in the reaction mixture, in the presence of the by-product ethyl bromide, excess TMSBr and the NMR standard trimethoxybenzene (TMB). A solution of the diethyl phosphonate **35e** or **35b** and TMB (0.33 eq.) in dry $CDCl_3$ (0.6 mL) under N_2 was transferred to an NMR tube which was flushed with N_2 and sealed with a septum. TMSBr (4 eq.) was added through the septum and the reaction progress was monitored by ^1H and ^{31}P NMR spectroscopy until the reaction was complete.

Bis(trimethylsilyl) {2-[(5-acetyl-4-methyl-1,3-thiazol-2-yl)amino]-2-oxoethyl}phosphonate 48

The general procedure 8 was followed, using **35e** (0.060 g, 0.18 mmol), TMB (0.010 g, 0.060 mmol) and TMSBr [0.095 mL (0.11 g), 0.72 mmol]. After completion of the reaction, the highly reactive *bis(trimethylsilyl) {2-[(5-acetyl-4-methyl-1,3-thiazol-2-yl)amino]-2-oxoethyl}-phosphonate* **48** was characterised without further purification; δ_H (600 MHz; $CDCl_3$) -0.03 (18H, s, 6xCH_3Si), 2.48 (3H, s, $CO.CH_3$), 2.66 (3H, s, CH_3) and 3.45 (2H, d, J=22.8 Hz, CH_2P); δ_C (150 MHz; $CDCl_3$) 1.7 (q, 6xCH_3Si), 15.4 (q, CH_3-4'), 29.9 (q, $CO.CH_3$), 38.4 (d, J_{C-P}=136.5 Hz, CH_2P), 125.4 (s, C-5'), 144.8 (s, C-4'), 160.4 (s, C-2'), 164.4 (s, NHC=O) and 189.0 (s, CH_3C=O); δ_P (243 MHz; $CDCl_3$) -0.69.

Bis(trimethylsilyl) [2-(isoxazol-3-ylamino)-2-oxoethyl]phosphonate 50

The general procedure 8 was followed, using **35b** (0.024 g, 0.090 mmol) and TMSBr [0.045 mL (0.052 g), 0.36 mmol]. After completion of the reaction, the highly reactive *bis(trimethylsilyl) [2-(isoxazol-3-ylamino)-2-oxoethyl]phosphonate* **50** was characterised without further purification; δ_H (600 MHz; $CDCl_3$) -0.04 (18H, s, 6xCH_3Si), 3.72 (2H, d, J=21.6 Hz, CH_2P), 7.00 (1H, d, J=1.8 Hz, 4'-H), 8.40 (1H, d, J=1.8 Hz, 5'-H) and 11.65 (1H, s, NH); δ_C (150 MHz; $CDCl_3$) 1.8 (q, 6xCH_3Si), 37.4 (d, J_{C-P}=141.0 Hz, CH_2P), 100.0 (d, C-4'), 154.8 (s, C-3'), 159.3 (d, C-5') and 162.2 (s, C=O); δ_P (243 MHz; $CDCl_3$) 0.00.

Procedure 9. Synthesis of diethyl (3-oxo-3-phenylpropyl)phosphonate 45.

The starting material, 3-chloropropiophenone 47 (1.00 g, 5.93 mmol), was placed in a dry, round-bottomed flask under N_2 and $P(OEt)_3$ [5.1 mL (4.94 g), 30 mmol] was added through a septum. The mixture was boiled under reflux (oil bath at 110 °C) for ca. 9 h. After cooling, hexane (20 mL) was added and the mixture stirred for ca. 20 min. The hexane layer did not separate from the product so the solvent and some of the excess $P(OEt)_3$ were evaporated in vacuo to yield diethyl (3-oxo-3-phenylpropyl)phosphonate 45 as a pale yellow oil, which was purified by column chromatography [on silica; elution with hexane-EtOAc (5:1)], (0.784 g, 49%) [Found: $(M+1)^+$, 271.1098. $C_{13}H_{19}O_4P$ requires M+1, 271.1099]; v/cm^{-1} 1687 (C=O) and 1018 (P-OR); δ_H (600 MHz; CDCl$_3$) 1.35 (6H, t, J=7.3 Hz, 2xCH$_3$), 2.19 (2H, m, CH$_2$P), 3.29 (2H, m, CO.CH$_2$), 4.11 (4H, q, J=7.3 Hz, 2xOCH$_2$), 7.46 (2H, t, J=7.4 Hz, 3'- and 5'-H), 7.57 (1H, d, J=7.4 Hz, 4'-H) and 7.97 (2H, d, J=7.4 Hz, 2'- and 6'-H); δ_C (150 MHz; CDCl$_3$) 16.3 (q, 2xCH$_3$), 19.8 (d, J_{C-P}=144.0 Hz, CH$_2$P), 31.7 (t, CO.CH$_2$), 61.7 (t, 2xOCH$_2$), 128.0 (d, C-2' and -6'), 128.7 (d, C-3' and -5'), 133.3 (d, C-4'), 136.3 (s, C-1') and 197.5 (s, C=O); δ_P (243 MHz; CDCl$_3$) 32.76; m/z 271 (MH$^+$, 18%) and 563 (100).

Procedure 10. Synthesis of disodium (3-oxo-3-phenylpropyl)phosphonate 46.

The phosphonate ester 45 (0.60 g, 2.2 mmol) was dissolved in dry CH$_2$Cl$_2$ (5 mL) under N_2 and TMSBr [1.2 mL (1.39 g), 8.8 mmol] was added dropwise. The mixture was stirred overnight at room temperature. After removal of the volatile compounds in vacuo, the residue was dissolved in water (2 mL) and then titrated with 0.4M-NaOH to a pH of ca. 8. After titration, the aqueous solution was added to methanol (ca. 200 mL) and evaporated to dryness in vacuo. Purification was carried out using reverse-phase column chromatography on C$_{18}$ cellulose, eluting with 1:1 MeOH/H$_2$O to yield disodium (3-oxo-3-phenylpropyl)phosphonate 46 as a cream solid (0.165 g, 29%), decomposes above 300 °C (lit.,[126,127] 115-117 and 123-124 °C); [Found: $(M-1)^+$, 213.0312. $C_9H_9O_4P$ requires M-1, 213.0317]; v/cm^{-1} 3196 (NH), 1645 (C=O) and 1119 (P-O); δ_H (600 MHz; CDCl$_3$) 2.00 (2H, dt, J=17.4 and 7.8 Hz, CH$_2$P), 3.38 (2H, t, J=7.8 Hz, CO.CH$_2$), 7.60 (2H, t, J=7.4 Hz, 3'- and 5'-H), 7.73 (1H, d, J=7.4 Hz, 4'-H) and 8.06 (2H, d, J=7.4, 2'- and 6'-H); δ_C (150 MHz; CDCl$_3$) 23.0 (d, J_{C-P}=130.5 Hz, CH$_2$P), 33.4 (t, CO.CH$_2$), 128.4 (d, C-2' and -6'), 129.0 (d, C-3' and -5'), 134.2 (d, C-4'), 136.5 (s, C-1') and 214.8 (s, C=O); m/z 271 [(M-H)$^+$, 77%] and 421 (100).

115

Procedure 11. Synthesis of 3-chloro-*N*-arylpropanamides 41a-e. (Adapted from a literature method.[72])

A solution of the relevant primary amine (**37a-e**) in dry THF was stirred under N_2. NaH (60% dispersion in mineral oil; 1 eq.) was added slowly to allow controlled evolution of H_2. Chloropropionyl chloride (1 eq.) was then added slowly through a dropping funnel and the mixture was stirred overnight at room temperature. The solvent was removed *in vacuo* and the residue dissolved in EtOAc (2 x 50 mL). The resulting solution was washed sequentially with saturated aqueous $NaHCO_3$ (2 x 100 mL), water (2 x 100 mL) and brine (2 x 100 mL). The combined aqueous layers were then re-extracted with EtOAc (100 mL). The organic layers were combined, dried with anhydrous Na_2SO_4 or $MgSO_4$ and evaporated *in vacuo* to afford the 3-chloro-*N*-arylpropanamide product **41a-e**.

3-Chloro-*N*-(pyridin-2-yl)propanamide 41a and side-products 42-44

The general procedure 11 was followed, using 2-aminopyridine **37a** (2.64 g, 28 mmol), THF (30 mL), NaH (1.20 g, 30 mmol) and chloropropionyl chloride [2.7 mL (3.56 g), 28 mmol]. The crude product (1.87 g, 36%) was isolated as a yellow solid. The mixture of products from the crude reaction mixture was separated using reverse-phase HPLC [on C18; elution with MeOH:H_2O (1:1)] to afford 4 products.

i) 3-Chloro-*N*-(pyridin-2-yl)propanamide 41a as an off-white solid (0.046 g, 39%), mp 190-196 °C (lit.,[128] §); (Found: C, 47.1; H, 4.9; N, 13.5. $C_8H_9ON_2Cl$ requires C, 52.0; H, 4.9; N, 15.2%); v/cm⁻¹ 1685 (C=O); δ_H (600 MHz; D_2O) 3.05 (2H, t, *J*=7.2 Hz, CO.CH$_2$), 4.79 (2H, t, *J*=7.2 Hz, CH$_2$Cl), 7.39 (1H, d, *J*=8.7 Hz, 3'-H), 7.49 (1H, t, *J*=6.6 Hz, 5'-H), 8.28 (1H, t, *J*=8.7 Hz, 4'-H) and 8.34 (1H, d, *J*=6.6 Hz, 6'-H); δ_C (150 MHz; D_2O) 28.4 (t, CO.CH$_2$), 50.7 (t, CH$_2$Cl), 115.8 (d, C-3'), 120.4 (d, C-5'), 141.5 (d, C-6'), 146.5 (d, C-4'), 147.8 (s, C-2') and 169.2 (s, C=O).

ii) N-*(3-Chloropropanoyl)*-N-*(pyridin-2-yl)prop-2-enamide 42 as a cream solid (0.008 g, 7%), mp 98-103 °C;[‡] v/cm⁻¹ 1679 and 1648 (C=O); δ_H (600 MHz; D_2O) 2.68 (2H, t, *J*=6.6 Hz, CO.CH$_2$), 4.33 (2H, t, *J*=6.6 Hz, CH$_2$Cl), 5.59 (1H, d, *J*=10.2 Hz, 3-H), 5.96 (1H, d, *J*=17.4 Hz, 3-H), 6.06 (1H, dd, *J*=17.4 and 10.2 Hz, 2-H), 6.83 (1H, t, *J*=6.6 Hz, 5''-H), 7.00 (1H, d, *J*=8.7 Hz, 3''-H), 7.76 (1H, t, *J*=8.7 Hz, 4''-H) and 7.78 (1H, d, *J*=6.6 Hz, 6''-H); δ_C (150 MHz; D_2O) 34.8 (t, CO.CH$_2$), 51.0 (t, CH$_2$Cl), 113.6 (d, C-5''), 116.3 (d, C-3''), 126.6 (dd, CH$_2$-3), 133.6 (d, C-2), 139.5 (d, C-6''), 142.5 (d, C-4''), 153.7 (s, C-2''), 175.3 (s, C=O-1) and 177.90 (s, C=O-1').

[‡] It was not possible to obtain mass spectrometry or elemental data for this compound due to its highly hygroscopic nature.

iii) *3-Chloro-*N*-(pyridin-2-yl)-*N*-[3-(pyridin-2-ylamino)propanoyl]propanamide* **43** as a cream solid (0.006 g, 5%), mp 88-91 °C;[‡] ν/cm^{-1} 1684 and 1645 (C=O); δ_H (600 MHz; D$_2$O) 2.72 (2H, t, J=6.5 Hz, 2-CO.CH$_2$), 2.93 (2H, t, J=6.5 Hz, 2''-CO.CH$_2$), 3.89 (2H, t, J=6.5 Hz, 3''-CH$_2$N), 4.42 (2H, t, J=6.5 Hz, 3-CH$_2$Cl), 6.94 (1H, t, J=6.8 Hz, 5'-H), 7.23 (1H, d, J=9.0 Hz, 3'-H), 7.26 (1H, t, J=5.8 Hz, 5'''-H), 7.75 (1H, d, J=7.8 Hz, 3'''-H), 7.88 (1H, t, J=7.8 Hz, 4'''-H), 7.90 (1H, d, J=6.8 Hz, 6'-H), 7.94 (1H, t, J=9.0 Hz, 4'-H) and 8.31 (1H, d, J=5.8 Hz, 6'''-H); δ_C (150 MHz; D$_2$O) 35.1 (t, CO.CH$_2$-2), 35.9 (t, CO.CH$_2$-2''), 39.0 (t, CH$_2$N-3''), 51.5 (t, CH$_2$Cl-3), 111.4 (d, C-3'), 113.4 (d, C-5') 116.3 (d, C-3'''), 121.4 (d, C-5'''), 139.7 (d, C-4'''), 141.1 (d, C-6'), 143.4 (d, C-4'), 147.9 (d, C-6'''), 149.8 (s, C-2'''), 152.5 (s, C-2'), 172.4 (s, C=O-1) and 177.9 (s, C=O-1'').

iv) *N*-(Pyridin-2-yl)prop-2-enamide **44** as a white solid (0.002 g, 2%), mp 76-78 °C (lit.,[129] §);[‡] ν/cm^{-1} 1648 (C=O); δ_H (600 MHz; D$_2$O) 5.88 (1H, d, J=10.3 Hz, 3-H), 6.36 (1H, d, J=17.1 Hz, 3-H), 6.45 (1H, dd, J=17.1 and 10.3 Hz, 2-H), 7.21 (1H, t, J=6.1 Hz, 5'-H), 7.83 (2H, m, 3'-H and 4'-H) and 8.28 (1H, d, J=4.6 Hz, 6'-H); δ_C (150 MHz; D$_2$O) 116.3 (d, C-3'), 121.3 (d, C-5'), 129.5 (dd, CH$_2$-3), 130.2 (d, C-2), 139.6 (d, C-4'), 147.9 (d, C-6'), 150.0 (s, C-2') and 167.0 (s, C=O).

*3-Chloro-*N*-(1,2-oxazol-3-yl)propanamide* **41b**

The general procedure 11 was followed, using 3-aminoisoxazole **37b** [2.1 mL (2.35 g), 28 mmol], THF (30 mL), NaH (1.20 g, 30 mmol) and chloropropionyl chloride [2.7 mL (3.56 g), 28 mmol]. The product was washed 3 times with hexane and dried to yield *3-chloro-*N*-(1,2-oxazol-3-yl)propanamide* **41b** as a pale yellow solid (6.34 g, 100%), mp 110-114 °C; [Found: (M+1)$^+$, 175.0256. C$_6$H$_7$N$_2$O$_2$Cl requires *M+1*, 175.0274]; ν/cm^{-1} 1667 (C=O); δ_H (600 MHz; CDCl$_3$) 2.94 (2H, t, J=6.6 Hz, CO.CH$_2$), 3.89 (2H, t, J=6.6 CH$_2$Cl), 7.13 (1H, d, J=1.2 Hz, 4'-H), 8.31 (1H, d, J=1.2 Hz, 5'-H) and 9.70 (1H, s, NH); δ_C (150 MHz; CDCl$_3$) 39.0 (t, CH$_2$Cl), 39.7 (t, CO.CH$_2$), 99.5 (d, C-4'), 157.4 (s, C-3'), 159.1 (d, C-5') and 167.9 (s, C=O); *m/z* 175 (MH$^+$, 100%).

3-Chloro-*N*-(1,3-thiazol-2-yl)propanamide **41c**

The general procedure 11 was followed, using 2-aminothiazole **37c** (2.80 g, 28 mmol), THF (30 mL), NaH (1.20 g, 30 mmol) and chloropropionyl chloride [2.7 mL (3.56 g), 28 mmol]. The product was washed 3 times with hexane and dried to yield 3-chloro-*N*-(1,3-thiazol-2-yl)propanamide **41c** as a yellow-brown solid (3.30 g, 62%), mp 129-132 °C (lit.,[130] 169 °C); [Found: (M+1)$^+$, 191.0020. C$_6$H$_7$N$_2$OSCl requires *M+1*, 191.0046]; ν/cm^{-1} 1688 (C=O); δ_H (600 MHz; CDCl$_3$) 3.01 (2H, t, J=6.6 Hz, CO.CH$_2$), 3.92 (2H, t, J=6.6 Hz, CH$_2$Cl), 7.04 (1H, d, J=3.6 Hz,

---

[‡] It was not possible to obtain mass spectrometry or elemental data for this compound due to its highly hygroscopic nature.

5'-H) and 7.49 (1H, d, J=3.6 Hz, 4'-H); δ_C (150 MHz; CDCl$_3$) 39.0 (t, CH$_2$Cl), 39.2 (t, CO.CH$_2$), 114.0 (d, C-5'), 136.5 (d, C-4'), 159.2 (s, C-2') and 167.5 (s, C=O); m/z 191 (MH$^+$, 62%) and 155 (100).

3-Chloro-*N*-(furan-2-ylmethyl)propanamide 41d

The general procedure 11 was followed, using furfurylamine **37d** [2.6 mL (2.72 g), 28 mmol], THF (30 mL), NaH (1.20 g, 30 mmol) and chloropropionyl chloride [2.7 mL (3.56), 28 mmol]. The product was washed 3 times with hexane and dried to yield the crude product as a brown solid (3.34 g, 63%). A portion of the crude product (0.10 g) was purified by column chromatography [on silica; elution with hexane-EtOAc (1:1)] to afford 3-chloro-*N*-(furan-2-ylmethyl)propanamide **41d** as a pale brown solid, mp 70-72 °C (lit.,[131] §); (Found: M$^+$, 187.0398. C$_8$H$_{10}$NO$_2$Cl requires M, 187.0400); ν/cm^{-1} 1633 (C=O); δ_H (600 MHz; CDCl$_3$) 2.65 (2H, t, J= 6.7 Hz, CO.CH$_2$), 3.81 (2H, t, J= 6.7 Hz, CH$_2$Cl), 4.46 (2H, d, J=5.3 Hz, CH$_2$N), 6.06 (1H, s, NH), 6.24 (1H, d, J= 3.3 Hz, 3'-H), 6.32 (1H, dd, J=3.3 and 1.9 Hz, 4'-H) and 7.35 (1H, d, J=1.9 Hz, 5'-H); δ_C (150 MHz; CDCl$_3$) 36.5 (t, CH$_2$N), 39.3 (t, CO.CH$_2$), 39.9 (t, CH$_2$Cl), 107.5 (d, C-3'), 110.4 (d, C-4'), 142.2 (d, C-5'), 150.9 (s, C-2') and 169.4 (s, C=O); m/z 187 (M$^+$, 82%) and 97 (100).

N-(5-Acetyl-4-methyl-1,3-thiazol-2-yl)-3-chloropropanamide 41e

The general procedure 11 was followed, using 5-acetyl-2-amino-4-methylthiazole **37e** (1.56 g, 10 mmol), THF (10 mL), NaH (0.43 g, 11 mmol) and chloropropionyl chloride [0.9 mL (1.27 g), 10 mmol]. The crude product was isolated as a yellow solid (2.07 g, 84%). A portion of the product was purified by column chromatography [on silica; elution with CHCl$_3$-EtOAc (1:1)] to afford *N*-(5-acetyl-4-methyl-1,3-thiazol-2-yl)-3-chloropropanamide **41e** as a pale yellow solid, mp 167-169 °C (lit.,[132] §); [Found: (M+1)$^+$, 247.0297. C$_9$H$_{11}$N$_2$O$_2$SCl requires M+1, 247.0308]; ν/cm^{-1} 1635 (C=O); δ_H (600 MHz; CDCl$_3$) 2.52 (3H, s, 4'-CH$_3$), 2.64 (3H, s, CO.CH$_3$), 2.95 (2H, t, J=6.0 Hz, CO.CH$_2$) and 3.89 (2H, t, J=6.0 Hz, CH$_2$Cl); δ_C (150 MHz; CDCl$_3$) 18.0 (q, C-4'), 30.4 (q, CO.CH$_3$), 38.6 (t, CH$_2$Cl), 39.3 (t, CO.CH$_2$), 125.6 (s, C-5'), 154.8 (s, C-4'), 158.5 (s, C-2'), 167.7 (s, NHC=O) and 190.6 (s, CO.CH$_3$); m/z 247 (MH$^+$, 7%) and 295 (100).

Procedure 12. Synthesis of phosphonate esters 39a-e.[72]

The 3-chloropropanamide starting material (**41a-e**) was placed in a dry, round-bottomed flask under N$_2$ and P(OEt)$_3$ (5 eq.) was added through a septum. The mixture was boiled under reflux (oil bath at 110 °C) for *ca.* 9 h. After cooling, hexane (20 mL) was added and the mixture stirred for *ca.* 20 min. The hexane was then decanted and stirring and decanting was repeated

with three further aliquots (20 mL each) of hexane. Evaporation of residual hexane and P(OEt)$_3$ *in vacuo* afforded the desired ester **39a-e**.

Diethyl [3-oxo-3-(pyridin-2-ylamino)propyl]phosphonate 39a

The general procedure 12 was followed, using **41a** (0.69 g, 3.7 mmol) and P(OEt)$_3$ [3.2 mL (3.11 g), 19 mmol] to yield *diethyl [3-oxo-3-(pyridin-2-ylamino)propyl]phosphonate* **41a** as an orange oil (0.36 g, 33%) [Found: (M+1)$^+$, 287.1161. C$_{12}$H$_{19}$N$_2$O$_4$P requires *M+1*, 287.1161]; v/cm^{-1} 1690 (C=O) and 1020 (P-OR); δ$_H$ (600 MHz; CDCl$_3$) 1.31 (6H, t, *J*=7.0 Hz, 2xCH$_3$), 2.18 (2H, dt, *J*=18.0 and 7.9 Hz, CH$_2$P), 2.70 (2H, dt, *J*=13.4 and 7.9 Hz CO.CH$_2$), 4.12 (4H, q, *J*=7.0 Hz, 2xOCH$_2$), 7.03 (1H, dd, *J*=7.3 and 5.0 Hz, 5'-H), 7.69 (1H, dd, *J*=8.8 and 7.3 Hz, 4'-H), 8.17 (1H, d, *J*=8.8 Hz, 3'-H), 8.27 (1H, d, *J*=5.0 Hz, 6'-H) and 8.52 (1H, s, NH); δ$_C$ (150 MHz; CDCl$_3$) 16.4 (q, 2xCH$_3$), 20.9 (d, *J$_{C-P}$*=142.5 Hz, CH$_2$P), 30.5 (t, CO.CH$_2$), 61.92 (t, 2xOCH$_2$), 114.0 (d, C-3'), 119.8 (d, C-5'), 138.4 (d, C-4'), 147.9 (d, C-6'), 151.3 (s, C-2') and 169.8 (s, C=O); *m/z* 287 (MH$^+$, 100%).

Diethyl [3-(1,2-oxazol-3-ylamino)-3-oxopropyl]phosphonate 39b

The general procedure 12 was followed, using **41b** (1.11 g, 6 mmol) and P(OEt)$_3$ [5.2 mL (5.04 g), 30 mmol] to yield *diethyl [3-(1,2-oxazol-3-ylamino)-3-oxopropyl]phosphonate* **39b** as an orange oil (1.29 g, 74%) [Found: (M+1)$^+$, 277.0962. C$_{10}$H$_{17}$N$_2$O$_5$P requires *M+1*, 277.0953]; v/cm^{-1} 1701 (C=O) and 1021 (P-OR); δ$_H$ (600 MHz; CDCl$_3$) 1.29 (6H, t, *J*=7.2 Hz, 2xCH$_3$), 2.16 (2H, dt, *J*=18.0 and 8.4 Hz, CH$_2$P), 2.79 (2H, dt, *J*=15.6 and 8.4 Hz, CO.CH$_2$), 4.11 (4H, m, 2xOCH$_2$), 7.02 (1H, d, *J*=1.2 Hz, 4'-H), 8.24 (1H, d, *J*=1.2 Hz, 5'-H) and 10.51 (1H, s, NH); δ$_C$ (150 MHz; CDCl$_3$) 16.3 (q, 2xCH$_3$), 20.6 (d, *J$_{C-P}$*=144.0 Hz, CH$_2$P), 29.4 (t, CO.CH$_2$), 62.1 (t, 2xOCH$_2$), 99.3 (d, C-4'), 157.6 (s, C-3'), 158.6 (d, C-5') and 170.0 (s, C=O); *m/z* 277 (MH$^+$, 35%) and 299 (100).

Diethyl [3-oxo-3-(1,3-thiazol-2-ylamino)propyl]phosphonate 39c

The general procedure 12 was followed, using **41c** (1.22 g, 6 mmol) and P(OEt)$_3$ [5.2 mL (5.04 g), 30 mmol]. The product *diethyl [3-oxo-3-(1,3-thiazol-2-ylamino)propyl]phosphonate* **39c** crystallised out of hexane as pale yellow crystals (1.29 g, 69%), mp 50-52 °C; [Found: (M+1)$^+$, 293.0723. C$_{10}$H$_{17}$N$_2$O$_4$PS requires *M+1*, 293.0725]; v/cm^{-1} 1686 (C=O) and 1028 (P-OR); δ$_H$ (600 MHz; CDCl$_3$) 1.32 (6H, t, *J*=7.2 Hz, 2xCH$_3$), 2.22 (2H, dt, *J*=6.6 and 1.2 Hz, CH$_2$P), 2.86 (2H, dt, *J*=6.6 and 1.2 Hz, CO.CH$_2$), 4.13 (4H, qd, *J*=7.2 and 1.2 Hz, 2xOCH$_2$), 6.99 (1H, d, *J*=3.4 Hz, 5'-H) and 7.53 (1H, d, *J*=3.4 Hz, 4'-H); δ$_C$ (150 MHz; CDCl$_3$) 16.4 (q, 2xCH$_3$), 20.8 (d, *J$_{C-P}$*=144.0 Hz, CH$_2$P), 29.3 (t, CO.CH$_2$), 62.0 (t, 2xOCH$_2$), 113.6 (d, C-5'), 136.9 (d, C-4'), 159.3 (s, C-2') and 169.2 (s, C=O); *m/z* 293 (MH$^+$, 100%).

Diethyl {3-[(furan-2-ylmethyl)amino]-3-oxopropyl}phosphonate **39d**

The general procedure 12 was followed, using **41d** (1.20 g, 6 mmol) and P(OEt)$_3$ [5.2 mL (5.04 g), 30 mmol] to yield *diethyl {3-[(furan-2-ylmethyl)amino]-3-oxopropyl}phosphonate* **39d** as a brown oil (1.48 g, 80%) [Found: (M+1)$^+$, 290.1169. C$_{12}$H$_{20}$NO$_5$P requires *M+1*, 290.1157]; ν/cm^{-1} 1654 (C=O) and 1020 (P-OR); δ$_H$ (600 MHz; CDCl$_3$) 1.29 (6H, t, *J*=7.2 Hz, 2xCH$_3$) 2.08 (2H, dt, *J*=17.8 and 8.0 Hz, CH$_2$P), 2.49 (2H, dt, *J*=14.7 and 8.0 Hz, CO.CH$_2$), 4.04 (4H, qd, *J*=7.2 and 2.9 Hz, 2xOCH$_2$), 4.41 (2H, d, *J*=5.5 Hz, CH$_2$N), 6.21 (1H, dd, *J*=3.2 and 0.6 Hz, 3'-H), 6.29 (1H, dd, *J*=3.2 and 1.9 Hz, 4'-H), 6.67 (1H, s, NH) and 7.33 (1H, dd, *J*=1.9 and 0.6 Hz, 5'-H); δ$_C$ (150 MHz; CDCl$_3$) 16.4 (q, 2xCH$_3$), 21.0 (d, *J$_{C-P}$*=142.5 Hz, CH$_2$P), 29.0 (t, CO.CH$_2$), 36.6 (t, CH$_2$N), 61.8 (t, 2xOCH$_2$), 107.4 (d, C-3'), 110.4 (d, C-4'), 142.1 (d, C-5'), 151.3 (s, C-2') and 170.8 (s, C=O); *m/z* 290 (MH$^+$, 14%) and 312 (100).

Diethyl {3-[(5-acetyl-4-methyl-1,3-thiazol-2-yl)amino]-3-oxopropyl}phosphonate **39e**

The general procedure 12 was followed, using **41e** (0.050 g, 0.2 mmol) and P(OEt)$_3$ [0.2 mL (0.17 g), 1 mmol] to yield *diethyl {3-[(5-acetyl-4-methyl-1,3-thiazol-2-yl)amino]-3-oxopropyl}-phosphonate* **39e**, which crystallised out of acetone as a white solid (0.028 g, 40%), mp 195-198 °C; [Found: (M+1)$^+$, 349.1003. C$_{13}$H$_{21}$N$_2$O$_5$PS requires *M+1*, 349.0987]; ν/cm^{-1} 1668 (C=O) and 1017 (P-OR); δ$_H$ (600 MHz; CDCl$_3$) 1.33 (6H, t, *J*=7.3 Hz, 2xCH$_3$), 2.21 (2H, dt, *J*=17.9 and 7.7 Hz, CH$_2$P), 2.49 (3H, s, CO.CH$_3$), 2.59 (3H, s, 4'-CH$_3$), 2.87 (2H, dt, *J*=15.4 and 7.7 Hz, CO.CH$_2$), 4.18 (4H, qd, *J*=7.3 and 3.6 Hz, 2xOCH$_2$) and 11.51 (1H, s, NH); δ$_C$ (150 MHz; CDCl$_3$) 16.4 (q, 2xCH$_3$), 18.2 (q, CH$_3$-4'), 20.5 (d, *J$_{C-P}$*=144.0 Hz, CH$_2$P), 29.0 (t, CO.CH$_2$), 30.4 (q, CO.CH$_3$), 62.5 (t, 2xOCH$_2$), 125.1 (s, C-5'), 155.7 (s, C-4'), 158.9 (s, C-2'), 169.9 (s, NHC=O) and 190.7 (s, CO.CH$_3$); *m/z* 349 (MH$^+$, 17%) and 719 (100).

Procedure 13. Hydrolysis of phosphonate esters 39a-e in DCM.

The relevant phosphonate ester (**39a-e**) was dissolved in dry CH$_2$Cl$_2$ (3.5 mL) under N$_2$ and TMSBr was added dropwise. The mixture was stirred overnight at room temperature. After removal of the volatile compounds *in vacuo*, the residue was dissolved in water (2 mL) and then titrated with 0.4M-NaOH to a pH of *ca.* 8. After titration, the aqueous solution was added to methanol (*ca.* 200 mL) and evaporated to dryness *in vacuo*. Purification of the products was carried out using reverse-phase column chromatography on C$_{18}$ cellulose, eluting with 1:1 H$_2$O:MeOH. Compounds **40b**, **40c**, **40d** and **40e** were further purified by reverse-phase HPLC (LUNA 10u C$_{18}$ column, 250 x 10.00 mm; elution with H$_2$O).

Disodium [3-oxo-3-(pyridin-2-ylamino)propyl]phosphonate **40a**

The general procedure 13 was followed, using **39a** (0.20 g, 0.69 mmol) and TMSBr [0.37 mL (0.43 g), 2.8 mmol]. *Disodium [3-oxo-3-(pyridin-2-ylamino)propyl]phosphonate* **40a** was isolated as a light brown solid (0.052 g, 100%),[‡] δ_H (600 MHz; D$_2$O) 1.77 (2H, t, J=8.4 Hz, CH$_2$P), 2.67 (2H, t, J=8.4 Hz, CO.CH$_2$), 7.26 (1H, t, J=6.0 Hz, 5'-H), 7.77 (1H, d, J=7.9 Hz, 3'-H), 7.90 (1H, t, J=7.9 Hz, 4'-H) and 8.33 (1H, d, J=6.0 Hz, 6'-H); δ_C (150 MHz; D$_2$O) 25.3 (d, J_{C-P}=129.0 Hz, CH$_2$P), 32.6 (t, CO.CH$_2$), 116.3 (d, C-3'), 121.1 (d, C-5'), 139.5 (d, C-4'), 147.8 (d, C-6'), 150.3 (s, C-2') and 176.6 (s, C=O).

Disodium [3-(1,2-oxazol-3-ylamino)-3-oxopropyl]phosphonate **40b**

The general procedure 13 was followed, using **39b** (0.50 g, 1.8 mmol) and TMSBr [0.96 mL (1.11 g), 7.2 mmol]. *Disodium [3-(1,2-oxazol-3-ylamino)-3-oxopropyl]phosphonate* **40b** was isolated as a brown solid (0.038 g, 27% from HPLC), decomposes 184-187 °C; [Found: (M+1-Na$_2$)$^+$, 219.0191. C$_5$H$_7$N$_2$O$_5$P requires *M+1-46*, 219.0191]; v/cm^{-1} 3184 (NH), 1683 (C=O) and 1047 (P-O); δ_H (600 MHz; D$_2$O) 1.79 (2H, dt, J=16.8 and 8.4 Hz, CH$_2$P), 2.68 (2H, dt, J=16.8 and 8.4 Hz, CO.CH$_2$), 6.78 (1H, d, J=0.6 Hz, 4'-H) and 8.54 (1H, d, J=0.6 Hz, 5'-H); δ_C (150 MHz; D$_2$O) 25.3 (d, J_{C-P}=129.0 Hz, CH$_2$P), 32.6 (t, CO.CH$_2$), 99.8 (d, C-4'), 158.0 (s, C-3'), 160.8 (d, C-5') and 176.3 (s, C=O); m/z 219 [(MH-Na$_2$)$^+$, 5%] and 371 (100).

Disodium [3-oxo-3-(1,3-thiazol-2-ylamino)propyl]phosphonate **40c**

The general procedure 13 was followed, using **39c** (0.80 g, 2.7 mmol) and TMSBr [1.4 mL (1.62 g), 11 mmol]. *Disodium [3-oxo-3-(1,3-thiazol-2-ylamino)propyl]phosphonate* **40c** was isolated as a brown solid (0.009 g, 13.9 % from HPLC), decomposes above 266 °C; [Found: (M-1)$^+$, 234.9943. C$_6$H$_7$N$_2$O$_4$SP requires *M-1*, 234.9942]; v/cm^{-1} 3356 (NH), 1658 (C=O) and 1068 (P-O); δ_H (600 MHz; D$_2$O) 1.73 (2H, dt, J=16.8 and 8.4 Hz, CH$_2$P), 2.66 (2H dt, J=8.9 and 8.4 Hz, CO.CH$_2$), 7.11 (1H, d, J=3.6 Hz, 5'-H) and 7.39 (1H, d, J=3.4 Hz, 4'-H); δ_C (150 MHz; D$_2$O) 24.3 (d, J_{C-P}=130.5 Hz, CH$_2$P), 31.0 (t, CO.CH$_2$), 114.1 (d, C-5'), 136.8 (d, C-4'), 158.9 (s, C-2') and 174.5 (s, C=O); δ_P (243 MHz; D$_2$O) 20.9; m/z 235 [(M-H)$^+$, 91%] and 217 (100).

Disodium {3-[(furan-2-ylmethyl)amino]-3-oxopropyl}phosphonate **40d**

The general procedure 13 was followed, using **39d** (0.30 g, 1.0 mmol) and TMSBr [0.55 mL (0.64 g), 4.2 mmol]. *Disodium {3-[(furan-2-ylmethyl)amino]-3-oxopropyl}phosphonate* **40d** was

---

[‡] It was not possible to obtain mass spectrometry or melting point data for this compound due to its highly hygroscopic nature.

isolated as a red-brown solid (0.23 g, 81%), decomposes above 273 °C; [Found: $(M-1)^+$, 232.0384. $C_8H_{10}NO_5P$ requires $M-1$, 232.0375]; v/cm^{-1} 3252 (NH), 1633 (C=O) and 1048 (P-O); δ_H (600 MHz; D_2O) 1.62 (2H, dt, J=17.1 and 4.4 Hz, CH_2P), 2.38 (2H, dt, J=8.3 and 4.4 Hz, $CO.CH_2$), 4.30 (2H, s, CH_2N), 6.25 (1H, d, J=3.0 Hz, 3'-H), 6.35 (1H, dd, J=3.0 and 1.9 Hz, 4'-H) and 7.40 (1H, d, J=1.9 Hz, 5'-H); δ_C (150 MHz; D_2O) 25.2 (d, J_{C-P}=130.5 Hz, CH_2P), 31.8 (t, $CO.CH_2$), 36.4 (t, CH_2N), 107.4 (d, C-3'), 110.7 (d, C-4'), 142.8 (d, C-5'), 151.3 (s, C-2') and 177.7 (s, C=O); δ_P (243 MHz; D_2O) 21.29; m/z 232 [$(M-H)^+$, 37%] and 421 (100).

Disodium {3-[(5-acetyl-4-methyl-1,3-thiazol-2-yl)amino]-3-oxopropyl}phosphonate 40e

The general procedure 13 was followed, using **39e** (0.233 g, 0.67 mmol) and TMSBr [0.35 mL (0.41 g), 2.7 mmol]. *Disodium {3-[(5-acetyl-4-methyl-1,3-thiazol-2-yl)amino]-3-oxopropyl}-phosphonate* **40e** was isolated as a yellow solid (0.138 g, 61%), decomposes above 260 °C;[‡] v/cm^{-1} 3122 (NH), 1704 (C=O) and 1041 (P-O); δ_H (600 MHz; D_2O) 1.70 (2H, dt, J=16.8 and 8.4 Hz, CH_2P), 2.51 (3H, s, 4'-CH_3), 2.53 (3H, s, $CO.CH_3$) and 2.68 (2H, dt, J=16.8 and 8.4 Hz, $CO.CH_2$); δ_C (150 MHz; D_2O) 17.5 (q, CH_3-4'), 24.4 (d, J_{C-P}=129.0 Hz, CH_2P), 29.4 (q, $CO.CH_3$), 31.6 (t, $CO.CH_2$), 125.8 (s, C-5'), 156.5 (s, C-4'), 161.5 (s, C-2'), 175.7 (s, NHC=O) and 195.6 (s, $CO.CH_3$).

Procedure 14. Synthesis of diethyl *N*-(trimethylsilyl)phosphoramidate 59.[117]

A solution of diethyl phosphoramidate **53** (5.0 g, 33 mmol) in benzene (10 mL) was made up under Ar. Hexamethyldisilazane [4.1 mL (3.2 g), 20 mmol (20% mol excess)] was added through a septum, with stirring. The mixture was then boiled under reflux in an oil bath (80 °C) under Ar for 3 h. The solvent and excess hexamethyldisilazane were removed *in vacuo* at 50-60 °C for 1 h to afford diethyl *N*-(trimethylsilyl)phosphoramidate **59** as a pale brown oil which crystallised on cooling to form off-white crystals which were highly hygroscopic (7.16 g, 97%),[‡] δ_H (600 MHz; $CDCl_3$) 0.18 (9H, s, $3xSiCH_3$), 1.30 (6H, t, J=7.2 Hz, $2xCH_3$), 2.39 (1H, s, NH) and 4.04 (4H, q, J=7.2 Hz, $2xOCH_2$); δ_C (150 MHz; $CDCl_3$) 0.6 (q, $3xSiCH_3$), 16.2 (q, $2xCH_3$) and 61.9 (t, $2xOCH_2$); δ_P (243 MHz; $CDCl_3$) 10.14.

Procedure 15. Synthesis of diethyl *N*-(2,2-diethoxyethyl)phosphoramidate 54.[117]

A suspension of NaH [60% dispersion in mineral oil; 1.44 g, 36 mmol (1.2 eq.)] was stirred in hexane (30 mL) under N_2 and then allowed to settle. The hexane was removed with a syringe

---

[‡] It was not possible to obtain mass spectrometry data for this compound due to its highly hygroscopic nature.

and the washing was repeated with 3 more aliquots (30 mL each) of hexane to remove the mineral oil. Dry benzene (20 mL) was added to the flask, followed by a solution of the protected phosphoramidate **59** (6.76 g, 30 mmol) in dry benzene (30 mL; added dropwise over 30 min to allow for evolution of H_2). Bromoacetaldehyde diethyl acetal [4.5 mL (5.9 g), 30 mmol] and tetrabutylammonium bromide (0.97 g, 3 mmol) were then added and the mixture was boiled under reflux in an oil bath (80 °C) under N_2 for 4 h. EtOH (25 mL) was then added slowly and the mixture was stirred for 1 h at 80 °C. After cooling, EtOAc (100 mL) was added and the mixture was washed three times with water (3 x 10 mL). The combined aqueous layers were then washed with EtOAc (3 x 10 mL) and the organic layers were combined and dried with $MgSO_4$. Evaporation of the solvent at 30-40 °C for 1 h afforded diethyl N-(2,2-diethoxyethyl)phosphoramidate **54** as a brown oil (7.29 g, 90%), (lit.,[133] §); δ_H (600 MHz; $CDCl_3$) 1.19 (6H, q, J=7.2 Hz, 2xCH_3), 1.28 (6H, q, J=7.2 Hz, 2xPOCH$_2$CH_3), 3.10 (1H, s, NH), 3.32 (2H, d, J=5.4 Hz, NCH$_2$), 3.59 (4H, dq, J=70.8 and 7.2 Hz, 2xOCH$_2$), 4.04 (4H, q, J=7.2 Hz, 2xPOCH$_2$) and 4.62 (1H, t, J=5.4 Hz, CH); δ_C (150 MHz; $CDCl_3$) 15.1 (q, 2xCH_3), 16.1 (q, 2xPOCH$_2$CH_3), 31.7 (t, NCH$_2$), 62.3 (t, 4xOCH$_2$) and 101.3 (d, CH); δ_P (243 MHz; $CDCl_3$) 10.24.

Procedure 16. Attempted synthesis of *diethyl (2-oxoethyl)amidophosphate* 55.[75]

The alkylated phosphoramidate **54** (0.50 g, 1.9 mmol) was placed in a round-bottomed flask and 2M-HCl (5 mL) was added. The mixture was stirred at room temperature overnight and then extracted with EtOAc (3 x 50 mL). The organic layers were combined and dried with $MgSO_4$. Removal of the solvent *in vacuo* afforded a brown oil (0.31 g, 86%), NMR analysis of which showed very little of the desired aldehyde **55** and suggested cleavage of the phosphoramidate substrate. The reaction was repeated at room temperature for reaction times of 3.5 days and 3 h and at 40 °C for 4 h with similar results.

3.2. Kinetic study of the reaction of phosphonate esters with bromotrimethylsilane

The study was conducted using a Bruker Biospin 600 MHz NMR spectrometer. Temperature calibration of the spectrometer was carried out between 283 K and 333 K using a standard solution of 4% MeOH in MeOD for 'nominal' temperatures between 283 K and 298 K, and a standard solution of 80% ethylene glycol in DMSO-d_6 for 'nominal' temperatures between 297 K and 333 K. The differences (Δ ppm) between the -CH_3 and -OH signals for methanol and the -CH_2 and -OH signals for ethylene glycol were measured at each 'nominal' temperature and used to calculate the actual temperature using the equations: T = (4.109 − Δ)/0.008708 for methanol and T = (4.218 - Δ)/0.009132 for ethylene glycol.[134,135] The reported temperatures for each of the kinetic runs are the corrected values.

Measurement of the ^{31}P T_1 relaxation times

Diethyl phosphonate **35e** (0.060 g, 0.18 mmol), and 1,3,5-trimethoxybenzene (TMB; 0.012 g, 0.068 mmol) were dissolved in dry $CDCl_3$ (0.6 mL; stored over molecular sieves and basic alumina) under N_2. The solution was transferred to an NMR tube which was then flushed with N_2 and sealed with a septum. The ^1H and ^{31}P NMR spectra [calibrated using 1M-phosphoric acid in D_2O as an external standard (0.00 ppm)] of the substrate **35e** and TMB were recorded and TMSBr [1 eq.; 0.024 mL (0.028 g), 0.18 mmol] was then added through the septum. The reaction mixture was shaken and left to stand overnight at room temperature. The T_1 relaxation times of the phosphorus nuclei (in compounds **35e**, **49** and **48**) were measured by recording the inversion recovery ^{31}P spectra in a series of 12 experiments involving different recovery times ranging from 100 ms to 20 s. The ^{31}P signals were integrated and the intensity plotted against the delay time to give the T_1 relaxation times using curve fitting in Topspin.

Kinetics of the reaction of phosphonate ester **35e** with TMSBr

For each kinetic run, weighed quantities of the substrate **35e** and TMB were dissolved in dry $CDCl_3$ (0.6 mL; stored over molecular sieves and basic alumina) under N_2. The solution was transferred to a graduated NMR tube, flushed with N_2 and sealed with a septum. The NMR spectrum of a ^{31}P standard (1 mL of 1M-phosphoric acid in D_2O) was obtained and the signal was calibrated to 0.00 ppm. The ^1H and ^{31}P spectra of the substrate solution were recorded and TMSBr (4 eq.) was then added. The total volume of the reaction mixture was recorded and the tube was immediately replaced in the probe. The NMR experiments were set to record both the ^1H and ^{31}P spectra, followed by a delay of 90 s between acquisitions. The experiments were repeated at different temperatures ranging from 283 K to 305 K.

124

3.3. Enzyme-binding and inhibition studies

Expression and purification of EcDXR[69,101]

EcDXR was expressed and purified by Taryn Bodill in the Rhodes Centre for Chemico- and Biomedicinal Research, according to standard procedures.[69,101] In brief, XL-1 Blue competent cells were transformed with EcDXR plasmid DNA. Isopropylthiogalactoside (IPTG) was used to induce expression of the recombinant EcDXR gene. EcDXR was then purified by a combination of Ni^{2+} affinity- and size exclusion-chromatography. The protein was stored at -20 °C in a sodium phosphate buffer of pH 7.

Saturation transfer difference (STD) NMR experiments[95]

Standardisation of the STD experiment.[136]

An STD assay using bovine serum albumin (BSA) as the protein with *L*-tryptophan and glucose as ligands was carried out to validate and optimise the STD parameters. Solutions of BSA (84 x 10^{-6} M), *L*-tryptophan (7.75 x 10^{-3} M) and glucose (α/β) (53.25 x 10^{-3} M) were made up in 50 mM Tris/HCl buffer (pH 7.3). A sample containing BSA (240 µL), Tris/HCl buffer (120 µL), *L*-tryptophan (130 µL), glucose (19 µL) and D_2O (25 µL) was made up in an NMR tube to give a final assay solution containing 40 µM BSA, 2 mM *L*-tryptophan and 2 mM glucose in 50 mM Tris/HCl buffer (pH 7.3). An STD NMR experiment was run on a Bruker Biospin 600 MHz NMR spectrometer using water suppression at 4.7 ppm with the on-resonance pulse train set to 0.5 ppm and the off-resonance pulse train set to 20 ppm with phase cycling. The pre-saturation Gaussian pulse was applied 4 times and 2048 scans were run. A second identical experiment was then carried out on a BSA sample (240 µL) which had been freeze-dried and resuspended in an equal volume (240 µL) of D_2O.

STD experiment using compounds 35a-e, 36a-e, 39a-e and 40b-e.

EcDXR was extracted and purified as described above. The ligands to be tested were divided into four groups (35a-e; 36b-e; 39a-e and 40b-e + 36a) and an STD experiment was run on each group. EcDXR in 50 mM Na_2PO_4 buffer (pH 7.0) was freeze dried and re-suspended in D_2O to make a final concentration of 15.0 µM. Each group of ligands was dissolved in this solution to give a final ligand concentration of 600 µM and thus a protein:ligand ratio of 1:40. The STD assay was optimised in terms of the number of pre-saturation Gaussian pulses and the power level of the saturation pulse. Saturation of the protein was achieved using a train of 40 Gaussian bell-shaped pulses separated by a 1 ms delay at an attenuation power level of 40 dB. The frequency of the saturating on-resonance pulse was at 0.73 ppm and the off-resonance

pulse at 20 ppm. Phase cycling between the on- and off-resonances was used to minimise the effects of slight changes in temperature or magnetic field homogeneity. No spin-lock filter was used. A 3-9-19 water suppression pulse was applied at 4.7 ppm and 6000 scans were acquired. The on- and off-resonance spectra were subtracted from each other and processed using Topspin software from Bruker. For the last two groups of compounds, after running the STD experiment, fosmidomycin **19** was added (to a concentration of 600 μM) and the experiment was re-run under the same conditions to test for non-specific binding.

DXR inhibition assay[40,57,69]

Assays were conducted in a reaction mixture containing 100 mM Tris-HCl (pH 7.5), 1 mM MgCl$_2$, 0.3 mM NADPH and 0.3 mM DOXP **9** in a total volume of 100 μL. Equal volumes of *Ec*DXR and ligand were incubated at 37 °C for 5 min; 100 μL of this enzyme-ligand mixture was then added to the rest of the assay components to make a total of 200 μL with a final *Ec*DXR concentration of 5 μg.mL^{-1}. The decrease in absorbance at 340 nm due to the decreasing concentration of NADPH ($\varepsilon_{NADPH} = 6.3 \times 10^3$ L.mol^{-1}.cm^{-1}) was followed for 10 min at 37 °C, relative to a blank lacking the DOXP substrate. For each ligand, enzyme activity in the absence of inhibitor was deemed to be 100% (*i.e.* 0% inhibition) and the % relative inhibition was determined in triplicate.

3.4. *In silico* studies

Molecular modelling and simulated docking of synthetic ligands

Geometry optimisation and energy minimisation of ligands

The structures of ligands **35a-e** and **36a-e** were drawn in Discovery Studio Visualizer 2.0[109] (in their phosphonate ester, protonated and deprotonated phosphonic acid forms) and an *in vacuo* global minimum was located for each of the ligands by means of a systematic conformational search using Cerius^2.[106] For the esters **35a-e**, the torsion angles were rotated in increments of 60° whilst, for the acids **36a-e**, the torsion angles were rotated in increments of 30° because the acids have fewer rotatable torsions. The energy maximum was set to 10.00 kcal.mol^{-1} and a maximum of 10 000 conformers was generated for each compound. The lowest energy conformers were then subjected to geometry optimisation and energy minimisation with frequency analysis at the DFT (B3LYP) level with the 6-31G(d) basis set, using (IEFPCM) solvent correction (water) as implemented in Gaussian 03.[107]

Preparation of the protein model for docking

The X-ray crystal structure of *E.coli* DXR 1Q0L[47] was obtained from the Protein Data Bank (PDB; E.C. 1.1.1.267).[48] As the divalent cation, M^{2+} was not present in the 1Q0L crystal structure, this structure was compared with the crystal structure 1ONP,[36] which includes Mn^{2+}. The distances from Mn^{2+} to the carbonyl and hydroxamate moieties of fosmidomycin (2.302 Å and 2.131 Å respectively) were measured in 1ONP and used to position a Mn^{2+} ion in the 1Q0L model relative to fosmidomycin. The Mn^{2+}-coordinating water molecule was also added at a distance of 2.232 Å from the metal ion and in a position consistent with an octahedral coordination sphere around the metal ion. Fosmidomycin **19** and the structural water molecules were removed from the active site in the modified 1Q0L model, but the NADPH cofactor was retained.

Flexible docking

The geometry optimised and energy minimised ligands were imported into AutoDock 4.0, Gasteiger[112] charges were added and non-polar hydrogens were merged using AutoDock 4.0.[108] All possible torsions in the ligands were allowed. The protein was prepared using AutoDock 4.0, Gasteiger charges were calculated, non-polar hydrogens were merged and a +2 charge was assigned manually to the Mn^{2+} ion.[112] The active-site residues Ser186, Ser222, Asn227, Lys228 and Glu231 were selected as flexible residues, and atom maps were created

for possible interactions between the active-site residues and the ligand. The active site was represented by a grid box of dimensions 60 x 60 x 60 units with grid-point spacing of 0.375 Å and offset from centre by 0.806, 7.056 and 1.806 Å along the x, y and z directions respectively. The dockings were simulated using a Lamarckian genetic algorithm in AutoDock 4.0 and 10 docking runs were carried out for each ligand.[108] The parameters for the genetic algorithm were: population size = 150; mutation rate = 0.02; crossover rate = 0.8, allowing for a maximum of 27 000 generations and 2 500 000 energy evaluations. After the docking, the lowest energy conformers for each of the 10 docking runs were visualised using the Discovery Studio Visualizer 2.0.[109] A single-point DFT energy calculation was then carried out on each of the lowest energy conformers at the B3LYP 6-31G(d) level as implemented in Gaussian 03.[107]

Refinement of the charge on the metal cofactor

The Mg cofactor and its coordinating ligands (fosmidomycin **19**, Glu151, Asp149, Glu230 and the crystal structure water HOH3153) were removed as a group from the *Ec*DXR crystal structure 2EGH.[53] The amino acid residues were capped with hydrogen atoms where they had been removed from the polypeptide chain and the group was assigned an overall charge of -3. A single point energy calculation was carried out on the group at the Hartree-Fock level using the 6-31G(d) basis set as implemented in Gaussian 03.[107]

4. REFERENCES

(1)   Sherman, I. W. A Brief History of Malaria and Discovery of the Parasite's Life Cycle. In *Malaria, Parasite Biology, Pathogenesis, and Protection*; Sherman, I. W., Ed.; American Society for Microbiology: Washington, DC, 1998; pp 3-10.

(2)   Ntsaluba, A. *Guidelines for the Prevention of Malaria in South Africa*; The National Department of Health: Pretoria, 2003; pp 7-41.

(3)   Areqawi, M.; Cibulskis, R.; Otten, M.; Williams, R.; Dye, C. *World Malaria Report*; World Health Organisation: Geneva, 2008; pp 1-215.

(4)   Trigg, P. I.; Kondrachine, A. V. The Current Global Malaria Situation. In *Malaria, Parasite Biology, Pathogenesis, and Protection*; Sherman, I. W., Ed.; American Society for Microbiology: Washington, DC, 1998; pp 11-22.

(5)   Casman, E. A.; Dowlatabadi, H. Introduction. In *The Contextual Determinants of Malaria*; Casman, E. A., Dowlatabadi, H., Eds.; Resources for the Future: Washington, DC, 2002; pp 1-5.

(6)   World Health Organisation. Roll Back Malaria. http://www.rbm.who.int/rbmvision/ (accessed July 20, 2010).

(7)   Milhous, W. K.; Kyle, D. E. Introduction to the Modes of Action and Mechanisms of Resistance to Antimalarials. In *Malaria, Parasite Biology, Pathogenesis, and Protection*; Sherman, I. W., Ed.; American Society for Microbiology: Washington, DC, 1998; pp 303-316.

(8)   Desowitz, R. S. Great Expectations, Malaria Vaccines and Antimalaria Drugs for the Next Century. In *The Contextual Determinants of Malaria*; Casman, E. A., Dowlatabadi, H., Eds.; Resources for the Future: Washington, DC, 2002; pp 216-231.

(9)   Bannister, L.; Mitchell, G. *Trends Parasitol.* **2003**, *19*, 209-213.

(10) Silvie, O.; Mota, M. M.; Matuschewski, K.; Prudêncio, M. *Curr. Opin. Microbiol.* **2008**, *11*, 352-359.

(11) Phillips, R. S. *Clin. Microbiol. Rev.* **2001**, *14*, 208-226.

(12) Chitnis, C. E.; Blackman, M. J. *Parasitol. Today* **2000**, *16*, 411-415.

(13) Ghosh, A.; Edwards, M. J.; Jacobs-Lorena, M. *Parasitol. Today* **2000**, *16*, 196-201.

(14) Breman, J. G. *Sci. Prog.* **2009**, *92*, 1-38.

(15) Sharma, S.; Pathak, S. *J. Vect. Borne Dis.* **2008**, *45*, 1-20.

(16) Cowman, A. F. The Molecular Basis of Resistance to the Sulfones, Sulfonamides, and Dihydrofolate Reductase Inhibitors; In *Malaria, Parasite Biology, Pathogenesis, and Protection*; Sherman, I. W., Ed.; American Society for Microbiology: Washington, DC, 1998; pp 317-330.

(17) Vaidya, A. B. Mitochondrial Physiology as a Target for Atovaquone and Other Antimalarials; In *Malaria, Parasite Biology, Pathogenesis, and Protection*; Sherman, I. W., Ed.; American Society for Microbiology: Washington, DC, 1998; pp 355-370.

(18) Meshnick, S. R. From Quinine to Qinghaosu: Historical Perspectives; In *Malaria, Parasite Biology, Pathogenesis, and Protection*; Sherman, I. W., Ed.; American Society for Microbiology: Washington, DC, 1998; pp 341-354.

(19) Bennett, T. N.; Patel, J.; Ferdig, M. T.; Roepe, P. D. *Mol. Biochem. Parasitol.* **2007**, *153*, 48-58.

(20) Krogstad, D. J.; De, D. Chloroquine: Modes of Action and Resistance and the Activity of Chloroquine Analogs; In *Malaria, Parasite Biology, Pathogenesis, and Protection*; Sherman, I. W., Ed.; American Society for Microbiology: Washington, DC, 1998; pp 331-340.

(21) Dondorp, A. M.; Nosten, F.; Yi, P.; Das, D.; Phyo, A. P.; Tarning, J.; Lwin, K. M.; Ariey, F.; Hanpithakpong, W.; Lee, S. J.; Ringwald, P.; Silamut, K.; Imwong, M.; Chotivanich, K.; Lim, P.; Herdman, T.; An, S. S.; Yeung, S.; Singhasivanon, P.; Day, N. P. J.; Lindegardh, N.; Socheat, D.; White, N. J. *N. Engl. J. Med.* **2009**, *361*, 455-467.

(22) Müller, O.; Sié, A.; Meissner, P.; Schirmer, R. H.; Kouyaté, B. *Lancet* **2009**, *374*, 1419.

(23) Rohmer, M. *Pure Appl. Chem.* **1999**, *71*, 2279-2284.

(24) Rohmer, M. *Nat. Prod. Rep.* **1999**, *16*, 565-574.

(25) Rohmer, M.; Seemann, M.; Horbach, S.; Bringer-Meyer, S.; Sahm, H. *J. Am. Chem. Soc.* **1996**, *118*, 2564-2566.

(26) Wiesner, J.; Jomaa, H. *Curr. Drug Targets* **2007**, *8*, 3-13.

(27) Vial, H. J. *Parasitol. Today* **2000**, *16*, 140-141.

(28) Lichtenthaler, H. K. *Biochem. Soc. Trans.* **2000**, *28*, 785-789.

(29) Wiesner, J.; Borrmann, S.; Jomaa, H. *Parasitol. Res.* **2003**, *90*, S71-S76.

(30) Argyrou, A.; Blanchard, J. S. *Biochemistry* **2004**, *43*, 4375-4384.

(31) Munos, J. W.; Pu, X.; Liu, H. *Bioorg. Med. Chem. Lett.* **2008**, *18*, 3090-3094.

(32) Dumas, R.; Biou, V.; Halgand, F.; Douce, R.; Duggleby, R. G. *Acc. Chem. Res.* **2001**, *34*, 399-408.

(33) Henriksson, L. M.; Unge, T.; Carlsson, J.; Åqvist, J.; Mowbray, S. L.; Jones, T. A. *J. Biol. Chem.* **2007**, *282*, 19905-19916.

(34) Proteau, P. J. *Bioorg. Chem.* **2004**, *32*, 483-493.

(35) Radykewicz, T.; Rohdich, F.; Wungsintaweekul, J.; Herz, S.; Kis, K.; Eisenreich, W.; Bacher, A.; Zenk, M. H.; Arigoni, D. *FEBS Lett.* **2000**, *465*, 157-160.

(36) Steinbacher, S.; Kaiser, J.; Eisenreich, W.; Huber, R.; Bacher, A.; Rohdich, F. *J. Biol. Chem.* **2003**, *278*, 18401-18407.

(37) Hoeffler, J. F.; Tritsch, D.; Grosdemange-Billiard, C.; Rohmer, M. *Eur. J. Biochem.* **2002**, *269*, 4446-4457.

(38) Singh, N.; Cheve, G.; Avery, M. A.; McCurdy, C. R. *Curr. Pharm. Des.* **2007**, *13*, 1161-1177.

(39) Okuhara, M.; Kuroda, Y.; Goto, T. *J. Antibiot.* **1980**, *33*, 13-17.

(40) Kuzuyama, T.; Shimizu, T.; Takahashi, S.; Seto, H. *Tetrahedron Lett.* **1998**, *39*, 7913-7916.

(41) Jomaa, H.; Wiesner, J.; Sanderbrand, S.; Altincicek, B.; Weidemeyer, C.; Hintz, M.; Türbachova, I.; Eberl, M.; Zeidler, J.; Lichtenthaler, H. K.; Soldati, D.; Beck, E. *Science* **1999**, *285*, 1573-1576.

(42) Cooke, B. M. *Parasitol. Today* **2000**, *16*, 407-408.

(43) Lim, L.; McFadden, G. I. *Philos. Trans. R. Soc. B: Biol. Sci.* **2010**, *365*, 749-763.

(44) Takahashi, S.; Kuzuyama, T.; Watanabe, H.; Seto, H. *Proc. Natl. Acad. Sci. U.S.A.* **1998**, *95*, 9879-9884.

(45) Kuzuyama, T.; Takahashi, S.; Takagi, M.; Seto, H. *J. Biol. Chem.* **2000**, *275*, 19928-19932.

(46) Voet, D.; Voet, J. G. Amino acid metabolism; In *Biochemsitry*; John Wiley & Sons Inc: New Jersey, 2004; pp 1023-1024.

(47) Mac Sweeney, A.; Lange, R.; Fernandes, R. P. M.; Schulz, H.; Dale, G. E.; Douangamath, A.; Proteau, P. J.; Oefner, C. *J. Mol. Biol.* **2005**, *345*, 115-127.

(48) Protein Data Bank. Crystal Structure of DXR in Complex with Fosmidomycin. http://www.rcsb.org/pdb/explore.do?structureId=1Q0L/ (accessed February 25, 2008).

(49) Yajima, S.; Nonaka, T.; Kuzuyama, T.; Seto, H.; Ohsawa, K. *J. Biochem.* **2002**, *131*, 313-317.

(50) Singh, N.; Cheve, G.; Avery, M. A.; McCurdy, C. R. *J. Chem. Inf. Model.* **2006**, *46*, 1360-1370.

(51) Goble, J. L.; Adendorff, M. R.; de Beer, T. A. P.; Stephens, L. L.; Blatch, G. L. *Protein Pept. Lett.* **2010**, *17*, 109-120.

(52) Silber, K.; Heidler, P.; Kurz, T.; Klebe, G. *J. Med. Chem.* **2005**, *48*, 3547-3563.

131

(53)   Yajima, S.; Hara, K.; Iino, D.; Sasaki, Y.; Kuzuyama, T.; Ohsawa, K.; Seto, H. *Acta Crystallogr., Sect. F: Struct. Biol. Cryst. Comm.* **2007**, *63*, 466-470.

(54)   Giessmann, D.; Heidler, P.; Haemers, T.; Van Calenbergh, S.; Reichenberg, A.; Jomaa, H.; Weidemeyer, C.; Sanderbrand, S.; Wiesner, J.; Link, A. *Chem. Biodiversity* **2008**, *5*, 643-656.

(55)   Koppisch, A. T.; Fox, D. T.; Blagg, B. S. J.; Poulter, C. D. *Biochemistry (N.Y.)* **2002**, *41*, 236-243.

(56)   Bock, C. W.; Katz, A. K.; Markham, G. D.; Glusker, J. P. *J. Am. Chem. Soc.* **1999**, *121*, 7360-7372.

(57)   Perruchon, J.; Ortmann, R.; Altenkämper, M.; Silber, K.; Wiesner, J.; Jomaa, H.; Klebe, G.; Schlitzer, M. *ChemMedChem* **2008**, *3*, 1232-1241.

(58)   Cheng, F.; Oldfield, E. *J. Med. Chem.* **2004**, *47*, 5149-5158.

(59)   Ortmann, R.; Wiesner, J.; Silber, K.; Klebe, G.; Jomaa, H.; Schlitzer, M. *Arch. Pharm.* **2007**, *340*, 483-490.

(60)   Haemers, T.; Wiesner, J.; Busson, R.; Jomaa, H.; Van Calenbergh, S. *Eur. J. Org. Chem.* **2006**, *17*, 3856-3863.

(61)   Meyer, O.; Grosdemange-Billiard, C.; Tritsch, D.; Rohmer, M. *Org. Biomol. Chem.* **2003**, *1*, 4367-4372.

(62)   Reichenberg, A.; Wiesner, J.; Weidemeyer, C.; Dreiseidler, E.; Sanderbrand, S.; Altincicek, B.; Beck, E.; Schlitzer, M.; Jomaa, H. *Bioorg. Med. Chem. Lett.* **2001**, *11*, 833-835.

(63)   Courtois, M.; Mincheva, Z.; Andreu, F.; Rideau, M.; Viaud-Massuard, M. *J. Enzyme Inhib. Med. Chem.* **2004**, *19*, 559-565.

(64)   Hemmi, K.; Takeno, H.; Hashimoto, M.; Kamiya, T. *Chem. Pharm. Bull.* **1982**, *30*, 111-118.

(65)   Devreux, V.; Wiesner, J.; Goeman, J. L.; Van Der Eycken, J.; Jomaa, H.; Van Calenbergh, S. *J. Med. Chem.* **2006**, *49*, 2656-2660.

(66)   Devreux, V.; Wiesner, J.; Jomaa, H.; Rozenski, J.; Van Der Eycken, J.; Van Calenbergh, S. *J. Org. Chem.* **2007**, *72*, 3783-3789.

(67)   Kurz, T.; Geffken, D.; Wackendorff, C. *Z. Naturforsch., B: J. Chem. Sci.* **2003**, *58*, 457-461.

(68)   Kurz, T.; Geffken, D.; Wackendorff, C. *Z. Naturforsch., B: J. Chem. Sci.* **2003**, *58*, 106-110.

(69)   Kuntz, L.; Tritsch, D.; Grosdemange-Billiard, C.; Hemmerlin, A.; Willem, A.; Bach, T. J.; Rohmer, M. *Biochem. J.* **2005**, *386*, 127-135.

(70)   Phaosiri, C.; Proteau, P. J. *Bioorg. Med. Chem. Lett.* **2004**, *14*, 5309-5312.

(71)   Fox, D. T.; Poulter, C. D. *J. Org. Chem.* **2005**, *70*, 1978-1985.

(72) Salisu, S. T. ATP Mimics as Glutamine Synthetase Inhibitors - an Exploratory Synthetic Study. Ph.D. Thesis, Rhodes University, Grahamstown, 2008.

(73) Mutorwa, M.; Salisu, S.; Blatch, G. L.; Kenyon, C.; Kaye, P. T. *Synth. Commun.* **2009**, *39*, 2723-2736.

(74) Deng, L.; Sundriyal, S.; Rubio, V.; Shi, Z. Z.; Song, Y. *J. Med. Chem.* **2009**, *52*, 6539-6542.

(75) Ortmann, R.; Wiesner, J.; Reichenberg, A.; Henschker, D.; Beck, E.; Jomaa, H.; Schlitzer, M. *Bioorg. Med. Chem. Lett.* **2003**, *13*, 2163-2166.

(76) Kurz, T.; Schlüter, K.; Kaula, U.; Bergmann, B.; Walter, R. D.; Geffken, D. *Bioorg. Med. Chem.* **2006**, *14*, 5121-5135.

(77) Park, S. H.; Gwon, H. J.; Lee, H. S.; Park, K. B. *Bull. Korean Chem. Soc.* **2005**, *26*, 1701-1705.

(78) Bhattacharya, A. K.; Thyagarajan, G. *Chem. Rev.* **1981**, *81*, 415-430.

(79) Krise, J. P.; Stella, V. J. *Adv. Drug Deliv. Rev.* **1996**, *19*, 287-310.

(80) Wiesner, J.; Ortmann, R.; Jomaa, H.; Schlitzer, M. *Arch. Pharm. (Weinheim)* **2007**, *340*, 667-669.

(81) Kumar, K. G. D.; Saenz, D.; Lokesh, G. L.; Natarajan, A. *Tetrahedron Lett.* **2006**, *47*, 6281-6284.

(82) McKenna, C. E.; Higa, M. T.; Cheung, N. H.; McKenna, M. C. *Tetrahedron Lett.* **1977**, *18*, 155-158.

(83) Mutorwa, M. Rhodes University, Grahamstown. Unpublished work, 2010.

(84) Strelko Jr., V.; Streat, M.; Kozynchenko, O. *React. Funct. Polym.* **1999**, *41*, 245-253.

(85) Semionova, N. A.; Yushmanov, V. E. *Radiobiologiya* **1993**, *33*, 388-391.

(86) Schmid, R.; Sapunov, V. N. General Reaction Types; In *Non-formal Kinetics*; Dyllick-Brenzinger, C., Ed.; Verlag Chemie: Weinheim, 1982; Vol. *14*, pp 14-19.

(87) Schmidbaur, H.; Seeber, R. *Chem. Ber.* **1974**, *107*, 1731-1738.

(88) Frost, A. A.; Schwemer, W. C. *J. Am. Chem. Soc.* **1952**, *74*, 1268-1273.

(89) Burkhard, C. A. *J. Ind. Eng. Chem.* **1960**, *52* , 678.

(90) Keusch, P. Chemical Kinetics Rate Laws, Arrhenius Equation - Experiments. http://www.uniregensburg.de/Fakultaeten/nat_Fak_IV/Organische_Chemie/Didaktik/Keusch/kinetics.htm/ (accessed July 20, 2009).

(91) Laidler, K. J.; King, M. C. *J. Phys. Chem.* **1983**, *87*, 2657-2664.

(92) Kaye, P. T.; Mphahlele, M. J.; Brown, M. E. *J. Chem. Soc., Perkin Trans. 2* **1995**, 835-838.

(93) Lobb, K. A. Rhodes University, Grahamstown. Unpublished computer programme, 2010.

(94) Conibear, A. C.; Lobb, K. A.; Kaye, P. T. *Tetrahedron* **2010**, *66*, 8446-8449.

(95) Mayer, M.; Meyer, B. *Angew. Chem. Int. Ed.* **1999**, *38*, 1784-1788.

(96) Marchioro, C.; Davalli, S.; Provera, S.; Heller, M.; Ross, A.; Senn, H. Experiments in NMR-Based Screening. In *BioNMR in Drug Research*; Zerbe, O., Ed.; Wiley-VCH: Weinheim, 2003; Vol. *16*, pp 321-339

(97) Yan, J.; Kline, A. D.; Mo, H.; Shapiro, M. J.; Zartler, E. R. *J. Magn. Reson.* **2003**, *163*, 270-276.

(98) Ji, Z.; Yao, Z.; Liu, M. *Anal. Biochem.* **2009**, *385*, 380-382.

(99) Chen, A.; Johnson C. S.; Lin, M.; Shapiro, M. J. *J. Am. Chem. Soc.* **1998**, *120*, 9094-9095.

(100) Mayer, M.; James, T. L. *J. Am. Chem. Soc.* **2002**, *124*, 13376-13377.

(101) Kuzuyama, T.; Takahashi, S.; Watanabe, H.; Seto, H. *Tetrahedron Lett.* **1998**, *39*, 4509-4512.

(102) Desjardins, R. E.; Canfield, C. J.; Haynes, J. D.; Chulay, J. D. *Antimicrob. Agents Chemother.* **1979**, *16*, 710-718.

(103) Taryn Bodill, Bioassay Technician, Centre for Chemico- and Biomedicinal Research, Rhodes University, Grahamstown, 2010.

(104) Haemers, T.; Wiesner, J.; Van Poecke, S.; Goeman, J.; Henschker, D.; Beck, E.; Jomaa, H.; Van Calenbergh, S. *Bioorg. Med. Chem. Lett.* **2006**, *16*, 1888-1891.

(105) Joseph, G. The Global Institute for Bioexploration; *Screens-to-Nature Manual;* Rutgers University, 2009, *1*, pp 1-63.

(106) *Cerius²*, Version 4.10 L revision 05.0708; Accelrys Inc.: Taipei Hsien, 1997.

(107) *Gaussian 03*, Revision E.01, Frisch, M. J.; Trucks, G. W.; Schlegel, H. B.; Scuseria, G. E.; Robb, M. A.; Cheeseman, J. R.; Montgomery Jr., J. A.; Vreven, T.; Kudin, K. N.; Burant, J. C.; Millam, J. M.; Iyengar, S. S.; Tomasi, J.; Barone, V.; Mennucci, B.; Cossi, M.; Scalmani, G.; Rega, N.; Petersson, G. A.; Nakatsuji, H.; Hada, M.; Ehara, M.; Toyota, K.; Fukuda, R.; Hasegawa, J.; Ishida, M.; Nakajima, T.; Honda, Y.; Kitao, O.; Nakai, H.; Klene, M.; Li, X.; Knox, J. E.; Hratchian, H. P.; Cross, J. B.; Bakken, V.; Adamo, C.; Jaramillo, J.; Gomperts, R.; Stratmann, R. E.; Yazyev, O.; Austin, A. J.; Cammi, R.; Pomelli, C.; Ochterski, J. W.; Ayala, P. Y.; Morokuma, K.; Voth, G. A.; Salvador, P.; Dannenberg, J. J.; Zakrzewski, V. G.; Dapprich, S.; Daniels, A. D.; Strain, M. C.; Farkas, O.; Malick, D. K.; Rabuck, A. D.; Raghavachari, K.; Foresman, J. B.; Ortiz, J. V.; Cui, Q.; Baboul, A. G.; Clifford, S.; Cioslowski, J.; Stefanov, B. B.; Liu, G.; Liashenko, A.; Piskorz, P.; Komaromi, I.; Martin, R. L.; Fox, D. J.; Keith, T.; Al-Laham, M. A.; Peng, C. Y.; Nanayakkara, A.; Challacombe, M.; Gill, P. M. W.; Johnson, B.; Chen, W.; Wong, M. W.; Gonzalez, C.; Pople, J. A.; Gaussian, Inc.: Wallingford, CT, 2004.

(108) Morris, G. M.; Goodsell, D. S.; Halliday, R. S.; Huey, R.; Hart, W. E.; Belew, R. K.; Olson, A. J. *J. Comput. Chem.* **1998**, *19*, 1639-1662.

(109) *Discovery Studio Visualizer*, Release 2.0; Accelrys Software Inc.: San Diego, 2007.

(110) Pettersen, E. F.; Goddard, T. D.; Huang, C. C.; Couch, G. S.; Greenblatt, D. M.; Meng, E. C.; Ferrin, T. E. *J. Comput. Chem.* **2004**, *25*, 1605-1612.

(111) Wiley, E. A.; MacDonald, M.; Lambropoulos, A.; Harriman, D. J.; Deslongchamps, G. *Can. J. Chem.* **2006**, *84*, 384-391.

(112) Gasteiger, J.; Marsili, M. *Tetrahedron* **1980**, *36*, 3219-3228.

(113) Curioni, A.; Mordasini, T.; Andreoni, W. *J. Comput. Aided Mol. Des.* **2004**, *18*, 773-784.

(114) Morris, G. M.; Ruth, H.; Lindstrom, W.; Sanner, M. F.; Belew, R. K.; Goodsell, D. S.; Olson, A. J. *J. Comput. Chem.* **2009**, *30*, 2785-2791.

(115) Huey, R.; Morris, G. M. *Using Autodock 4 with AutoDock Tools; A Tutorial*; Scripps Research Institute: California, 2008; Vol. *1*, pp 56.

(116) Hirsch, A. K. H.; Fischer, F. R.; Diederich, F. *Angew. Chem. Int. Ed.* **2007**, *46*, 338-352.

(117) Zwierzak, A. *Synthesis* **1982**, *11*, 920-922.

(118) Still, W. C.; Kahn, M.; Mitra, A. *J. Org. Chem.* **1978**, *43*, 2923-2925.

(119) Al-Zaydi, K. M.; Al-Shamary, A.; Elnagdi, M. H. *J. Chem. Res.* **2006**, 408-411.

(120) Shionogi & Co., Ltd. Japanese Patent JP 59128326 A 19840724, 1984.

(121) Cesur, Z. *Pharmazie* **1987**, *42*, 716-717.

(122) Speziale, A. J.; Hamm, P. C. *J. Am. Chem. Soc.* **1956**, *78*, 5580-5584.

(123) Speziale, A. J.; Hamm, P. C. *J. Am. Chem. Soc.* **1956**, *78*, 2556-2559.

(124) Sayed, S. M.; Selim, M. A.; Raslan, M. A.; Khalil, M. A. *Heteroat. Chem.* **2000**, *11*, 362-369.

(125) Dang, Q.; Kasibhatla, S. R.; Reddy, K. R.; Erion, M. D.; Reddy, M. R.; Agarwal, A. International Patent WO 2000014095 A 120000316, 2000.

(126) Cooper, R. J.; Camp, P. J.; Henderson, D. K.; Lovatt, P. A.; Nation, D. A.; Richards, S.; Tasker, P. A. *Dalton Trans.* **2007**, 1300-1308.

(127) Myers, T. C.; Harvey, R. G.; Jensen, E. V. *J. Am. Chem. Soc.* **1955**, *77*, 3101-3103.

(128) Bechstein, U.; Liebscher, J. *J. Prakt. Chem. (Liepzig)* **1989**, *331*, 153-6.

(129) Eriksson, J.; Åberg, O.; Långström, B. *Eur. J. Org. Chem.* **2007**, 455-461.

(130) Takatori, Y. Japanese Patent JP 4402809119691120, 1969.

(131) Schlesinger, A. H.; Prill, E. J. *J. Am. Chem. Soc.* **1956**, *78*, 6123-6127.

(132) AKos Consulting & Solutions GmbH; *Catalogue Publication, AKI-VT-00393425,* 2009.

(133) Moskva, V. V.; Pavlov, V. A.; Zykova, T. V.; Razmov, A. I. *Zh. Obsh. Khim.* **1980**, *50* , 2805-2806.

(134) Nicholls, A. W.; Mortishire-Smith, R. J. *Magn. Reson. Chem.* **2001**, *39*, 773-776.

(135) Van Geet, A. L. *Anal. Chem.* **1968**, *40*, 2227-2229.

(136) Krishnan, V. V. *Curr. Anal. Chem.* **2005**, *1*, 307-320.